Integrated Hydrological and Hydrogeological System Analysis of the Lake Tana Basin, Northwestern Ethiopia

Sileshi Mamo Fantaye

A Thesis Submitted to the School of Earth Sciences

Presented in Partial Fulfillment of the Requirements for the Degree of Doctor of Philosophy (Hydrogeology)

Addis Ababa University

Addis Ababa, Ethiopia

June, 2015

Addis Ababa University

School of Graduate Studies

This is to certify that the thesis prepared by Sileshi Mamo, entitled: Integrated Hydrological and Hydrogeological System Analysis of the Lake Tana Basin, Northwestern Ethiopia and submitted in partial fulfillment of the requirements for the Degree of Doctor of Philosophy (Hydrogeology) complies with the regulations of the University and meets the accepted standards with respect to originality and quality.

Signed by the Examining Committees:

Principal Advisor: Prof. Tenalem Ayenew Signature……. Date……..

Examiner(Internal): Dr. Dessie Nedaw Signature…….Date……

Examiner(External):Prof. Moumtaz Razack Signature…….Date……

Chair of School or Graduate

Program Coordinator:…… Signature…….Date……

ABSTRACT

Integrated Hydrological and Hydrogeological System Analysis of the Lake Tana Basin, Northwestern Ethiopia

Sileshi Mamo

Addis Ababa University, 2015

Integrated hydrological, hydrogeological, hydrogeochemical and isotopes hydrological studies have been done in Lake Tana basin to understand the nature of aquifers and aquifer systems and their interactions and groundwater flow regime, to reveal and estimate the basin groundwater outflow and decipher the out flowing area, estimate groundwater inflow to and leakage rate from the Tana Lake and trace leakage area, determine groundwater and surface waters interaction, evaluate the basin groundwater recharge rate, and determine the origin of local high groundwater salinity.

The basin is characterized by different volcanic rocks overlain by sediments. The lithologic units include Quaternary lacustrine sediments, basalt and rhyolite, Tertiary flood basalts: Lower, Middle and Upper basalts, and Mio-Pliocene Shield volcanic rocks: Sekela Basalt, Degoma Basalt, Guna Tuff, Guna Basalt and trachyte flows and plugs.

These lithostratigraphic units have been grouped into hydrostratigraphic aquifers and confining units. The aquifers are ranked from low to moderate to high productivity. Productivity increases when the whole multi layers volcanic aquifers are intersected in fractured area. The results of the study revealed three aquifer systems, which are termed as the upper, intermediate and lower aquifer systems. The Upper Aquifer System has set of independent unconfined and (semi)confined aquifers in the northern, eastern, southwestern and western areas, and has isolated shallow and deep groundwater flow systems in the area that all flow toward the Tana Lake. The shallow unconfined aquifer interacts with and often feeds the rivers and the lake, while the deep groundwater in this system underflows out of the basin to Tis Abay area. The intermediate and lower aquifer systems have been ascertained to be found in the

eastern area below the Upper Aquifer System and are under confined condition, and have regional outflow to Tis Abay area.

Recharge rates of 195.6, 284.0 and 285.4 mm/year have been estimated based on baseflow analysis, chloride mass balance (CMB) and soil water balance (SWB) methods, respectively. Baseflow separation method shows shallow groundwater recharge that returns to streams. The recharge estimates from CMB and SWB are nearly similar and the average of the two (284.7 mm/year) can be taken as the mean basin recharge rate. The difference between the basin recharge and the baseflow to streams (89.1 mm $year^{-1}$ or 31.3% of the recharge) contributes to deep groundwater recharge and groundwater discharge to the Lake Tana.

Basin water balance evaluation has given inter basin groundwater outflow of 3333.5 hm^3/year. Hydrogeochemistry and isotopic data suggest that the basin groundwater outflow is mainly to the adjacent low lying Tis Abay area. Tana Lake balance study has also given leakage outflow of 954.8 hm^3/year, which mixes with groundwater mainly in the Beles basin and to certain extent in the Tis Abay area. Groundwater inflow directly to the lake is found to be not significant.

Origin of groundwater salinity in the volcanic area is mainly silicate hydrolysis. However, in lacustrine sediments aquifer, pockets of ground waters attain relatively high salinity (brackish) due to dissolution of evaporites and cation exchange.

Key words: hydrogeological system analysis, groundwater recharge**,** inter basin groundwater outflow, leakage, Lake Tana**,** Ethiopia

ACKNOWLEDGMENT

I would like first and for most to thank and acknowledge the School of Earth Sciences of the Addis Ababa University for giving me the opportunity to pursue my PhD study. Besides, I gratefully acknowledge the School for granting the research and isotope laboratory analysis.

I highly acknowledge my institution, the Geological Survey of Ethiopia, for allowing me to conduct the PhD study, granting the research and for hydrochemistry laboratory analysis.

I sincerely thank and acknowledge members of the School graduate and Supervisory committees for their genuine and deliberate follow up and management of the progress and accomplishment of the research works.

It is my pleasure to express my sincere thank to my principal supervisor Prof. Tenalem Ayenew for giving me the opportunity to do the research under his supervision, encouragement and allotting much of his time for guiding and shaping the research and reviewing the manuscript of the thesis.

I highly thank my co-advisor Dr Seifu Kebede for his encouragement, supervision and support during the execution of the research and reviewing the manuscript of the thesis.

Most importantly, I would like to thank Prof Gezahgne Yiergu for consultation and reviewing the geology part of the thesis. I sincerely thank Dr Tilahun Mammo for various consultations.

Moreover, I would like to thank my colleagues in the Groundwater Resource Assessment Directorate of the Geological Survey of Ethiopia for various assistances during the accomplishment of the research works.

Various offices referred are greatly acknowledged for data supply and consultations.

ACCRONIYUMS

Symbols

P	Precipitation over the basin
ET_o	Reference potential evapotranspiration
E_{ol}	Open evaporation from Tana Lake
E_{osm}	Evapotranspiration from seasonal marsh
E_{opm}	Open evaporation from permanent marsh
AET	Actual evapotranspiration
A	Slope of the saturation vapour pressure versus temperature curve at the mean air temperature, in mm of mercury per °C
H_n	Net radiation in mm of evaporable water
E_a	Parameter including wind velocity and saturation deficit
γ	Pychrometric constant = 0.49 mm of mercury per °C
H_a	Incident solar radiation out side the atmosphere on a horizontal surface, expressed in mm of evaporable water
a	A constant depending upon the latitude Θ and is given by a = 0.29 cosΘ
b	A constant with an average value of 0.52
n	Actual duration of bright sunshine in hours
N	Maximum possible hours of bright sunshine
r	Reflection coefficient (albedo) = 0.05 for water surface
σ	Stefan-Boltzman constant = 2.01×10^{-9} mm/day
T_a	Mean air temperature in degree Kelvin = 273 + °C
e_a	Actual mean vapour pressure in the air in mm of mercury
u_2	Mean wind speed at 2 m above ground in km/day
e_w	Saturation vapour pressure in mean air temperature in mm of mercury
R_n	Net radiation at the crop surface (MJ/m^2d)
G	Soil heat flux density (MJ/m^2d)
T	Mean daily air temperature at 2m height (ºC)
e_s	Saturation vapour pressure (kPa)
Δ	Slope vaspour pressure curve (kPa/ ºC)
Q_t	Stream flow at time step t

q_t	Direct runoff at time step t
α	Filter parameter associated with the catchment
C_{gw}	Cl in groundwater
C_p	Cl in bulk precipitation
Q	Runoff
C_q	Cl content of runoff
D	Dry Cl deposition
R	Recharge rate
ET_c	Crop evapotranspiration
K_c	Crop coefficient
T	Transsmissivity
SC	Specific capacity
Sm	Soil moisture
dSm	Change in soil moisture
I	Inflow
O	Outflow
ε	Undetermined balance elements, measurement and estimation errors
dt	Time increment
S_i	Surface inflow to the basin/ volumetric gauged and un-gauged surface inflow to the lake
G_i	Lateral groundwater inflow from adjacent aquifer/ volumetric groundwater inflow to the lake
A_r	Artificial recharge and return flow
S_o	Surface water outflow from the basin or Tana Lake
G_o	Basin groundwater outflow/ leakage rate from Tana Lake to adjacent basins
E_o	Open water evaporation
W	Withdrawal for consumptive uses
ds	Storage changes in open waters (rivers, lakes, reservoirs, ponds and wetlands), unsaturated zone and saturated zone.
A	Area
eG_o	Uncertainty introduced in the estimated value due to measurement error
eP	Measurement error for precipitation

eS_o	Surface outflow measurement error
eE_o	Error for evaporation measurement
V_L	Lake volume
P_l	Precipitation over the lake
C_L	Chloride content of Tana Lake
C_{Si}	Chloride content of surface inflow
C_{Gi}	Chloride content of groundwater inflow
C_{Pl}	Chloride content of precipitation over the Tana Lake
C_{So}	Chloride content of surface outflow
C_{Go}	Chloride content of groundwater outflow or leakage water
C_{Eol}	Chloride content of evaporation over the Tana Lake
eP_l	Measurement error for precipitation over the lake
Na^+	Sodium
K^+	Potassium
Ca^{2+}	Calcium
Mg^{2+}	Magnisium
HCO_3^-	Bicarbonate
Cl^-	Chloride
F^-	Fluoride
SO_4^{2-}	Sulfate
NO_3^-	Nitrate
SiO_2	Silca
Br^-	Bromide
pH	The negative logarithm of hydrogen ion activity
Z_i	Standard score of sample i
X_i	Value of sample i
X	Mean
s	Standard deviation
CO_2	Carbondioxide
PCO_2	Partial pressure of carbon dioxide
$\alpha CO_2(aq)$	Activity of aqueous carbon dioxide
^{18}O	Oxygen-18
^{2}H	Deuterium
^{3}H	Tritum

δ	Delta
a_o	Initial tritium activity
a_t	Tritium activity after time *t*
λ	Decay constant = $\ln 2/t_{1/2}$
$t_{1/2}$	Half life of tritium (12.43 TU)
E	Surface elevation
D	Borehole depth
WS	Depth to groundwater level strike
SWL	Depth to static groundwater level
Q	Yield
s	Drawdown
S	Storativity
Ma	Million annum

Units

mm	Millimeter
cm	Centimeter
m	Meter
km	Kilometer
h	Hecto
l	Liter
s	Second
d	Day
mg	Milligram
kg	Killogram
meq	Milli equivalent
mmol	Milli mol
µS	Micro Siemen
‰	Permil
TU	Tritium unit
δ	Delta
ºC	Degree Celcius

Abrevations

ITCZ	Inter-tropical convergence zone
RH	Relative humidity
GIS	Geographical information system
DEM	Digital elevation model
Fig	Figure
BFI	Baseflow index
DRO	Direct runoff
SWB	Soil water balance
CMB	Chloride mass balance
EN	Electro neutrality
EC	Electric conductivity
TH	Total hardness as $CaCO_3$
TDS	Total dissolved solids
HCA	Hierarchical cluster analysis
PCA	Principal component analysis
RCA	Residual carbonate alkalinity
SI	Saturation index
GNIP	Global network of isotopes in precipitation
FAO	Food and Agricultur Organization
VSMOW	Vienna standard mean ocean water
LMWL	Local mdeteoric water line
UAS	Upper aquifer system
IAS	Intermediate aquifer system
LAS	Lower aquifer system
WWDSE	Water Works Design and Supervision Enterprise
a.s.l	Above see level
NNE	North-north-east
SSW	South-south-west
WWN	West-west-north
EES	East-east-south
N	North
S	South
NE	Northeast

SW	Southwest
NNW	North-north-west
SSE	South-south-east
NW	Northwest
SE	Southeast
Lab	Laboratory
AWWCE	Amhara Water Works Construction Enterprise
ADSWE	Amhara Design and Supervision Enterprise

CONTENTS **PAGE**

ABSTRACT ii
1. INTRODUCTION 1
1.1. Background 1
1.2. Previous Studies 2
1.3. Rationale and Relevance of the Study 5
1.4. Objectives 8
1.5. Approach and Methodology 9
1.6. Materials and Tools 14
1.7. Limitation 16
1.8. Structure of the Thesis 16
2. DESCREPTION OF THE AREA 18
2.1. Location 18
2.2. Topography 19
2.3. Soil and Land Cover 19
2.3.1. Soil 19
2.3.2. Land cover 23
3. GEOLOGY 24
3.1. Regional Geology 24
3.2. Geology of the Tana Basin 29
3.2.1. Lithologic units and stratigraphy 29
3.3. Tectonic Structures 44
4. HYDROMETEOROLOGY 47
4.1. Climate 47
4.2. Meteorological Elements 47
4.2.1. Meteorological stations and data quality 47
4.2.2. Precipitation 51
4.2.3. Evapotranspiration 58
4.2.4. Temperature 66
4.2.5. Relative humidity, sunshine hours and wind speed 67
4.3. Hydrology 70
4.3.1. Rivers 70
4.3.2. Tana Lake and Reservoirs 71
4.3.3. Wetland 73
4.3.4. Baseflow analysis 73
4.3.5. Estimation of runoff coefficient 79
5. HYROGEOLOGY 79
5.1. General 79
5.2. Hydrostratigraphic Units and Aquifer Characterization 82
5.2.1. Intergranular Aquifers 82
5.2.2. Fractured Aquifers 91
5.2.3. Aquitard 100
5.3. Groundwater Flow Regime 101
5.4. Groundwater Recharge and Discharge Conditions 101
6. EVALUATION OF GROUNDWATER RECHARGE 102
6.1. General 102
6.2. Baseflow Separation Method 103
6.3. Soil Water Balance Method 104
6.4. Chloride Mass Balance Method 107
7. BASIN WATER BALANCE EVALUATION 112

8. HYDROLOGICAL AND CHEMICAL MASS BALANCE OF LAKE TANA 114
9. HYDROGEOCHEMISTRY 118
9.1. General 118
9.2. Sampling and Evaluation of Accuracy of Laboratory Analysis 119
9.3. Evaluation of Hydrochemical Parameters and Ions 121
9.3.1. Hydrochemical parameters 122
9.3.2. Major ions 126
9.4. Multivariate Analysis and Hydrochemical Facies 134
9.5. Origin of Groundwater Salinity, Hydrogeochemical Evolution and Inverse ..... Hydrogeochemical Modeling.....149
9.5.1. Origin of salinity and hydrogeochemical evolution.....149
9.5.2. Inverse hydrogeochemical modeling……... …165
10. ENVIRONMENTAL ISOTOPES HYDROLOGY 167
10.1. General 167
10.2. Deuterium and Oxygen-18 168
10.2.1. Local meteoric water line (LMWL).....168
10.2.2. Altitude effect 170
10.2.3. Deuterium and Oxygen-18 data evaluation 173
10.3. Tritium 184
11. SYNTHESIS 190
11.1. Analysis of Aquifers, Aquifer Systems and Groundwater Flow Regime 190
11.2. Groundwater Recharge Estimates 201
11.3. Inter Basin Groundwater Outflow Rate and Deciphering Outflow Area 203
11.4. Groundwater and Surface Waters Interaction 204
11.4.1. Groundwater- streams interaction 204
11.4.2. Groundwater-Tana Lake interaction 205
11.5. Origin of Groundwater Salinity 209
11.6. Origin of Wetlands 211
12. CONCLUSIONS AND RECOMMENDATIONS.....211
REFERENCES.....213

FIGURES

Figure 1.1. Out line of the research methodology. 15
Figure 2.1. Location map.....18
Figure 2.2. Physiographic regions in the Tana basin. 20
Figure 2.3. Topographic elevation map (meter). 21
Figure 2.4. Soil map. 23
Figure 2.5. Land cover map. 25
Figure 3.1. Geological map of the northern Ethiopian plateau (Keiffer et al., 2004). .28
Figure 3.2. Conceptual stratigraphic relationships between lithologic units exposed in different sectors of the study area and their possible correlations. 30
Figure 3.3. Geological sketch map and tectonic structures (Compiled and modified from Workeneh Haro et al., 2010; 2011; Dejene Hailemaryam et al., 2012 and Efrem Beshawered et al., 2010). 31
Figure 3.4. A geological cross-section from Guna volcano (B) in the west to Tana Lake (B') in the east. Vertical scale has been exaggerated 10 times. 33
Figure 3. 5. A geological-cross section from Gonder area (C) in the north to Tana Lake.....33
(C') in the south , not exaggerated. 33
Figure 3.6. Contact between Middle and Upper basalts. 35
Figure 3.7. Contact between Sekela and Quaternary basalts. 38
Figure 3.8. Contact between Guna Tuff and a)Upper Basalt and b) Guna Basalt 39
Figure 3.9. Contact between Trachyte flow and Upper Basalt near Gorgora town. 40
Figure 3. 10. Contact between Quaternary basalt and Sekela Basalt. 41
Figure 3.11. Contact between rhyolite dome and a) Quaternary basalt, ...43
b) Upper Basalt. 43
Figure 3.12. Rose diagram for strikes of faults. 45
Figure 3.13. Rose diagram for lineaments. 46
Figure 4.1. Climatic zones of the basin. 49
Figure 4.2. Spatial distribution of meteorological stations. Number indicates class of the station. 51
Figure 4.3. Graph depicting precipitation regimes in Ethiopia (Andarge Mekonen, 2010). 54
Figure 4.4. Temporal variation of precipitation in selected stations. 54
Figure 4.5. Spatial variation of precipitation (in mm). 56
Figure 4.6. Relationship of rainfall (P) and altitude (H). 57
Figure 4.7. Thiessen polygons used to estimate aerial depth of precipitation. 60
Figure 4.8. Thiessen polygons used to estimate mean precipitation over the Tana Lake.....61
Figure 4.9. Thiessen polygons used for averaging the reference potential evapotratnspiration. 64
Figure 4.10. Sub-basins in the area. 72
Figure 4.11. Trends of water level for Tana Lake. 73
Figure 4.12. Map showing the specific discharge values of gauged catchments. 77
Figure 4.13. Plot of specific discharge (SD) versus BFI. 78
Figure 4.14. The total and groundwater baseflow hydrographs for a) Gilgel Abay b) Gemero stations. Red and blue lines show the total and groundwater baseflow hydrographs, respectively. 79
Figure 5.1. Groundwater and surface waters points inventoried and used in data analysis. 83
Figure 5.2. Hydrogeological map of the area. 84

Figure 5.3. Hydrogeological cross sections along a) A-A', b) B-B', c) C-C'. The lines are indicated in Fig. 8.2. Vertical exaggerations are indicated at title of vertical axes. 87
Figure 5.4. Graphs depicting variation of the hydraulic parameters of the different aquifers. a) borehole depth, b) borehole yield, c) spring yield (spring with discharge as large as 108 l/s was observed for Quaternary basalt), d) transsmissivity 90
Figure 5.5. Fractures and vesicles in Quaternary basalt aquifer. 91
Figure 5.6. Diagnostic curve for Bahir Dar test borehole (GW226). 93
Figure 5.7. Moench fracture flow solution for Bahir Dar test borehole (GW226). 93
Figure 5.8. Joints in the Middle Basalt aquifer. 94
Figure 5.9. Muli layered fractured aquifers a) around Gonder (GW3) b) Debretabor borehole no.10 (GW9). Violet and pink colors indicate depths to water strike and the final static groundwater level, respectively (Source: ADSWE drilling logs). 97
Figure 5.10. Diagnostic curve for borehole GW3.....98
Figure 5.11. Moench fracture flow solution to estimate transsmissivity and storativity. 98
Figure 5.12. Joints in the Upper Basalt aquifer. 99
Figure 6.1. Elements of recharge (After Nyagwambo, 2002).....103
Figure 9.1. Graph showing electro neutrality of water samples. 120
Figure 9.2. Plot of field measured pH versus laboratory measured pH values of groundwater samples. 121
Figure 9.3. Spatial distribution of Electric conductivity (EC) in µS/cm. 122
Figure 9.4. Spatial distribution of pH. 125
Figure 9.5. Spatial distribution of total hardness (mg/l). 126
Figure 9.6. Spatial distribution of Ca^{2+}. 127
Figure 9.7. Spatial distribution of Mg^{2+}. 128
Figure 9.8. Spatial distribution of Na^{+}. 129
Figure 9.9. Spatial distribution of HCO_3^{-} 130
Figure 9.10. Spatial distribution of chloride. 132
Figure 9.11. Spatial distribution of sulfate.....133
Figure 9.12. Spatial distribution of fluoride.....134
Figure 9.13. Dendogram showing clusters or subgroups (SG) of ground waters. Dashed red line is the phenon line. Labels of X axis are sample numbers (see Appendix 4). 136
Figure 9.14. Further classification by PCA. Numbers indicate subgroups based on HCA classification. 139
Figure 9.15. Piper diagram of groundwater subgroups, surface waters and rainfall. Size of symbols is proportional to their total dissolved solids content. 140
Figure 9.16. Spatial distributions of groundwater subgroups. 145
Figure 9.17. Spatial distributions of hydrochemical facies. Number indicates subgroup to which the groundwater sample belongs. 146
Figure 9.18. Box plot showing variation of borehole depth for groundwater 148
subgroups. 148
Figure 9.19. Plot of Na^{+} versus Cl^{-}; SG stands for subgroup. 150
Figure 9.20. Plot of Na^{+} versus HCO_3^{-}. 151
Figure 9.21. Plot of Ca^{2+} versus HCO_3^{-}. 151
Figure 9.22. Plot of Ca^{2+} versus SO_4^{2-}. 152
Figure 9.23. Plot of $(Ca^{2+} + Mg^{2+})$-$(HCO_3^{-} + SO_4^{2-})$ versus $(Na^{+} + K^{+} - Cl^{-})$. 152
Figure 9.24. Plot of Cl^{-} versus TDS. 155
Figure 9.25. Plot of HCO_3^{-} versus TDS. 155

Figure 9.26. Plot of Na^+ versus TDS. 156
Figure 9.27. Plot of Ca^{2+} versus TDS. 156
Figure 9.28. Plot of concentrations of ions and chemical parameters versus groundwater subgroups. 157
Figure 9.29. Plot of Br^- versus Cl^- 159
Figure 9.30. Plot of Br^-/Cl^- versus Cl^-. 159
Figure 9.31. Plot of $\delta^{18}O$ (‰) versus electric conductivity (µS/cm). a) samples are grouped by subgroups b) grouped by aquifers. 161
Figure 9.32. Plots of electric conductivity (µS/cm) versus altitude. a) grouped by groundwater subgroups, b) grouped by aquifers. 163
Figure 10.1. Local meteoric water line for Tana and surrounding areas (data in ‰). 170
Figure 10.2. Altitude effect a) based on delta ^{18}O (‰), b) based on delta ^{2}H (‰) 171
Figure 10.3. Spatial distribution of delta ^{18}O (‰). 175
Figure 10.4. Plot of delta deuterium versus oxygen-18 (‰). a) grouped by groundwater subgroups, b) grouped by aquifers, c) grouped by type of schemes 179
Figure 10.5. Plot of delta Oxygen-18 versus altitude a) grouped by groundwater subgroups and b) grouped by sub-areas. 180
Figure 10.6. Spatial distribution of tritium (in TU). 186
Figure 10.7. Plot of tritium versus altitude. 189
Figure 10.8. Plot of tritium versus delta ^{18}O. 189
Figure 11.1. Plot of tritium versus electric conductivity. a) grouped by groundwater subgroups, b) grouped by aquifers. 194
Figure 11.2. Plot of HCO_3^- versus pH showing open and closed systems in the area. 196
Figure 11.3. Cross section along D-D' depicting inter basin groundwater outflow from Tana basin to Tis Abay area. Vertical scale is exaggerated 100 times. Cross section line is shown in Figure 5.2. 204
Figure 11.4. Map showing the groundwater outflow area from Tana basin and leakage area from Tana Lake. 208

TABLES

Table 2.1. Land covers of Tana basin. 23
Table 4.1. Ethiopian climate. 48
Table 4.2. Meteorological stations and their characteristics. 50
Table 4.3. Characterization of precipitation pattern in Ethiopia. 53
Table 4.4. Mean monthly precipitation values of stations (1995-2009. 55
Table 4.5. Estimated mean meteorological parameters for the basin (1995-2009), in mm. 59
Table 4.6. Open water evaporation (E_o) data calculated based on Penman's equation and Pitche evaporation (in mm). 68
Table 4.7. Mean monthly temperature of four selected stations (in °C). 68
Table 4.8. Relative humidity, sunshine hours and wind speed for selected stations. 69
Table 4.9. Area of sub-basins. 71
Table 4.10. Mean gauged and ungauged total runoff (hm3/year) 71
Table 4.11. Morphometric characteristics. 71
Table 4.12. Mean (1995-2009) BFI and specific discharge values of gauged catchments in the basin. 76

Table 5.1. Aquifer classification criteria (After, Geoffery and Gall, 1991). 81
Table 5.2. Hydraulic data of lacustrine sediments aquifers. 88
Table 5.3. Hydraulic data of Guna Tuff aquifer. 91
Table 5.4. Hydraulic data of Quaternary basalt and the underlying Tertiary basalts aquifers. 93
Table 5.5. Hydraulic data of the Middle Basalt aquifer. 95
Table 5.6. Hydraulic data of the Upper Basalt aquifer. 100
Table 6.1. Recharge estimate based on baseflow separation method. 105
Table 6.2. Soil water balance (mm); available water capacity 165 mm. 108
Table 8.1. Percentage changes in G_o and G_i for the changes in the respective input parameters by ±20%. 118
Table 9.1. Summary statistics for hydrochemical parameters and ions (mg/l). 123
Table 9.2. Variance and loadings of variables to principal components. 138
Table 9.3a. Mean values of ions and hydrochemical parameters for groundwater clusters or subgroups (mg/l). 141
Table 9.3b. Mean values of ions and hydrochemical parameters for surface waters and rainfall (mg/l). 142
Table 9.4. Hydrochemical facies associated with ground waters subgroups, surface and rain waters. 144
Table 9.5. RCA and selected ions and ionic ratios. 165
Table 9.6. Saturation indices (SI) and selected mass transfer model solutions (mmol/kg of water) when Subgroup3 evolves to subgroups 1b and 1d. 166
Table 10.1. Meteorological stations where rainfall samples collected. 172
Table 10.2. Weighted (by precipitation) mean delta deuterium and oxygen-18 value of the rainfall at the stations. 173
Table 10.3. Summary statistics for environmental isotopes data. 183

APPENDICES

Appendix 1. Groundwater inventory data. 223
Appendix 2a. Field and laboratory measured hydrochemical parameters for groundwater. 233
Appendix 2b. Laboratory measured hydrochemical data for groundwater. 240
Appendix 2c. Field and laboratory measured hydrochemical parameters for rainfall and surface waters. 247
Appendix 2d. Laboratory measured hydrochemical data for rainfall and surface waters. 249
Appendix 3a. Isotopic data of groundwater samples. 251
Appendix 3b. Isotopic data of surface waters. 257
Appendix 3c. Isotopic data of rainfall. 258
Appendix 4. Groundwater subgroups. 260

1. INTRODUCTION

1.1. Background

The Lake Tana basin is located in the northwestern Ethiopian volcanic terrain with limited extent of lacustrine sediments. Previous geophysical investigations reported Mesozoic sedimentary rocks beneath the volcanic rocks. The rainfall amount is high in the region.

Water use competition is seen in Tana basin among hydroelectric, irrigation, tourism, water supply, navigation and environmental needs such as sustaining the river baseflow and wetlands, and this will be a serious issue in the future. Groundwater is the major source of water supply for towns and rural communities. Currently, there is an attempt by the Federal Government to develop groundwater using deep boreholes and rivers using dams for medium and large scale irrigation and flood control in the basin.

Many wells drilled have poor productivity and some with poor quality. Drying of wells and springs has also been reported after prolonged drought. This shows that the effective use of groundwater has been hampered due to complex nature of aquifers in the basin and partly because the hydrogeological system and sustainable yield of the aquifers and the basin were not adequately explored. This led to difficulties in locating productive aquifers and sustainably develops the groundwater. Besides, the intended groundwater development for irrigation will entails drying of streams flow that will have adverse effect on the current irrigation schemes using rivers and on riparian ecology, as well as on existing and future groundwater supply schemes.

Water supply investigations of specific towns and studies and researches that cover part of the Tana sub-basins and a few that cover the whole Tana basin as well as regional ones that consist of the basin have been done to solve the problem. However, these studies often use the conventional hydrogeological methods and some with limited hydrochemistry input. Others are regional to investigate the area in detail. Thus, integrated hydrogeological,

hydrogeochemistry and environmental isotope hydrology studies are essential to understand the hydrogeological system and the groundwater resource of the area, which have implication for proper utilization and management of the groundwater resources.

The present research is the first attempt in the basin to do integrated and detailed hydrogeological, hydrogeochemistry and environmental isotopes hydrology studies for better understanding of the hydrogeological systems. This can improve the understanding of the aquifer systems present and how they functions under natural condition and with existing man made features (interaction with surface waters, basin groundwater outflow condition, etc), and gives the renewable groundwater resource or recharge and discharge. Furthermore, it gives answer to the source of groundwater salinity in the area, and particularly to pockets of relatively highly saline (brackish) ground waters in the lacustrine sediments.

The account period for hydrometeorological data analysis and hydrological evaluations is between 1995 and 2009. Because, a lot of activities are being done since 2010, which include house hold irrigation using streams whose consumption is unknown, making dams and diverting the Tana Lake by tunnel for power development, which disturb the natural system.

1.2. Previous Studies

The geology of the Tana basin has been mapped by Mengesha et al. (1996), BCEOM (1998) and Pietrangeli (1990), which show that Tertiary Tarmaber Basalt, Quaternary Basalt and Quaternary unconsolidated lacustrine and alluvial sediments cover the area. According to Kieffer et al. (2004), Mio-Pliocene volcanic rocks including Choke (22.4 Ma) and Guna (10.7 Ma), and Quaternary volcanic rocks cover the Tana basin. Begosew Abate et al. (1998) did petrographic and geochemical studies in basaltic and rhyiodacitic rocks of Lake Tana and Gimjabet-Kosober areas. These studies are more regional. The floor of the Tana Lake is covered by clay (Lamb et al., 2007).

The geological and structural maps of the different parts of the basin have been prepared at a scale of 1:250000 by the Geological Survey of Ethiopia (Workeneh Haro et al., 2010; 2011; Dejene Hilemaryam et al., 2012 and Ephrem Beshawered et al., 2010), which have been done on four map sheets including the study area. Geological base map for Tana basin has been compiled from these maps and was verified and modified in this study.

Thick (1.5 to 2 km) Mesozoic sedimentary rocks were reported in Tana basin by magneto telluric imaging technique beneath the 250 m thick flood basalt (Hautot et al., 2006). Tadesse Meselu (2009) has also reported basalt up to 295 m, which is underlain by Mesozoic sedimentary rocks that extends between 295 m and 3.6 km based on gravity method in Debretabor area. Metamorphic rocks underlie the sedimentary rocks. However, deep test well drilled around Bahir Dar town has encountered granite below volcanic rocks, which could probably be Precambrian, at a depth of 350 m up to the final depth of the borehole (500 m). Besides, deep test well drilling in the northern plain area shows volcanic rocks up to the final depth of 400 m below lacustrine sediments.

Tana area has been built through a series of uplift due to mantle plume activity. Flood basalts and three garbens have been formed during this process, which are Gonder, Debretabor and Dengel grabens. Dengel graben occupies the present southwestern area, but increased rate of uplift and volcanism has reversed the topography. Subsequent subsidence occurred due to tensile forces and the Tana Lake occupied the center of the subsidence and graben convergence (Chorowicz et al., 1998).

Hydrogeological studies within and regional ones that include the Tana basin have been done by Tesfaye Chernet (1990), BCEOM (1998), Bayissa Asfaw (2003), Molla Fetene (2004), SMEC (2007), Beruke Abel (2009), Matebie Meten (2009), Zelalem Leyew (2009), Zenaw Tessema (2011) and Sogreah (2012). These studies are mainly conventional and the same hydrogeological units have been classified with different aquifer productivity by these authors.

Previous studies used mainly conventional hydrogeology with little hydrogeochemical inputs. Hydrogeochemical and isotopic studies in Abay Basin and in Tana basin conducted by Seifu Kebede et al. (2005 and 2012) have shown different groundwater types in Tana basin based on their hydrogeochemical and isotopic signatures. Addis Hailu (2011) has also conducted hydrogeochemical and isotopic study in Abay Basin that include the study area.

Groundwater- surface water interaction attempt have been done by different authors. According to WWDSE (2007) water from the Tana Lake percolates through its floor to aquifers of Tertiary volcanic and Mesozoic sedimentary rocks, which are found in the eastern area. Seifu Kebede et al. (2004), Getachew Hadush (2008) and Samson Mengistu (2010) concluded that groundwater contribution is less than 7% of the total inflow to the Lake Tana based on baseflow separation and numerical modeling techniques. However, according to SMEC (2007) groundwater inflow to the lake is negligible. About 130.5 hm^3/year groundwater outflow was estimated to the Tana Lake from northern catchment areas using numerical groundwater flow modeling (Nigussie Ayele, 2010). Samson Mengistu (2010) did numerical groundwater flow modeling for Tana basin and found that the baseflow to streams is 1809 hm^3/year, and groundwater contribution to the lake is 243.1 hm^3/year (2.8% of the total inflow). According to this author, recharge from influent streams to the aquifer is 7.04 hm^3/year.

On the other hand, Girum Admasu (2010) concluded based on isotopes and hydrochemistry studies that the rivers feed the groundwater in the volcanic terrain and plains of the Megech, Rib and Gumara sub-basins. The works of Seifu Kebede et al. (2012) and SMEC (2007), Getachew Hadush (2008) and numerical flow modeling done by Samson Mengistu (2010) showed that leakage from the lake and inter basin groundwater outflow were not considered, and considered a closed basin and lake in terms of groundwater outflow. The results of these studies seem to be contradictory, and this has been resolved by the present integrated studies.

Un-gauged catchments flow has been determined by Abeyu Wale (2008) to be 41% (2729 hm^3/year) of the total river inflow to the lake based on HBV model.

Getachew Hadush (2008) estimated un-gauged catchments inflow to be 900 hm^3/year (18% of the total inflow to the lake) using the lake water balance evaluation method, and 650 hm^3/year using a mixing cell approach. Seifu Kebede et al. (2012) calculated using isotope mass balance method that the surface water inflow from un-gauged catchments to the lake is 1727 hm^3/year, and the evaporative water loss in the vast flood plains adjoining the lake to be 483 hm^3/year. This variation is attributed to the limitation and uncertainty of each method, and because groundwater inflow to and outflow from the lake were not included in the model.

Recharge estimation attempt using different hydrograph separation and Chloride mass balance methods have given 184.3, 161.7, 70-120, 142.7 mm/year by Sogreah (2012), Getachew Zewde (2010), Getachew Hadush (2008) and BCEOM (1998), respectively. However, the chloride mass balance method did not take into account the surface runoff. These values are variable because of limitations of the methods used and uncertainties in the input parameters.

1.3. Rationale and Relevance of the Study

The previous studies mainly used conventional hydrogeological methods with limited hydrochemical input. However, geological and hydrological studies often give fragmentary or incomplete information to the sub-surface groundwater system. The available groundwater table contour map also gives the shallow groundwater or aquifers head as depths of boreholes are shallow. Therefore, there is lack of sufficient and sound data to justify and support the previous ideas, and to discern the hydrogeological system in this basin. Besides, the results of the previous studies are variable and contradictory.

Most of the previous studies were done in some parts of the area and only a few cover the whole Tana basin. Existing studies speculated the presence of shallow and deep aquifers. Furthermore, hydrochemical and isotopic studies in Tana and Abay basin as whole showed that there are ground waters with different geochemical characteristics than the previous anticipation. However, the aquifers

present, nature of aquifers and their flow regime and interactions are poorly known until now. This suggests further integrated and detailed study.

Deep test wells drilled by the Ministry of Water, Irrigation and Energy (MoWIE) and for Gonder town water supply and at Bahir Dar area have been used and provided additional hydrogeological information including groundwater level, geological logs and pumping test data, which help to upgrade the previous studies and visualize the shallow, intermediate and deep aquifers conditions together with hydrogeochemistry and isotopic data. Analysis of litho-stratigraphy, deep boreholes geological logs, groundwater level and pumping test data, and hydrogeochemical and isotopic data under this study has revealed the presence muylti layers of aquifers in the upper, intermediate and lower aquifer systems.

Origin, groundwater flow regime, recharge and discharge conditions, interaction and mixing among the different ground waters of the upper, intermediate and lower aquifer systems were poorly known until this study. Origin of the wet lands in Tana basin has been dealt by some previous authors and it is further addressed in this study. Hydrogeochemical and isotopes investigations have been done together with the conventional hydrogeological method to fill this gap.

Most of the previous recharge estimations were done based on different river hydrograph separation methods. The recharge estimates of previous authors are variable and often under estimated. Besides, baseflow separation method gives only the shallow aquifer recharge that interacts with the rivers. Therefore, the chloride mass balance that accounts surface runoff, soil water balance and baseflow separation methods were used here to estimate reliable basin recharge rate under this study. The recharge estimated by these different methods also helped to understand the streams-groundwater interaction.

Previous conclusions concerning the interaction between groundwater and streams were contradictory. Girum Admasu (2010) concluded that the rivers feed the groundwater in the volcanic terrain and plains of the Megech, Rib and Gumara sub-basins while others considered that the groundwater feeds the streams. The interaction between streams and groundwater was better understood in this study.

Besides, most authors believe that the inflow from the groundwater to and outflow from the Lake Tana to the groundwater is negligible. Moreover, all previous lake balance studies (Abeyu Wale, 2008; Getachew Hadush, 2008 and Seifu Kebede et al., 2012) did not take into account the groundwater inflow to and leakage outflow from the lake. However, WWDSE (2007) speculated possible lake water underflow to deep Chilga groundwater basin, which is the northern adjoining basin, and no outflow to Beles basin, and there is significant lake water outflow to the deep aquifers in the eastern area via the lake floor. Thus, this controversial issue had to be resolved and interaction of the Lake Tana with the shallow and deep aquifers should have to be determined by this study. The lake balance has been evaluated, which considered the groundwater inflow and outflow, and the un-gauged catchment runoff.

No attempts were done for inter basin groundwater outflow condition by the previous studies. Most previous studies considered the basin and Tana Lake as a closed system in terms of groundwater inflow and outflow. Besides, numerical groundwater flow modeling done so far assumed no inter basin groundwater and lake leakage outflow in their model or considered a closed system. Quantity of the Tana basin groundwater outflow and outflow area and presence of significant leakage rate from Tana Lake and leakage area, and minor groundwater inflow to the lake have been ascertained in this study.

Ground waters with relatively high salinity, which are not fit for drinking and irrigation, have been reported by previous studies within the lacustrine sediments. Origin of salinity for these pockets of ground waters was not known except Seifu et al. (2012) that concluded to be due to dissolution of evaporites that are deposited associated with evaporation of river flood pools after the rainy period. Further works have been done in this study to understand and ascertain the origin or sources of salinity to these ground waters. Besides, sources ions for the different ground waters in the basin have been determined.

To this end, the study gave better answer than ever done works, for the hydrogeological problems in the area by providing new first hand information and crucial knowledge on aquifer systems present and their groundwater flow regimes,

basin recharge rate, groundwater discharge, how the hydrogeological system functions, inter basin groundwater outflow rate and outflow area, groundwater and surface waters interactions, groundwater inflow to and leakage rate from the Tana Lake and leakage area, and on the origin of groundwater salinity. It is anticipated that the study has valuable implication to sustainable and effective planning of groundwater development and management by reducing the uncertainty of understanding the hydrogeological system and by giving the dynamic groundwater resource or basin recharge rate. It can also be used as a reference for hydrogeological studies that will be conducted in similar hydrogeological setting.

1.4. Objectives

The present research is designed with the aim to better understand the hydrogeological system of the basin and estimate recharge rate to unravel and resolve the controversial issues mentioned in Section 1.3, and to determine the origin of groundwater salinity. The output of the study will aid to improve sustainable and effective groundwater provision and management in the area.

Specifically the followings are the main objectives of the research.

- Understand nature of aquifers and the aquifer systems present and their interaction, and characterize aquifers
- Understand and analyze the groundwater flow regimes, evolution and origin of the ground waters of each aquifer system
- Determine groundwater recharge rate over the basin
- Determine the groundwater discharge
- Understand the recharge and discharge processes of aquifers and aquifer systems
- Evaluate the inter basin groundwater outflow rate and identify outflow areas
- Estimate groundwater inflow to and outflow (leakage rate) from Tana Lake, and trace leakage area

- Understand the groundwater and surface waters (Tana Lake, reservoirs and streams) interactions
- Origin of ground waters salinity
- Origin of wetlands

1.5. Approach and Methodology

Tana basin has complex and diversified geological formations, tectonic structures and evolution of the basin, relief features and hydrogeological conditions. Application of a single method in such environment could not properly address the actual field conditions. Hydrogeology of this complex system can be more explored through application and integration of multiple disciplines. Geomorphic, geological, hydrogeological, hydrogeochemical and environmental isotopes investigations have been done in this study. The results from each data set have been synchronized and integrated to describe and understand the hydrogeological system of the study area and recharge rate. The research works have been accomplished in three phases: Desk Works, Field Works and Post Field Works.

A. Desk (pre-field) Works

The following works have been done during the desk study.

- Acquire and review literatures, available soil, land use/land cover, geological, hydrogeological reports and data
- Collect and interpret new boreholes and pumping test data from different offices
- Acquire and process meteorological and hydrological data
- Purchase and interpret topographic maps
- Interpret satellite imagery and SRTM data
- Structural analysis
- Prepare preliminary geological and hydrogeological maps
- Identify research gaps, develop hypothesis, methodology and plan the field works

The preliminary geological base map has been compiled from four different geological map sheets. Satellite imagery interpretation has been done to verify and modify the map and to map structures. Then, the data gap has been identified. Field geological traverses and observation points have been planned to fulfill the gap and make the geological and structural map.

The hydraulic characters of existing aquifers have been judged from the existing literatures, borehole lithological logs and pumping test data. Existing groundwater points have been overlaid in the preliminary geological base map and the previously sampled sites identified. Present sampling sites were selected from some previously sampled sites where it is essential and from new water points.

B. Field Works

Geological and structural mapping, hydrogeological characterization and groundwater points' inventory, and sampling from groundwater and surface waters have been conducted during this phase.

Geological and structural mapping

Geological and structural mapping have been done based on DEM (SRTM) data, land sat imagery interpretation and field traverses and observations. Eleven rock samples have been collected from different units and petrography analysis was done.

Hydrogeological characterization

Field hydraulic properties of each hydrogeologic unit such as fracturing and texture of sediments have been studied. Additional borehole geological logs and pumping test data have been collected from different offices, which helped to aquifers characterization. Springs and some available open hand dug wells have been inventoried. Boreholes are caped and pumps are installed to make inventory.

Water sampling

For better representation of hydrogeologic units, surface waters and to cover the anticipated groundwater outflow areas, 110, 112 and 70 water samples have been collected from the groundwater and surface waters, which are for chemistry, ^{2}H &

^{18}O and tritium analysis, respectively. All samples for chemistry and stable isotopes (^{2}H & ^{18}O) and 51 samples for tritium have been analyzed.

Cold fresh, brackish and cold salty ground waters and thermal fresh ground waters have been sampled from springs, hand dug wells, boreholes and deep test wells (301 to 500 m) in the Tana basin, and from possible basin groundwater outflow and Tana Lake leakage areas.

Tana Lake was sampled from the shores and at the center. Inflow rivers to the Tana Lake, reservoirs and Abay River at the Tana Lake surface outflow area have also been sampled.

Precipitation sampling

Rainfall sampling sites have been selected at 5 meteorological stations with marked difference in altitude, and which are located at the different parts of the basin and the surrounding area. These stations are Gonder, Gassay, Bahir Dar, Gish Abay or Sekela and Gilgel Beles that is outside the Tana basin. Rainfall was collected daily from each station and stored into Jericans, which were kept in cool and dark room. Samples have been taken monthly for ^{2}H & ^{18}O (32 samples) and chemical (9 samples) analysis. Rainfall sampling was done during the wet season starting from April until October, 2012. All samples have been analyzed.

Field measurement

Electric conductivity, pH and temperature have been measured at the site. Furthermore, discharge of springs and depths to static water level have been measured in some open hand dug wells.

C. Post Field Works

Laboratory analysis

Water samples for chemical analysis have been analyzed at the Geological Survey laboratory for complete chemical analysis and Bromide. Isotope samples for deuterium and oxygen-18 and tritium have been analyzed at the Isotope Hydrology Laboratory of the School of Earth Sciences, Addis Ababa University.

Data processing and interpretation

The data attained from desk and field studies together with laboratory results have been processed, interpreted, analyzed and integrated during this phase to achieve the research goals The following major works have been accomplished.

- **Geology**

  The geological and structural map of Tana basin has been finalized.

- **Hydrogeology**

  The following works have been done.

  - Estimation of hydraulic parameters (transsmissivity, specific capacity and yield) of hydrogeological units making use of boreholes and pumping test data
  - Analysis of structural data to understand their implications to leakage outflow and on the groundwater potential of the aquifers.
  - Classification of hydrostratigraphic units; aquifers were evaluated and ranked according to their potential and hydrogeological map has been prepared
  - The upper, intermediate and lower aquifer systems and the aquifer types, and set of aquifers and their lateral extensions in the upper aquifer system have been ascertained and characterized using hydrogeological, hydrogeochemical and isotopic data
  - Groundwater flow regime of these aquifer systems and recharge and discharge conditions as well as their interaction have been ascertained

- **Basin water balance evaluation**

  Water balance of the Tana basin has been done and the presence of inter basin groundwater outflow has been ascertained and estimated.

- **Evaluation of recharge rate**

  Land cover, soil map, hydrometeorological elements and environmental tracer (Cl) data have been used to assess the groundwater recharge in the basin. Recharge rate has been estimated using baseflow separation approach, soil water balance and chloride mass balance methods.

- **Hydrological and chemical mass balance of Lake Tana**

  Leakage rate from the lake and groundwater inflow condition to the lake have been assessed and quantified by integrating the hydrological and chemical mass balances of the lake.

- **Hydrogeochemistry**
  - Accuracy of laboratory analysis has been evaluated
  - Evaluation of hydrochemical parameters and major ions, and their statistical and spatial variation in the basin have been done
  - Multivariate analysis (Hierarchical Cluster Analysis and Principal Component Analysis) have been done to classify ground waters into objective groups that are related with geography and geology, and hydrochemical facies were determined
  - Different plots and inverse hydrogeochemical modeling have been done to determine sources of groundwater salinity, evolution and mass transfer when the initial groundwater evolves to final groundwater
  - Hydrogeochemical results helped to verify, characterize and analyze aquifer system and aquifers present in the area, flow regime of the aquifer systems, to identify inter basin groundwater outflow areas from the basin, and to determine origin of groundwater salinity and mass transfer, origin of wetland, and interaction between groundwater and surface waters (Tana Lake, reservoirs and rivers).

- **Isotope hydrology**
  - Different plots for deuterium, oxygen-18 and tritium have been prepared and interpretation was done to verify leakage outflow areas from Tana Lake, and to analyze aquifer systems and aquifers and their recharge processes and mechanism, area and time. Isotopic data also helped to determine ground waters age, mixing or interaction and ground waters flow regime, discharge processes and identify paleo groundwater, and to determine origin of wetland and groundwater- surface waters interactions.

Results from the different disciplines have been synchronized and integrated to give the research out puts. Details of the methodologies have been further discussed under their respective chapters and sections. Methodology and work flow is outlined in Figure1.1.

1.6. Materials and Tools

Water samples were collected in new and clean and dry standard double caped polyethylene bottles. Different analytical methods have been used to analyze the different ions. Na^+, K^+, Ca^{2+} and Mg^{2+} have been analyzed by atomic absorption method. HCO_3^-, CO_3^{2-} and Cl^- were analyzed by titration method while SiO_2 and SO_4^{2-} were measured using UV spectrophotometer, and Br^- and F^- by electrode method.

The waters were analyzed for $\delta^{18}O$ and δ^2H using LGR laser isotope analyzer (DCT-100). The uncertainties are ±0.2 and ±2 ‰ for $\delta^{18}O$ and δ^2H, respectively. The results are given as permil (‰) deviations from the internationally accepted standard V-SMOW. Water samples for tritium were analyzed using Packard Liquid Scintillation Analyzer (TRI-CARB 3170TR/SL) after distillation and enrichment processes. The uncertainty with the measured tritium data is ±0.5 TU. The results are given in tritium unit (TU).

Various soft wares were employed to assist the processing, interpretation and mapping of the data sets. ArcGIS 9.3 (www.esri.com), ENVI 4.7 (www.ittvis.com), Global Mapper version 11 (www.globalmapper.com), Surfer 10 (www.goldensoftware.com), AutoCAD 2009 (http://www.autodesk.com) and Micro soft excel were used for quarrying, mapping and analyzing the spatial and temporal data.

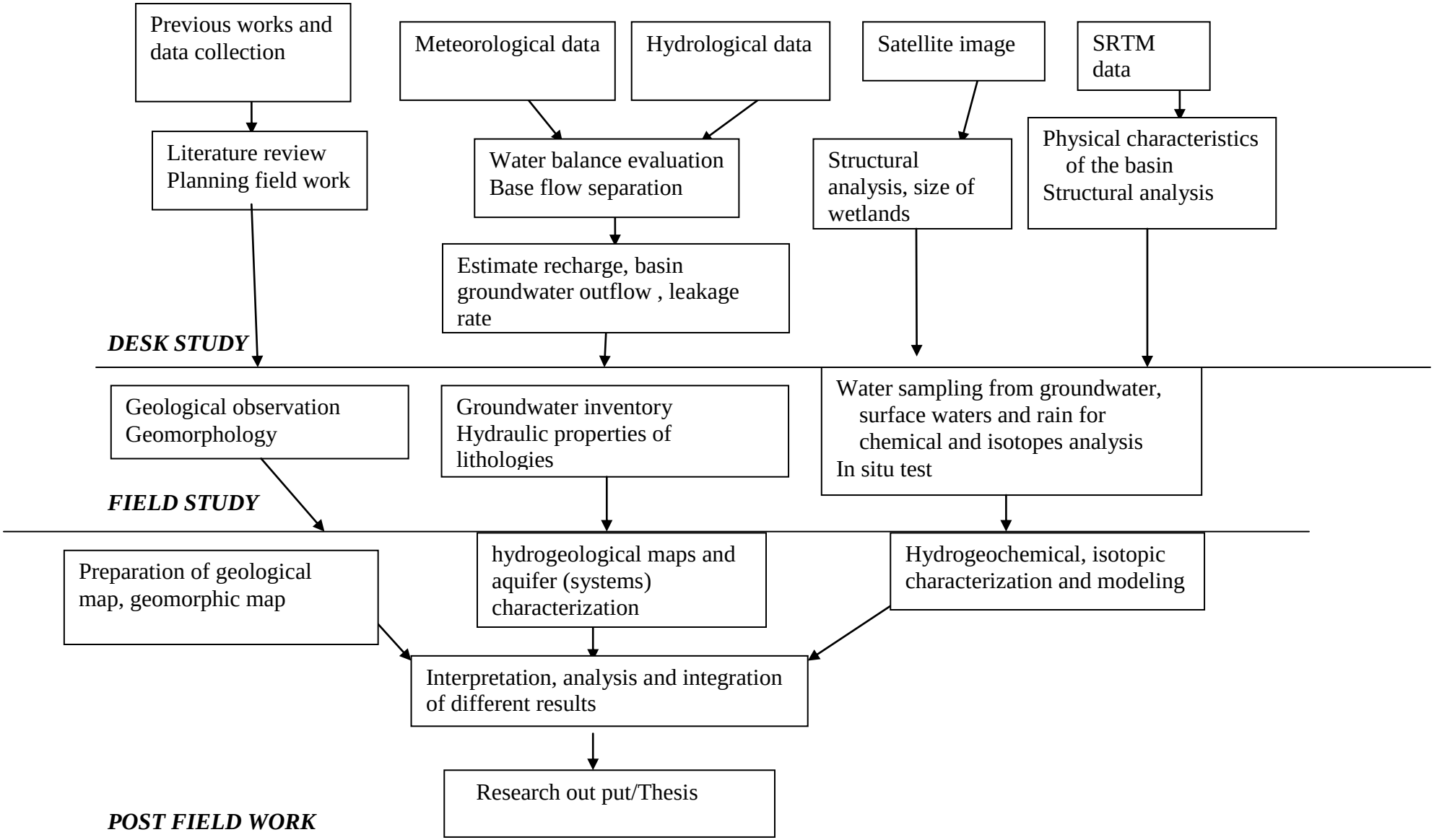

Figure 1.1. Out line of the research methodology.

Hydrochemical data have been processed and interpreted using Aquachem version 4.0.284 (http://www.waterloohydrogeologic.com), STATISTICA version 8 (Stat Soft Inc.2008), PhreeqC version 2.8.0.0 (USGS, 2003), and Micro soft excel soft wares. River Analysis Package version 3.0.3.0 software (Marsh et al., 2003) was used for baseflow separation and Cropwat (FAO, 2009) software was used to estimate the reference potential evapotranspiration. Aquifer Test Pro version 4.2.0.2 (www.swstechnology.com) has also been used for pumping test data analysis.

1.7. Limitation

Scarcity of drilled boreholes in some parts of the area, scarcity of borehole depth and pumping test data, and lack of sufficient number of deep boreholes penetrating the whole depth of the stratified multy layers volcanic aquifer systems are the major encountered limitations.

1.8. Structure of the Thesis

The thesis is structured into 12 chapters. Chapter one deals with general introductions. It includes detailed overview and description about the background to the study, previous studies, main problems or research rationale and relevance, objectives, approaches and methodologies and materials and tools. Chapter two consists of description of the study area. Location and description of the physical features such as topography, soil and land covers are given. Regional geology and the geology of the area including the stratigraphy, lithology and structures are treated in Chapter three.

Chapter four consists of description and analysis of hydrometeorological data. Climate and estimation of the various meteorological elements such as basin precipitation, reference potential evapotraspiration, actual evapotranspiration, mean precipitation over the lake and open water evaporation have been dealt. Moreover, surface waters such as rivers, reservoirs, wet land and Tana Lake, and baseflow separation from river hydrographs have been treated in this Chapter.

In Chapter 5, the hydrogeology of the area is discussed. Grouping of lithostratigraphic units into hydrostratigraphic aquifers and confining units, and characterization and ranking of aquifers have been done here. Groundwater flow systems recharge and discharge conditions of aquifers and aquifer systems are described in detail in this chapter.

Evaluation of groundwater recharge rate based on baseflow analysis, soil water balance and chloride mass balance methods is addressed in Chapter six. Basin water balance evaluation is given in Chapter 7. Inter basin groundwater outflow rate from Tana basin has been estimated under this chapter. Hydrological and chemical mass balances of the Tana Lake are dealt in Chapter 8. Groundwater inflow to, and leakage rate from the lake have been estimated in this chapter.

Chapter nine deals with the subject of hydrogeochemistry. Evaluation of accuracy of laboratory analysis, evaluation of hydrochemical parameters and ions, multivariate (HCA and PCA) analysis and hydrochemical facies, origin of groundwater salinity, hydrogeochamical evolution and inverse hydrogeochemical modeling are included in this chapter. Detail description are given on the implication of the results to the aquifers/aquifer systems and groundwater flow systems analysis, identifying inter basin groundwater outflow area, interaction between groundwater and surface waters, and on the sources of ground waters salinity.

Environmental isotopes hydrology is given in Chapter 10. Stable isotopes of deuterium and oxygen-18 and tritium are discussed in detail here. Implications of isotopic results for aquifers/aquifer systems and groundwater flow systems analysis, tracing of Tana Lake leakage path, interaction between aquifers, and groundwater and surface waters interactions are discussed in detail.

Results of the different disciplines treated in each chapter have been integrated, synthesized and analyzed in Chapter 11 so as to meat and realize the research goals and objectives.

The thesis ends with conclusions and concrete clues (Chapter 12), which have implications for the forthcoming groundwater development and management undertakings in the area.

2. DESCREPTION OF THE AREA

2.1. Location

Tana basin is located within UTM zone 37, between 252788 and 396487 m E longitude, and 1218577 and 1410176 m N latitude (Fig. 2.1). The basin has a total area of 14 845.5 km^2, of which Tana Lake occupies 3 057.4 km^2. The Seasonal and perennial wetlands have area of 382.1 and 11.9 km^2, respectively.

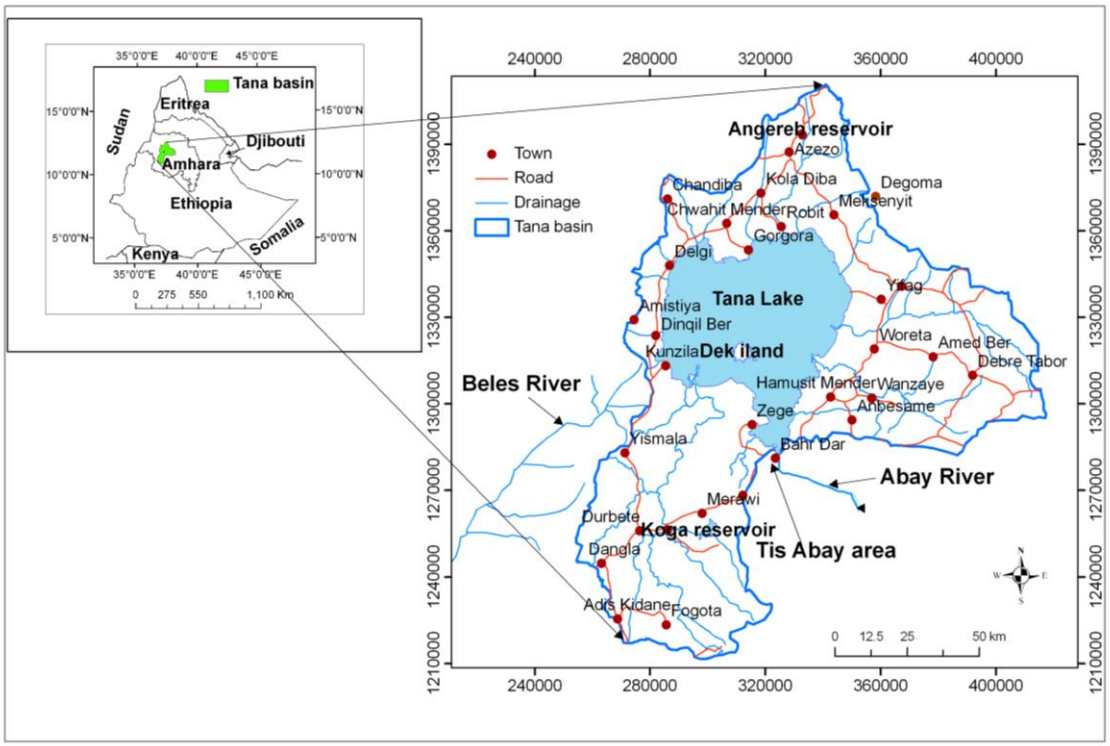

Figure 2.1. Location map.

2.2. Topography

Tana basin can be divided into different physiographic regions. These include plateau top, rugged mountainous volcanic terrain, escarpment, low relief terrain in Quaternary volcanic rocks and sediments and flat and gentle plains covered with lacustrine sediments (Fig.2.2).

Topographic slope generally decreases towards the Tana Lake from all sides. The minimum and maximum elevations are 1679 and 4089 m, respectively. Figure 2.3 shows spatial variation of surface elevations.

2.3. Soil and Land Cover

2.3.1. Soil

Soils existing in Tana basin have been classified by FAO (1997), and further have been described in detail by BCEOM (1999) and SMEC (2007) on the basis of cation exchange capacity, base saturation percentage, color, soil horizons developed, land form/slope and chemistry, which are summarized as given below (Fig. 2.4). The following soil types can be identified in the basin.

Chromic Luvisols

It is dark brown over yellowish brown clay, moderately to well drained and deep to very deep. It covers an area of 2 255 km^2 (19.3% of the basin).

Eutric Cambisols

It is moderately to deep and well drained silty clay soil. It covers 10 km^2 areas, which is 0.08% of the area.

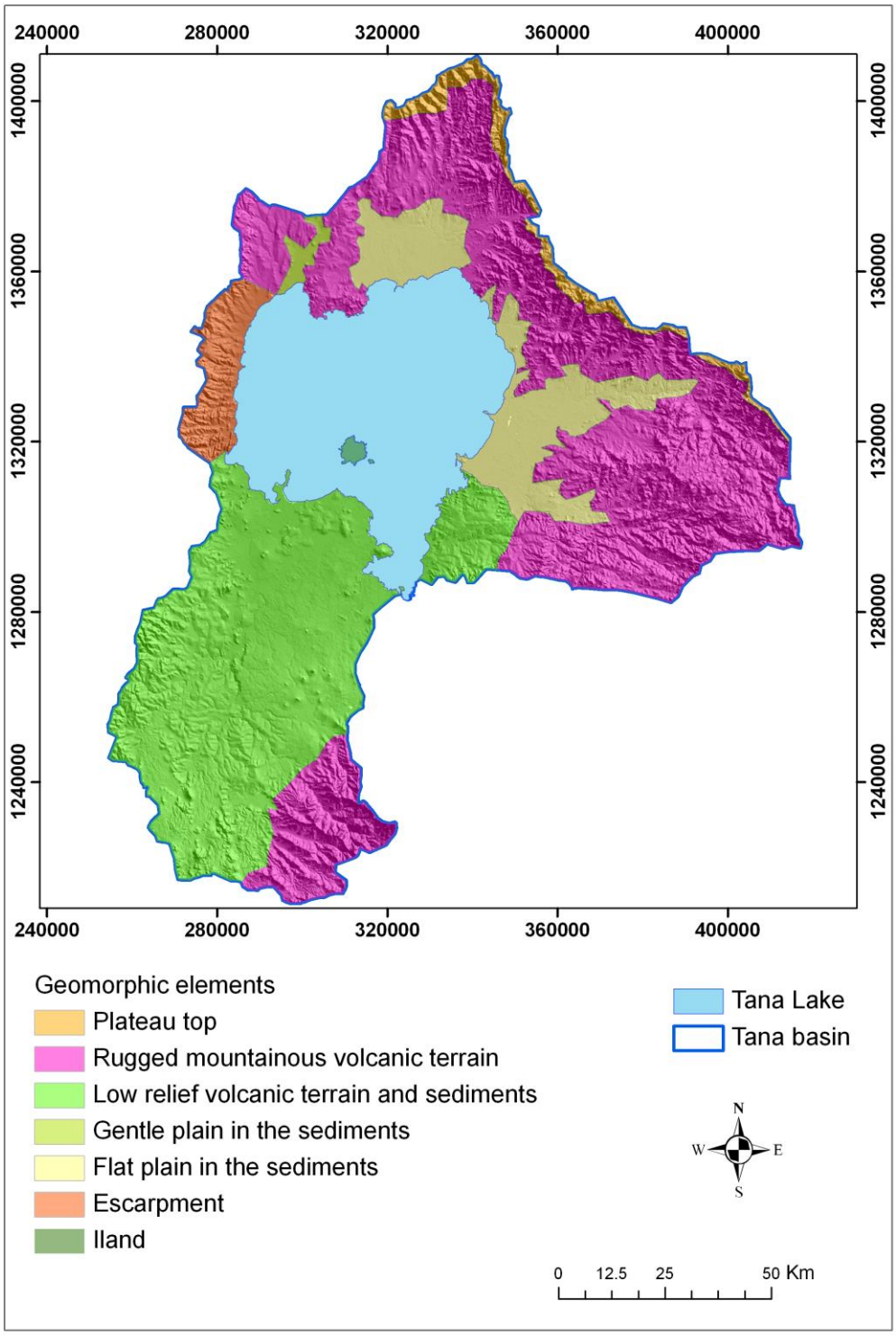

Figure 2.2. Physiographic regions in the Tana basin.

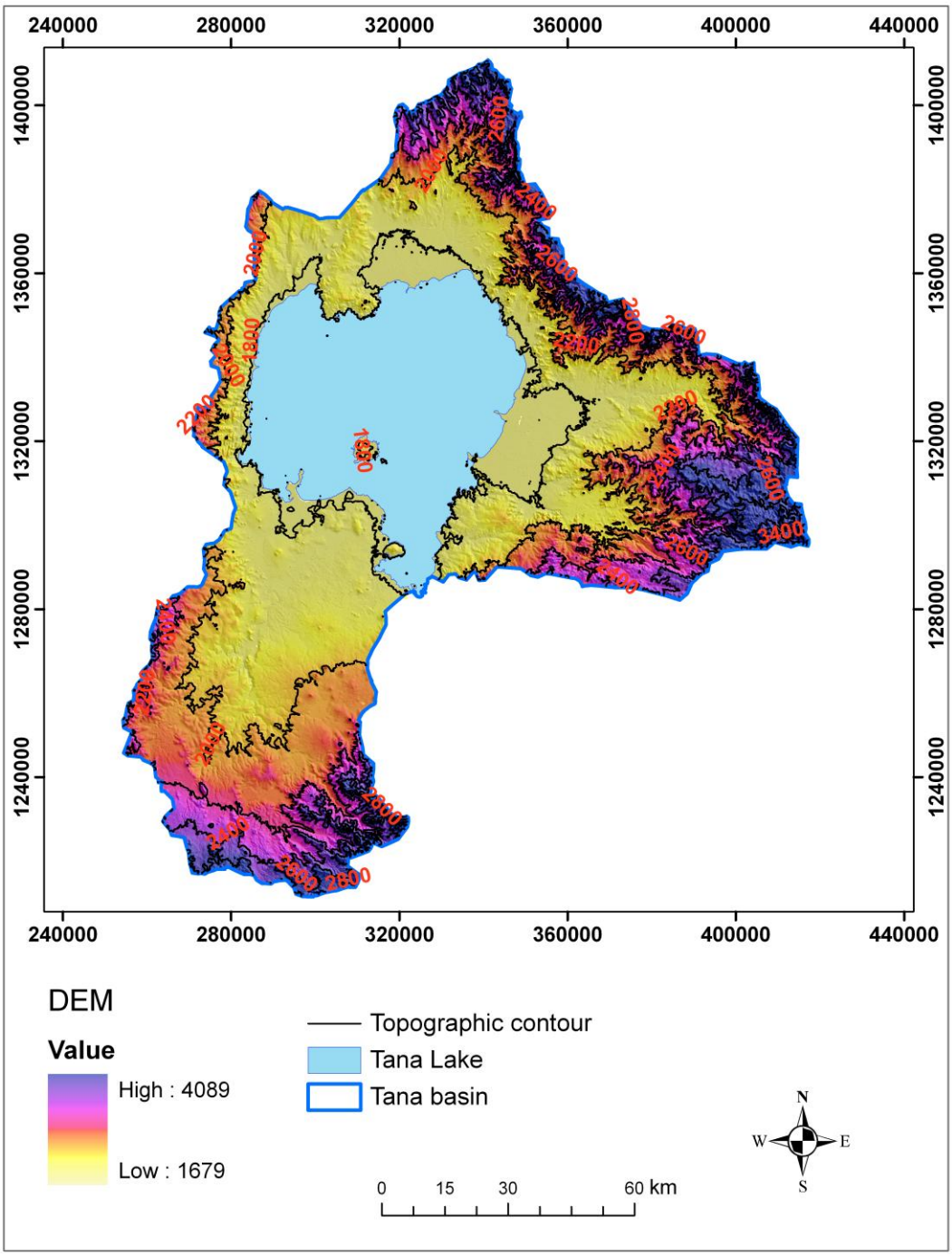

Figure 2.3. Topographic elevation map (meter).

Eutric Fluvisols

It is dark olive brown over black clay, moderately well to imperfectly drained, very deep, firm to friable when moist, and sticky and plastic when wet. It is clay loam. It covers 1477 km^2 area (12.7% of the area).

Eutric Leptosols

This soil is dark brown clay, excessively drained, hard when dry, firm to friable when moist and sticky and plastic when wet. It covers an area of 1 800 km^2 (15.4% of the area).

Eutric Regosols

It is excessively drained, shallow and dark brown clays. It is slightly hard when dry, friable when moist, and sticky and plastic when wet. It occupies 39 km^2 areas (0.34% of the area).

Eutric Vertisols

It is very deep, imperfectly to poorly drained, very dark grey to reddish brown clay. It has an area of 1 724 km^2 (14.8% of the area).

Haplic Alisols

It is reddish brown, well drained, deep to very deep clay. It covers 711 km^2 area or 6.1% of the area.

Haplic Luvisols

This soil is well drained silty clay to clay (SMEC, 2007). It covers 3 008 km^2 area (25.8% of the area).

Haplic Nitisols

It is moderately well drained silty clay to clay soil (SMEC, 2007), which occupies 191 km^2 area (1.6% of the area).

Lithic Leptosls

It is moderately deep to deep clay loam. It occupies 457 km^2 areas (3.9% of the area).

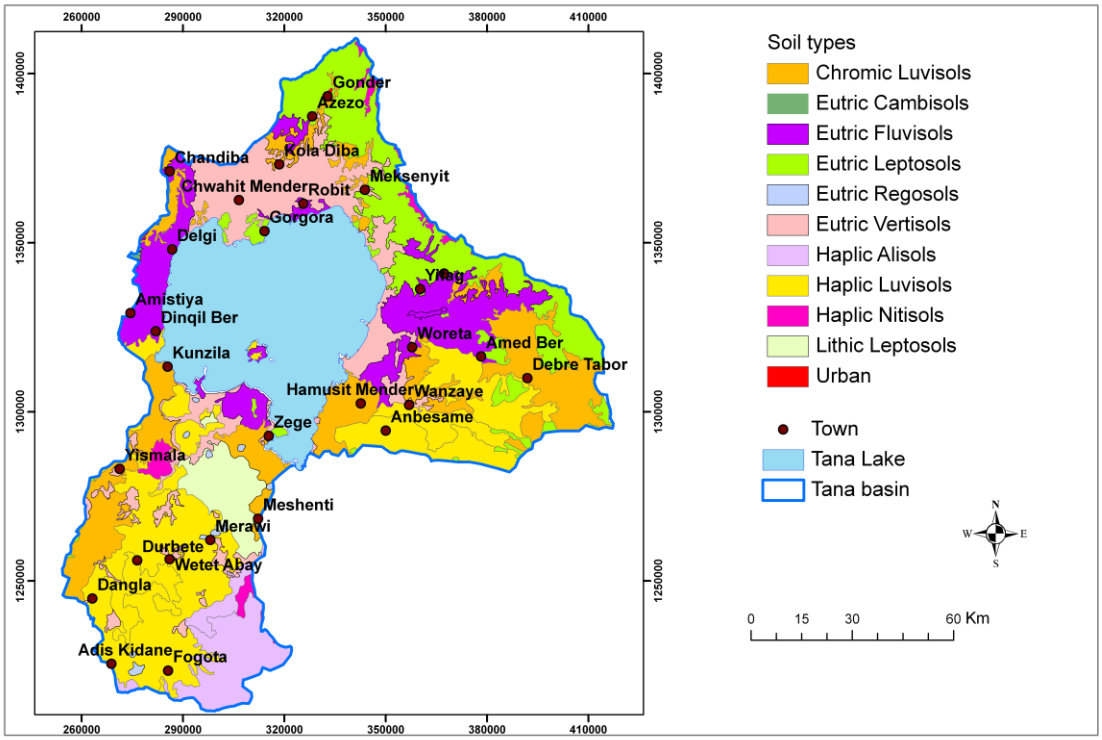

Figure 2.4. Soil map.

2.3.2. Land cover

Tana basin has the following land covers (After FAO, 1997). Table 2.1 and Figure 2.5 show land covers of the basin.

Table 2.1. Land covers of Tana basin.

Land cover	Area (km^2)	Percent of the area
Afro-Alpine heath vegetation	33.1	0. 3
Bush, shrub and grass land	1486.4	12.6

Cultivated land	9912.1	83.8
Perennial swamp	11.9	0.1
Seasonal marsh	382.1	3.2

3. GEOLOGY

3.1. Regional Geology

The Ethiopian flood basalts and associated felsic pyroclastic rocks (Ethiopian Trap Basalts) are continental volcanic rocks that erupted before the onset of continental rifting and sea-floor spreading in the Afar, which is believed to be associated with the Afar plume activity. The bulk of these volcanics erupted mainly around 30 Ma ago during a relatively short, <5 Myr period (Fig.3.1) (Berhe et al., 1987; Hofmann et al., 1997; Kieffer et al., 2004). Following this peak of fissural activity, large shield volcanoes developed on the surface of the volcanic plateau. In many cases the shield volcanism was comagmatic with the flood volcanism that formed the main volcanic plateau (Keiffer et al., 2004).

The entire plateau volcanic sequence is sub-divided into the following formations: Ashangi basalts, Aiba basalts, Alaji basalts/ rhyolites and Tarmaber basalts, from the oldest to the youngest. According to a number of previous studies, e.g. Zanettin et al. (1974), Mengesha Tefera et al (1996) and Tesfaye Chernet (1993), these formations have the following characteristics.

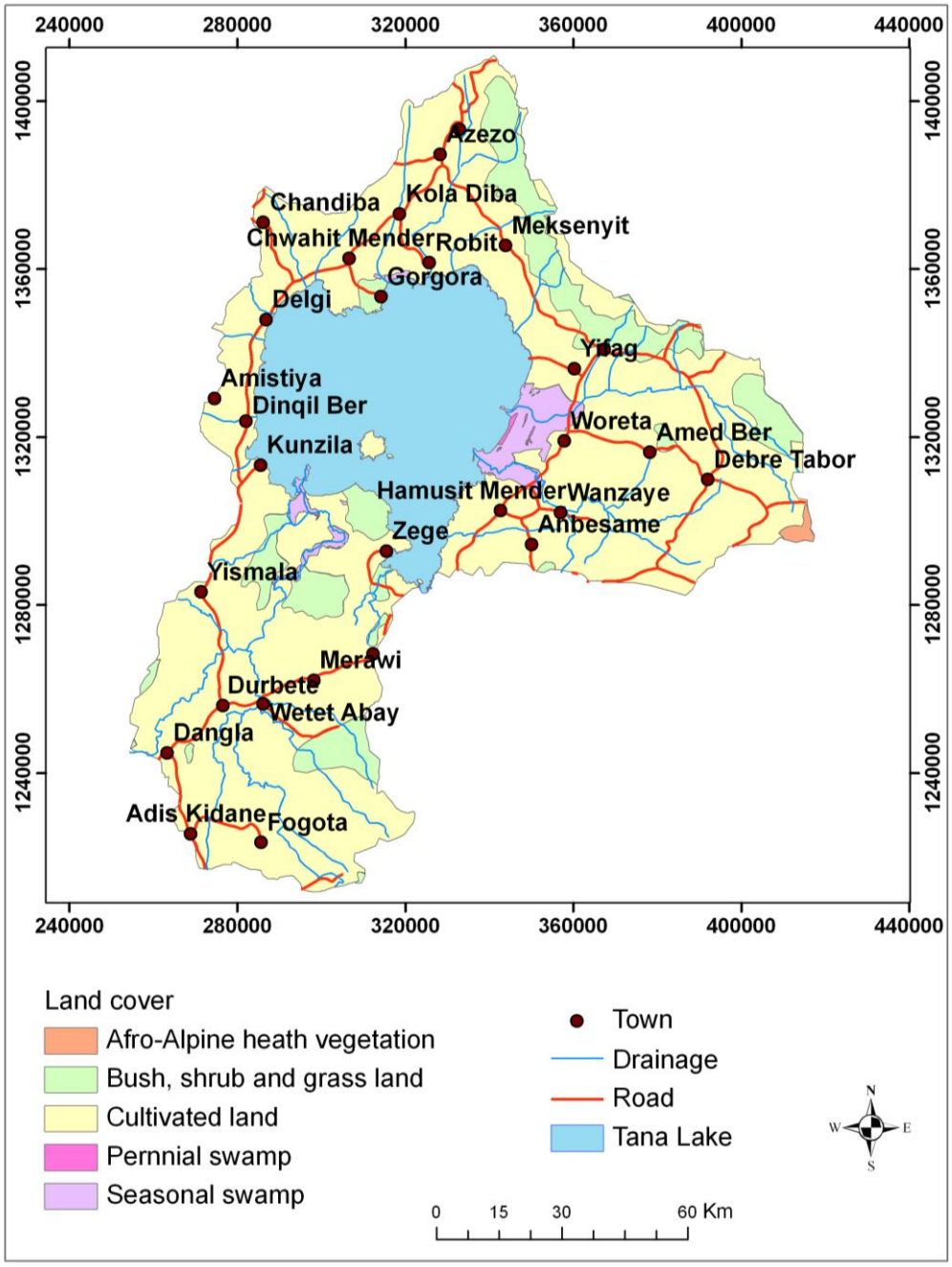

Figure 2.5. Land cover map.

Ashani Basalt Formation

The Ashangi Formation constitutes the lower sequence unconformably lying on the Mesozoic marine sediments. It is characterized by thin lava flows, (< 10 m) forming

relatively smooth or less steep topography. The Ashangi basalt sequence, on the western half of the northern Ethiopian plateau (e.g. Lima Limo section), is flat-lying and undeformed. On the other hand, there is observational evidence for minor faulting and tilting within the Ashangi basaltic pile north of the Wereta-Woldia road and east of upper Tekezze River suggesting that deformation of the flood basalts occurred during their emplacement. This formation is essentially made up of a series of extensive basalt flows, and at places with minor interbeds of acidic layers (rhyolitic pyroclastics). The basalts are commonly aphyric and strongly weathered. Intercalations of tuff and paleosols are also found. The total thickness of Ashangi basalts is estimated to be 200 to 1200 m (Tesfaye Cherenet, 1993). The basalt sequence is commonly injected by dolorite sills and dykes.

The Ashangi Basalt cycle is distinct from those of Aiba, Alaji and Tarmaber. The stratigraphic reconstruction of the terrains is often difficult by the bad stage of preservation of the rocks themselves. In the absence of evident unconformities, the distinction between Ashangi basalts and Aiba basalts is based on the fact that the former is more intensively weathered and at places faulted and tilted, while the latter can be found in clearly fresh, compact, continuous and unbroken flows (Zanettin et al., 1974).

Aiba Basalt Formation

Aiba Formation constitutes the second pulse of fissural basalt volcanism. This sequence is composed of thicker basalt flows (10-50 m) that characteristically form steep topographic cliffs. This sequence sometimes contains minor amounts of felsic products with variable thicknesses. The basalts flows are extensive, flat-lying, layered and generally aphyric. The overall thickness of this sequence on average is 200m and the maximum is 600m (Tesfaye Chernet, 1993)). Aiba basalts unconformabley overlie the tilted Ashangi basalts in the eastern portion of the north-eastern plateau.

Alaji Basalt/Rhyolite Formation

The Alaji Formation lies directly over the Aiba basalts without a major unconformity. This formation essentially constitutes a thick series of felsic rocks made up of pyroclastic

flow (welded and un-welded ignimbrites) and fall deposits (welded and un-welded ash/ tuff deposits). The Alaji rhyolites are absent on the western portion of the north-western plateau (e.g. Lima Limo area) and are quite thick on the eastern sector of the plateau nearer the Afar and Ethiopian Rift margins reaching an overall measured thicknesses of ~500m. This implies that major magmatic centers (e.g. stratovolcanoes) had developed by 29 Ma and the collapse of these volcanic structures produced calderas, fuelled Plinian to Ultraplinian eruptions.

In some woks and reports (e.g. Mengesha Tefera et al., 1996), the Alaji Formation has been described to include aphyric basalt flows together with felsic pyroclastics. In this case the basalts are indistinguishable from the underlying Aiba basalts in the field.

Tarmaber Basalt Formation

Superimposed on the Alaji rhyolitic pyroclastics and flood lavas, locally thick sequences of basalt flows have been outpoured, during mid-Miocene, from low-angled shield volcanoes that have built prominent land features such as the Simien, Meghezez and Choke-Menghistu and Guna volcanic massifs. The shield volcanic formation contains sequences of alternating basalts, rhyolitic and trachytic lava flows, tuff and ignimbrite, particularly near the summits (Keffer et al, 2004). The formation is commonly cut by a network of mafic and felsic dyke swarms. Tarmaber basalt flows are thinner and less continuous than the underlying Ashanghi and Aiba flood basalts. Tarmaber basalts are heterogeneous but characteristically more porphyritic, containing abundant and often large phenocrysts of plagioclase, pyroxene and olivine. After shield volcanic activity, subsequent volcanism was largely confined to regions of rifting (Keffer et al, 2004).

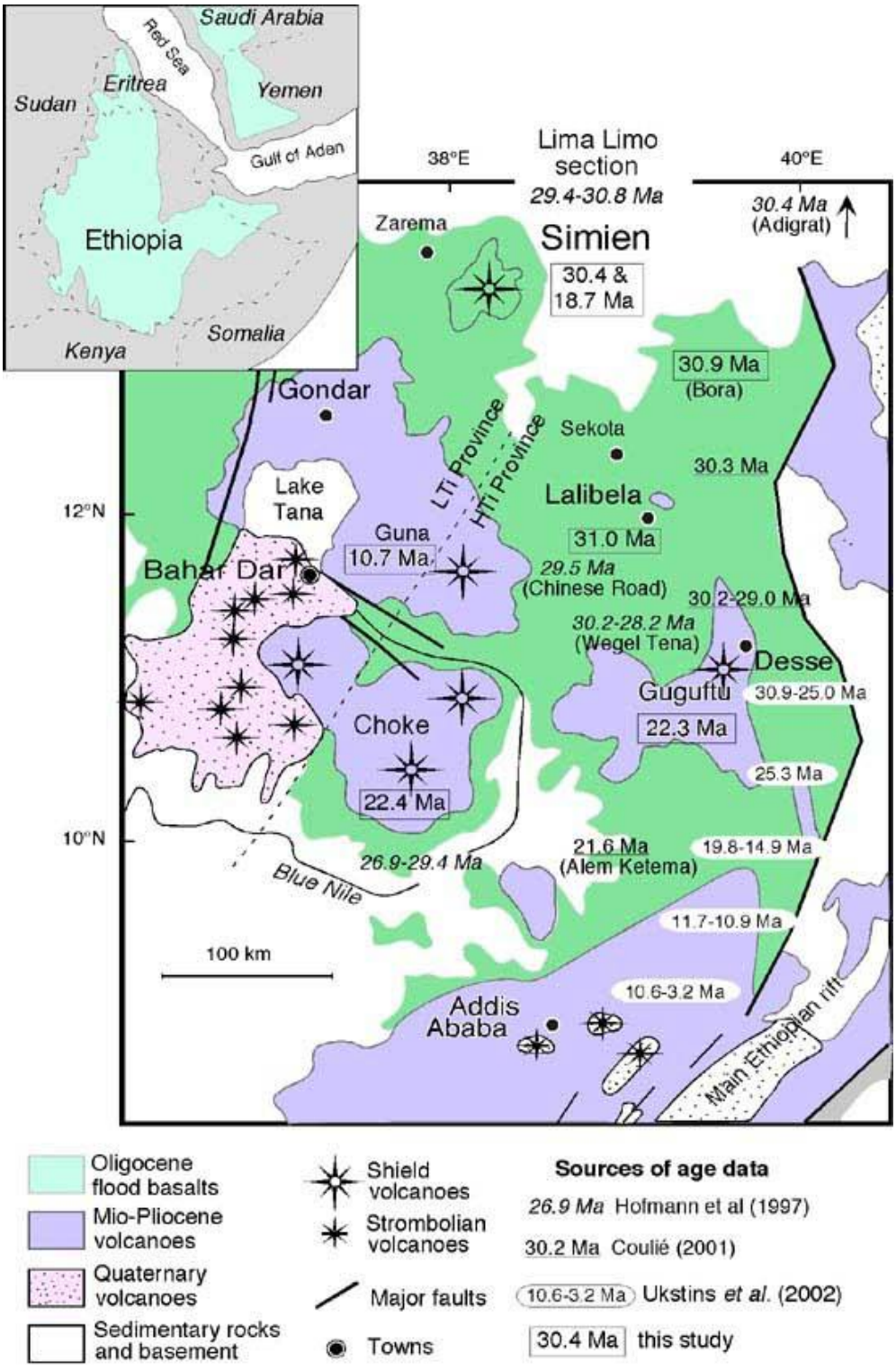

Figure 3.1. Geological map of the northern Ethiopian plateau (Keiffer et al., 2004).

3.2. Geology of the Tana Basin

3.2.1. Lithologic units and stratigraphy

3.2.1.1. Stratigraphy

Previous regional studies have described the geology of the Tana basin as consisting of Tarmaber Basalt Formation, Quaternary basalts and lacustrine sediments only. Recently, the Geological Survey of Ethiopia has published four different map sheets (Workeneh Haro et al., 2010; 2011; Dejene Hailemaryam et al., 2012 and Efrem Beshawered et al., 2010) in which the Tana basin includes volcanic rock units belonging to the Ashangi, Aiba, Alaji and Tarmaber formations. Trachyte flows and plugs in the eastern area have been reported to be part of Tarmaber Formation (Workeneh Haro et al., 2010). On the other hand, trachyte flow in the Gorgora (northern) area has been mapped as lavas of Quaternary age (Workeneh Haro et al., 2011). Quaternary basalt and lacustrine sediments have also been mapped by these authors in the basin.

In the present study, the geology of the Tana basin was first synthesized in a simplified form from the four map sheets published by the Geological Survey of Ethiopia. This was followed by geological and tectonic interpretation of satellite images. In a subsequent study field work was undertaken to further verify, identify and describe the lithological units and tectonic structures. Observations of contacts between lithologic units and structural measurements have been made during the field work. Eleven representative rock samples have been taken from different exposures for further laboratory investigations.

On the basis of the geological maps published by the Geological Survey of Ethiopia, field observations and laboratory petrographic studies of representative samples, the lithologic units exposed in the study area have been grouped as follows:

1. Middle Basalt: (Aiba Basalt Formation)
2. Upper Basalt: (Alaji Basalt/Rhyolite Formation)
3. Degoma Basalt, Sekela Basalt, Guna volcanics (Guna Tuff, Guna Basalt, Guna Phonolite), Trachyte flows and plugs: (Tarmaber Basalt Formation)

4. Quaternary basalts and rhyolites: Tana Basalts
5. Quaternary lacustrine sediments.

Lithological logs from boreholes drilled in the northern area revealed presence of Lower Basalt (Ashangi Formation) underlying the Middle Basalt. The stratigraphic relationships between the various lithologic units exposed in the eastern, northern and southern sectors of the Tana basin together with their correlations are shown in Figure 3.2.

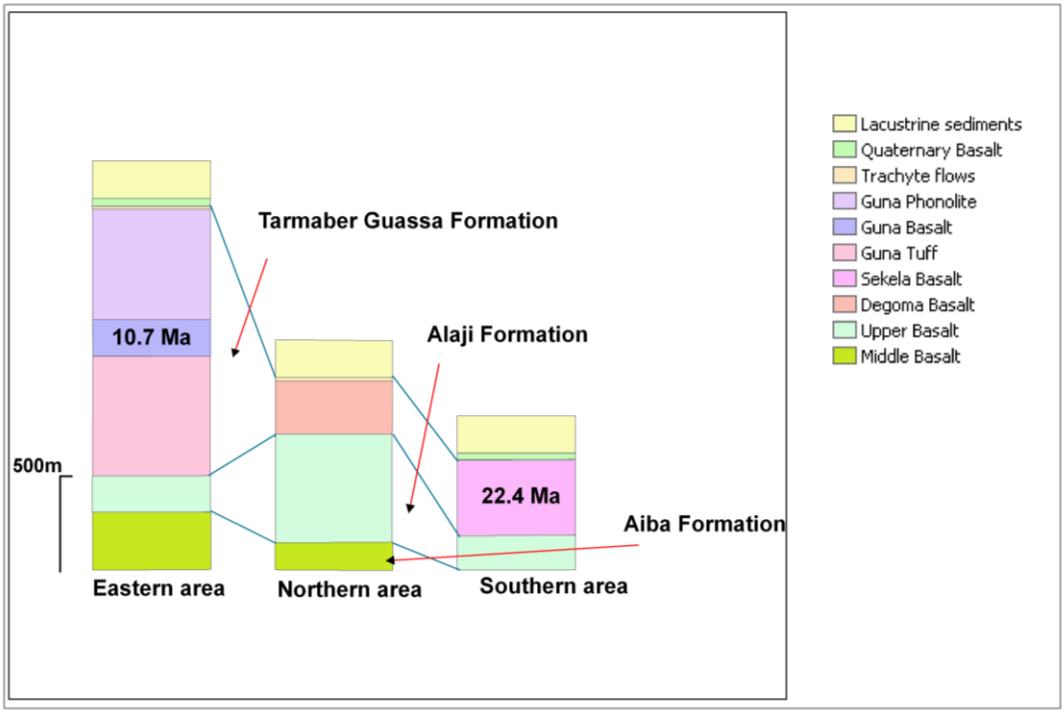

Figure 3.2. Conceptual stratigraphic relationships between lithologic units exposed in different sectors of the study area and their possible correlations.

A final geological sketch map of Tana basin produced from the compilation of existing geological maps, interpretation of satellite images and field investigations is shown in Figure 3.3. The map shows the mappable lithologic units together with major tectonic

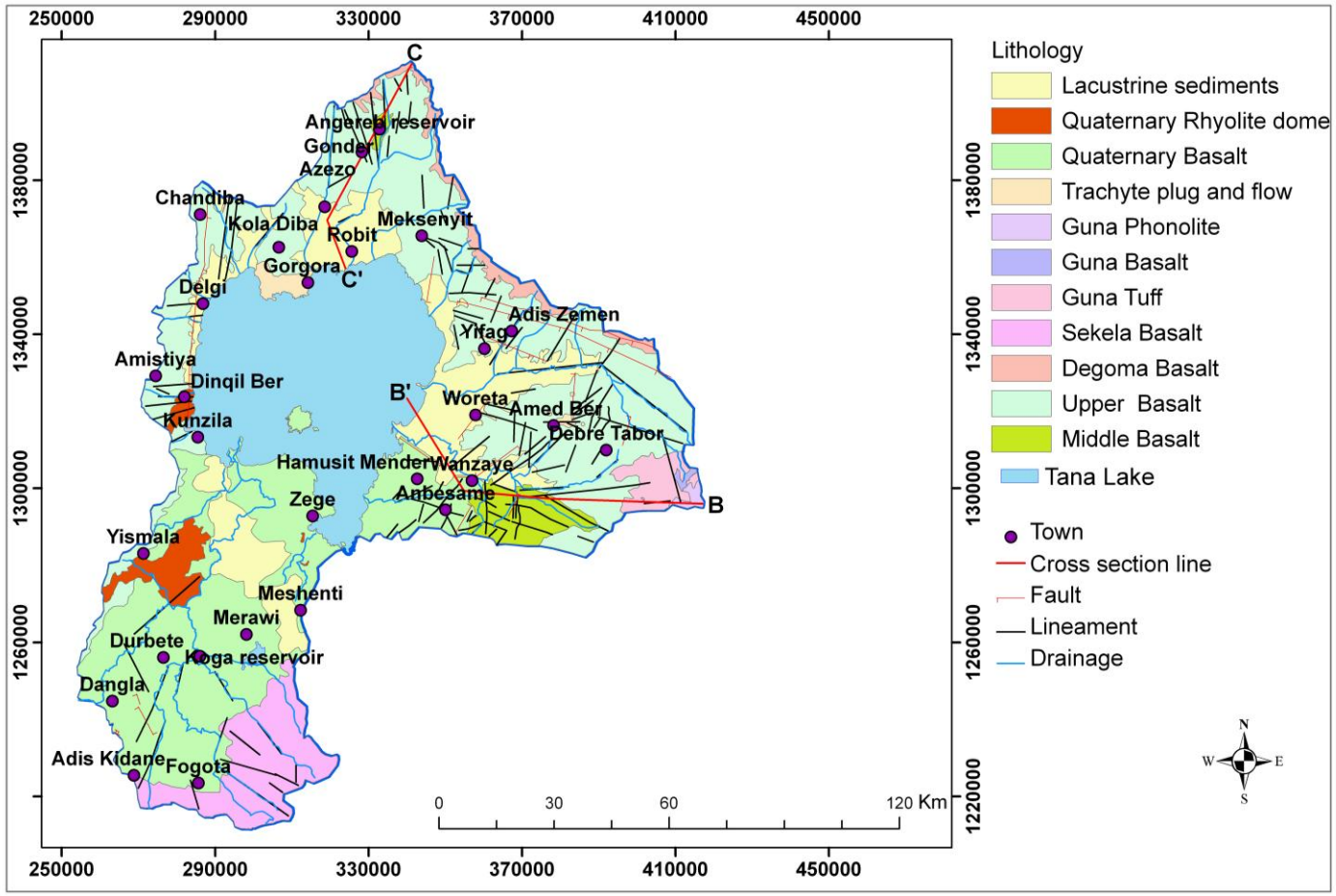

Figure 3.3. Geological sketch map and tectonic structures (Compiled and modified from Workeneh Haro et al., 2010; 2011; Dejene Hailemaryam et al., 2012 and Efrem Beshawered et al., 2010).

structures affecting the study area. Representative geological cross-sections along selected transects are shown in Figures 3.4, and 3.5.

The oldest lithology exposed in the area is Lower Basalt or the Ashangi Basalts in a locality near but outside the study area (Workineh Haro et al., 2010; 2011 and Dejene Hilemaryam et al., 2012) as well as in boreholes drilled within the Tana basin. These basalt flows are overlain by the Middle Basalt Unit, which is correlated with Aiba Basalt Formation by the above authors. The name Middle Basalt Unit is adopted in this study. The basalt flows are thinly layered (7-10m), dense and compact, resistant to erosion at places and form isolated hills. This unit covers a wide area laterally indicating fissural eruption.

The Middle Basalt Unit is overlain by another series of basalt flows, termed as Upper Basalt Unit with paleosol of 0.5m thick in between. Workineh Haro et al. (2010 & 2011) and Dejene Hilemaryam et al. (2012) correlated the Upper Basalt Unit to Alaji Basalt/ Rhyolite Formation. The unit consists of ignimbrite and pyroclastic deposits of up to more than 100 m thickness in its upper part. It laterally covers wide areas.

The Alaji Basalt in the north and north-eastern parts of the study area is directly overlain by a series of basalt flows grouped here under the Degoma Basalt Unit. These basaltic flows are believed to have been emplaced from shield volcanoes and are hence correlated to Tarmaber Guassa Formation. The basalt flows are fresh and form plateau morphology and have limited lateral area coverage.

A variety of lava flows and pyroclastic deposits are found on Guna volcano and have been subdivided lithologically into the following sub-units: Guna Tuff, Guna Basalt and Guna Phonolite. These rocks have limited aerial extent around the volcano and belong to the Tarmaber Guassa Formation. The age of Guna basalt was dated to be 10.7 Ma (Keiffer et al., 2004).

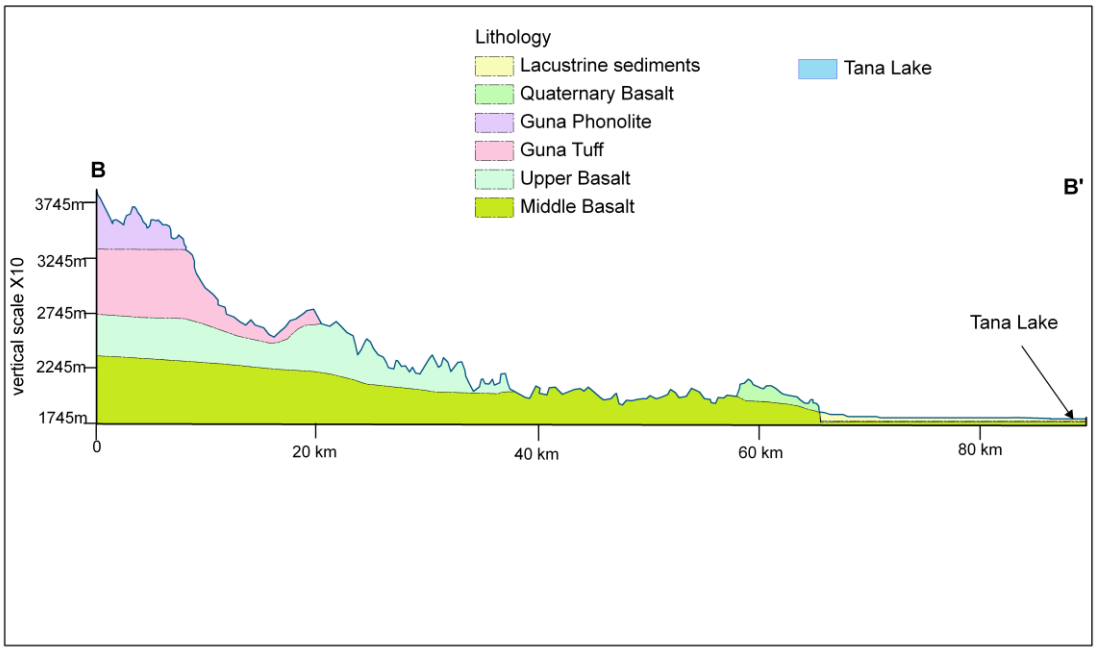

Figure 3.4. A geological cross-section from Guna volcano (B) in the west to Tana Lake (B') in the east. Vertical scale has been exaggerated 10 times.

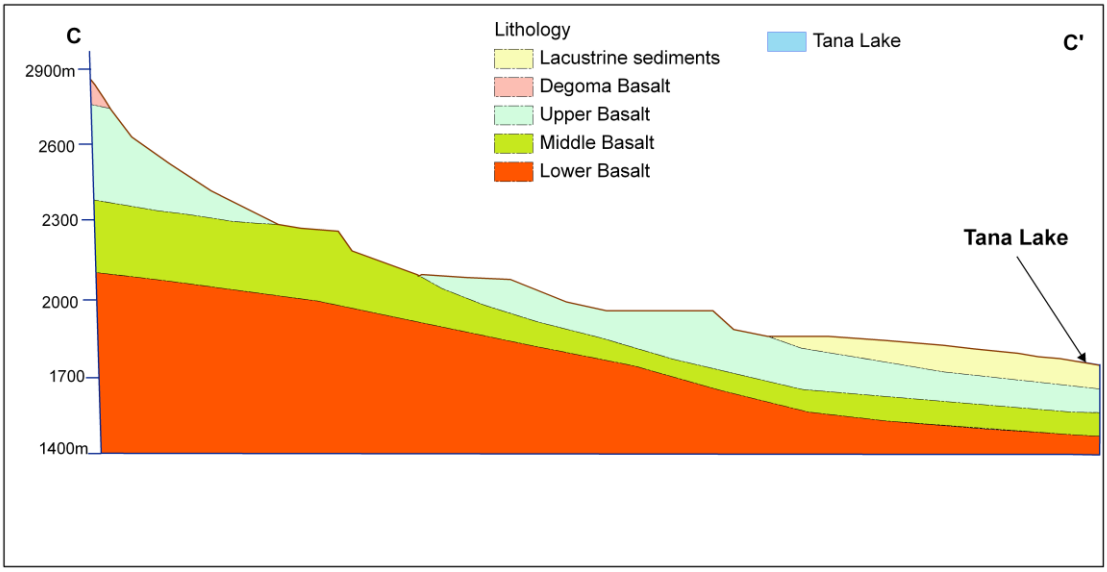

Figure 3. 5. A geological-cross section from Gonder area (C) in the north to Tana Lake (C') in the south , not exaggerated.

In the southern part of the Tana Basin, the Upper Basalt Unit or Alaji Basalt/Rhyolite formation is overlain by basalt flows collectively named as Sekela Basalt Unit. This unit appears to be part of the nearby Choke shield volcano which has been dated to be 20.4 Ma (Keffer et al., 2004). Sekela Basalt hence belongs to Tarmaber Guassa Formation.
A number of isolated trachyte flows, lava domes and plugs, commonly forming prominent topographic features, such as those around Addis Zemen, Debretabore and Gorgora towns, are found in the study area. These rocks are believed to have been emplaced at the later stages of shield volcanic activity, and are correlated to Tarmaber Guassa Formation. Around Gorgora town, the trachyte flows overlie the Alaji Basalt/Rhyolite Formation, with about 0.5m thick paleosol in between.

Recent basalt flows and associated scoria cones covering wide areas in the south-west and east of the Tana basin have been mapped in previous studies to be Quaternary age and this age is adopted in this study. These basalts are also known in the literature as Tana Basalts. In some places rhyolite domes have been emplaced through the Quaternary Basalts and the underlying Alaji Basalts/Rhyolites with steep contact relations.

Fluivio-lacustrine sediments are found around the shores of Lake Tana. These sediments have been deposited during the Quaternary when the lake level was much higher than today.

3.2.1.2. Lithologic descriptions

It has been shown above that the geology of the Tana basin constitutes a succession of volcanic rocks and lacustrine sediments of Tertiary and Quaternary age. The volcanic rocks have also been grouped into lithologic units and correlated with major known volcanic formations in the region. Detail descriptions of the lithologic units as well as their macroscopic and petrographic characteristics are given below.

Middle Basalt (Aiba Basalt Formation)

Middle Basalt forms the oldest volcanic rocks exposed in the area. It is unconformably overlain by Upper Basalt (Alaji Formation), with reddish clay silt and white gray silty paleosols of about 0.5m thick (Fig.3.6). This basalt is underlain by Lower Basalt (Ashangi Formation) a few kilometers outside the study area (Workineh Haro et al.,2010; 2011 and Dejene Hilemaryam et al., 2012), and in the boreholes drilled in the area.

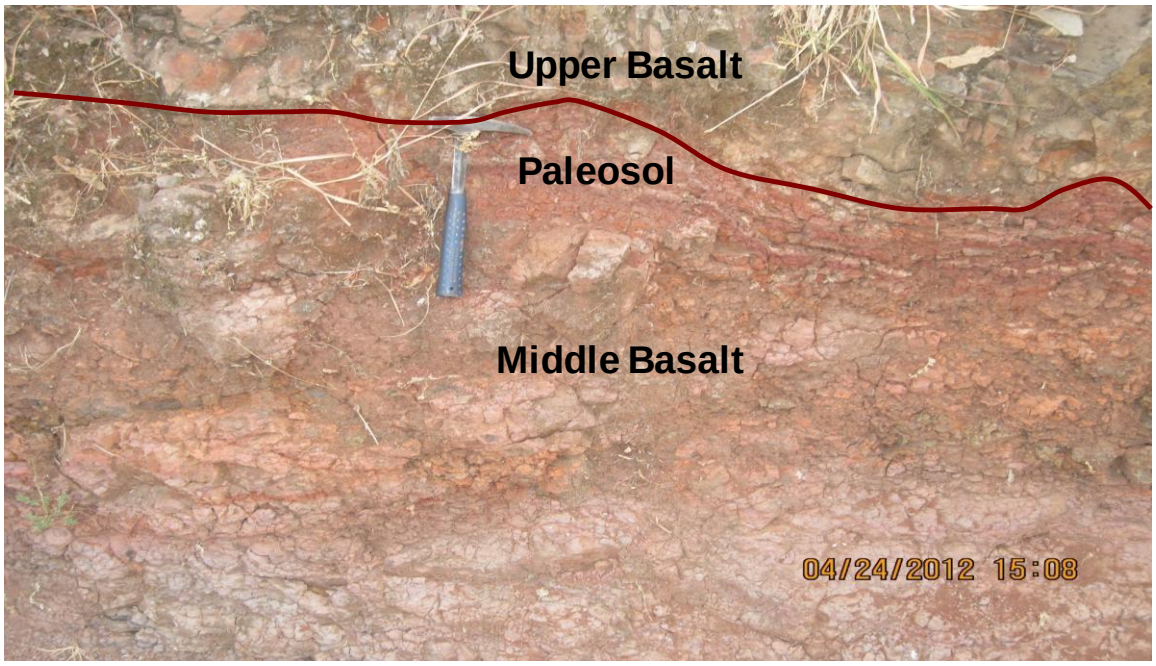

Figure 3.6. Contact between Middle and Upper basalts.

It is dense, compact and thinly stratified. This basalt is often fine grained but at places plagioclase and olivine phyric. This rock is of Oligocene age (Keffer et al., 2004). It is exposed around Gonder town in the north and in the eastern part of the area. It is slightly vesicular and often filled by zeolites. It is highly weathered on top near the contact with Upper Basalt and is relatively massive below, and forms frequent erosional peaks. Small out crops of Middle Basalt occur along the road from Addis Zemen to Maksegnit towns. In the eastern area, it is thinly layered. It is affected by faults, lineaments and macroscopic joints.

Petrographic study of a sample taken at (UTM 37) 334859 mE, 1393316 mN showed modal composition of plagioclase (35%), clinopyroxene (33%), olivine (12%), opaques (10%), volcanic glass (10%).

The Middle Basalt has exposure thickness of up to 300 m in the east, and ~147m in the nearby north areas (Workineh Haro et al., 2011). Boreholes drilled in the northern part of the area encountered this basalt between the overlying Upper Basalt and the underlying Lower Basalt, which are separated by paleosols. The thickness of Middle Basalt in these boreholes varies from 71 to 90 m, with an average of 77 m. Middle Basalt covers 382.4 km^2 areas (3.2% of the area).

Upper Basalt, (Alaji Basalt/Rhyolite Formation)

Upper Basalt is exposed at wide area in the northern, eastern and western and south western parts of the area estimated to be 4 300 km^2 (36.3% of the area). The maximum measured thickness of Upper Basalt is 572 m in northern area and 196 m in the eastern area, and 185 m in the southwestern area. Boreholes drilled in this basalt unit have shown thickness of 46 to 188 m, with the average of 112 m.

It is often fine grained but with plagioclase-hornblende, olivine and pyroxene-olivine phyric at places. It unconformably overlies the Middle Basalt and is overlain by the Degoma Basalt unit in the north, the Guna tuff in the east and Quaternary basalt in the southwest. It consists of ignimbrite and tuff layers towards the top as in the eastern area. It is cut by faults, lineaments and macrosopic joints and also by columnar joints.

Thin section analysis for the basalt sample taken at (UTM 37, 375256 mE, 1287196 mN) has shown modal composition of plagioclase (45%), clinopyroxene (40%) and opaques (15%). A sample taken at (UTM 37, 280303 mE, 131637 mN) showed fine grained basalt with modal composition of plagioclase (40%), clinopyroxene (35%), opaques (15%) and volcanic glass (10%).

Degoma Basalt, Sekela Basalt, Guna volcanics (Guna Tuff, Guna Basalt, Guna Phonolite), Trachyte flows and plugs: (Tarmaber-Guassa Formation)

Degoma Basalt

Degoma Basalt is found in northern and northeastern summit areas forming small plateau. It overlies the Upper Basalt, and is younger and fresh. Degoma Basalt is plagioclase, olivine, Olivine-plagioclase phyric and fine grained basalts. It is dark gray and black, slightly weathered and massive, columnarly jointed at places. It is layered. Pyroclastic deposits found on the top. Thickness of this basalt reaches 289 m. Thin section analysis from fine grained basalt has shown the following composition (Workineh Haro et al., 2011): plagioclase (44%), clinopyroxene (15%), glass (13%) and olivine (3%). Zeolite and calcite infillings are reported.

This basalt covers an area of 213 km^2, which is 1.8% of the area.

Sekela Basalt

Sekela Basalt is found at the southwest elevated terrain of Gish Abay or Sekela area. It is underlain by Upper Basalt out side the study area. It is part of Choke volcano and has age of 22.4 Ma (Keffer et al., 2004).

This basalt is plagioclase-olivine-pyroxene and olivine phyric. It is dark gray in fresh and reddish to yellowish brown when weathered. Sample taken from plagioclase-olivine-pyroxene phyric basalt (UTM 37, 297701 mE, 1215366 mN) shows the following modal composition: plagioclase (36%), clinopyroxene (35%), olivine (15%), opaque (5%), volcanic glass (5%), calcite (2%), chalcedony 2(%). Moreover, sample taken from olivine phyric basalt at (UTM 37, 289691 mE and 1222799 mN) showed modal composition of plagioclase (37%), clinopyroxene (36%), opaque (12%), olivine (10%) and volcanic glass (5%).

Sekela Basalt is moderately fractured with northeast and northwest trending macroscopic joints.

This basalt is unconformably overlain by Quaternary basalt in the south western part, with paleosol of about 0.3 m thickness in between them (Fig.3.7). Its thickness is about 400 m. It covers an area of 845.3 km^2.

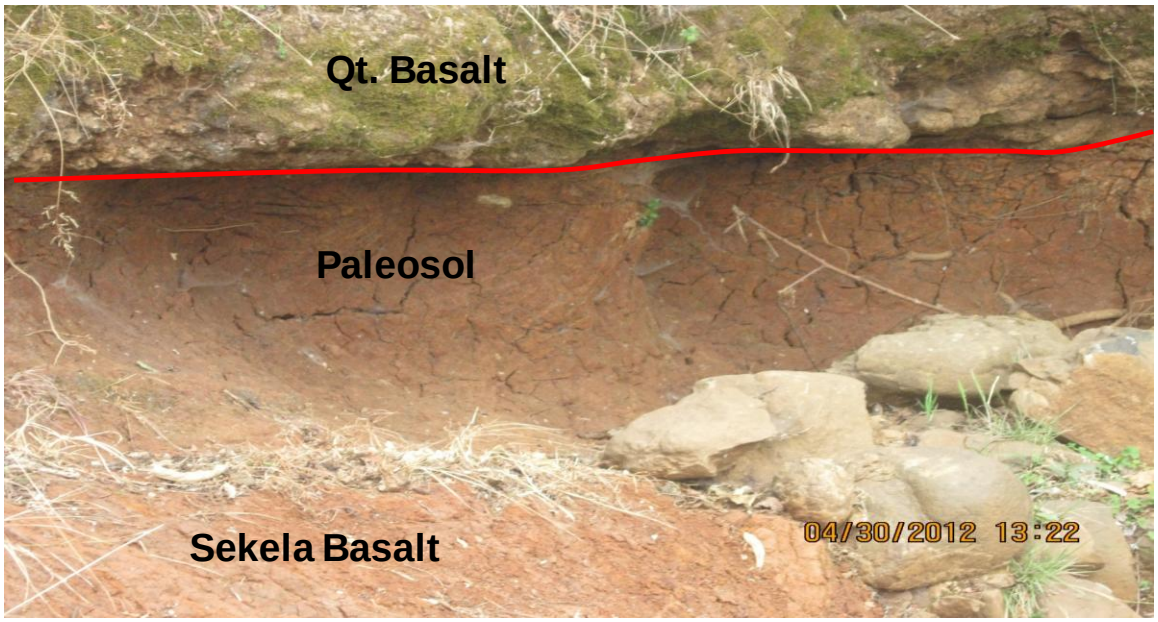

Figure 3.7. Contact between Sekela and Quaternary basalts.

Guna Volcanics

Guna Tuff

Guna tuff is found at the eastern part of the area. It is light colored, loose to weekly compacted, and contains compact welded tuff beds. It is overlain and underlain by Guna basalt and Upper Basalts, respectively (Figs3.8a&b). The tuff consists of rock fragments of mainly pumice and basalt, and at some places shows cross-bedding indicating surge deposits (Workineh Haro et al., 2010).

Its thickness reaches 640 m. Guna Tuff is believed to be the first edifices of the Guna volcano and belong to Tarmaber Guassa Formation. It covers an area of 183.7 km^2 (1.6 % of the area).

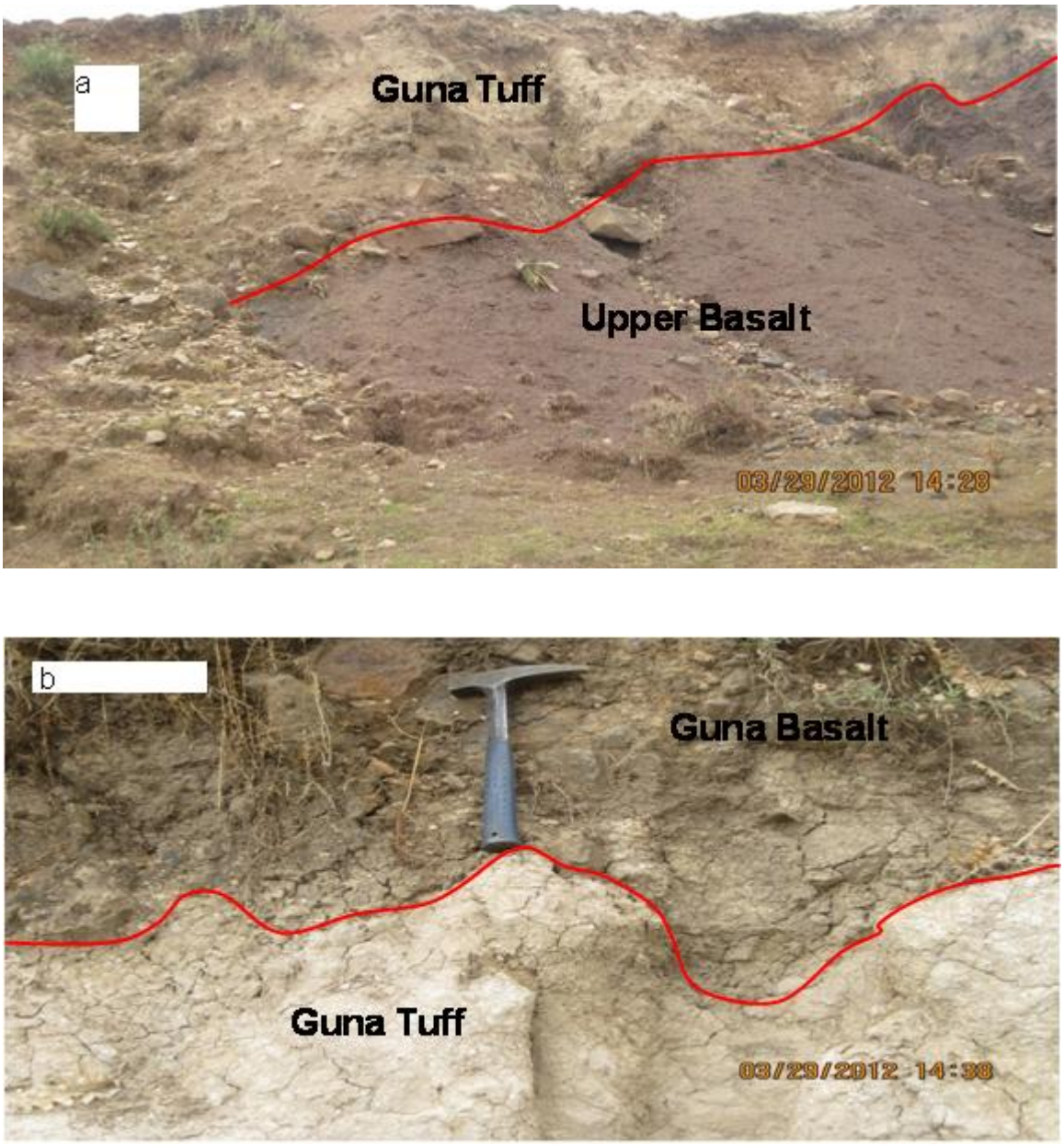

Figure 3.8. Contact between Guna Tuff and a)Upper Basalt and b) Guna Basalt

Guna Basalt

Guna Basalt is olivine phyric and a fine grained, and layered. It is slightly weathered and columnarly jointed at places. It overlies the Guna Tuff (Fig.3.9) and underlies the Guna Phonolite. Its thickness reaches 193 m. It covers an area of 47.6 km^2, which is 0.4% of the total area. Its age has been dated to be 10.7 Ma by Keffer et al. (2004).

Guna Phonolite

Guna Phonolite forms the top summit of Guna Mountain. It is dark greenish gray color, relatively fresh and columnarly jointed. Its thickness reaches 590 m. It overlies the Guna Basalt. Guna Phonolite is porphyritic with phenocrists of sandine, nephline, nosean, lucite, augite and sphene. Ground mass consists of minerals that are found as phenocrists (Addise Mekonen, 2006). It has an area of 15.8 km^2 (0.1% of the area).

Trachyte Flows and Plugs

Trachyte flows overlies unconformably the Upper Basalt near Gorgora town (Fig3.9) at the northern shore of the lake. It is highly fractured. Trachyte flow was also seen overlying the Upper Basalt at the road to Debretabor from Wereta town, which is close to Amora gedel trachyte plug. It is fractured. Trachyte plugs are also found within Upper Basalt in the eastern part of the area. The trachyte is sandine and quartz phyric.

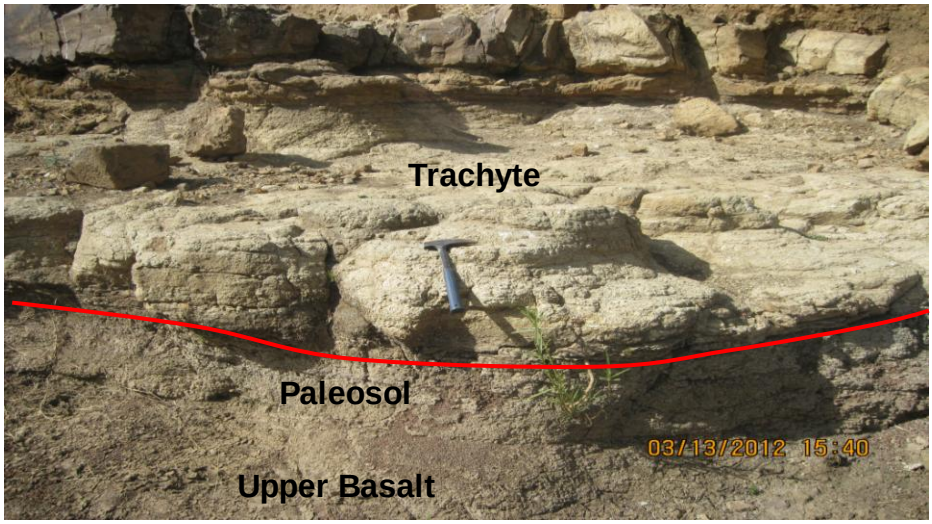

Figure 3.9. Contact between Trachyte flow and Upper Basalt near Gorgora town.

The modal composition of the trachyte around Gorgora has been reported as follows (Werkineh Haro et al., 2011): sandine (20%), augite (15%), acicular sandine (10%), quartz (10%), hematite (15%), crypto crystalline materials (30%). Trachyte flow near Gorgora town has been reported to be Quaternary by Werkineh Haro et al. (2011). However, it is believed here to belong to Tarmaber Formation as that of the plugs, which has been emplaced at the end of shield volcanic activity.

Tarchyte flows have less than 25 m thickness. Trachyte flows and plugs cover about 99.9 km^2 area, which is 0.8% of the area.

Tana Quaternary Basalts and Rhyolite

Quaternary Basalt

Quaternary Basalt occupies the southwestern and southeastern areas. It is dark and dark gray and consists of aphanatic, olivine, plagioclase-pyroxene-olivine phyric basalts, which is scoraceous and vesicular. Scoria cones are found within these rocks.

It overlies the Sekela Basalt (Fig3.10) and Upper Basalt in the southwestern areas, which are separated by paleosols.

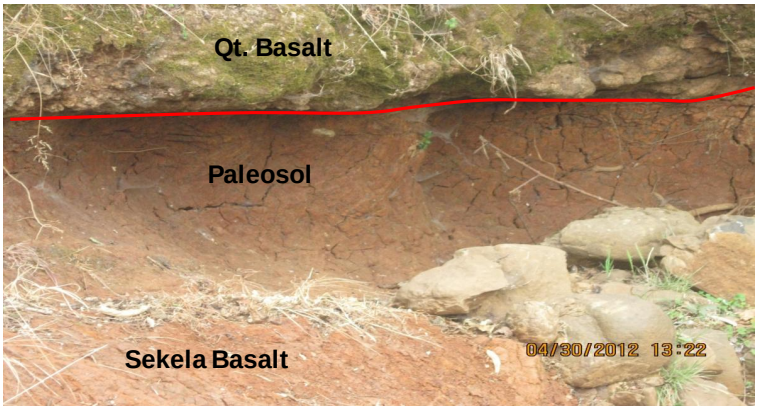

Figure 3. 10. Contact between Quaternary basalt and Sekela Basalt.

Fine grained and dark basalt at eastern area (UTM 37, 350291 mE, 1292521 mN) has modal composition of plagioclase (45%), clinopyroxene (38%), opaque (12%) and volcanic glass (5%). Olivine phyric vesicular and scoraceous basalt at (UTM 37, 309808 mE and 1266612 mN) has shown plagioclase (40%), clinopyroxene (36%), olivine (15%), opaque (5%) and volcanic glass (4%). Sample taken from olivine basalt at (UTM 37, 281202 mE and 1226309 mN) shows plagioclase (35%), clinopyroxene (30%), volcanic glass (13%), olivine (12%), opaque (8%) and calcite (2%).

The Quaternary Basalt is jointed and three vertical, horizontal and northeast trending major sets are observed, which are open and interconnected. It is highly vesicular at places.

Quaternary Basalt is emplaced after the formation of the Tana rift and is overlain by lacustrine sediments. Its thickness is 24 to 49 m as encountered in boreholes, and it covers an area of 3 390.1 km^2 (28.6% of the area).

Quaternary Rhyolite Domes

Rhyolite form small domes and broad based gentle sloping circular to elliptical hills. The rhyolite is light grey to pink with K-feldspar, plagioclase and quartz porphyry. K-feldspar is altered. It is moderately weathered on top. The rhyolite was considered to be Quaternary flow below the Quaternary Basalt by Efrem Beshawered et al. (2010). However, the rhyoltite has been found to have sub vertical dip with the adjacent Upper and Quaternary basalts (Figs.3.11 a&b). Therefore, it is believed that this rhyolite domes are placed post Quaternary basalt. Intercalation of unwelded tuff and ash are seen at places toward the top.

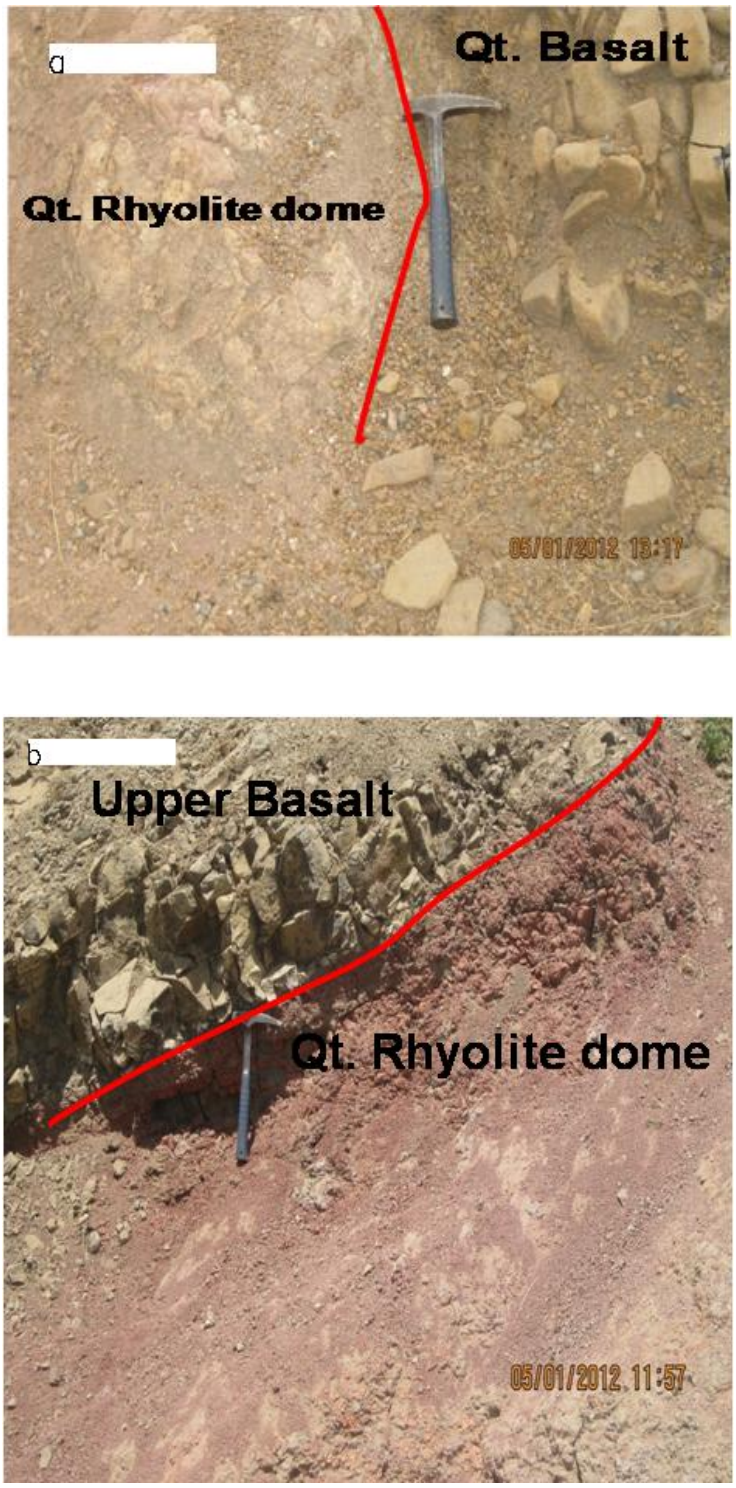

Figure 3.11. Contact between rhyolite dome and a) Quaternary basalt,

b) Upper Basalt.

Samples taken from rhyolite dome (UTM 37, 312121 mE, 1280878 mN) showed modal composition of plagioclase (40%), sanidine (24%), quartz (20%), chalcedony (7%), calcite (5%), opaque (3%) and pyroxene (1%). Rhyolite sample taken from around Dengel ber town has also shown quartz (40%), plagioclase (15%), chalcedony (14%), sanidine (11%), volcanic glass (15%), opaque (3%), calcite (1%) and pyroxene (1%).

Quaternary rhyolite covers an area of 300.4 km^2, which is 2.5% of the area.

Quaternary Lacustrine Sediments

Lacustrine sediments are found close to the lake shore in the east, north and west and southwest. These sediments are deposited during the high lake level probably during the pluvial period, where erosion rate from the adjacent mountains was intense.

These sediments are unconsolidated dark and dark brown clay soil, which develops cracks at places. Bedded tuff inter bedded with mud stone, which is loose and friable are reported at Rib river, near Woreta town, indicating paleo lake sediment (Workineh Haro et al., 2010). Boreholes drilled at the eastern margin of this deposit show sand and gravel beds at various depths suggesting fluviatile deposits during high river loads. Thickness of this deposit varies from few meters up to about 180 m. It covers an area of 2 088.9 km^2 (17.6% of the area).

3.3. Tectonic Structures

A number of normal faults with dominant NNE-SSW and WWN-EES trends are found on the western escarpment and eastern parts of the Tana Basin (Figures 3.12). A major N-S normal fault with down throw to the east forms the escarpment on the west of the lake. The WWN-EES trending normal faults have down throws either to the SSW or NNE, while the NNE-SSW normal faults are down thrown to EES. All these faults have their fault planes with very steep dips. Figure3.12 is a rose diagram showing strike directions of 19 measured normal faults in the area.

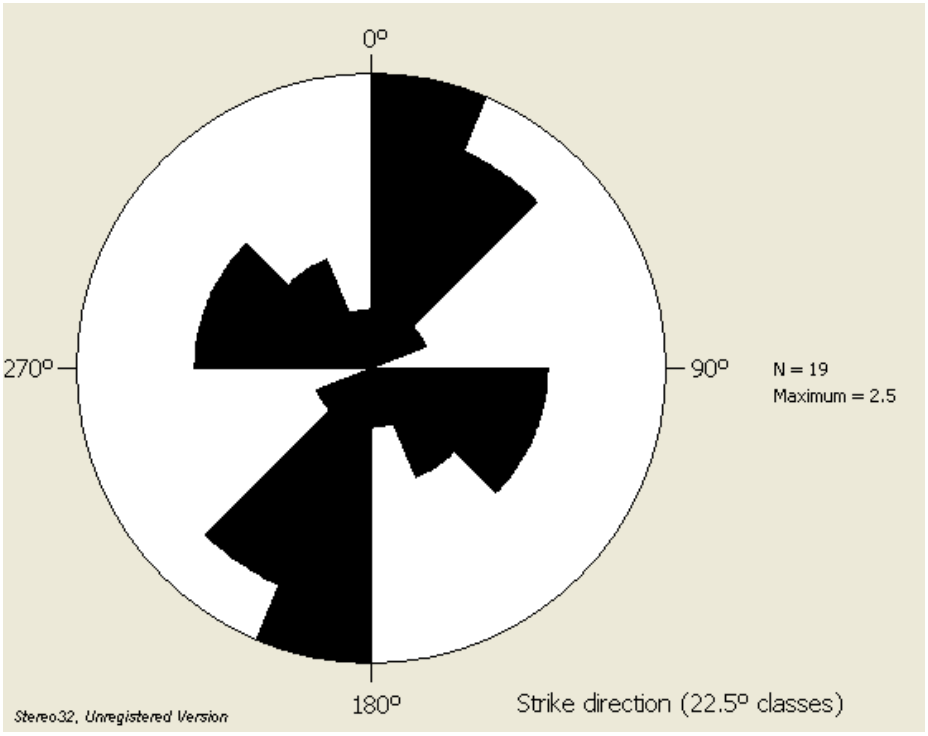

Figure 3.12. Rose diagram for strikes of faults.

On the basis of cross-cutting relationships among the observed normal faults and influence on drainage, the N-S trending faults seem to be the oldest followed by the WWN-EES ones. The NNE-SSW faults are the youngest ones.

Other linear features or lineaments, probably of tectonic origin, have also been interpreted from satellite imageries of the study area. These lineaments have the following trends: NNE-SSW, NE-SW, NNW-SSE and NW-SE. Figure 3.13 shows the rose diagram of the lineaments identified in the area. The NNE-SSW and NE-SW lineaments control the morphology and drainage system in the eastern part of the area suggesting their relatively younger age. In the western escarpment area, the WWN- EES trending lineaments are much more dominant.

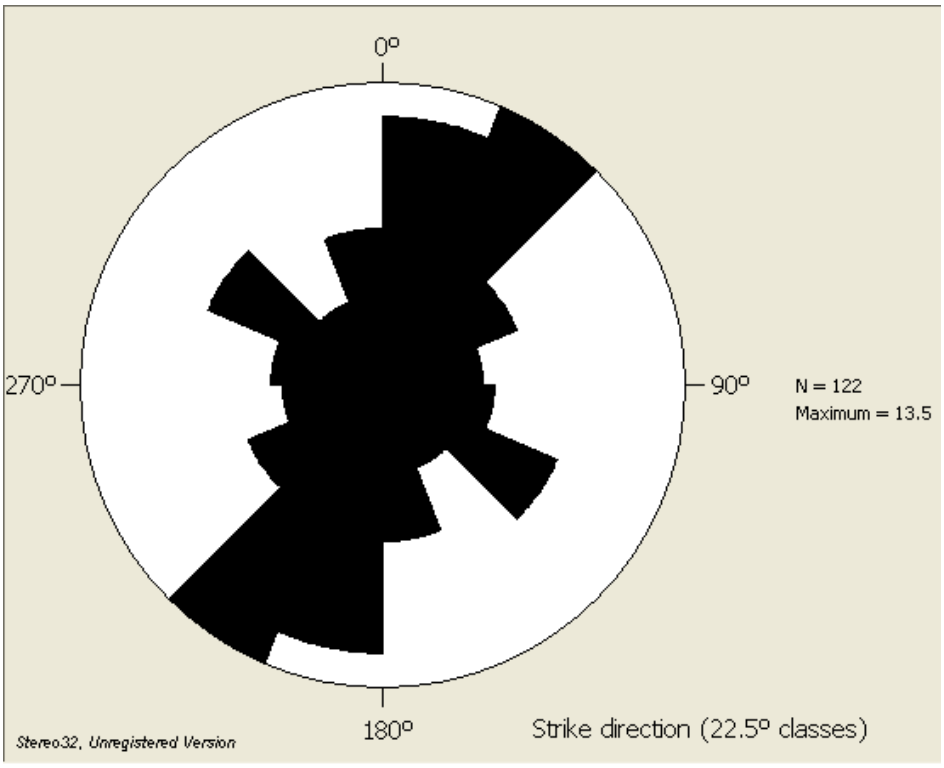

Figure 3.13. Rose diagram for lineaments.

Macroscopic joints with NE-SW and NW-SE trends commonly cut through all the exposed rock formations: Middle, Upper, Shield volcanic Formations and Quaternary basalts. The joints are frequently open, closely spaced (often less than 1m) and interconnected.

According to Chorowicz et al. (1998), Tana basin was formed due to subsidence, which occurred at the focus of the three half grabens called the Gonder, Debretabore and Dengle grabens. The first subsidence was in Mid-Tertiary while the subsequent subsidences were due to reactivation of graben faults in Late Miocene and Quaternary. Subsidence was due to purely tensional forces.

4. HYDROMETEOROLOGY

4.1. Climate

The climatic conditions of Ethiopia are strongly influenced by altitude. According to Daniel Gemechu (1997), there are wide varieties in climatic zones in Ethiopia. The climatic zones defined by Gozálbez and Cebrián (2006) and Daniel Gemechu (1997) are presented in Table 4.1.

The climatic zones of the basin have been prepared based on the climatic region classification given in Table 4.1, making use of the elevation and precipitation data of the study area. Figure 4.1 shows the climatic zones in the basin.

4.2. Meteorological Elements

4.2.1. Meteorological stations and data quality

Rainfall data is the most readily available climatic information in the study area. Most of these stations have long year's records with very good data quality. Thirteen stations with data from 1995 to 2009 have been purchased from the Ethiopian Meteorological Agency and used in the analysis. Data with missing records greater than 3 months have been discarded while the mean value of the given period is assigned for the missing data of less than 3 months of a given hydrological year.

Stations that are used, their locations, altitude, class and mean annual precipitation values are shown in Table 4.2. Figure 4.2 shows spatial distribution of these meteorological stations.

Table 4.1. Ethiopian climate.

Name/Altitude, Mean annual temperature	Precipitation (below 900 mm)	Precipitation (900 - 1400 mm)	Precipitation (>1400 mm)
High wurch (Kur) > 3700 m.a.s.l < 5°C			Afro-alpine meadows of grazing land and steppes, no farming helichrysum, lobelia
Wurch (Kur) 3700-3200 m.a.s.l 5-10°C		Sub-afroalpine barely erica, hypericum	Sub-afroalpine barely erica, hypericum
Dega 3200-2300 m.a.s.l 10-15°C		Afro-mountain (temperate) forest-wood land barely, wheat, pulses juniperus, hagenia, podocarpus	Afro-mountain (temperate) bamboo forest barely, wheat, nug, pulses juniperus, hagenia, podocarpus, bamboo
Weina Dega 2300-1500 m.a.s.l 15-20°C	Savannah (Sub-tropical) wheat, teff, some corn acacia savannah	Shrub-savannah (Sub-tropical) corn, sorghum, teff, enset, wheat, barely acacia, cordia, ficus	Wooded-savannah (Sub-tropical) corn, teff, nug, enset, barely acacia, cordia, ficus, bamboo
Kolla 1500-500 m.a.s.l >30°C	Tropical sorgham and teff acacia bush	Tropical sorgham, teff, nug, peanuts acacia, cordia, ficus	Wet tropical mango, sugar cane, corn, coffee, orange cyatheal, albizia
Bereha < 500 m.a.s.l >40°C	Semi-desert and desert crops only with irrigation thorny acacia, commiphora		

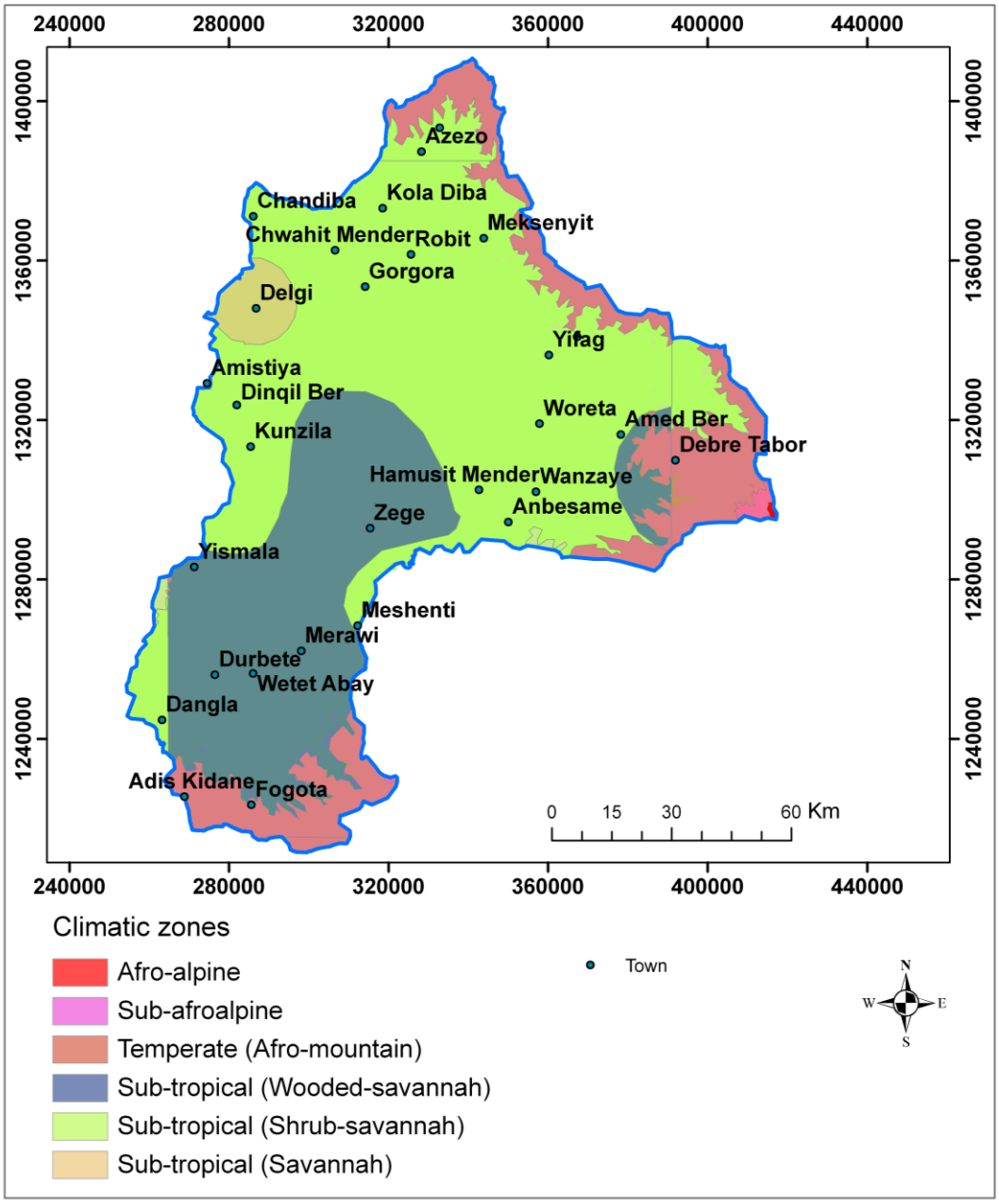

Figure 4.1. Climatic zones of the basin.

The total aerial coverage of the different climatic zones is 0.04, 0.3, 15.2, 28.9, 53.3 and 2.2 % for Afro-alpine, Sub-afroalpine, Temperate (Afro-mountain), Subtropical (Wooded-savannah), Subtropical (Shrub-savannah) and Subtropical (savannah) climatic zones, respectively.

Table 4.2. Meteorological stations and their characteristics.

Station	X	Y	Altitude (m)	Class*	Annual precipitation (mm)
Zege	316149	1292779	1801	3	1657.2
Bahir Dar	321281	1282896	1800	1	1239.5
Dangila	265076	1264911	2116	1	1583.0
Gonder	329703	1384771	1973	1	1275.0
Debretabor	390674	1312089	2612	1	1546.4
Gorgora	315176	1354866	1816	1	1101.0
Addis Zemen	376034	1339063	1940	1	1032.0
Sekela or Gish Abay	304802	1215226	2715	4	1870.3
Delgi	287368	1348448	1798	4	718.3
Kunzila	284673	1313544	1807	4	1126.8
Woreta	358067	1318378	1819	3	1309.0
Dek Estifanos	306855	1313215	1815	3	1738.0
Gassay	406941	1304349	2789	3	NC*

NC*- no complete data

Class 1: rainfall, temperature, relative humidity, sunshine hour, wind speed

Class 3: rainfall and temperature

Class 4: rainfall

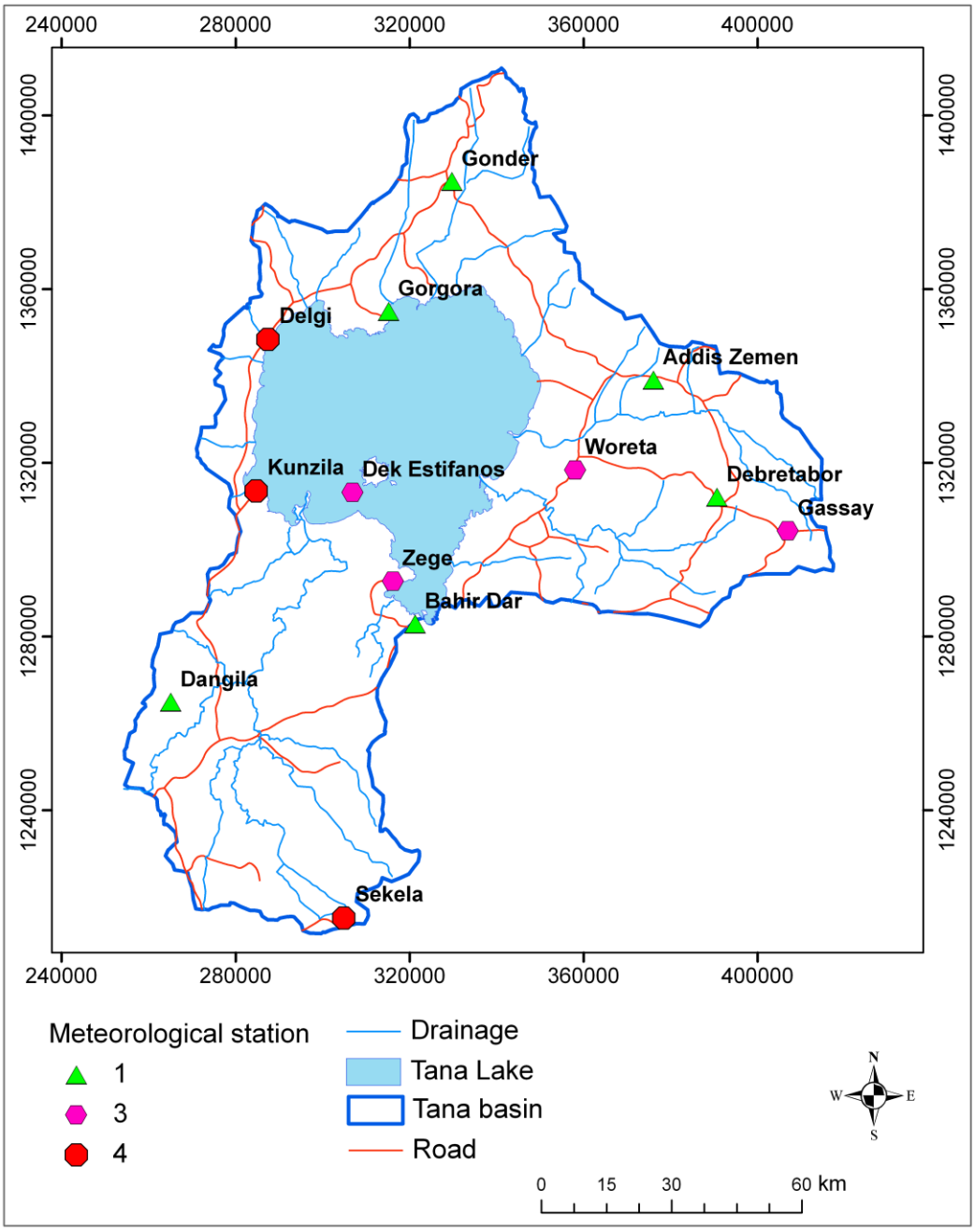

Figure 4.2. Spatial distribution of meteorological stations. Number indicates class of the station.

4.2.2. Precipitation

4.2.2.1. Precipitation pattern and temporal variation

The precipitation in Ethiopia falls almost entirely in the form of rainfall. The Ethiopian territory is divided into four zones marked as A, B, C and D, each of them with different precipitation patterns. The seasonal classification and precipitation regime of Ethiopia (after NMSA, 1996) are characterized in Table 4.3 and shown in Figure 4.3.

Tana basin belongs to Zone B (b2 &b3), which is characterized with one dry and other wet season. The rainfall is uni modal and is mainly between April/May to October/November. The rain fall during summer originates from the Atlantic and Indian oceans when the Inter Tropical Convergence Zone (ITCZ) moves to about 19°N, just to the north of Lake Tana. From October to May, the ITCZ shifts south wards and dry conditions persists in the region (Lamb et al., 2006).

Mean monthly precipitations of six selected meteorological stations are shown in Figure 4.4 and Table 4.4. Most of the rainfall occurs during the months of July and August for all stations.

4.2.2.2. Spatial variation of precipitation and rainfall- altitude relationship

The spatial distribution of precipitation is shown in Figure 4.5. Precipitation varies spatially. There is marked difference between highlands and lowlands due to large difference in altitude. However, there are stations such as Zege and Dek Estifanos, with relatively high precipitation values unlike their relatively lower altitude, which are close outside in the land (shoreline) and in the iland within the Tana Lake, respectively (see Fig. 4.5). This seems to be due to moisture recycling associated with Tana Lake.

Table 4.3. Characterization of precipitation pattern in Ethiopia.

Zone	Precipitation pattern
A	This region mainly covers the central and central eastern part of the country. It is characterized by three distinct seasons, and by bimodal precipitation pattern with small peaks in April and the main rainy season during mid June to mid September with peak in July
B	This region covers the western part of the country. It is characterized by a single precipitation peak. Two distinct seasons, one being wet and the other dry, are encountered in this region. The analysis of mean monthly precipitation patterns shows that this zone can be split into south western (b1) with the wet season during February/March to October/November, western (b2) with the wet season during April/May to October/November, and northwestern (b3) with the wet season during June to September
C	This region mainly covers the southern and southeastern parts of the country. It has two distinct precipitation peaks with a dry season in between. The first wet season is from March to May and the second is from September to November
D	The red Sea region in the extreme northeastern part of the country receives diffused precipitation with no distinct pattern, however, precipitation occurs mainly during the winter.

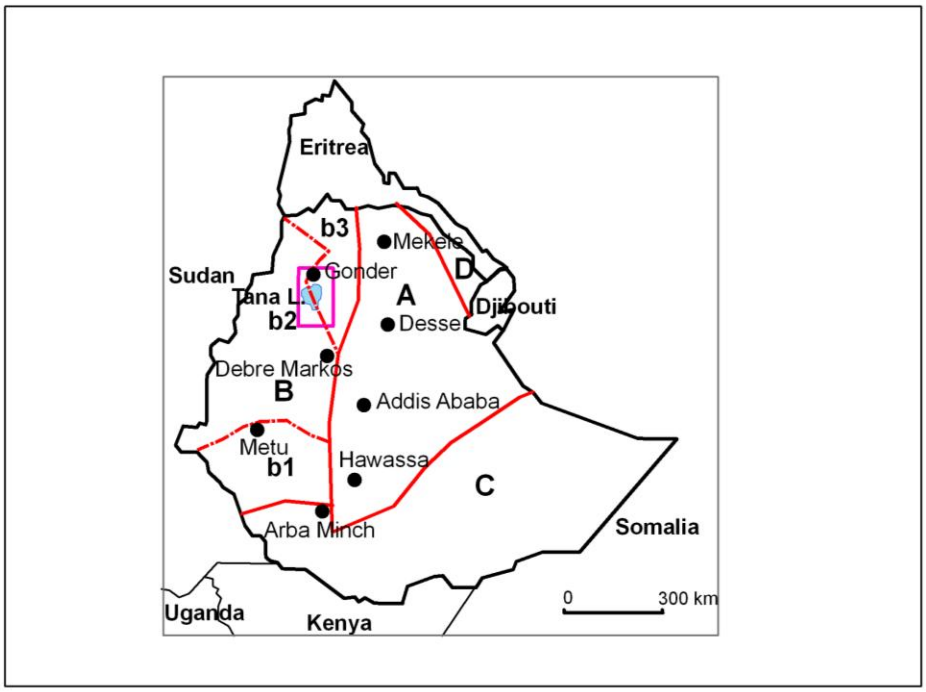

Figure 4.3. Graph depicting precipitation regimes in Ethiopia (Andarge Mekonen, 2010).

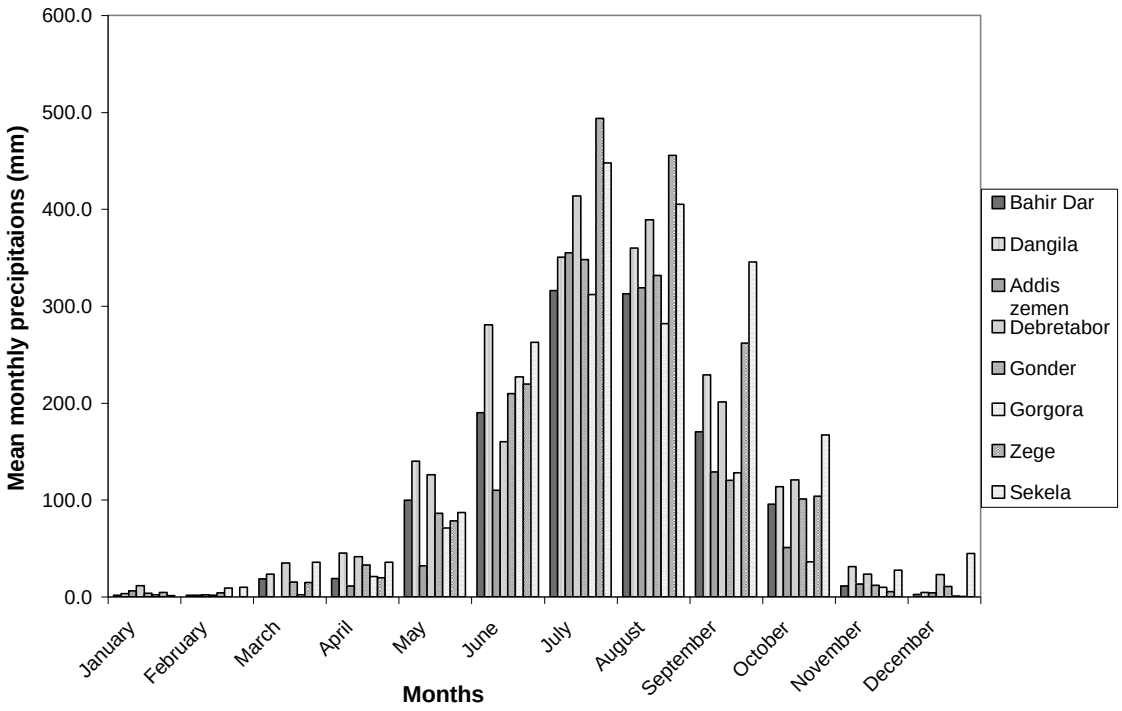

Figure 4.4. Temporal variation of precipitation in selected stations.

Table 4.4. Mean monthly precipitation values of stations (1995-2009.

Month	Bahir Dar	Dangila	Addis Zemen	Debretabor	Gonder	Gorgora	Zege	Sekela
January	1.7	3.3	6	11.4	3.5	2	4.6	1.1
February	1.7	1.8	2	1.4	4.1	9	0.1	9.9
March	18.6	23.6	0	34.9	15.3	2	14.7	35.9
April	19.0	45.0	11	41.5	32.8	21	19.5	35.8
May	99.9	139.8	32	126.0	86.2	71	78.5	87
June	190.1	280.9	110	160.0	209.6	227	219.4	262.8
July	316.1	350.6	355	413.5	348.1	312	493.8	447.8
August	312.8	360.0	319	389.3	331.4	282	455.4	405.1
September	170.3	229.1	129	201.1	120.4	128	261.6	345.4
October	95.8	113.5	51	120.7	101.0	36	103.7	167.1
November	11.2	31.2	13	23.6	11.8	10	5.3	27.5
December	2.5	4.4	4	23.1	10.8	1	0.4	44.9
Annual	1239.5	1583.0	1032.0	1546.4	1275.0	1101.0	1657.2	1870.3

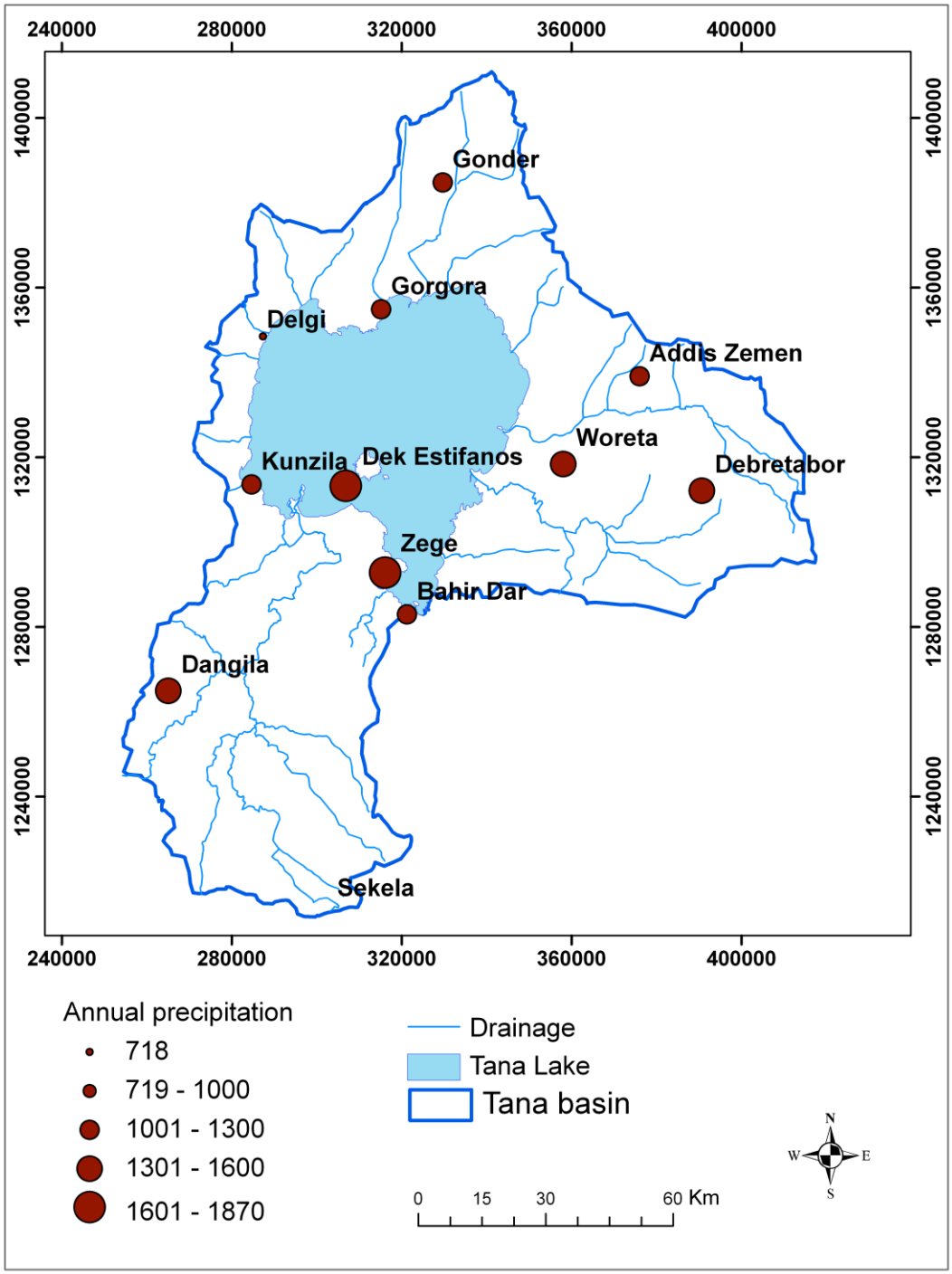

Figure 4.5. Spatial variation of precipitation (in mm).

Plot of rainfall versus altitude (Fig. 4.6) does not show a clear trend and has poor correlation coefficient (R^2 = 0.25) because of the same reason mentioned above.

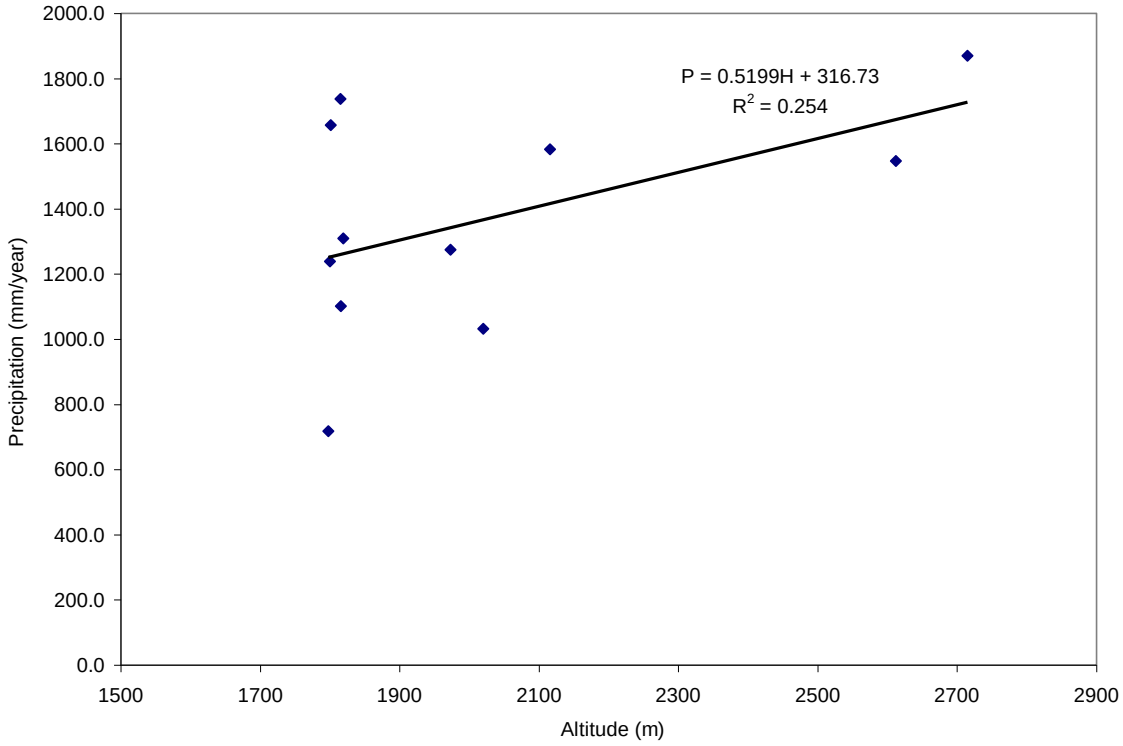

Figure 4.6. Relationship of rainfall (P) and altitude (H).

4.2.2.3. Estimation of aerial depth of precipitation

Precipitation over the basin

Monthly precipitation data (1995-2009) of 8 stations have been used to estimate the mean aerial precipitation over the basin. Bahir Dar, Dangila, Addis Zemen, Debretabor, Gonder, Gorgora, Zege and Sekela stations have been used to estimate the basin average precipitation (*P*). After the mean monthly data of each station is calculated, the aerial average has been estimated using Thiessen polygonal method on monthly basis.

Thiessen polygonal averaging method is effective for rugged terrain and where distribution of station is not uniform. Once constructed, it can be used to calculate aerial average of the different periods if the location of stations does not change (Surbamanya, 2004). Isoheytal method of aerial depth precipitation estimation is also good. However, the number of stations is not enough for establishing isoheyets. Table 4.5 depicts the

mean monthly precipitation data of the basin. Location of meteorological stations and Thiessen polygons used to estimate aerial average precipitation is shown in Figure 4.7.

Precipitation over the Tana Lake

Thiessen polygonal averaging method has also been employed to estimate the mean annual precipitation (P_l) over the Tana Lake on annual basis. Wereta, Gorgora, Delgi, Kunzila, Dek Estifanos, Bahir Dar and Zege stations, which are close and within the lake have been used in this computation. Figure 4.8 shows the Thiessen polygons used in this estimation.

4.2.3. Evapotranspiration

Evapotranspiration is known as a loss of water or moisture through the process of transpiration by plants and evaporation of water from the soil and water bodies. If sufficient moisture is available for the need of vegetation covering the area under the given set of atmospheric conditions, the resulting evapotranspiration is called potential evapotraspiration. However, the real evapotranspiration occurring in a specific atmospheric and soil moisture situation is called actual evapotranspiration.

Table 4.5. Estimated mean meteorological parameters for the basin (1995-2009), in mm.

	Jan	Feb	Mar	Apr	May	Jun	Jul	Aug	Sep	Oct	Nov	Dec	Annual
P	4.5	3.9	16.4	27.7	88.6	207.9	382.7	358	194.1	91.5	15.8	9.5	1400.4
ET_o	110	120	138	136	131	103	85	84	102	110	103	103	1329
E_{ol}	129.0	145.7	168.1	191.8	159.4	95.6	94.0	93.4	113.7	108.5	125.4	118.9	1543.9
E_{osm}	3.1	2.7	11.2	19.0	60.7	94.2	74.8	93.4	113.7	108.5	125.4	57.6	764.2
E_{opm}	129.0	145.7	168.1	191.8	159.4	95.6	94.0	93.4	113.7	108.5	125.4	118.9	1543.9
AET	3.1	2.7	11.2	19.0	60.7	94.2	74.8	73.9	89.8	96.8	90.7	57.6	674.4

P: precipitation, ET_o: reference potential evapotranspiration, E_{ol}: lake evaporation, E_{osm}: evapotranspiration from seasonal marsh, E_{opm}: open evaporation from permanent marsh, AET: actual evapotranspiration

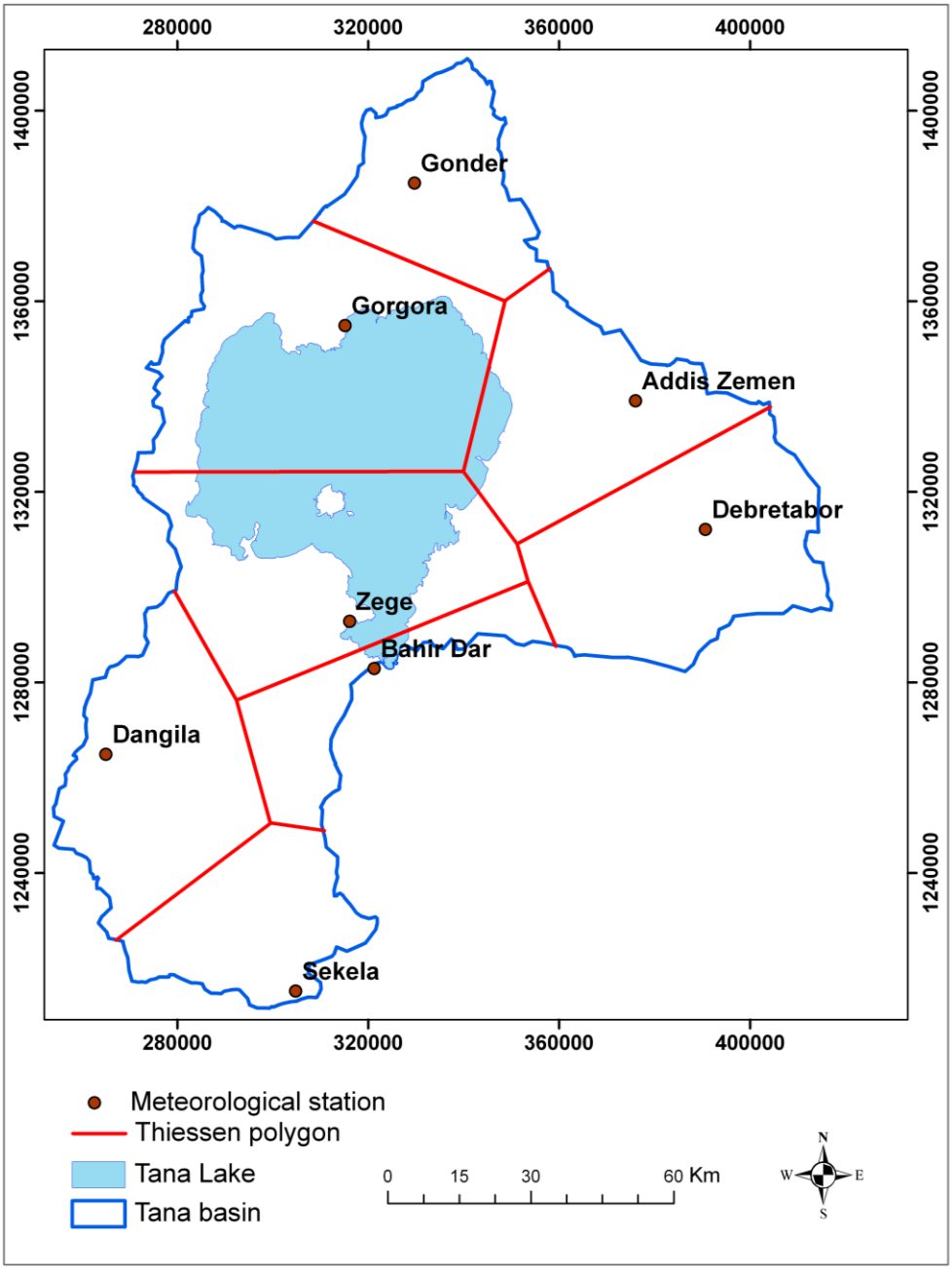

Figure 4.7. Thiessen polygons used to estimate aerial depth of precipitation.

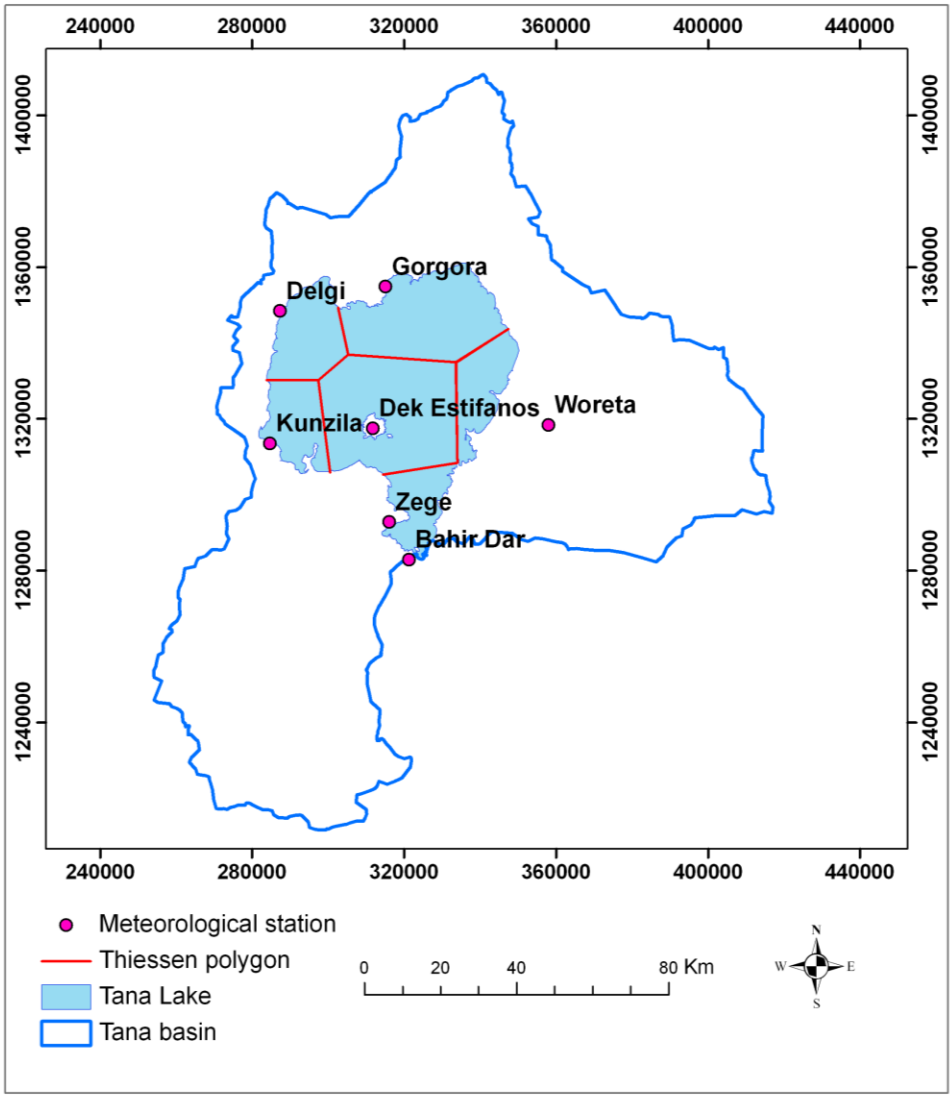

Figure 4.8. Thiessen polygons used to estimate mean precipitation over the Tana Lake.

4.2.3.1. Estimation of reference potential evapotraspiration (ET_o)

The mean monthly reference potential evapotranspiration (ET_o) has been estimated for Bahir Dar, Dangila, Addis Zemene, Gonder, Gorgora and Debretabor stations using Penman-Monteith method (Equation 1) with the help of the FAO (2009) software known as Cropwat version 8.0. FAO Penman-Monteith method is a combination of energy, aerodynamic and surface resistance equations and is given below (FAO, 2009).

$$ET_o = \frac{0.408\Delta(R_n - G) + \gamma(900/T+273)u_2(e_s - e_a)}{\Delta + \gamma(1+0.34\,u_2)} \quad \ldots\ldots\ldots\ldots\ldots\ldots\ldots\ldots\ldots\ldots\ldots\ldots (1)$$

Where,

ET_o = reference evapotranspiration (mm/d)

R_n = net radiation at the crop surface (MJ/m^2d)

G = soil heat flux density (MJ/m^2d)

T = mean daily air temperature at 2m height (ºC)

u_2 = wind speed at 2 m height (km/d)

e_s = saturation vapour pressure (kPa)

e_a = actual vapour pressure (kPa)

e_s-e_a = saturation vapour pressure deficit (kPa)

Δ = slope vaspour pressure curve (kPa/ ºC)

γ = psychrometric constant (kPa/ ºC)

Penman-Monteith equation is appropriate for temperate climate, which describes successfully the most aspects of evapotranspiration of temperate crops. Evaporation from the soil is generally small in temperate region, where as, in semi arid and arid regions crops and vegetations are lacking and soil evaporation dominates than transpiration (Bruin, 1988).

Most part of the study areas have Subtropical (Shrub- savannah), Subtropical (Wooded-savannah), and Temperate (Afro-mountain) climates while other have Subtropical (Savannah), Sub-Afroalpine and Afro-Alpine type of climates. Therefore, this method gives reasonable reference evapotranspiration estimation for the area.

The aerial average monthly reference potential evapotraspiration has then been estimated with the help of Thiessen polygonal method (Table 4.5). Figure 4.9 shows Thiessen

polygons used to estimate the aerially average reference potential evapotraspiration in the basin.

4.2.3.2. Estimation of actual evapotranspiration

Actual evapotranspiration (AET) has been calculated using soil water balance computation (Table 4.5).

4.2.3.3. Estimation of open water evaporation

Open water evaporation (E_{ol}) from the Lake Tana has been estimated using Penman's method. Penman's equation is based on theoretical reasoning, which is a combination of the energy balance and mass transfer approach. It is given as follows (Surbamanya, 2004; Shaw, 1994):

$$E_{ol} = (AH_n + E_a\gamma)/A + \gamma \quad (2)$$

Where,

E_{ol} = mean monthly lake evaporation in mm/year

A = slope of the saturation vapour pressure versus temperature curve at the mean air temperature, in mm of mercury per °C

H_n = net radiation in mm of evaporable water

E_a = parameter including wind velocity and saturation deficit

γ = psychrometric constant = 0.49 mm of mercury per °C

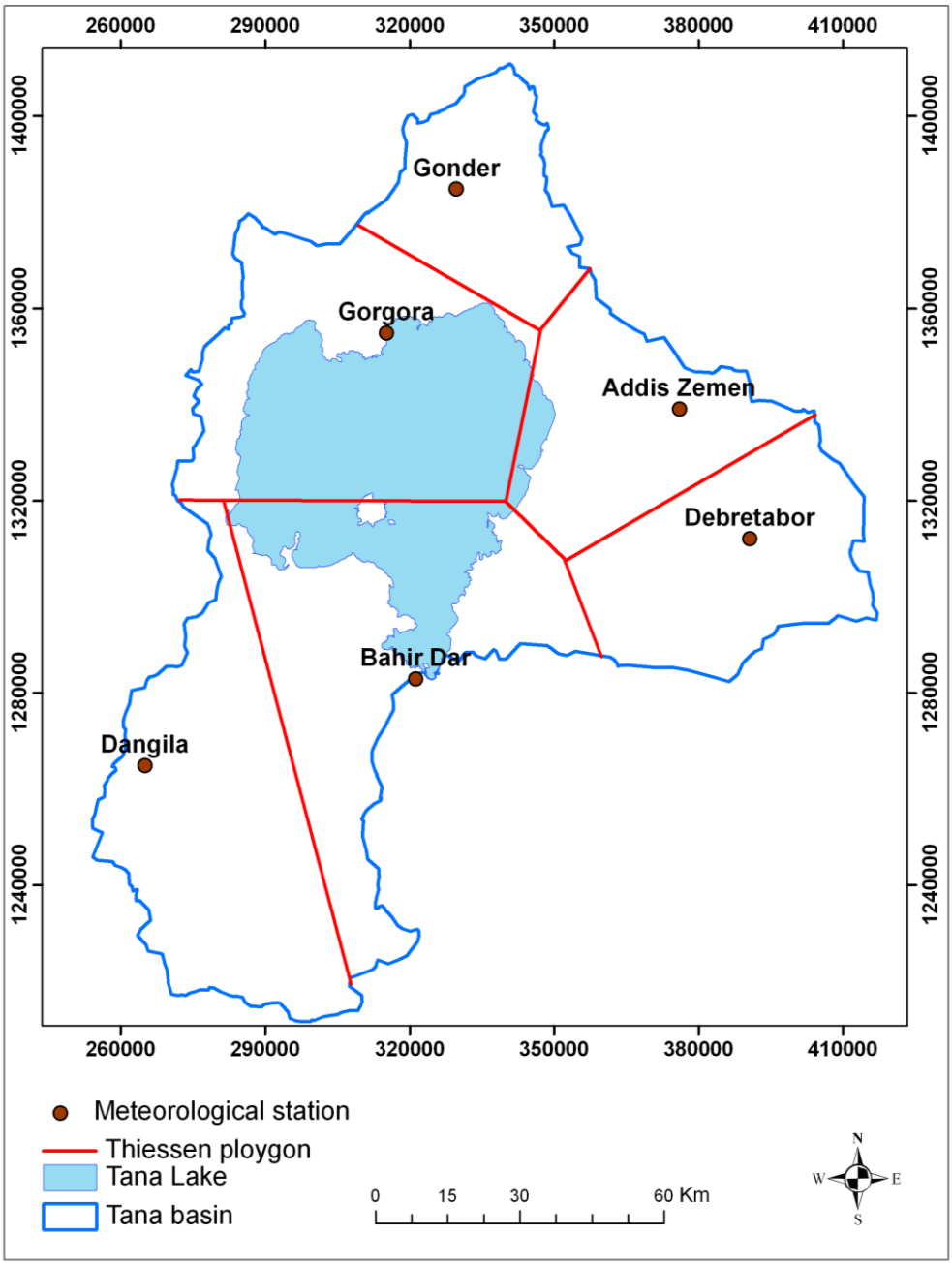

Figure 4.9. Thiessen polygons used for averaging the reference potential evapotratnspiration.

The parameter Hn is estimated as:

$$H_n = H_a(1-r)(a+b\times n/N)-\sigma T^4_a(0.56-0.092e_a^{0.5})(0.10+0.90n/N) \quad \ldots\ldots\ldots\ldots\ldots\ldots (3)$$

Where,

H_a = incident solar radiation out side the atmosphere on a horizontal surface, expressed in mm of evaporable water (a function of the latitude and period of the year)

a= a constant depending upon the latitude Θ and is given by a = 0.29 cosΘ

b = a constant with an average value of 0.52

n = actual duration of bright sunshine in hours

N = maximum possible hours of bright sunshine (a function of latitude)

r = reflection coefficient (albedo) = 0.05 for water surface

σ = Stefan-Boltzman constant = 2.01×10^{-9} mm/day

T_a = mean air temperature in degree Kelvin = 273 + °C

e_a = actual mean vapour pressure in the air in mm of mercury

The parameter E_a is also estimated as given below:

$$E_a = 0.35(0.5 + u_2/160)(e_w-e_a) \quad \ldots\ldots\ldots\ldots\ldots\ldots\ldots\ldots\ldots\ldots\ldots\ldots\ldots\ldots\ldots\ldots\ldots\ldots (4)$$

Where,

u_2 = mean wind speed at 2 m above ground in km/day

e_w = saturation vapour pressure in mean air temperature in mm of mercury

e_a = actual vapour pressure defined earlier

Estimation of the Tana Lake evaporation based on the Penman's method has been done using Bahir Dar and Gorgora meteorological stations data, which are close to the lake.

Open evaporation has also been calculated from mean monthly (1995-2009) Pitche evaporation measurement at Bahir Dar station. A conversion factor of 0.75 (Tenalem Ayenew, 1998) has been used to estimate the lake evaporation. Then, average value of the evaporation rates obtained by Penman's equation and from Pitche evaporation data have been estimated (Tables 4.5 and 4.6) and used for the basin water balance and Tana Lake balance evaluations.

The permanent marsh consists of the Tana Lake water on the surface and groundwater underneath, which are in hydraulic continuity. Hence, open water evaporation is assumed to dominate here and evaporation similar to the Tana Lake (E_{opm}) has been used. Transpiration from grasses may occur but can not be quantified. Isotope data showed that the dominant process in the permanent wetland is evaporation.

Seasonal marshes are also used to form following the inundation of the land by the rise of the Tana Lake and rivers' flood. This marsh often occurs between August and November. Therefore, open evaporation that is similar to the lake is considered during this period while the mean actual evapotranspiration values (E_{osm}) are used for the rest dry months. These data are given in Table 4.5.

4.2.4. Temperature

Monthly maximum and minimum temperatures data (1995-2009) have been obtained for six stations within the study area. The mean monthly temperatures have been calculated for each station. The mean monthly temperature data for Bahir Dar, Dangila, Debretabore and Gonder stations are given in Table 4.7.

Temperature varies in the study area and does not show strict relationship with altitude. The mean annual temperature for these stations vary from the minimum 15.8 °C for Debretabore station to the maximum of 20.6 °C for Gonder station.

4.2.5. Relative humidity, sunshine hours and wind speed

Relative humidity is measured three times a day, which is at 6:00, 12:00 and 18:00 hours. Relative humidity is found to be higher at Dangila station (76.6 %) and lower for Gonder station (51.8 %). Generally, relative humidity is higher during rainy season than dry period in all stations (Table 4.8).

Daily sunshine hours are low during wet season than during dry period in all stations. Bahir Dar station has the highest mean annual daily sunshine hours (8.1 hours) while Debretabore station has the lowest sunshine hours (6.9 hours), see Table 4.8.

Wind speed is measured at 2 m above the ground surface. The highest wind speed (133.7 km/d) is seen for Gonder station and the lowest (54 km/d) is for Bahir Dar station. Wind speed is generally high during summer season in all stations.

Long term mean monthly relative humidity, sunshine hours and wind speed data for four selected stations are given in Table 4.8.

Table 4.6. Open water evaporation (E_o) data calculated based on Penman's equation and Pitche evaporation (in mm).

	Jan	Feb	Mar	Apr	May	Jun	Jul	Aug	Sept	Oct	Nov	Dec	Annual
E_o, penman (Bahir Dar)	131	137	153	233	165	58	123	123	135	85	127	109	1580
E_o, pitche (Bahir Dar)	110.3	133.7	162.3	165.5	139.1	81.1	49.4	47.9	57.9	83.8	104.4	110.2	1245.6
E_o, penman (Gorgora)	145.7	166.3	189.0	177.0	174.2	147.8	109.6	109.3	148.3	156.7	144.8	137.4	1806.1
E_o, average	129.0	145.7	168.1	191.8	159.4	95.6	94.0	93.4	113.7	108.5	125.4	118.9	1543.9

Table 4.7. Mean monthly temperature of four selected stations (in °C).

	Jan	Feb	Mar	Apr	May	Jun	Jul	Aug	Sep	Oct	Nov	Dec	mean annual
Bahir Dar	18.1	19.9	21.3	23.0	22.2	20.9	19.3	19.4	19.8	20.1	19.1	18.5	20.1
Dangila	15.2	17.2	18.2	19.2	18.9	17.6	16.8	16.8	16.9	16.6	15.7	15.1	17.0
Debretabor	15.5	16.9	17.6	18.2	17.4	16.3	14.3	14.4	14.8	14.9	14.8	14.8	15.8
Gonder	20.1	21.9	22.8	23.4	22.6	20.1	18.5	18.6	19.4	19.8	20.2	20.0	20.6

Table 4.8. Relative humidity, sunshine hours and wind speed for selected stations.

Parameter	Station	Jan	Feb	Mar	Apr	May	Jun	Jul	Aug	Sep	Oct	Nov	Dec	Mean	max	Min
Relative	Debretabore	45.4	40.4	44.5	44.1	45.7	73.9	85.0	85.5	80.2	69.1	58.9	50.8	60.3	85.5	40.4
Humidity	Dangila	70.7	60.8	59.7	61.2	77.3	85.1	89.2	88.9	86.9	86.1	80.1	73.1	76.6	89.2	59.7
(%)	Bahir Dar	52.5	45.2	43.7	44.6	52.5	69.6	77.0	80.1	74.2	66.1	59.3	54.7	59.9	80.1	43.7
	Gonder	35.2	32.8	32.4	37.0	45.8	65.7	77.2	77.5	69.9	59.7	46.6	41.6	51.8	77.5	32.4
Sunshine	Debretabore	8.1	9.1	8.7	8.1	6.8	5.5	2.3	2.2	6.1	8.7	8.9	8.6	6.9	9.1	2.2
hours	Dangila	9.5	9.2	8.5	8.5	7.9	6.4	4.4	4.4	6.2	6.8	8.5	8.9	7.4	9.5	4.4
	Bahir Dar	9.8	9.9	9.0	9.0	8.5	7.0	4.8	4.5	6.6	8.7	9.7	10.0	8.1	10.0	4.5
	Gonder	9.5	9.2	8.4	7.6	7.1	5.2	4.3	4.7	7.2	7.7	8.8	9.0	7.4	9.5	4.3
Wind	Debretabore	100.5	110.0	111.5	117.8	117.8	111.5	98.2	109.2	100.5	79.3	84.8	96.6	103.2	117.8	79.3
speed	Dangila	86.4	100.4	105.8	110.2	112.3	109.1	104.8	100.4	176.0	73.4	62.6	68.0	100.8	176.0	62.6
(km/d)	Bahir Dar	43.5	48.5	58.0	68.3	61.2	63.5	54.7	54.9	51.8	53.4	48.5	42.2	54.0	68.3	42.2
	Gonder	140.0	151.2	155.5	149.5	159.8	163.3	116.6	103.7	117.5	108.9	117.5	121.0	133.7	163.3	103.7

4.3. Hydrology

4.3.1. Rivers

The Lake Tana basin is drained by a number of perennial and seasonal streams and rivers. In general, eleven sub-basins can be identified in the Lake Tana basin (Fig. 4.10). All streams and rivers flow into the lake. The main ones include Gilgel Abay, Rib, Gumara and Megech sub-basins. They account to 75.6% of the drainage basin. Surface outflow from the lake is only through the Abay or the well known Blue Nile River. Areas of sub-basins are shown in Table 4.9.

River inflow to the lake has been gauged at 10 sites in the different rivers (Fig. 4.10). Daily rivers discharge data (1995-2009) have been collected from the Ministry of Water, Irrigation and Energy and used to analyze the groundwater baseflow and surface water components.

River inflow to the Tana Lake from gauged catchments has been estimated using the eight hydrological stations, excepting Amen and Gelda stations, in annual basis, which are showen in Table 4.9. Amen station is within the Gilgel Abay sub-basin.

However, there is also surface water inflow to the lake from un-gauged catchments. The ungauged catchment accounts to 44.6% of the total catchment area. The un-gauged surface runoff has been estimated using runoff coefficient of 0.314 (Section 4.3.5) multiplied by the annual aerial average precipitation (1400.4 mm/year) and the total un-gauged catchment area of 5134.1 km^2 (Table 4.10).

The mean monthly surface water outflow of Lake Tana basin is through the Abay River (gauged), which is also given in Table 4.10.

Table 4.9. Area of sub-basins.

Sub-basin	Gelda	Gumera	Ribb	Megech	Dirma	Escarpment	Gilgel Abay	Gemero	Garno	Sew Gedel	Gabikura
Area (km^2)	350.7	1624.3	2007.8	756.1	434.9	495.7	4527.3	587.4	484.7	315.1	204.2

Table 4.10. Mean gauged and ungauged total runoff (hm3/year).

Streams	Gilgel Abay	Kilty	Dirma	Gumera	Ribb	Gelda	Garno	Gemero	Megech	Ungauged runoff	Abay River
Discharge	1691.4	276.5	235.5	1208.4	493.4	49.0	26.5	48.2	227.4	2260	4733.4
Calculated gauged area (km^2)	1946.7	595.3	377.0	1189.7	1704.5	35.6	102.2	184.4	518.6	5134.1	14845.5

4.3.2. Tana Lake and Reservoirs

Tana Lake, Angereb and Koga reservoirs are found within Tana basin. Morphometric parameters of the lake and reservoirs are given in Table 4.11.

Table 4.11. Morphometric characteristics.

Water body	Mean depth (m)	Area (km^2)	Volume (hm^3)
Tana Lake	9	3057.4	27516.6
Koga reservoir	4.8	17.4	81.3
Angereb reservoir	12.3	0.43	5.3

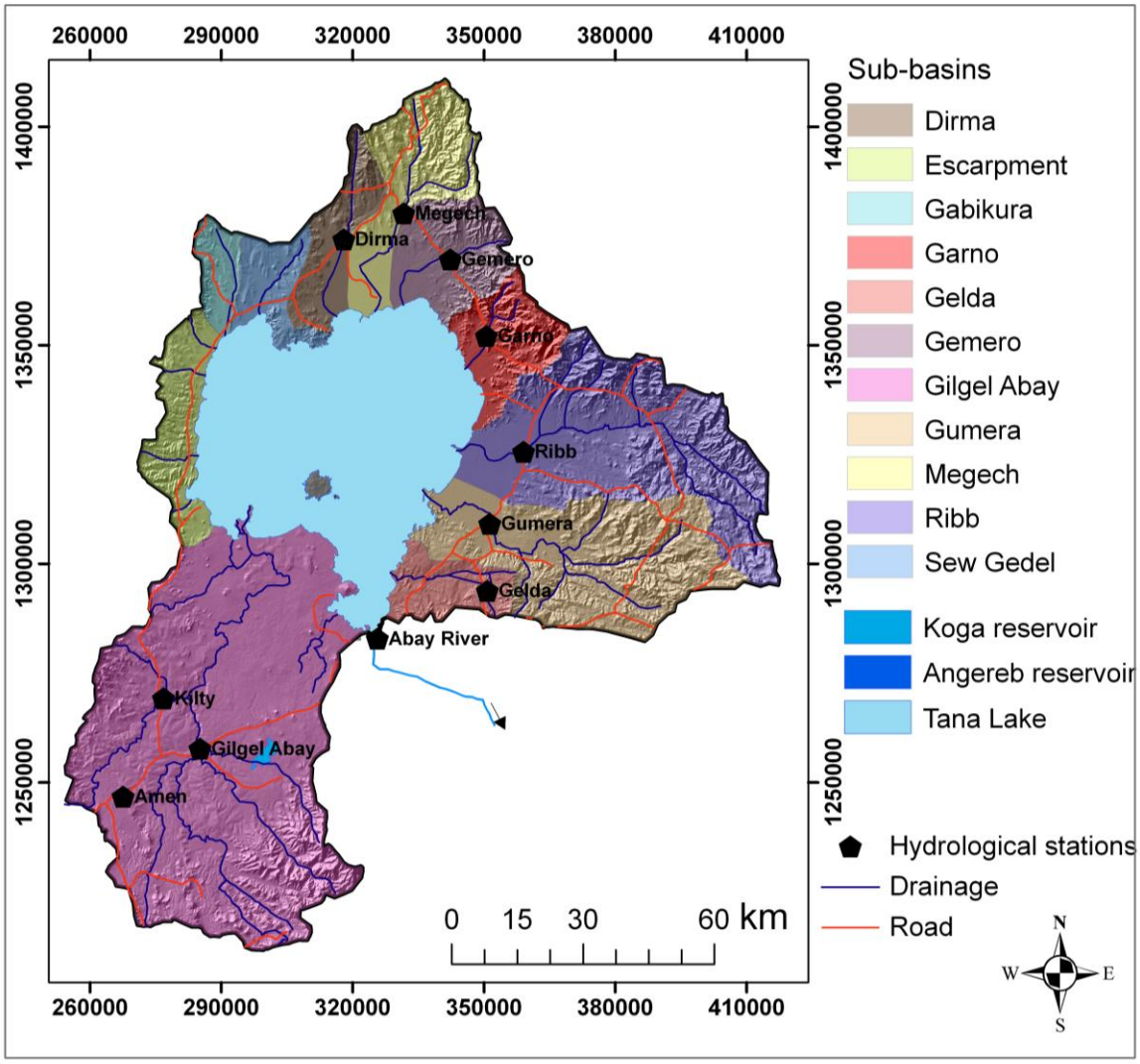

Figure 4.10. Sub-basins in the area.

Water level of Tana Lake varies within one meter amplitude from the mean starting from 1980 to 2008 (Fig. 4.11). A one meter variation in the Tana Lake water level results to negligible area variation compared to its large area (Seifu Kebede et al., 2005). Relatively higher lake level rise has been observed between 1994 and 1999. Then, the lake level declined between 1999 and 2004, which is due to the construction of Chara diversion weir at the out let of the lake to augment the dry season outflow to regularly supply water

for the Tis Abay hydroelectric power development. The lake tends to rise between 2004 and 2008.

4.3.3. Wetland

Perennial marsh that exist through out the year and seasonal marsh that occur between August and November because of river food pools and inundation by the lake water during the rainy summer are found in the basin within lacustrine sediments. They cover an area of about 11.9 and 382.1 km^2, respectively (Fig. 2.5 and Table 2.1).

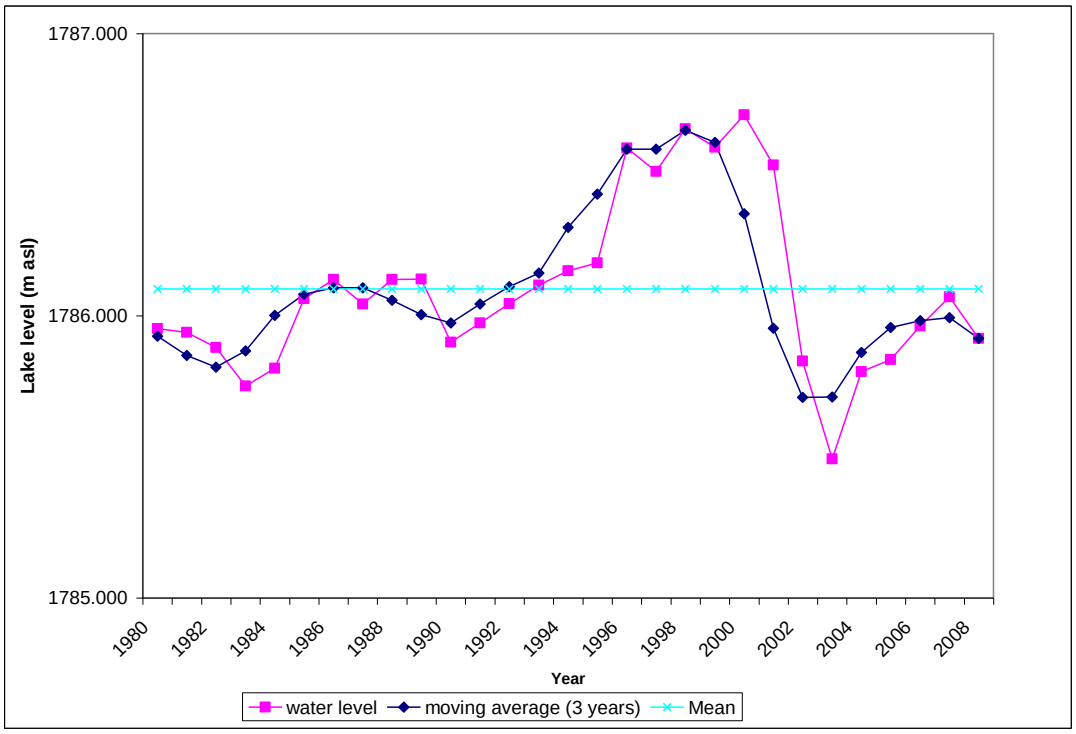

Figure 4.11. Trends of water level for Tana Lake.

4.3.4. Baseflow analysis

River hydrograph consists of surface runoff, interflow, groundwater baseflow and channel precipitation. Interflow includes quick or rapid and delayed components, which used to discharge to streams soon in the soil and after long time in the intermediate or subsurface zones, respectively. Interflow and the contributions from the precipitation are usually taken lumped to surface runoff during hydrograph separation and referred here as direct runoff (DRO).

The main purpose of baseflow analysis is to estimate the mean rate of groundwater recharge or discharge as baseflow (Rutledge and Mesko, 1996). Baseflow separation method is applied here over long period of hydrological records so that the effect of change in storage can be considered negligible. Baseflow separation has been done using 15 years (1995-2009) daily streams flow data at 9 hydrological stations that are situated at different parts of the basin.

Baseflow indices (BFI), which is baseflow divided by total river runoff, have been estimated for each station and period used. In case where there is year with missing data of more than 3 months, it is omitted and BFI have been estimated separately for the different consecutive periods for a given station. Weighted mean BFI by the number of years used is then calculated for the station using all the data sets (Table 4.12). The following formula was used to calculate the BFI.

$$BFI\_M = \sum(BFI\_i \times Years\_i)/\sum Year\_i \ldots\ldots\ldots\ldots\ldots\ldots\ldots\ldots\ldots\ldots\ldots\ldots\ldots\ldots\ldots (5)$$

Where,

BFI_M: average BFI for entire analysis period

BFI_i: BFI in a single data period

Years_i: Number of years for the single data period

River Analysis Package software (RAP) developed by Monash University Melbourne (Australia) and Lyn-Hollick (1979) digital filter algorithm have been used to estimate the BFI.

Lyn-Hollick algorithm is given as follows:

$$q_t = \alpha \times q_{t-1} + (1+\alpha)/2 \times (Q_t - Q_{t-1}) \quad \ldots\ldots(6)$$

Where,

Q_t = stream flow at time step t

q_t = direct runoff at time step t

α = filter parameter associated with the catchment

The purpose of the filter is to create a relatively smooth transition from period of baseflow before a storm event to the usually elevated baseflow following the storm event (Marsh et al., 2003). The Lyn-Holick digital filter has one parameter, which is the α value. Grayson et al (1996) recommended a value of 0.975 for α (Marsh et al., 2003). This filter parameter value has been found appropriate and adapted in this analysis, and gave reasonable hydrograph separation.

The total river flow has been partitioned into baseflow and direct runoff using BFI values of each station. Direct runoff has been estimated as a product of one minus BFI and the total river runoff. Baseflow indices, direct runoff and specific discharge of each station are given in Table 4.12. BFI slightly varies from place to place. The maximum (0.41) and the minimum (0.21) BFI values are estimated for Garno and Gemero rivers' stations, respectively.

Furthermore, the specific groundwater discharge (base flow/area) show minor variation in the basin. The maximum (1.2 mm/km^2) was found for Garno river station while the minimum (0.05 mm/km^2) is for Rib river station. Variation in BFI and specific discharges among sub basins can be attributed to variation in the geomorphology, hydraulic

characteristics (aquifers storage and hydraulic conductivity) of the formations covering the catchment area and due to variation in the effective precipitation over the gauged catchment. Ribb station has wide plain area in lacustrine clayey sediments that has low permeability and effective precipitation, which reduce the groundwater recharge and baseflow.

Spatial distribution of the specific discharge is depicted in Figure 4.12. Plot of specific discharge versus BFI (Fig. 4.13) shows positive correlation with R^2 equals to 0.5. Gelda station has small area in lower topography but has exceptionally the highest total runoff and specific discharge than other stations when compared to its area although its BFI value is low. This may indicate that the data is subject to error and it was rejected from further analysis. Dirma station has no sufficiently long period records for baseflow analysis and was not used. Figures 4.14a&b show the total and groundwater baseflow hydrographs for Gilgel Abay and Gemero rivers' stations, respectively.

Table 4.12. Mean (1995-2009) BFI and specific discharge values of gauged catchments in the basin.

Station	BFI	Total flow (hm^3/year)	Base flow (mm/year)	Area (km^2))	Specific discharge (mm/km^2)
Ribb	0.282	493.4	81.6	1704.5	0.05
Megech	0.333	227.4	146.0	518.6	0.28
Kilty	0.305	276.5	141.7	595.3	0.24
Amen	0.296	22.7	75.5	89	0.85
G/Abay	0.326	1691.4	283.3	1946.7	0.15
Garno	0.414	26.5	107.3	102.2	1.05
Gelda	0.276	49.0	379.8	35.6	10.67
Gemero	0.21	48.2	54.9	184.4	0.30
Gumera	0.289	1208.4	293.5	1189.7	0.25

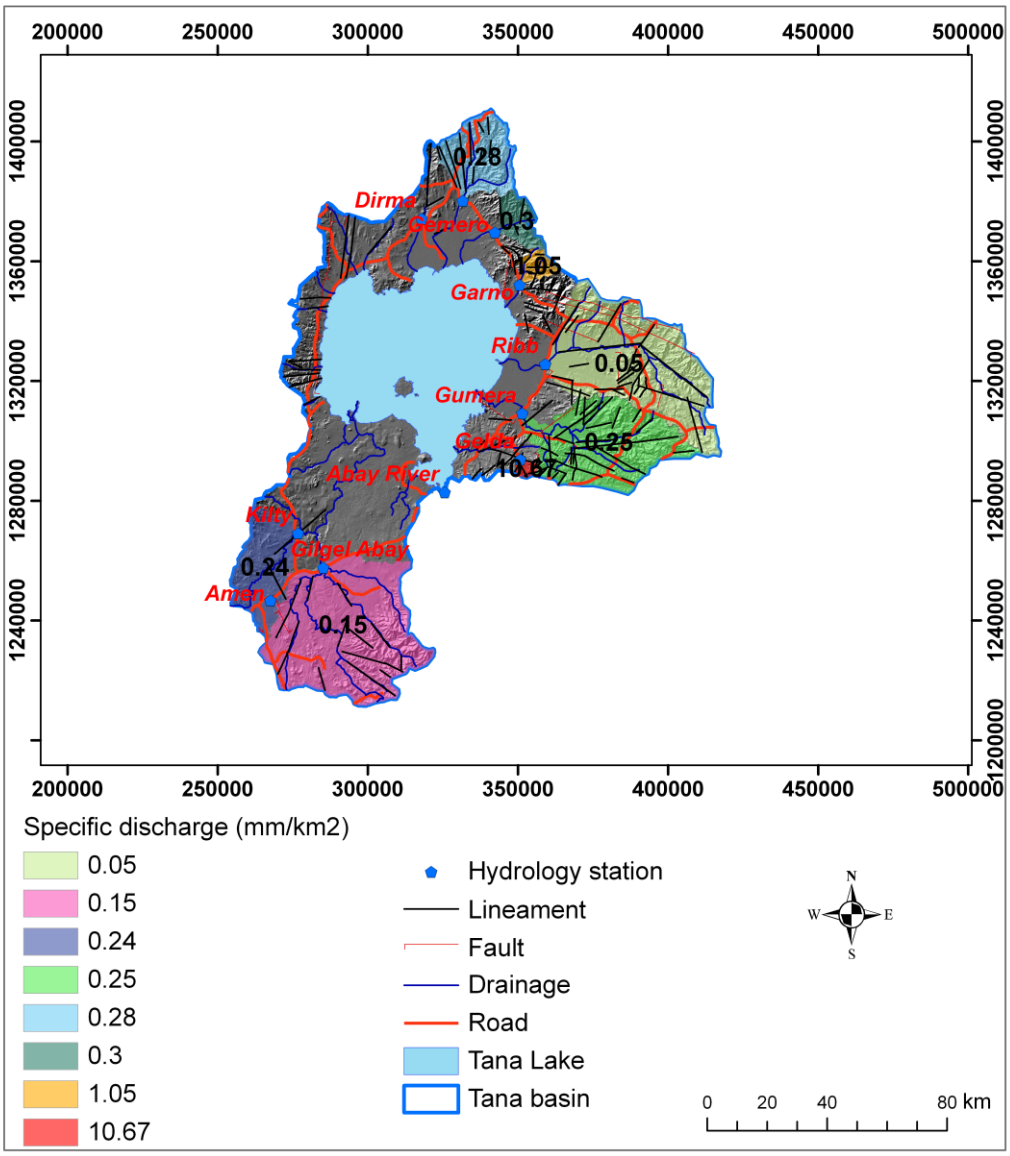

Figure 4.12. Map showing the specific discharge values of gauged catchments.

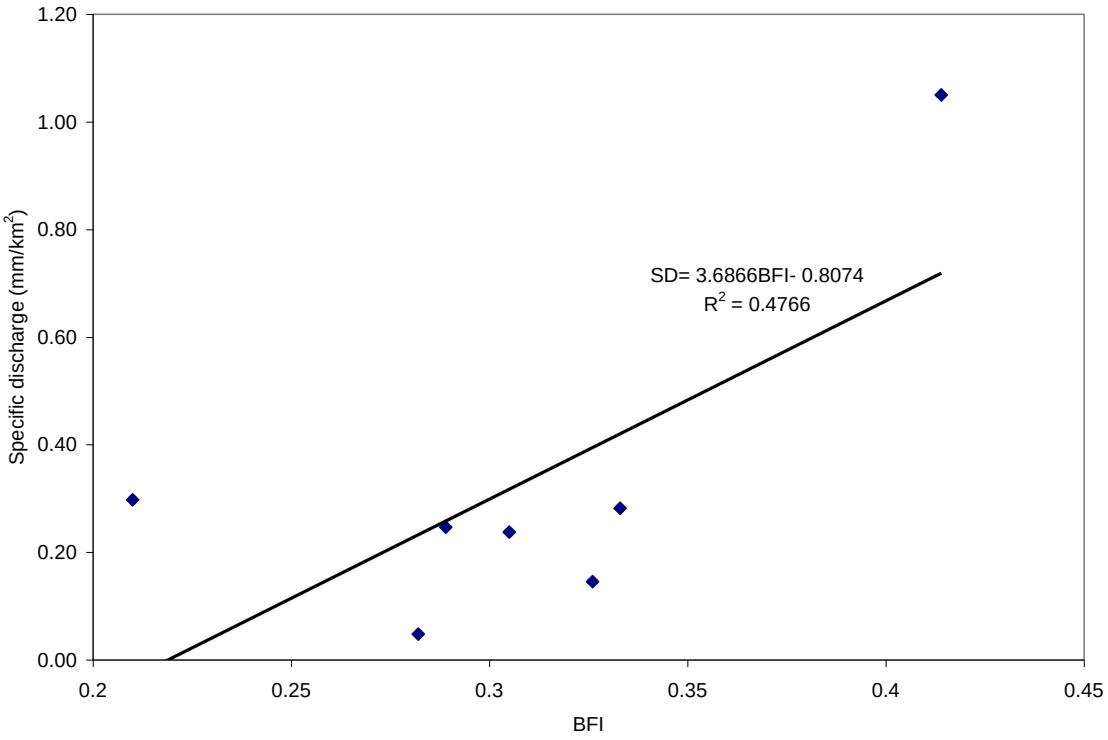

Figure 4.13. Plot of specific discharge (SD) versus BFI.

(a)

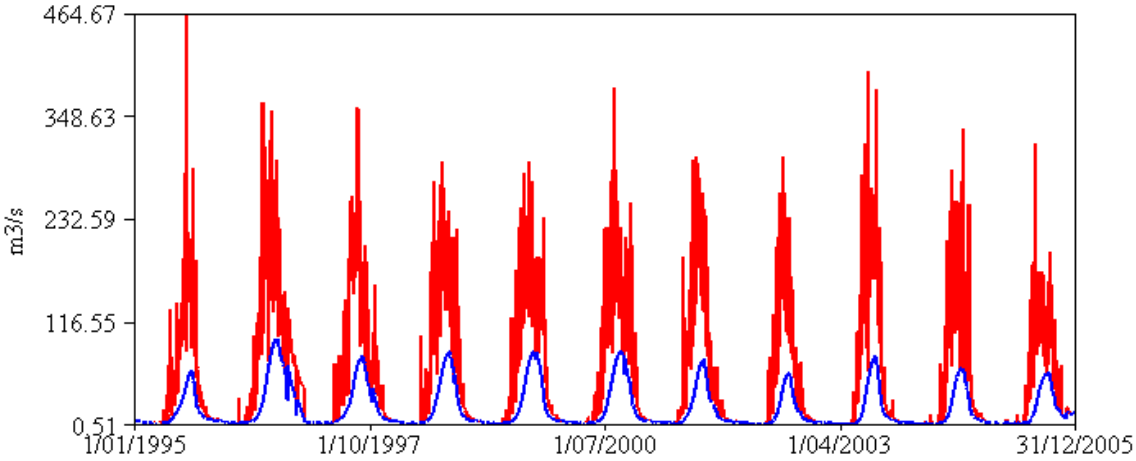

(b)

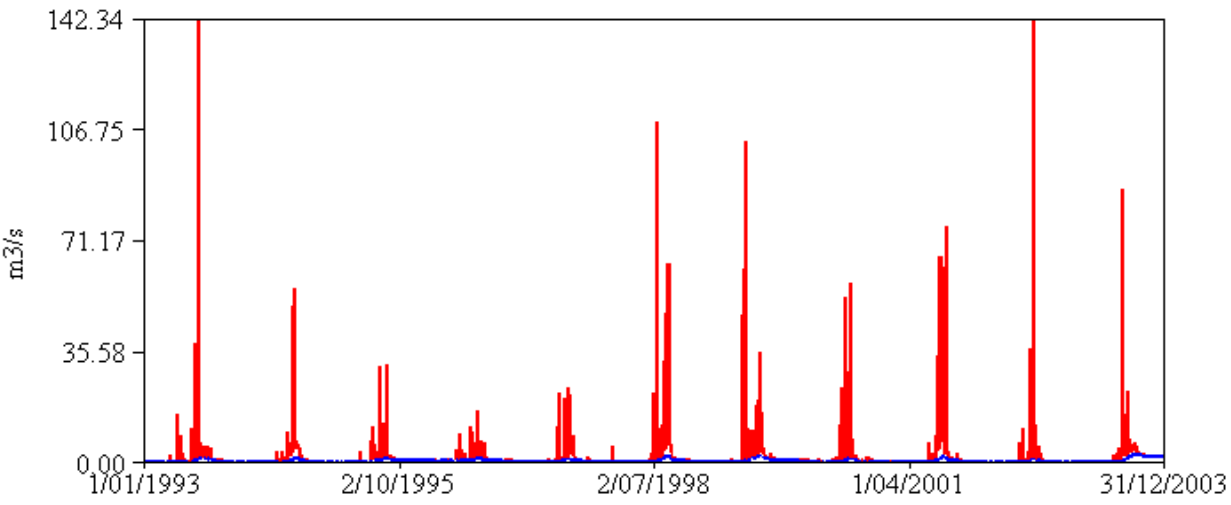

Figure 4.14. The total and groundwater baseflow hydrographs for a) Gilgel Abay b) Gemero stations. Red and blue lines show the total and groundwater baseflow hydrographs, respectively.

4.3.5. Estimation of runoff coefficient

The total rivers' runoffs have been partitioned as baseflow and direct runoff for each station. Then, the weighted (by stations areas) mean direct runoff has been estimated to be 440.7mm/year (Table 6.1).

The mean basin precipitation has been calculated based on Thiessen polygonal averaging method (Section 4.2.2.3) to be 1400.4 mm/year.

The mean basin runoff coefficient is estimated as quotient of the mean annual direct runoff and the aerial average annual basin precipitation to be 0.314.

5. HYROGEOLOGY

5.1. General

The water bearing or hydraulic characteristics of volcanic rocks are determined by their primary and secondary porosities as well as their openness and interconnections.

The top and lower vesicular and braciated parts of the individual flow of the formation, lava tubes and inter flow zones are porous and permeable, which favor horizontal flow. The middle part of the flow (entablature) generally contains columnar joints and favor vertical flow. However, if the entablature is totally massive, it may act as regional confining unit.

Tectonic structures enhance the porosity and permeability of volcanic rocks. The presence of pyroclastic inter layers also enhance the over all porosity and groundwater storage in volcanic aquifer systems. Alluvial and lacustrine deposits between lava flows are also important aquifers in volcanic terrain. Paleosol may acts as an aquifer or confining unit depending on the texture of the soil.

In regional flow systems, aquifers and confining units are defined using the concept of hydrostratigraphic unit (Andresson and Woessner, 1991; Weight, 2008). Several geologic or stratigraphic formations may be combined into a single hydrostratigraphic unit based on their similar hydrogeologic properties, or a single startigraphic formation may be divided into aquifers and confining units.

The different volcanic rocks and unconsolidated sediments that form three multi layers aquifer systems (upper, intermediate and lower aquifer systems; see Section 11.1) have been classified into different hydrostratigarphic units based on their field hydraulic properties, borehole and spring yields and pumping test data (transsmissivity). Furthermore, topographic setting and recharge conditions have been considered to evaluate the productivity of hydrostratigarphic units.

Hydrostratigraphic units have been grouped based on whether the groundwater flow is in porous or fracture dominated media as intergranular and fracture aquifer categories and aquitards.

Intergranular aquifer: groundwater is stored in and flow through pores of unconsolidated sediments. Guna Tuff and lacustrine sediments are categorized to this aquifer group.

Fracture aquifer: groundwater is stored in and flow through the weathered and fractured parts of the volcanic rocks and through primary flow features like vesicles and breccia, etc. The Tertiary and Quaternary volcanic rocks are classified to this aquifer groups. These volcanic rocks formed stratified multi layered aquifer systems, which are confined at depth by massive layers and/or paleosols.
Aquitard: groundwater stored in and flow via these rocks is minor to be considered as an aquifer. Quaternary rhyolite and trachyte plugs are grouped as an aquitard.

Each intergranular and fracture aquifers are ranked based on their productivity using the following criteria (Table 5.1).

Table 5.1. Aquifer classification criteria (After, Geoffery and Gall, 1991).

Aquifer Productivity	Transsmissivity (m^2/day), mean	Yield (l/s), mean
Very high	>500	>25
High	100-500	5-25
Moderate	50-100	2-5
Low	10-50	0.5-2
Very Low	1-10	0.05-0.5
Aquitard	< 1	< 0.05

Extensive aquifer: when the area is greater than 100 km^2.

Most boreholes only have yield and drawdown data while only few boreholes have pumping test data. Specific capacity has been estimated from borehole yield and draw down data. Then, transsmissivity is deduced using the Logan (1962) empirical equation, which is given below.

$$T = 1.22 \times SC \quad \text{(7)}$$

Where, T is transsmissivity and SC is specific capacity

Few available pumping test (constant and recovery tests) data has been analyzed using aquifer test pro version 4.2. Types of aquifer and analysis methods have been selected based on the diagnostic curves and lithological logs, and depths of water strikes and static groundwater levels. Consequently, transsmissivity and storativity have been deduced by the software.

Location of groundwater points have been shown in Figure 5.1 and the data are presented in Appendix1.

5.2. Hydrostratigraphic Units and Aquifer Characterization

Geological formations have been grouped into different hydrostratigraphic units based on their hydraulic properties as follows. Figure 5.2 shows the hydrogeological map of the area, and Figures 5.3a-c are the hydrogeological cross sections at indicated lines.

5.2.1. Intergranular Aquifers

5.2.1.1. Extensive and low to moderate productive intergranular aquifer

Aquifer associated with lacustrine sediments is classified to this aquifer group. Lacustrine sediments consist of unconsolidated sediments of clay at the top. No lithological logs are available to see the vertical facial changes. However, bedded tuff inter bedded with mud stone, and alternations of sand with clay at eastern part of the plain have been observed.

Borehole depth in this aquifer varies from 45 to 118 m. The mean and median depths are 72 and 60 m. Yield of boreholes varies from 2 to 6 l/s, with a mean and median of 3.4

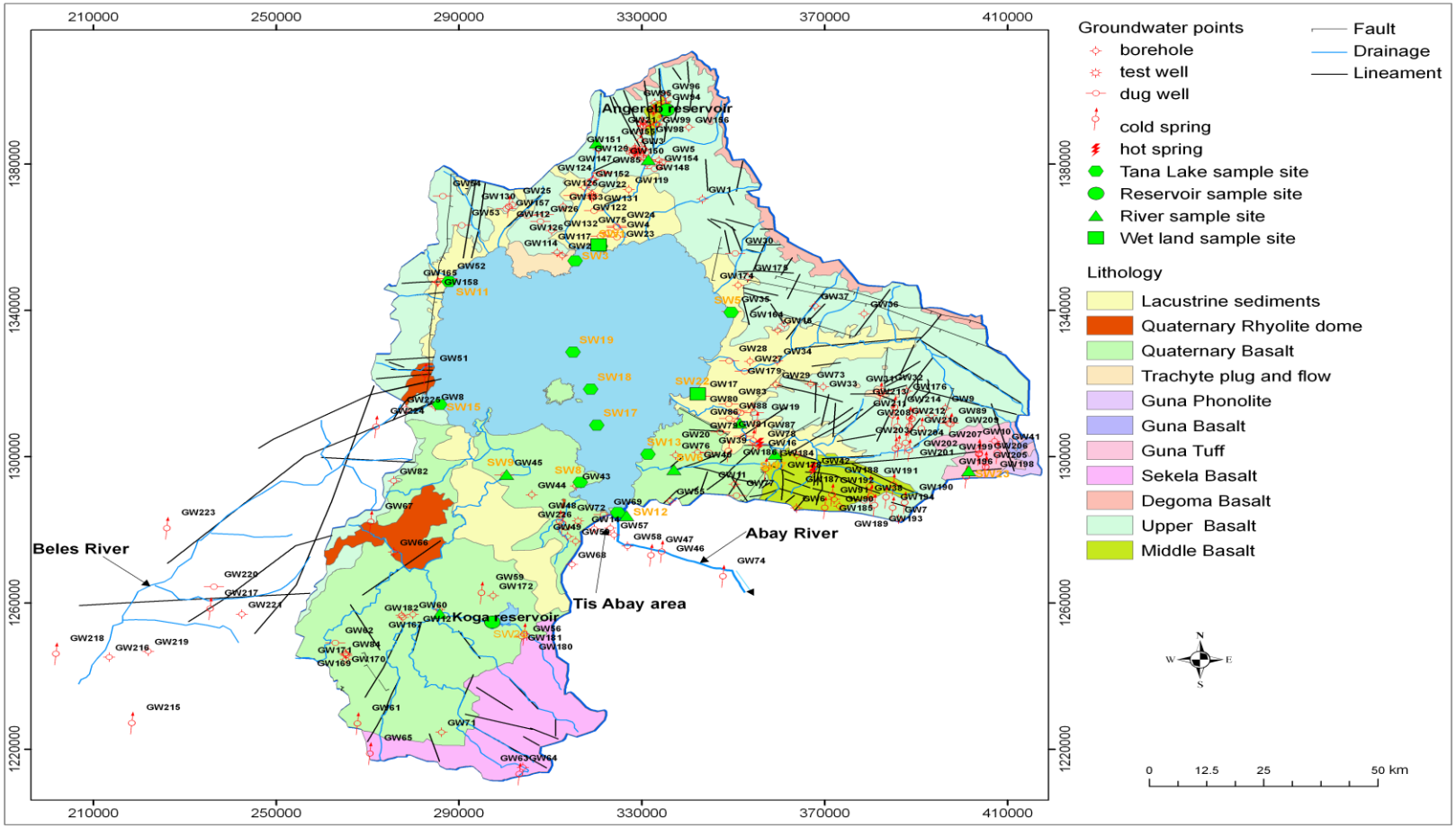

Figure 5.1. Groundwater and surface waters points inventoried and used in data analysis.

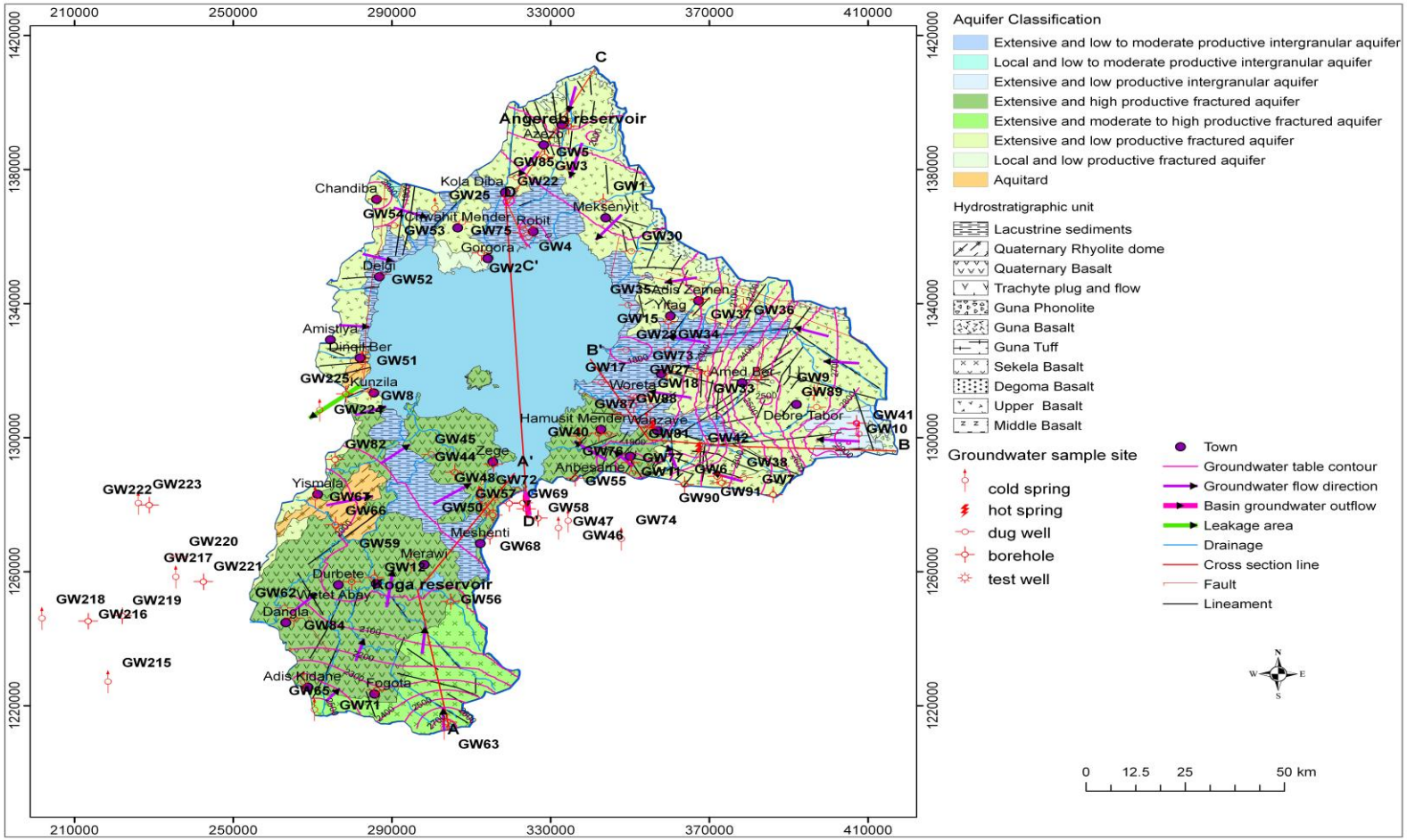

Figure 5.2. Hydrogeological map of the area.

(a)

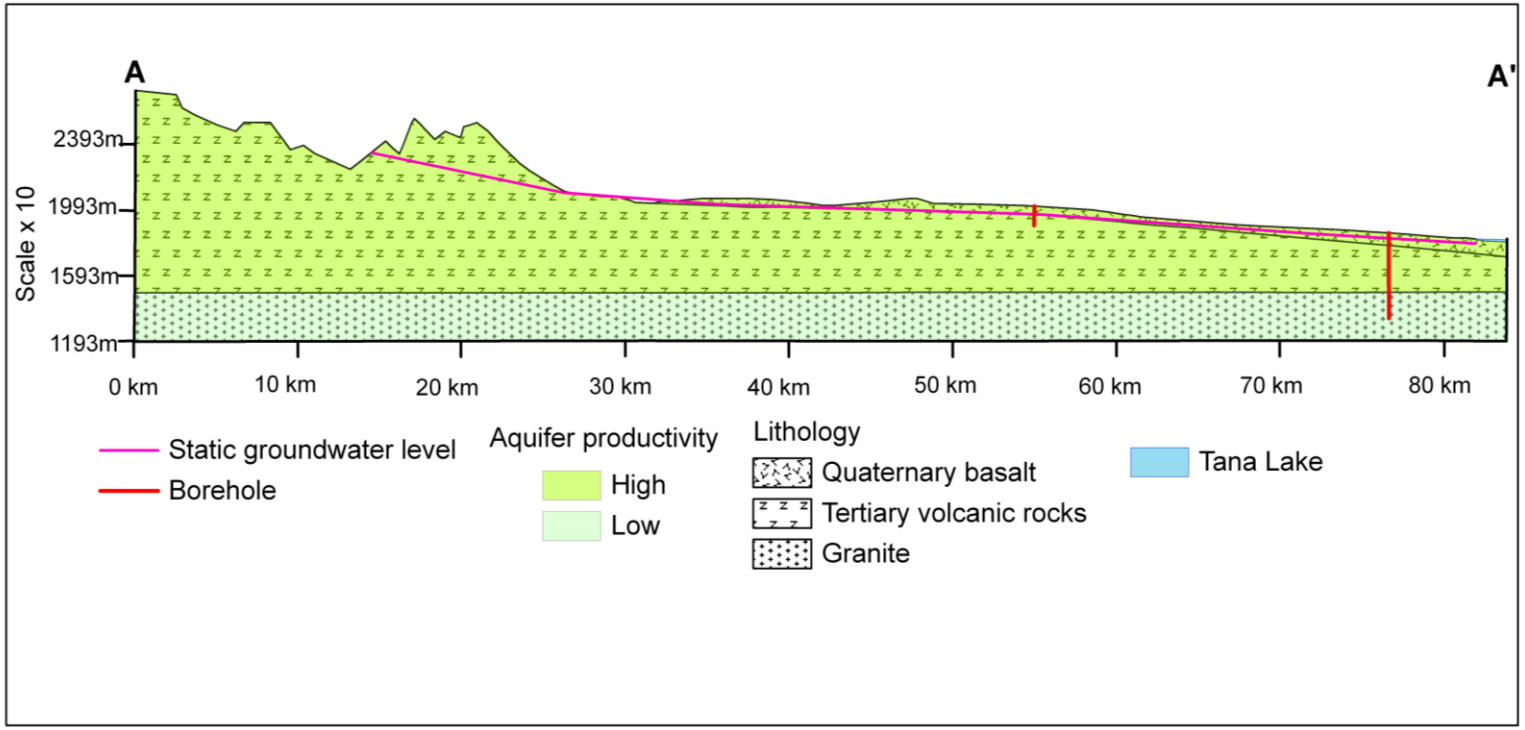
A
A'
2393m
1993m
1593m
1193m
Scale x 10
0 km
10 km
20 km
30 km
40 km
50 km
60 km
70 km
80 km
Static groundwater level
Borehole
Aquifer productivity
High
Low
Lithology
Quaternary basalt
Tertiary volcanic rocks
Granite
Tana Lake

(b)

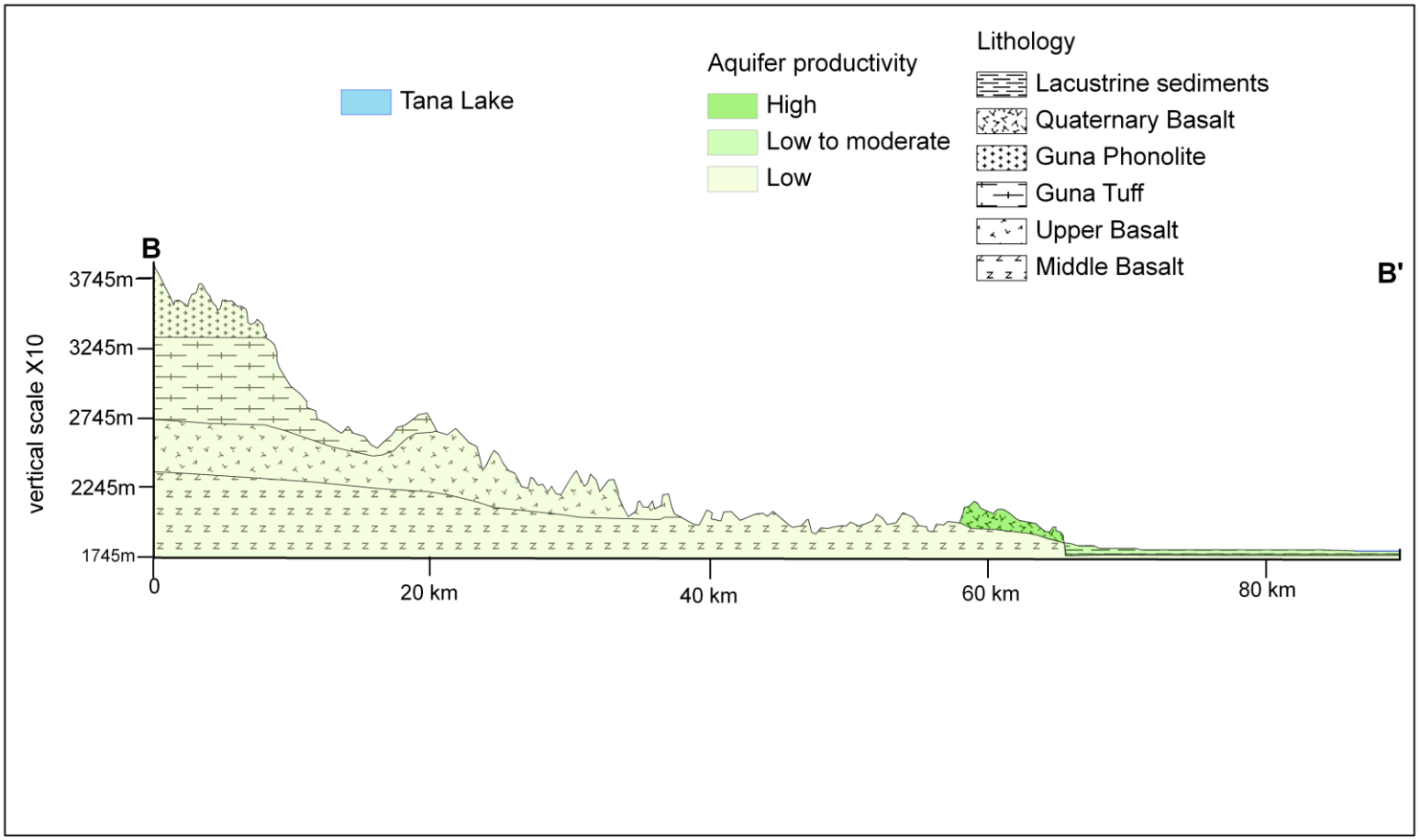
Tana Lake
Aquifer productivity
High
Low to moderate
Low
Lithology
Lacustrine sediments
Quaternary Basalt
Guna Phonolite
Guna Tuff
Upper Basalt
Middle Basalt
B
B'
vertical scale X10
3745m
3245m
2745m
2245m
1745m
0
20 km
40 km
60 km
80 km

(c)

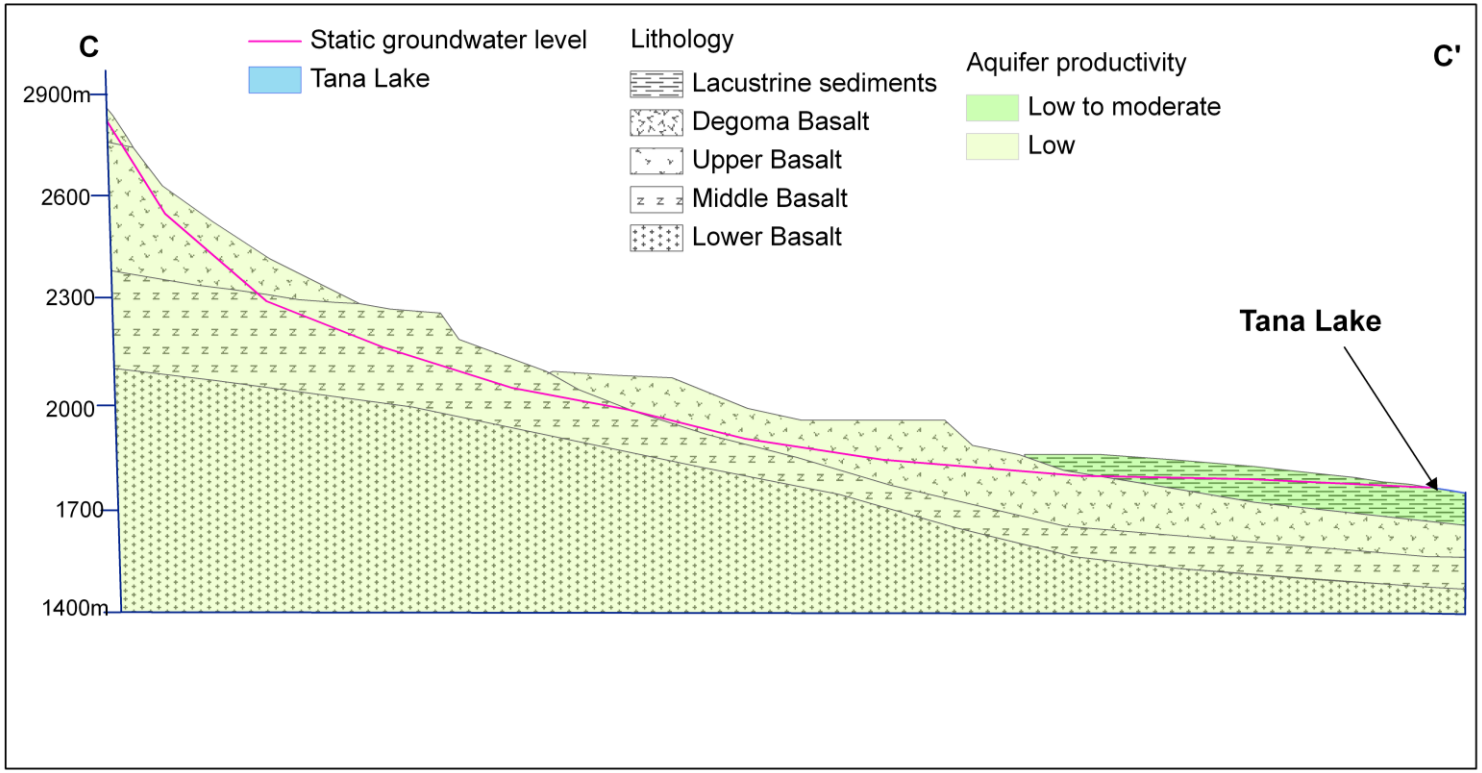

Figure 5.3. Hydrogeological cross sections along a) A-A', b) B-B', c) C-C'. The lines are indicated in Fig. 8.2. Vertical exaggerations are indicated at title of vertical axes.

and 2.8 l/s. Transsmissivity varies from 2.1 to 34.8, and a mean and median of 16.9 and 13.7 m^2/d. However, transsmissivity data are very few. Static groundwater level data varies from 3.5 to 20 m, with a mean and median values of 8.6 and 5.5 m (see Table 5.2 and Figs. 5.4a-d).

Table 5.2. Hydraulic data of lacustrine sediments aquifers.

Parameters	mean	median	max	min	number
Spring yield (l/s)			2		
Borehole yield (l/s)	3.4	2.8	6	2.0	8.0
Transsmissivity (m^2/d)	16.9	13.7	34.8	2.1	3.0
Static groundwater level (m)	8.6	5.5	20	3.5	10.0
Borehole depth (m)	72.0	60.0	118	45.0	10.0

(a)

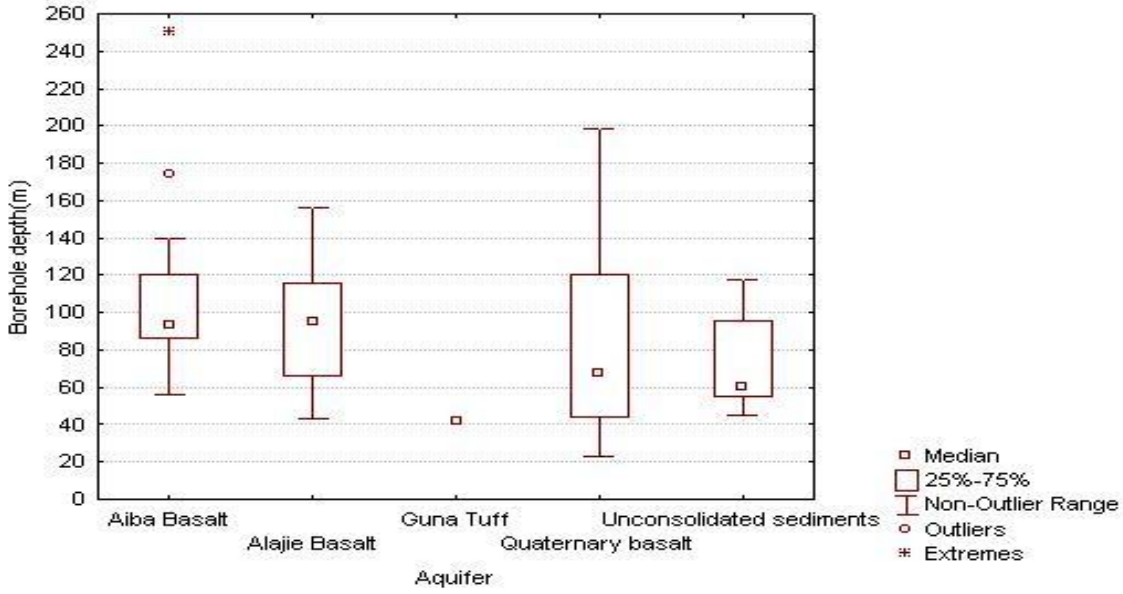

(b)

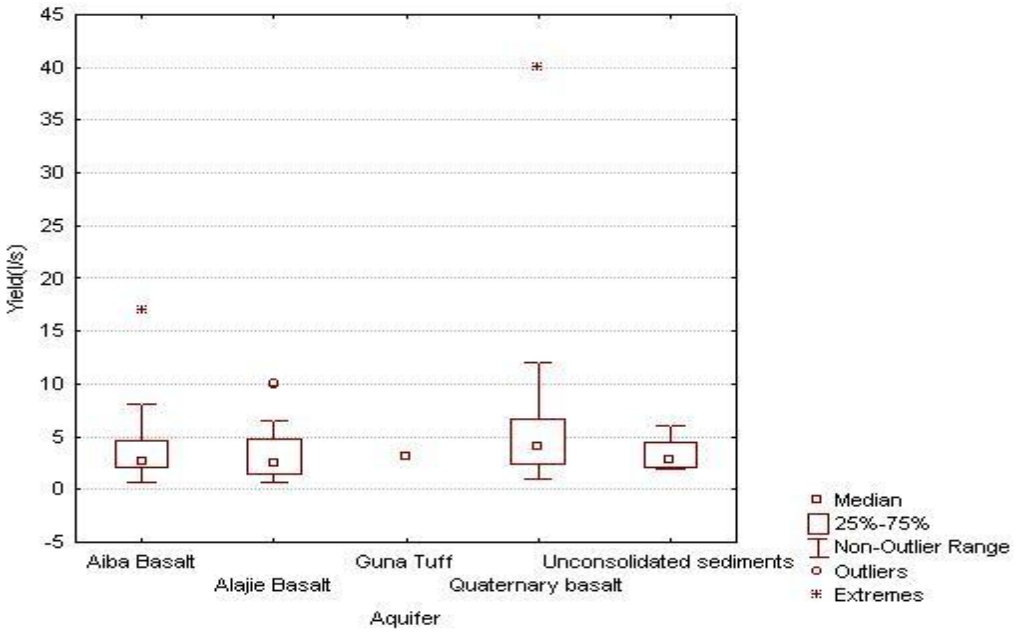
45
40
35
30
25
20
15
10
5
0
-5
Yield(l/s)
Aiba Basalt
Alajie Basalt
Guna Tuff
Quaternary basalt
Unconsolidated sediments
Aquifer
Median
25%-75%
Non-Outlier Range
Outliers
Extremes

(c)

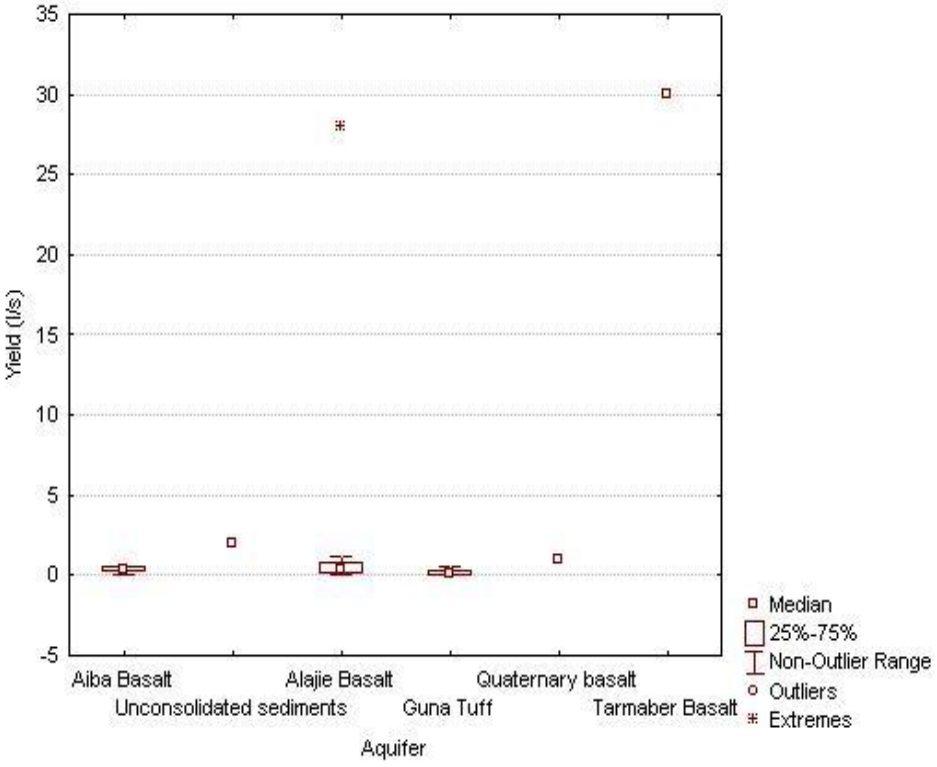
35
30
25
20
15
10
5
0
-5
Yield (l/s)
Aiba Basalt
Alajie Basalt
Quaternary basalt
Unconsolidated sediments
Guna Tuff
Tarmaber Basalt
Aquifer
Median
25%-75%
Non-Outlier Range
Outliers
Extremes

(d)

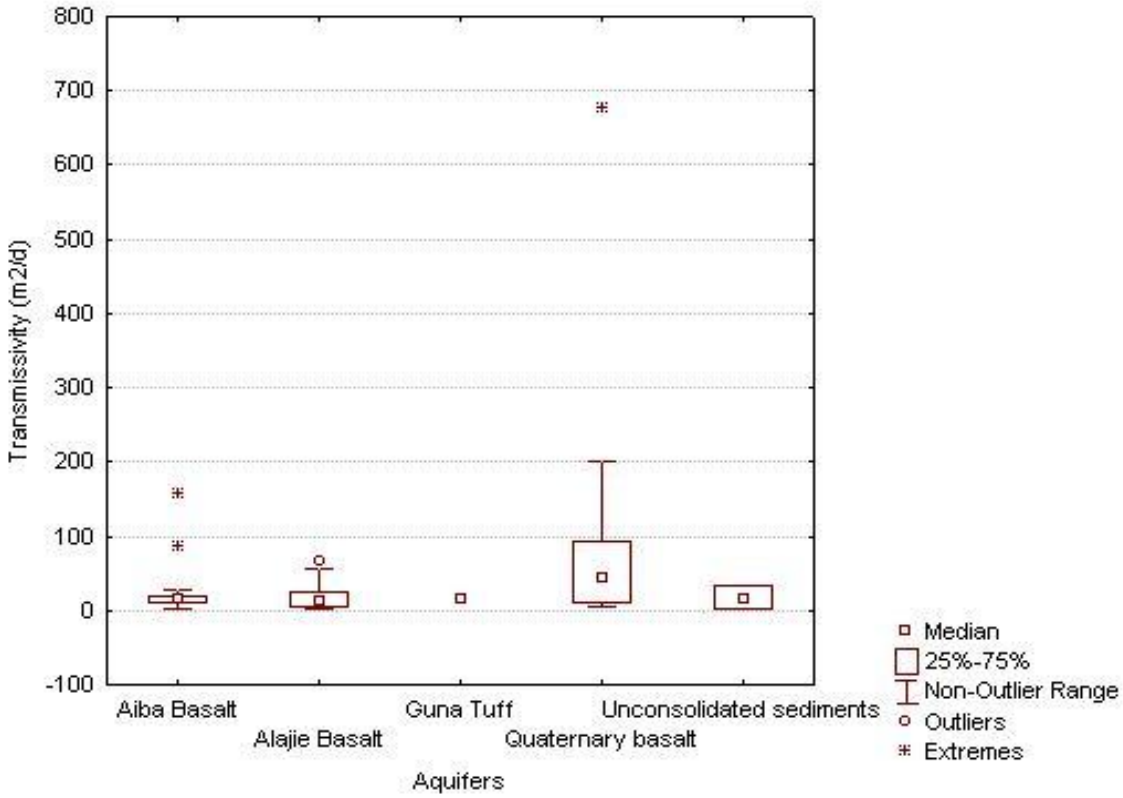

Figure 5.4. Graphs depicting variation of the hydraulic parameters of the different aquifers. a) borehole depth, b) borehole yield, c) spring yield (spring with discharge as large as 108 l/s was observed for Quaternary basalt), d) transsmissivity

5.2.1.2. Extensive and low productive intergranular aquifer

Guna Tuff is loose to weakly compact with welded tuff interbeds. Springs emerging from this aquifer have discharge of 0.02 to 0.5 l/s, with a mean of 0.19 and median of 0.1 l/s. Only one borehole has been drilled in this aquifer at Gassay town. It has depth of 42 m, yield of 3.1 l/s, transsmissivity of 13.7 m^2/d and a static groundwater level of 0.9 m (see Fig. 5.4a-d and Table 5.3).

Table 5.3. Hydraulic data of Guna Tuff aquifer.

Parameters	mean	median	max	min	number
Spring yield (l/s)	0.19	0.10	0.50	0.02	7.00
Borehole yield (l/s)			3.1		1.0
Transsmissivity (m^2/d)			13.7		1.0
Static water level (m)			0.9		1.0
Borehole depth (m)			42		1.0

5.2.2. Fractured Aquifers

5.2.2.1. Extensive and high productive fractured aquifer

Quaternary Basalt Aquifer

This basalt aquifer is found at the southwestern and in the eastern part of the area. This aquifer is vesicular and scoraceous and fractured. Often 3 sets of joints are seen which are open and interconnected (Fig. 5.5). It is covered by thin reddish brown clayey silty eluvium. This aquifer is underlain by Sekela Basalt and Upper Basalt, and the Middle and Lower Basalts aquifers seem to be found underneath.

Figure 5.5. Fractures and vesicles in Quaternary basalt aquifer.

Boreholes drilled through this aquifer to the underlying Tertiary basalts aquifers have depth of 23 to 198 m, with mean and median of 82.6 and 67.4 m. However, thickness of the Quaternary basalt aquifer is 24 to 49 m. These boreholes have partially penetrated the underlying Tertiary Basalts aquifers. Transsmissivity ranges from 6.3 to 676.7 m^2/d. The mean and median values are 118 and 43.7 m^2/d. Spring discharge in Quaternary basalt aquifer, within the study area and in the surrounding areas, ranges from 1 to 108 l/s with a mean and median of 49.4 and 51.8 l/s, respectively. Borehole yield varies from 1 to 40 l/s with a mean and median of 7.4 and 4 l/s, respectively. Static groundwater level ranges from 2.3 to 47.7 m and a mean and median of 17.7 and 12.9 m (see Table 5.4 and Fig. 5.2a-d).

A test borehole currently drilled around Bahir Dar town (GW226) with a depth of 500 m intersected the Quaternary and the underlying Upper, Middle and Lower basalts aquifer (0-356 m), and the underneath granite (356-500 m), which probably could be Precambrian. Granodiroite sill has been observed between 226 and 264 m depth interval. The static groundwater level was 35.05 m when the borehole was drilled up to 156 m. However, the static water level dropped to 36.3 m when the drilling depth reaches 500 m suggesting multi layered aquifers and the lower ones are in (semi)confined conditions with relatively lower head when compared to the upper one, which seems to be in unconfined condition. Pumping testing was conducted for 72 hours on this test borehole with discharge of 53 l/s and a drawdown of 43.6 m attained. Diagnostic curve shows double porosity confined aquifer where groundwater flow both in the block (rock matrix) and fractures (Fig. 5.6). Moench fracture flow analysis method for confined aquifer has given transsmissivity of 108 m^2/d and storativity of 3.45×10^{-4} (Fig. 5.7)

Table 5.4. Hydraulic data of Quaternary basalt and the underlying Tertiary basalts aquifers.

Parameters	mean	median	max	min	number
Spring yield (l/s)	49.40	51.75	108.00	1.00	6.00
Borehole yield (l/s)	7.4	4.0	40	1.0	12.0
Transsmissivity (m^2/d)	118.0	43.7	676.7	6.3	11.0
Static groundwater level (m)	17.7	12.9	47.7	2.3	10.0
Borehole depth (m)	82.6	67.4	198	23.0	16.0

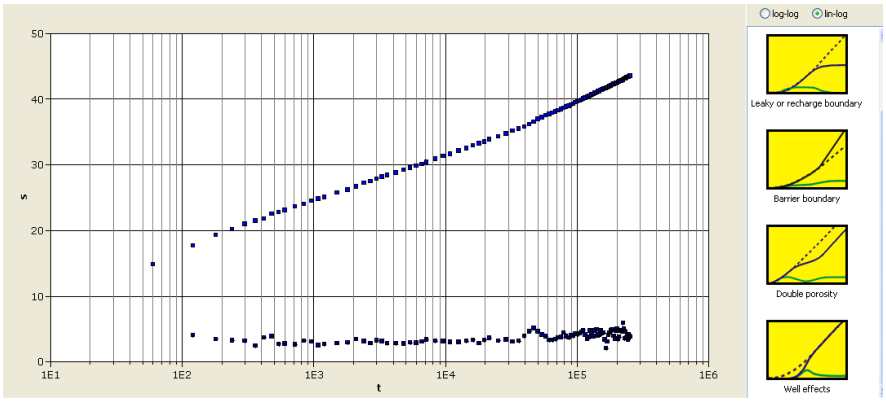

Figure 5.6. Diagnostic curve for Bahir Dar test borehole (GW226).

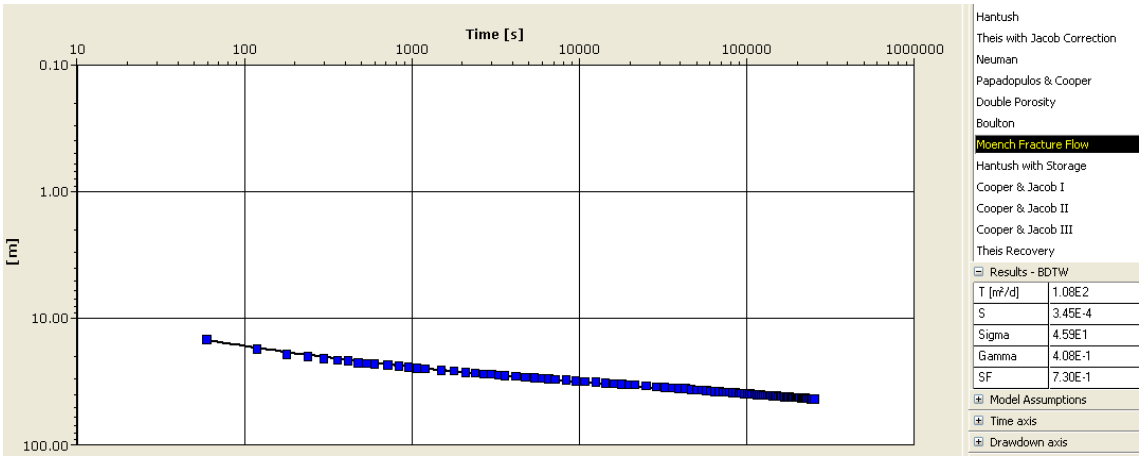

Figure 5.7. Moench fracture flow solution for Bahir Dar test borehole (GW226).

5.2.2.2. Extensive and moderate to high productive fractured aquifer

Sekela Basalt Aquifer

It is exposed on the southwestern part of the area at Gish Abay (Sekela) hill. It is weathered and moderately fractured with major ones trending to the northeast and northwest. Fractures are open and interconnected. Springs and boreholes are seen in this aquifer. However, discharge measurement was possible only to one spring which has about 30 l/s dry period discharge. This aquifer is reported to have 10 to 15 l/s springs' discharge in the near by out side the study area (Bayiesa Asefaw, 1993).

5.2.2.3. Extensive and low productive fractured aquifer

Middle Basalt Aquifer

This aquifer is exposed at limited area around Gonder town in the north and eastern areas, and found in boreholes below the Upper Basalt aquifer. It is highly weathered on top toward the contact with the Upper Basalt aquifer and they are separated by thin clayey silt paleosol. This aquifer is slightly vesicular, which is at palaces filled with zeolite, slightly to moderately fractured and weathered, and thinly layered (Fig. 5.8).

Figure 5.8. Joints in the Middle Basalt aquifer.

Borehole depth varies from 65 to 251 m, and the mean and median values are 109.8 and 95 m. Borehole yields range from 0.7 to 17 l/s with 4.2 and 2.6 l/s mean and median values. Transsmissivity show variation from 1.1 to 157.1 with a mean and median of 26.5 and 14.7 m^2/d. High values suggest that highly yielding boreholes can be obtained by electing suitable site in structurally affected areas. Spring discharge varies from 0.1 to 0.5 with a mean and median of 0.4 l/s. Static groundwater level varies from artesian at Angereb valley (near Gonder town) to 59 m. The mean and median values are 16.7 and 10.8 m. (see Table 5.5 and Fig. 5.4a-d).

Table 5.5. Hydraulic data of the Middle Basalt aquifer.

Parameters	mean	median	max	min	number
Spring yield (l/s)	0.4	0.4	0.5	0.1	6.0
Borehole yield (l/s)	4.2	2.6	17.0	0.7	20.0
Transsmissivity (m^2/d)	26.5	14.7	157.1	1.1	16.0
Static groundwater level (m)	16.7	10.8	59.0	artesian	9.0
Borehole depth (m)	109.8	95.0	250.6	65.0	17.0

Groundwater level drop and rise have been encountered at different places when the underlying aquifers beneath the Upper Basalt (Middle and Lower basalts) aquifer are intersected (Fig. 5.9a&b). Furthermore, groundwater has been stricken at different depths in theses aquifers suggesting multy layered aquifer system. The Middle and Lower basalt aquifers are in (semi) confined conditions.

(a)

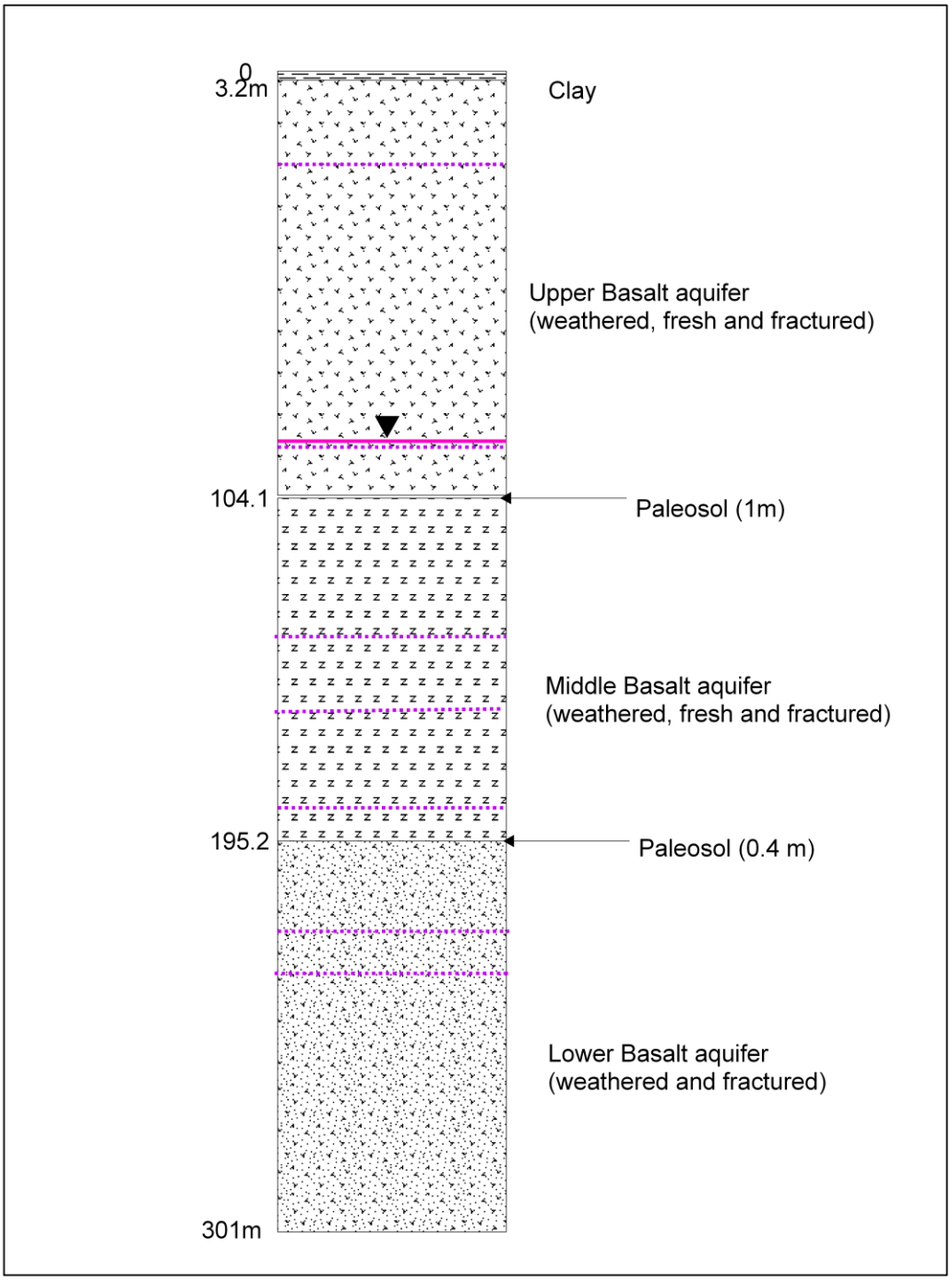
0
3.2m
Clay
Upper Basalt aquifer
(weathered, fresh and fractured)
104.1
Paleosol (1m)
Middle Basalt aquifer
(weathered, fresh and fractured)
195.2
Paleosol (0.4 m)
Lower Basalt aquifer
(weathered and fractured)
301m

(b)

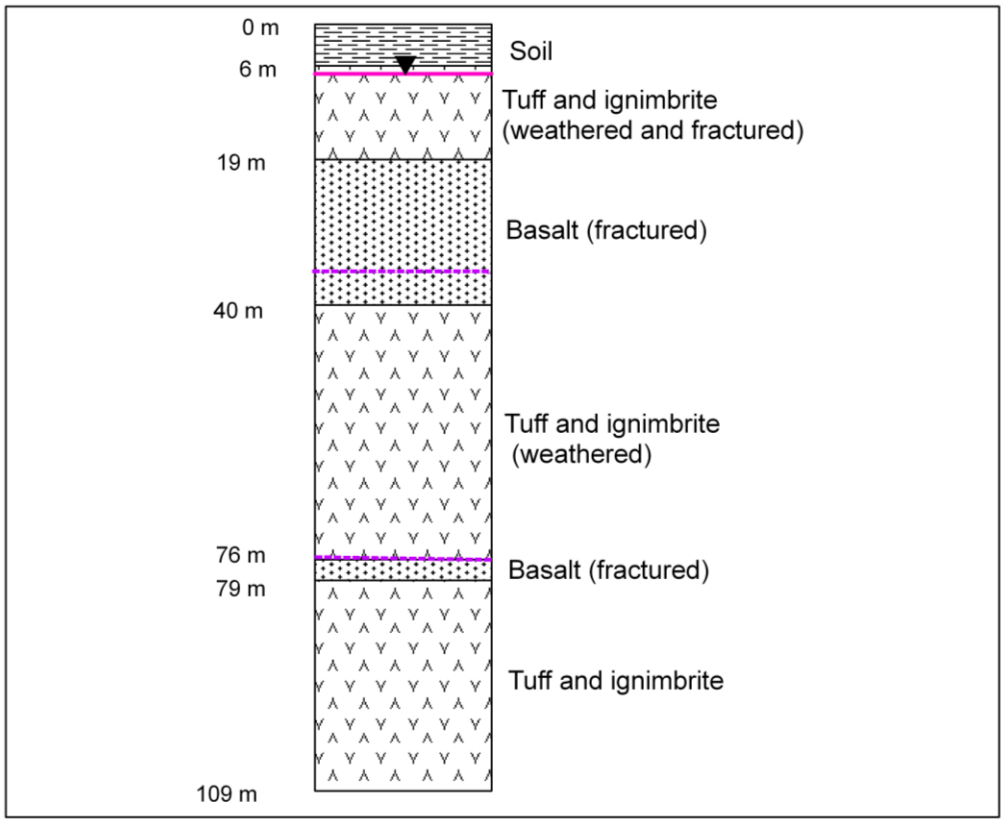

Figure 5.9. Muli layered fractured aquifers a) around Gonder (GW3) b) Debretabor borehole no.10 (GW9). Violet and pink colors indicate depths to water strike and the final static groundwater level, respectively (Source: ADSWE drilling logs).

Pumping test analysis was conducted for 24 hours for GW3 borehole, with a discharge of 18.2 l/s. A draw down of 17.34 m has been observed. The diagnostic curve and the fact that groundwater has been stricken at different depths and the drop in static water level for this borehole suggest double porosity flow in confined aquifer (Fig. 5.10). Moench fracture flow solution has given transsmissivity of 69 m^2/d and storativity of 7.85×10^{-4} (Fig. 5.11).

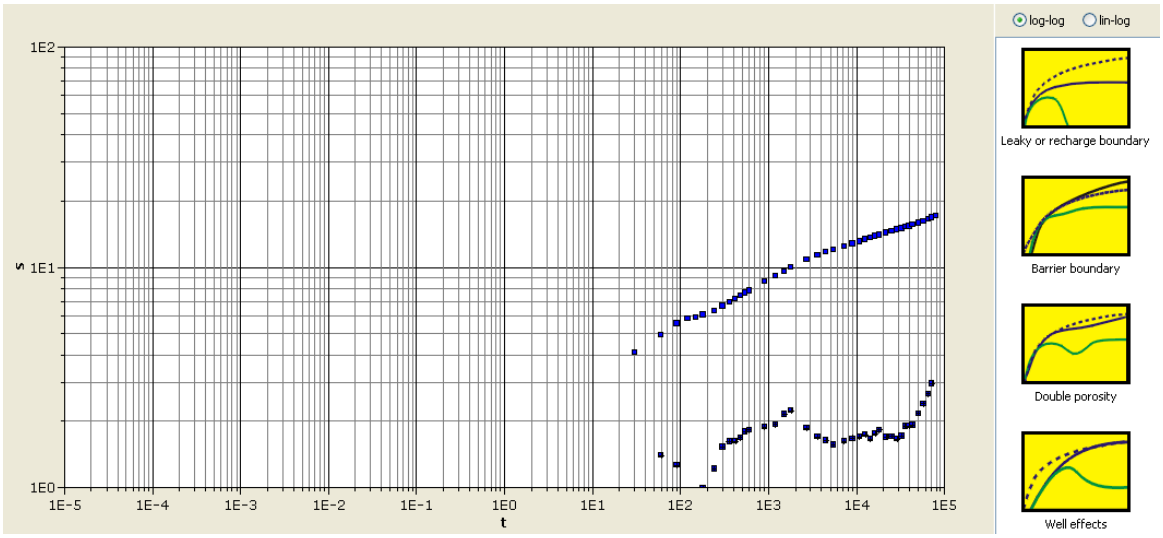

Figure 5.10. Diagnostic curve for borehole GW3.

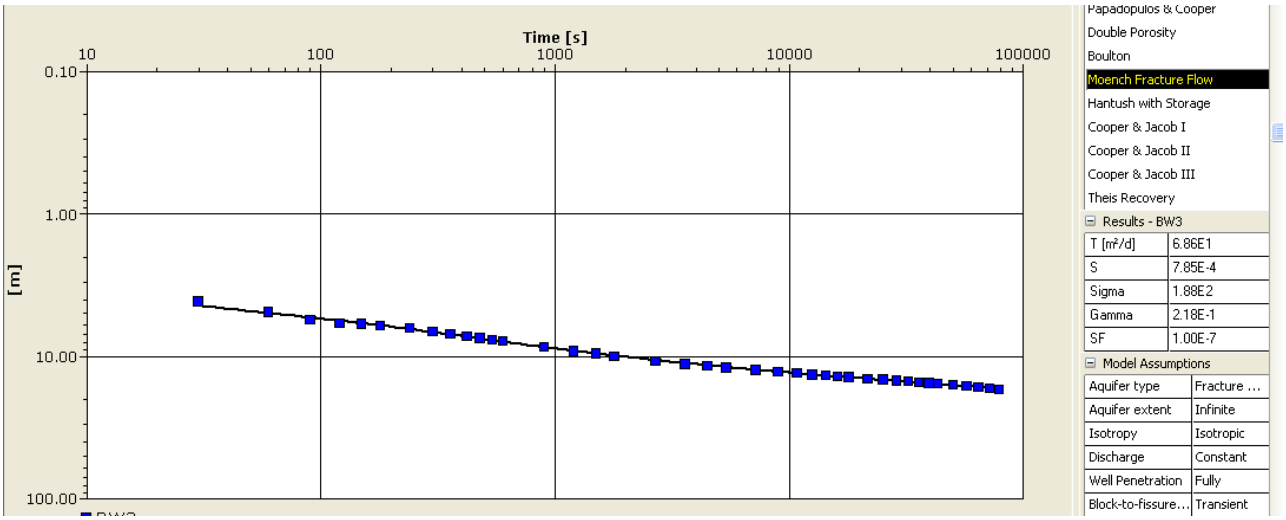

Figure 5.11. Moench fracture flow solution to estimate transsmissivity and storativity.

Upper Basalt aquifers

This hydrogeologic unit is exposed in most parts of the study area. It is highly weathered on top with thin clayey silt eluvium in moderate slopes. It is moderately fractured and columnarly jointed. Three sets of macroscopic joints with northwest, northeast and north-south trends are observed, which are interconnected and open. It is also found moderately

fractured in the eastern part of the area, south of Debretabore town. Else where it is slightly to moderately fractured. Figure 5.12 shows joints in Upper Basalt aquifer.

Figure 5.12. Joints in the Upper Basalt aquifer.

Boreholes drilled in this aquifer have depths of 43 to 156 m, with 91.8 and 92.5 m mean and median values, respectively. Borehole yield ranges from 0.6 to 10 l/s. The mean and median are 3.5 and 2.7 l/s. Spring yield varies from 0.04 to 28 l/s with a mean and median of 1.8 and 0.3 l/s. Transsmissivity varies between 3.2 and 67.3, with a mean and median of 19.8 and 14.7 m^2/d. This indicates that suitable sites should be sought to get better productivity (see Fig. 5.4a-d). Static groundwater level ranges from 2 to 18 m, with 7 and 5.4 m mean and median values, respectively. Table 5.6 shows the hydraulic data to this aquifer. This aquifer often form unconfined aquifer where exposed.

5.2.2.4. Local and low productive fractured aquifer

Degoma Basalt Aquifer

It is slightly weathered, columnarly jointed and fractured and layered. It is exposed on the northern and northeastern summit part of the area. No groundwater point is found in this

aquifer. It is classified to low productive aquifer and groundwater here may be developed by hand dug wells.

Table 5.6. Hydraulic data of the Upper Basalt aquifer.

Parameters	mean	median	max	min	number
Spring yield (l/s)	1.8	0.3	28.0	0.04	21.0
Borehole yield (l/s)	3.5	2.7	10.0	0.6	25.0
Transsmissivity (m^2/d)	19.8	14.7	67.3	3.2	18.0
Static groundwater level (m)	7.0	5.4	18.0	2.0	16.0
Borehole depth (m)	91.8	92.5	156.0	43.0	21.0

Guna Basalt Aquifer

It occupies the eastern part of the area. It is slightly weathered and highly fractured and columnarly jointed at places. Groundwater points are not available in this aquifer. It is situated in the steep slope, which acts as recharge area with low storage.

Guna Phonolite Aquifer

This aquifer occupies the top summit of the Guna volcano and has steep slope that can transmit but has low groundwater storage. It is fresh and columnarly jointed.

Trachyte Aquifers

Trachyte aquifer is found overlying the Upper Basalt aquifer. It is fractured but its thickness is low to be considered as an important aquifer.

5.2.3. Aquitard

Quaternary rhyolite domes and trachyte plugs are only slightly fractured and act as an aquitard.

5.3. Groundwater Flow Regime

Volcanic rocks and the overlying lacustrine sediments form stratified aquifers, which are interacting vertically. The upper aquifer is often in unconfined condition while deeper ones are in (semi) confined conditions. Spatially, independent sets of aquifers are found in the eastern, northern, western and southwestern parts of the area. These aquifers share common hydrologic characteristics and can be considered as one aquifer system, which is termed as the Upper Aquifer System (see Section 11.1). Groundwater in this aquifer system moves from all sides toward the Tana Lake (Fig. 5.2). Groundwater in the upper unconfined aquifer interacts with surface waters (streams, Tana Lake and reservoirs) while the deep groundwater converges as inter basin groundwater outflow to the adjacent low lying Tis Abay area (see Section 9.3 and 11.3).

Furthermore, intermediate and lower aquifer systems are ascertained to exist in eastern area, which are represented by ground waters that ascend through fault (borehole GW9 for Subgroup1c) and lineament (salty uprising cold spring, GW32 for Subgroup1a), underlying the Upper Aquifer System, see Section 11.1. The latter is plaeo groundwater. Groundwater flow regime of these aquifer systems are not clear as there are no deep boreholes penetrating aquifers of these systems. Further description of these aquifer systems are given in Chapters 9, 10 and 11.

5.4. Groundwater Recharge and Discharge Conditions

The Upper Aquifer System has active recharge. Recharge takes place from precipitation in volcanic terrains and little recharge from precipitation may take place in fluvio-lacustrine sediments aquifer at the plain. Recharge at the eastern and northern plain lacustrine sediments aquifer may also occur from influent streams and seasonal flood pools, and inundated Tana Lake water. Furthermore, groundwater recharge occurs from reservoirs made in the volcanic terrains. The Lower Aquifer System has no current recharge. It was recharged during Early Holocene humid period.

The shallow groundwater in the Upper Aquifer System discharges as baseflow into streams and as springs. Most of the streams are perennial throughout the year suggesting that the streams are fed by groundwater baseflow during the dry period. Groundwater discharge directly into the Tana Lake is minor although there is indication from hydreogeological, hydrochemical and isotopic signatures (see Chapter 8, Sections 9.4, 10.2 and 11.3. This may be due to the presence of massive and compact clay beneath and surrounding the lake.

Evapotranspiration from the shallow groundwater at the margins of the Tana Lake and abstraction are other mechanisms of the groundwater discharge.

6. EVALUATION OF GROUNDWATER RECHARGE

6.1. General

Recharge is the downward movement of water to the water table that adds water to the groundwater reservoir (Tenalem Ayenew and Tamiru Alemayehu, 2001). Recharge can be direct from precipitation and irrigation, indirect from streams and localized from surface ponds. The various processes for the recharge to take places are summarized in Figure 6.1.

There are several methods to directly calculate the groundwater recharge and the most reliable ones are to measure directly with lysimeter or to use tank model, and by monitoring the movement of water through the vadose zone with tensiometers. However, these methods give local information and are difficult to regionalize. The actual methods used to estimate recharge depend on the scale and accuracy required.

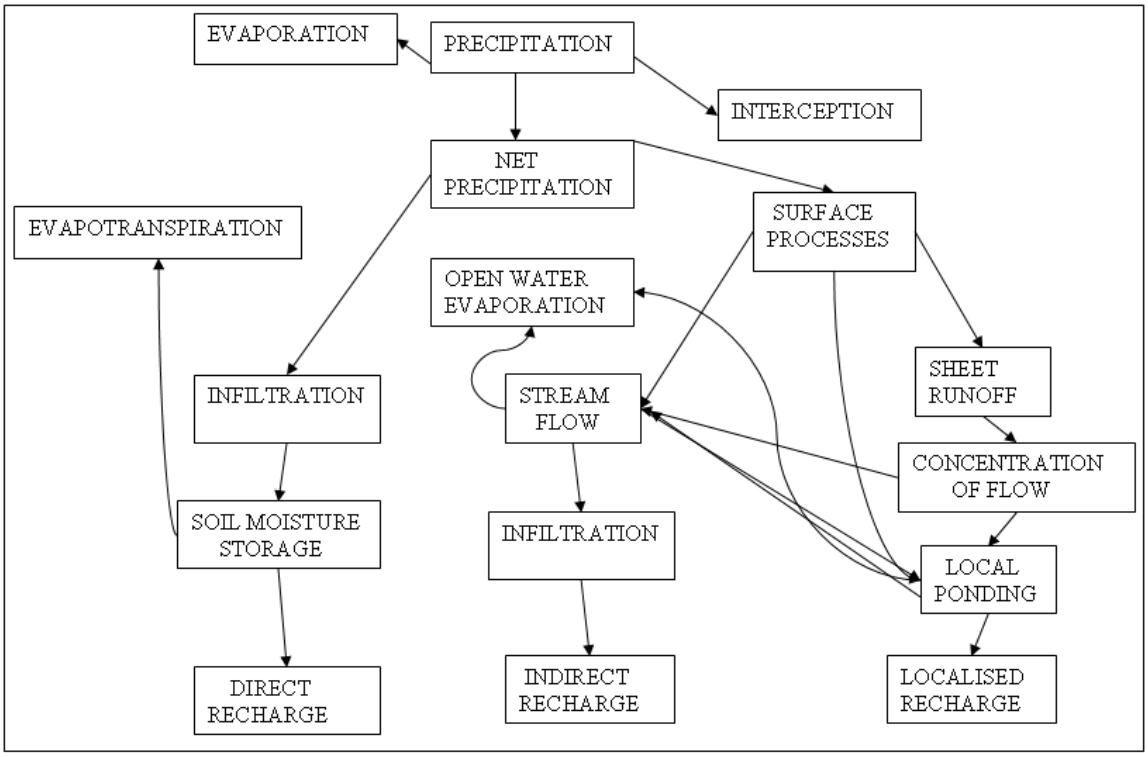

Figure 6.1. Elements of recharge (After Nyagwambo, 2002).

Recharge rate can be calculated based on different methods. Because of the uncertainties associated with each method, the use of many different approaches is recommended to constrain the recharge estimate (Scanlon et al., 2002). In humid areas like the Tana basin, baseflow separation and soil water balance methods are appropriate (Scanlon et al., 2002). These methods together with chloride mass balance method have been used here to estimate the recharge.

6.2. Baseflow Separation Method

The total rivers' runoffs have been portioned into baseflow and direct runoff, which is delt in Section 4.3.4.

The mean baseflow or groundwater discharge to rivers has been estimated as weighted (by area) of base flows of 7 stations distributed in the basin to be 195.6 mm $year^{-1}$ (Table 6.1). However, the actual mean groundwater recharge rate exceeds the mean baseflow or groundwater discharge to streams by the amount equal to the riparian evapotranspiration, consumptive uses, discharge to the lake and deep recharge that underflow beneath the stream beds.

Therefore, this value may indicate the minimum recharge rate of the shallow unconfined aquifer for the whole volcanic terrains including un-gauged catchments except the flat plain in eastern and northern parts of the area where the streams are influent to the groundwater here.

6.3. Soil Water Balance Method

Soil water balance method uses the surplus water as a recharge. This method is widely used for regional recharge estimation. Spatial changes in evapotranspiration due to changes in soil and vegetation types can be incorporated in this model and the model has a simple scheme to distribute surplus water into successive months (Tenalem Ayenew, 1998).

Soil and land cover maps of the Tana basin have been prepared. These maps have been overlaid using Arc GIS 9.3, and the aerially weighted available water capacity of the area have been estimated to be 165 mm using the available water capacity (% volume) of soils and rooting depth (meter) of vegetations (Thornthwaite and Mather, 1957).

Table 6.1. Recharge estimate based on baseflow separation method.

	BFI	Total flow (mm/year)	Base flow (mm/year)	Direct runoff (mm/year)	Catchment area (km^2)	DRO*Area	Base flow*Area
Ribb	0.282	289.5	81.6	207.8	1704.5	354273.3	139143.5
Megech	0.333	438.4	146.0	292.4	518.6	151644.6	75708.6
Kilty	0.305	464.5	141.7	322.8	595.3	192165.1	84331.5
G/Abay	0.326	868.9	283.3	585.6	1946.7	1140023.3	551405.9
Garno	0.414	259.3	107.3	151.9	102.2	15527.4	10969.9
Gemero	0.21	261.4	54.9	206.5	184.4	38074.4	10121.0
Gumera	0.289	1015.7	293.5	722.2	1189.7	859148.2	349217.8
Total					6241.4	2750856.4	1220898.2
Weighted mean DRO and baseflow (mm/year)						440.7	195.6

DRO: Direct runoff

Aerially averaged precipitation (*P*) and reference evapotranspiration (ET_o), based on Thiessen polygonal method, have been used in the soil water balance computation (Table 4.5).

The reference evapotranspiration is an approximation of a hypothetical reference grass evapotranspiration at particular location. The reference grass or crop assumed is adequately watered and an albedo of 0.23 (FAO, 2009).

The reference evapotranspiration is a climatic parameter and expresses the evaporative power of the atmosphere at a specific location and time of the year, and does not consider the crop characteristics (such as type, development and management practices) and soil factors (Allen et al., 1998). It is therefore necessary to define the crop evapotranspiration (ET_c) for each crop and stage of growth.

The crop evapotranspiration standard represents evapotranspiration from disease free, well fertilized crops, growing in large fields, under optimum soil water conditions, and achieving full production under the given climatic conditions. On the other hand, evapotranspiration from natural vegetation with out management practices is known as crop evapotranspiration non-standard (Allen et al., 1998).

The crop coefficient (K_c) integrates the effect of characteristics that distinguish a specific crop from the reference crop. ET_c is calculated by multiplying the ET_o by the suitable K_c. The crop coefficient is affected by crop type and to minor extent by climate and soil evaporation. K_c for a given crop varies with the growing stage, as ground cover, crop height and leaf area changes as the crops develop.

Evaluation of the soil water balance needs to assign K_c to deduce the ET_c from ET_o under specific site conditions.

Different types of crops (dominantly maize, sorghum, wheat, teff and rice in decreasing order) and natural vegetations (often grass and short bushes and shrubs) grow in the area,

and it is difficult to ascribe K_c values for each crop and vegetation as their area coverage is unknown. About 83.8% of the total study areas are agricultural land, and the farmers exercise crop management practices. The rainfall is frequent to wet the soil and the crops are often kept to dry in the field during the late growing season. The growing stages of these crops are not known. Therefore, average value of the average crop coefficients during the initial, mid and late growing periods (Allen et al., 1998), which is equal to 0.88, has been calculated and used for all months in the soil water balance computation.

Monthly direct runoffs that are used in the computation have been derived by multiplying the runoff coefficient of 0.314 to the aerially averaged mean monthly precipitation values.

Soil water balance computation has been done manually by the simple book keeping Thornthwaite and Mather (1957) method. The recharge is estimated as a residue of monthly precipitation values minus direct runoff, ET_c and the positive soil accretion (Table 6.2).

Soil water balance computation using the above described method and data gave annual recharge rate of 285.4 mm/year (Table 6.2). This value represents the net recharge reaching the groundwater table as the direct runoff used in the calculation incorporates interflow in the unsaturated zone that discharge to the near by streams, and seepage or through flow that emerges at the near by foot slopes is minor.

6.4. Chloride Mass Balance Method

The chloride mass balance (CMB) approach may be used both in unsaturated and saturated zones to estimate recharge. It is based on the assumption of conservation of mass between the input of atmospheric Cl and the Cl flux in the subsurface.

CMB method for saturated zone may be especially useful in areas where groundwater levels do not fluctuate or data on groundwater levels are lacking. CMB is often applied in

Table 6.2. Soil water balance (mm); available water capacity 165 mm.

	Jan	Feb	Mar	Apr	May	Jun	Jul	Aug	Sep	Oct	Nov	Dec	Annual
P	4.5	3.9	16.4	27.7	88.6	207.9	382.7	358.0	194.1	91.5	15.8	9.5	1400.4
DRO	1.4	1.2	5.2	8.7	27.9	65.4	120.4	112.7	61.1	28.8	5.0	3.0	440.7
ET_O	110.0	120.0	138.0	136.0	131.0	107.0	85.0	84.0	102.0	110.0	103.0	103.0	1329.0
ETc	96.8	105.6	121.4	119.7	115.3	94.2	74.8	73.9	89.8	96.8	90.6	90.6	1169.5
Sm	0.0	0.0	0.0	0.0	0.0	48.3	165.0	165.0	165.0	130.9	51.1	0.0	
dSm						48.3	116.7			-34.1	-79.8	-51.1	
AET	3.1	2.7	11.2	19.0	60.7	94.2	74.8	73.9	89.8	96.8	90.7	57.6	674.4
R	0.0	0.0	0.0	0.0	0.0	0.0	70.8	171.4	43.3	0.0	0.0	0.0	285.4

Sm: soil moisture, dSm: change in soil moisture, R: recharge

semi arid and arid regions where the impact of runoff is not taken into account and evaporation effect on the recharge water is significant. However, it is frequently used also in other areas.

Basin groundwater recharge can be estimated as follows **(**After, Eriksson and Khunakasem, 1969; Wilson and Guan, 2004**)**

$$R = (C_pP\text{-}C_qQ + D)/C_{gw} \quad \ldots\ldots\ldots\ldots\ldots\ldots\ldots\ldots\ldots\ldots\ldots\ldots\ldots\ldots\ldots\ldots\ldots\ldots(8)$$

Where, C_{gw} is Cl in groundwater, P is precipitation over the basin, C_p is Cl in bulk precipitation, Q and C_q are runoff and its Cl content, D is dry Cl deposition, R is recharge

In industrial areas, gases and aerosols that may contain substantial Cl may pollute the atmosphere and lead to high levels of dry deposition (Nyagwambo, 2002). Dry deposition must be considered in areas within or downwind of atmospheric pollution source. The amount of deposition is a function of the atmospheric concentration of gases, aerosols and the velocity at which they are deposited. However, there are no many industries in the area.

The bulk Cl deposition, which is measured in rain gauge monthly during wet season, incorporates the dry deposition of the preceding month. Thus, the bulk deposition nearly represents the total (dry + wet) atmospheric Cl deposition, and the wet season Cl concentration measured at the rain gauge can be taken in the calculation (Nyagwambo, 2002). The rain gauges, where the rain fall samples have been collected, have low height than the natural vegetations and most of the crops growing in the area. Hence, dry fall out from intercepted water by vegetation and crops can be captured by the rain gauge.

Chloride mass balance has been done with the following major assumptions.

– The bulk precipitation (dry fall and precipitation) is the only source of Cl in the system, and Cl is inert in the system

- Cl deposition rate and mean annual precipitation are accurately estimated and have been constant over the period of groundwater residence time
- The measured Cl content of groundwater accurately represents the mean value of the total groundwater

Limitations and uncertainties of the CMB method may be summarized as given below (Beekman and Xu, 2003).

- CMB should not be applied in areas underlain by evaporites or areas where upcoming or mixing of saline (groundwater) occurs
- In fractured rock system, the applicability of CMB method is complicated if additional Cl is produced through weathering of the rock matrix. Recharge in this case is a minimum
- When time is needed to develop new equilibrium between groundwater Cl concentrations in the rock matrix and fracture following change in environmental conditions
- If recharge water flow preferentially, it will not get enough time to evaporate and over estimate the recharge
- Measured atmospheric input of Cl for short period is assumed to be representative for a long period, where as rainfall and Cl deposition during the past may be different from today
- Uncertainty in the measured Cl content of rainfall and rainfall amount depend on the type of rain gauge used, pollution and analytical error

According to Cook (2003), despite the short comings, the CMB method is highly recommended even for fractured rock system (Beekman and Xu, 2003).

Aerial average basin precipitation, which is calculated using 15 consecutive years' (1995-2009) data have been used in CMB computation. Rainfall sampling was conducted for one hydrological year in four meteorological stations distributed within the basin. After the weighted mean (by precipitation) content of Cl in each station is calculated, harmonic

mean of the Cl content for the four stations has been estimated and used in the recharge estimation.

Mean weighted direct runoff was estimated by hydrograph separation method (Section 6.1). Cl concentration of rivers at different streams is measured and a harmonic mean of these data has been considered for CMB evaluation.

Cl input has been observed to groundwater in lacustrine sediments and for the deep source groundwater. Groundwater points with anomalously high Cl values, which are believed to be due to local dissolution of trace eviporites in the lacustrine sediments has been omitted. Furthermore, the old deep paleo groundwater with high Cl was not also used for CMB computation. Therefore, ground waters with minimum input of Cl from the aquifers have been taken in this calculation. Harmonic mean of Cl concentration of groundwater (boreholes, springs and hand dug wells) samples was taken in this computation.

The following values have been used for recharge estimation based on chloride mass balance method.

P= 1400.4 mm/year
C_p=1.2 mg/l
Q= 440.7 mm/year
C_q= 2.12 mg/l
C_{gw}= 2. 63 mg/l

Recharge of 284 mm/year has been estimated using the above data into Equation 7. The result shows effective recharge that joins the groundwater reservoir. Isotopic data revealed diffuse groundwater recharge during rainy summer season, which suggest no major recharge through preferential flow exists. Therefore, the recharge water can get time to evaporate in soil and weathered mantle of the volcanic aquifers so that the

recharge calculated by CMB does not overestimates and represents the actual mean recharge rate in the basin.

7. BASIN WATER BALANCE EVALUATION

The water balance approach is an application of the law of conservation of mass in hydrology. The catchment water balance can be given as follows (Kuzmin et al., 1974; Nyagwambo, 2006).

$$I - O \pm \varepsilon = \pm ds/dt \quad \text{.....(9)}$$

Where,
I = inflow [L/T^1], O = outflow [L/T], ε = undetermined balance elements, measurement and estimation errors [L/T], ds= change in storage [L], and dt is time increment [T].

Inflow includes precipitation over the basin (P), surface inflow (S_i), lateral groundwater inflow from adjacent aquifer (G_i) and artificial recharge and return flow (A_r). Outflow encompasses surface water outflow from the basin (S_o), basin groundwater outflow to adjacent basin (G_o), open water evaporation (E_o), actual evapotranspiration (AET) and withdrawal for consumptive uses (W). ds include storage changes in open waters (rivers, lakes, reservoirs, ponds and wet lands), unsaturated zone and saturated zone.

Tana basin consists of rivers, lakes, reservoirs, permanent and seasonal marshes and land areas. Water balance bodies, which are less than 2-3% of the basin area, can be omitted from the water balance computation (Kuzmin et al., 1974). Thus, very small Angereb reservoir and Koga reservoir constructed after 2010 have not been incorporated in the basin water balance evaluation.

The water balance equation given below has been applied for Tana basin. Computation was done on annual basis.

$$P+S_i+G_i+ A_r -S_o-G_o-AET-E_o-W\pm \varepsilon = \pm dS \quad \text{.....(10)}$$

Because there is no artificial recharge and return flow, and groundwater and surface water inflows from the adjacent catchment, A_r, S_i and G_i can be neglected from equation 10.

If inflow exceeds the outflow, there will be increase in storage while the storage tends to decrease if the inflow is less than the outflow. Water balance computation has been done over long period of time (1995-2009) and the change in storage (dS) can be assumed to be negligible or equal to zero.

Equation 10 can then be given as follows:

$$P\times A - S_o -G_o-AET\times A-E_{ol}\times A-E_{opm}\times A-E_{osm}\times A-W\pm \varepsilon = 0 \quad \text{……(11)}$$

Where, E_{ol} = evaporation from the Tana Lake, E_{opm} = open evaporation from permanent marsh, E_{osm} = evapotranspiration from seasonal marsh, A = area with respect to the parameters (areas of the seasonal and permanent marshes are 382.1 and 11.9 km^2, respectively). The data are given in Table 4.5.

Withdrawal has been calculated using population number residing in the area by considering average consumption of 25 l/s per head, which equals to 7.9 hm^3/year. Irrigation water use until 2009 is assumed to be negligible.

Uncertainty (eG_o) introduced in the estimated value due to measurement error is deduced using the following equation (Sacks et al., 1998). Undetermined water balance elements are not important for the area and estimation error is assumed to be minor.

$$eG_o = [(eP\times P)^2 + (eS_o\times S_o)^2]^{0.5} \quad \text{……(12)}$$

Measurement error for precipitation (eP) is about ± 5% in tropics, while surface outflow measurement error (eS_o) is ± 5% (Kuzmin et al., 1974).

All parameters except G_o in Equation 10 is known and has been equated to estimate the groundwater outflow (G_o). The total groundwater outflow from the basin, which includes leakage rate from the Tana Lake (Chapter 8), is therefore estimated to be 3333.5 hm^3/year.

The uncertainty or error bound for the estimated basin groundwater outflow (eG_o) due to measurement error of fluxes is also calculated using Equation 11 to be ±1066.1 hm^3/year.

8. HYDROLOGICAL AND CHEMICAL MASS BALANCE OF LAKE TANA

Lakes are complex dynamic systems, interacting with the local environment and connected to the hydrological cycle through both surface and underground inflows and outflows, as well as via precipitation and evaporation fluxes. The interaction with the local environment also includes chemical constituents and mineral phases that are transported from the catchment area to the lake via surface and underground inflows, which leave the lake together with out flowing water or accumulate in the lake sediments (Rozanski et al., 2001).

The water budget or hydrologic balance of the lake is based on the mass conservation law or hydrological continuity equation. Lakes' water budget is computed by measuring or estimating all of lake's water gains or losses, and the corresponding change in lake volume over the same time period and has the form (Rozanski et al., 2001; Sacks et al., 1998):

$$dV_L/dt = S_i+G_i+P_l-S_o-G_o-E_{ol} \quad \text{.....(13)}$$

Where, V_L is lake volume. S_i, G_i, S_o and G_o represent the volumetric surface and groundwater inflow and outflow fluxes, respectively. P_l stands for precipitation over the lake and E_{ol} is the evaporation flux from the lake. S_i includes both gauged and un-gauged surface water inflows. dt represents time period over which estimation is done.

The chemical mass balance approach uses naturally occurring conservative tracer (e.g. Cl) and combines the water budget equation with solute balance equation. This approach also applies mass conservation law to the tracer constituents, which are dissolved in water. The Cl tracer can be assumed as conservative that is not significantly involved in any geochemical or biological reactions that alter its concentration (Sacks et al., 1998), and it is often used in lake balance evaluation. The mass balance equation written for chemical tracer (Cl) has the following form:

$$C_L \times dV_L/dt + V_L \times dC_L/dt = C_{Si} \times S_i + C_{Gi} \times G_i + C_{Pl} \times P_l - C_{So} \times S_o - C_{Go} \times G_o - C_{Eol} \times E_{ol} \qquad (14)$$

Where, C with the respective subscripts represents the concentration of the tracer (Cl) in the lake and in all incoming and out going water fluxes.

Long term mean annual values (1995-2009) of P_l, S_i, S_o and E_{ol} have been used. Furthermore, average value of Cl of groundwater inflow (boreholes, springs and dug wells) from the shallow unconfined aquifer that interacts with the river inflows and the Tana Lake have been used. Cl content of precipitation sampled at Gonder and Bahir Dar meteorological stations, which are close to the Lake Tana, have been weighted with precipitation and the average of the two was used for the computation.

The lake is shallow with average depth of 9m (Lamb et al., 2007) and considered to be vertically mixed. Steady state condition with respect to the bulk mass of water and the Cl tracer are assumed here.

This implies:

$dV_L/dt = 0$ and $dC_L/dt = 0$

Therefore, Equation 13 and 14 can be given as:

$$G_i - G_o = S_o + E_{ol} - S_i - P_l = 0 \quad \text{.....(15)}$$

$$C_{Gi} \times G_i - C_{Go} \times G_o = C_{So} \times S_o + C_{Eol} \times E_{ol} - C_{Si} \times S_i - C_{Pl} \times P_l \quad \text{.....(16)}$$

The chloride content of the evaporating water flux is zero and the term $C_{Eol} \times E_{ol}$ will be eliminated in Equation 16.

The uncertainty associated with the measurement error of the hydrological fluxes used has been calculated in order to see the uncertainty with the computed groundwater inflow and outflow using Equation 17 (Sacks et al., 1998).

$$Error = [(eP_l \times P_l)^2 + (eS_i \times S_i)^2 + (eS_o \times S_o)^2]^{0.5} \quad \text{.....(17)}$$

Where, e with the respective subscripts shows error associated with each parameter. eP_l, eS_i and eS_o are taken to be 5% (Chapter 7).

The following values for fluxes and Cl concentration have been used for the parameters set in Equations 15 and 16.

P_l= 4016 hm^3/year

C_{Pl} =1.19 mg/l

E_{ol} = 4720.3 hm^3/year

S_i-gauged = 4207.3 hm^3/year (excepting Gelda station data)

S_i- ungauged = 2278.3 hm^3/year

C_{Si} = 2.97 mg/l

S_o = 4733.4 hm^3/year

C_{Gi} = 82.9 mg/l

The chloride content of the lake (Cl = 2.87 mg/l) has been assigned to surface water out flow (S_o) and groundwater outflow or leakage from the lake (G_o).

The above data have been assigned for the fluxes and Cl concentrations in Equations 15 and 16 to estimate the groundwater inflow (G_i) to and groundwater outflow or leakage rate (G_o) from the lake. Solving Equations 15 and 16 has given leakage rate of 954.8 hm^3/year and groundwater inflow of -93.1 hm^3/year. The groundwater inflow value is negative but small and close to zero, which is within the limit of error introduced in the estimate because of measurement errors. This suggests that there is no significant direct groundwater contribution to the lake.

River water loss to recharge the lacustrine sediments aquifer in the eastern and northern plain areas seems generally to be small that does not significantly alter the results, and was not accounted in the lake balance evaluation. Moreover, magnitude of rivers' floods to the wetland is unknown and is not considered.

Uncertainty or error bound of ±375.0 hm^3/year, which is propagated from measurement error to the estimated groundwater inflow and leakage outflow values, is calculated based on Equation 17. The hydrochemical data have electro neutrality less than 5%, which indicates acceptable accuracy that does not introduce significant error in the estimates.

Sensitivity Analysis

The uncertainty introduced with the derived G_o and G_i due to the variation in magnitude of fluxes and Cl content has also been assessed based on sensitivity analysis. G_o and G_i have been calculated for the range of ±20% Cl contents of precipitation, groundwater inflow and the Tana Lake, and for evaporation flux and un-gauged runoff. Table 8.1 depicts the percentage change on leakage rate and groundwater inflow for the changes of the respective input parameters.

Sensitivity analysis showed that the groundwater inflow estimate is highly susceptible and influenced by Cl content of the lake followed by evaporation rate. Change in Cl content of the groundwater inflow and precipitation have relatively less impact on the estimated groundwater inflow.

Leakage rate is highly sensitive to the change in lake evaporation rate and to lesser extent to ungauged runoff while the change in other input parameters has generally low influence on it.

Table 8.1. Percentage changes in G_o and G_i for the changes in the respective input parameters by ±20%.

	Change of the calculated parameter (%)*	
Parameters	G_o	G_i
Cl content of precipitation	-1.3/+1.3	-12.9/+13.0
Cl content of groundwater inflow	+1.7/-2.5	+17.2/-26.1
Cl content of Tana Lake water	+4.0/-4.2	+40.7/-43.2
Evaporation	-102.4/+ 102.4	-36.3/+36.4
Ungauged runoff	+47.7/-47.9	-0.5/+0.6

* The numbers in the columns correspond to the increase/decrease by 20% of the respective input parameters

9. HYDROGEOCHEMISTRY

9.1. General

Natural water consists of dissolved minerals, dissolved gases and suspended particulate matter. The chemical composition of natural water is derived from different sources of solutes including gases from the atmosphere, weathering and erosion of rock and soil, solution or precipitation reactions occurring below the land surface and effect resulting

from human activities (Hem, 1985). The chemistry of groundwater in the saturated zone is controlled by chemical reaction rate, residence time within the saturated zone, and mineralogy of the rock matrix, where residence time and flow path are determined by factors such as aquifer thickness, permeability and amount of recharge. These factors combine to different degrees to create diverse water types with compositions that vary in space and time.

The objectives of the hydrochemical investigations are to determine the sources, concentration, and fate of dissolved constituents within the physical framework of flow and transport. The approach divides the water samples into hydrochemical facies (water types), which are groups of samples with similar chemical characteristics that can then be correlated with geography and geology.

The analytical results (ions, hydrochemical parameters and water types) were presented spatially and as bi-variant plots to understand the groundwater flow systems, and allow visualization of the trends (evolution), sources of salinity and interaction among water of different provenance.

9.2. Sampling and Evaluation of Accuracy of Laboratory Analysis

Groundwater samples were collected from springs, hand dug wells and boreholes during field works. Water samples have also been collected from rivers, wet land, Tana Lake and rainfall using 5 meteorological stations.

A total of 119 water samples have been collected for chemical analysis. Besides, additional 6 samples with complete hydrochemical data have been used from secondary sources. Some of the boreholes sampled have no depth information, which makes interpretation difficult.

The accuracy of the chemical analysis results was evaluated based on electro neutrality (EN) using Aquachem soft ware. According to Fetter (2001), analysis of water samples with EN within ± 5% is regarded as acceptable.

109 samples (87.9%) have EN between ± 5%, while samples with ± 5-10% EN are 10 (8.1%). Five samples (4%) have EN exceeding ± 10% (Fig. 9.1).

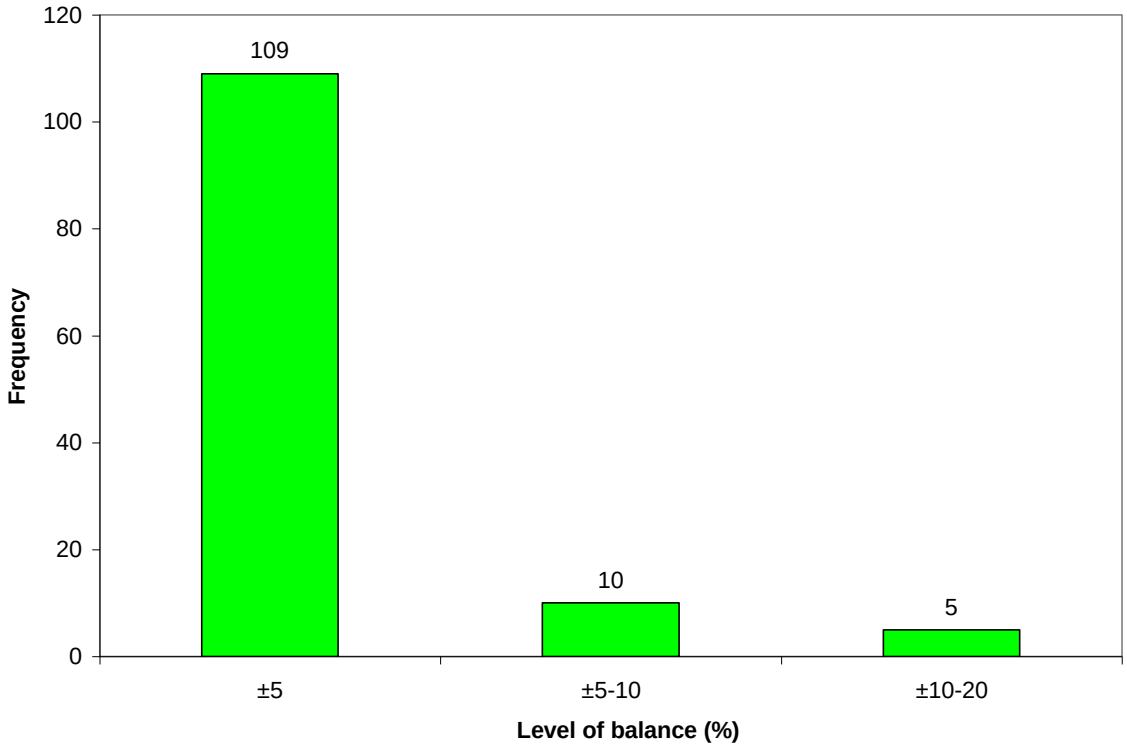

Figure 9.1. Graph showing electro neutrality of water samples.

All samples with balance error within ± 5% and 3 samples, which are important but with balance error between ± 5-10% (GW16, 27 and 54) have been used for data interpretation and analysis. Samples with EN exceeding ± 10% have been rejected.

Furthermore, plot of field measured pH against the laboratory measured pH values has shown very good correlation with R^2 equals to 0.73, which suggests that the laboratory analysis data are reliable.

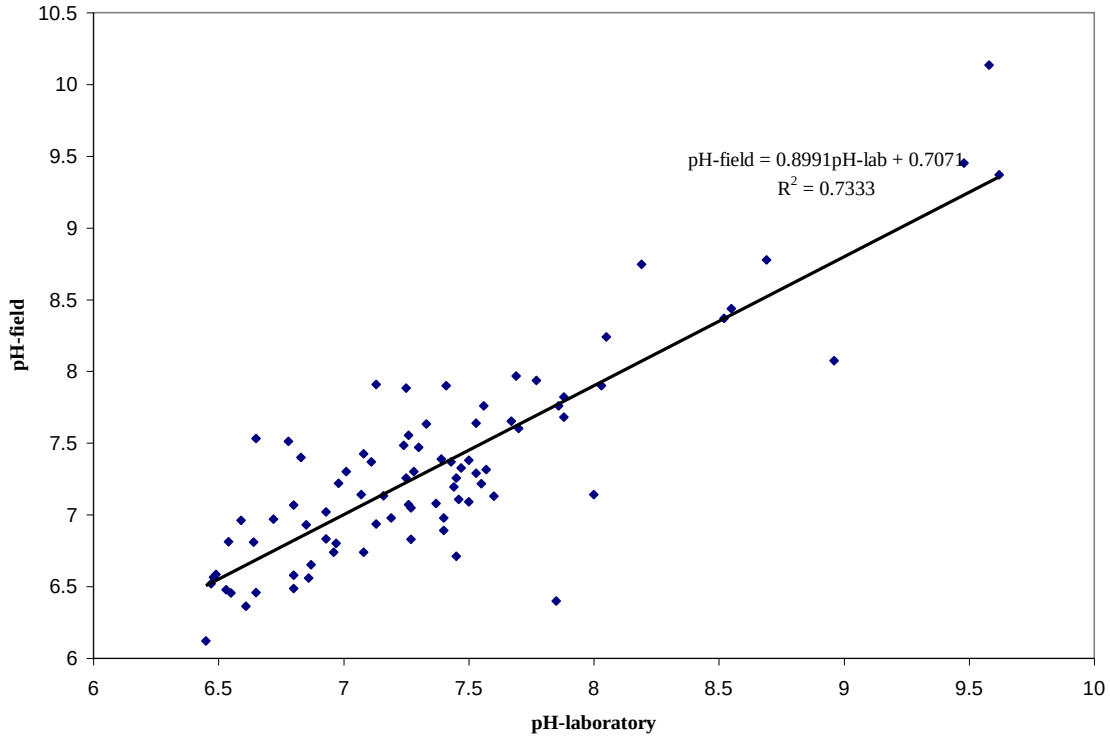

Figure 9.2. Plot of field measured pH versus laboratory measured pH values of groundwater samples.

9.3. Evaluation of Hydrochemical Parameters and Ions

Spatial variation of hydrochemical parameters and ions are evaluated to understand the hydrodynamics and identify possible sources. Hydrochemical parameters and ions vary spatially. Table 9.1 shows summary statistics for the groundwater samples in Tana basin. Chemical data are given Appendix 2.

9.3.1. Hydrochemical parameters

A. Total ionic concentration

The total ionic concentration is expressed in terms of electric conductivity (EC) or total dissolved solids (TDS). Figure 9.3 shows spatial distribution of EC.

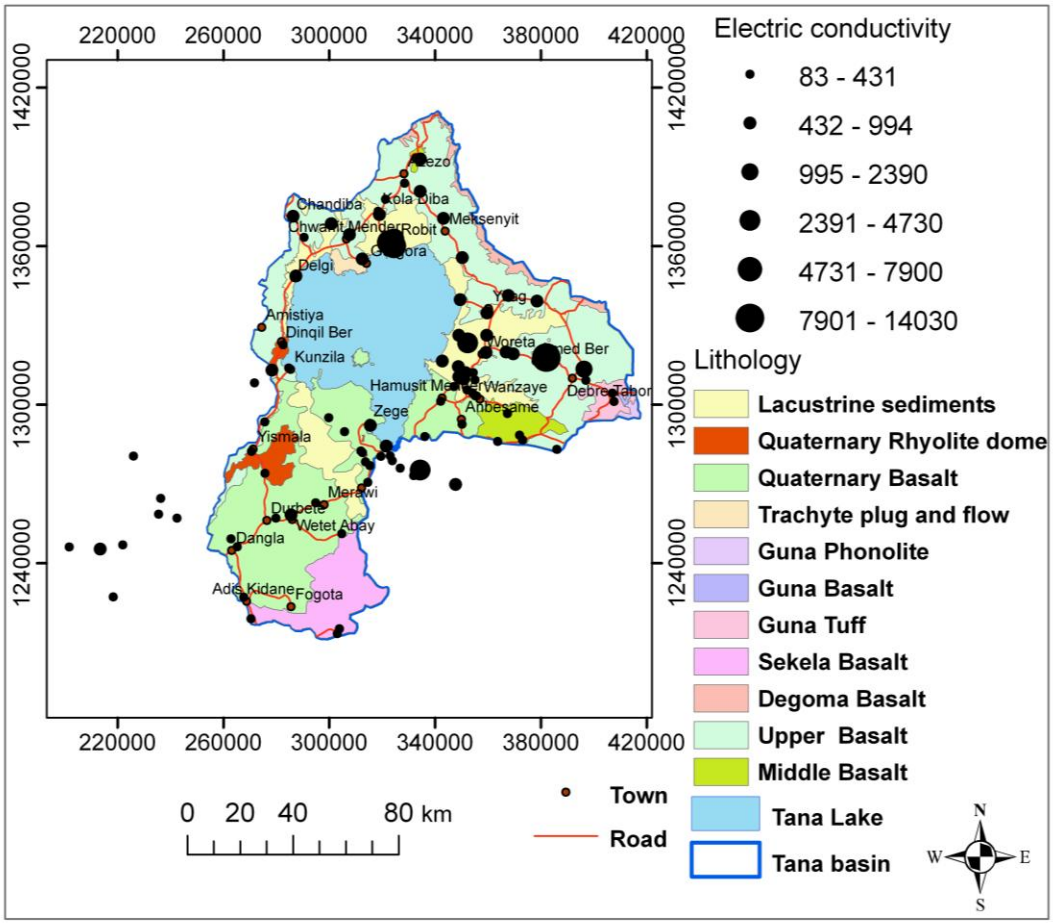

Figure 9.3. Spatial distribution of Electric conductivity (EC) in µS/cm.

EC varies form the minimum value of 83 µS/cm for GW63 (Gish Abay spring) at the southwestern area to 14030 µS/cm for GW32 (Serba Maryiam salty oozing spring) in the eastern area.

Table 9.1. Summary statistics for hydrochemical parameters and ions (mg/l).

	Na	K	Ca	Mg	HCO3	Cl	F	SO4	NO3	SiO2	Br	pH	EC (µS/cm)	TH
Mean	105.5	3.0	44.6	28.0	376.4	69.0	0.5	50.9	9.0	45.3	1.2	7.4	837.6	227.1
Median	20.0	1.3	29.5	11.9	221.0	4.0	0.3	4.9	4.9	44.0	0.5	7.3	382.5	127.3
Maximum	3700.0	88.0	680.0	400.0	7893.0	1872.0	5.5	2297.0	90.8	107.0	18.4	9.6	14030.0	3345.5
Minimum	2.1	0.2	0.0	0.1	27.0	0.0	0.1	0.1	0.0	10.0	0.1	6.5	83.0	2.9
Count	96.0	96.0	96.0	96.0	96.0	96.0	96.0	96.0	96.0	82.0	76.0	96.0	96.0	96.0
Standard deviation	398.9	9.1	77.5	66.6	873.6	281.7	0.6	265.1	14.5	19.8	2.9	0.7	1853.3	441.2

Ground waters in the southwestern area have less EC values than in eastern and northern areas. However, relatively high EC value was seen in southwestern area especially for deep (500m) test borehole, which equals to 1 247 µS/cm. Exceptionally high EC values of 14030 and 2390 µS/cm have also been observed for GW32 and GW9 (Debretabor borehole no.10), which are found in volcanic rocks in the eastern area. This may suggest that these samples represent deep ground waters. On the other hand, some hand dug wells in the lacustrine sediments aquifer of eastern and northern areas show EC ranging from 3980 µS/cm for GW27 to 7900 µS/cm for GW4 (see Section 9.5)

Deep (301m) borehole (GW3) that intersect the Upper, Middle and Lower basalts aquifers in the northern area and hot springs of GW42 and GW16 in the eastern volcanic area have low EC values of 294, 192 and 198 µS/cm, respectively.

In general, EC increases along groundwater flow direction. Some unexpected low values along down flow direction are due to shallow depth of boreholes and hand dug wells.

B. pH

pH varies from 6.47 for GW9 in the eastern area to 9.62 for GW3 in the northern area. (Fig. 9.4)

Most samples have pH between 6.73 to 7.77. Some boreholes (GW84, 11, 3) and hot springs (GW42, 16) are hyper alkaline (9.1 to 9.48). In general, groundwater in the southwest has low pH than other parts of the area. pH does not show systematic variation along groundwater flow direction.

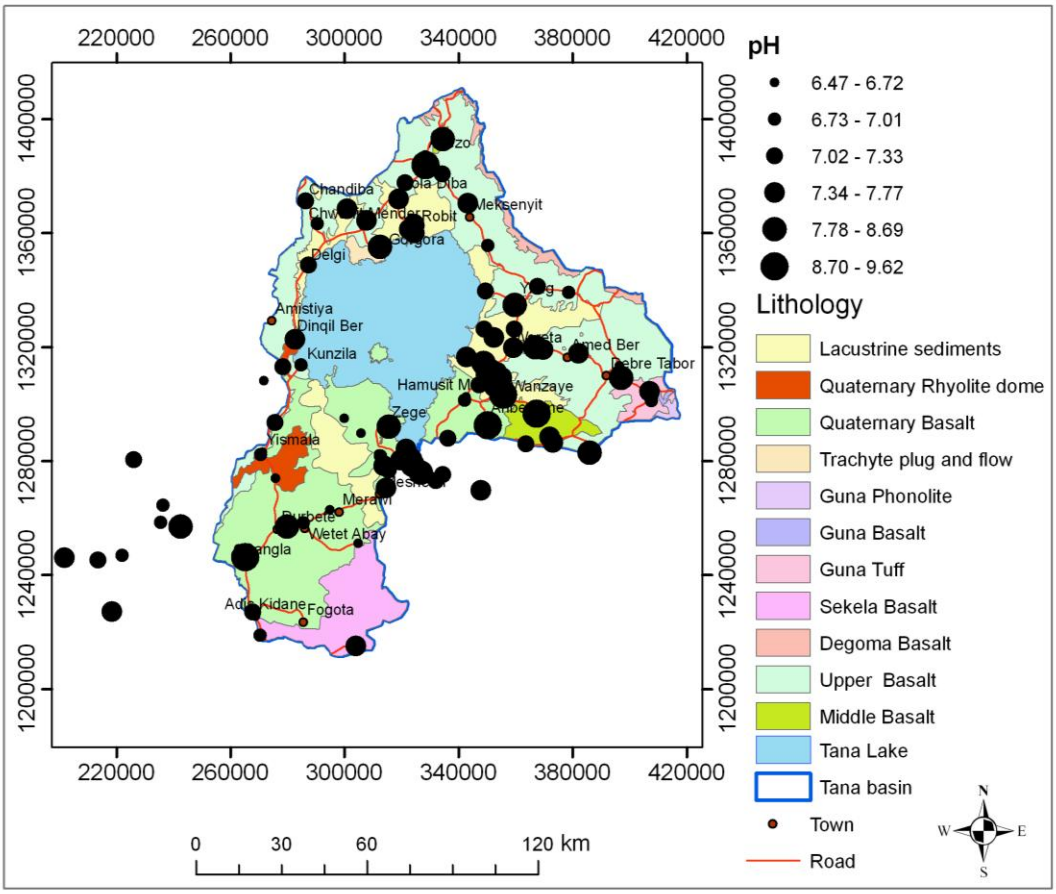

Figure 9.4. Spatial distribution of pH.

C. Total Hardness (TH as $CaCO_3$)

The minimum and maximum total hardnesses are 2.9 and 3346 mg/l which are observed at GW42 and GW4, respectively in the eastern and northern areas. Most samples have TH less than 159 mg/l. Relatively high values of 1892 and 1792 mg/l are observed in GW75 and 24 (Fig. 9.5) .

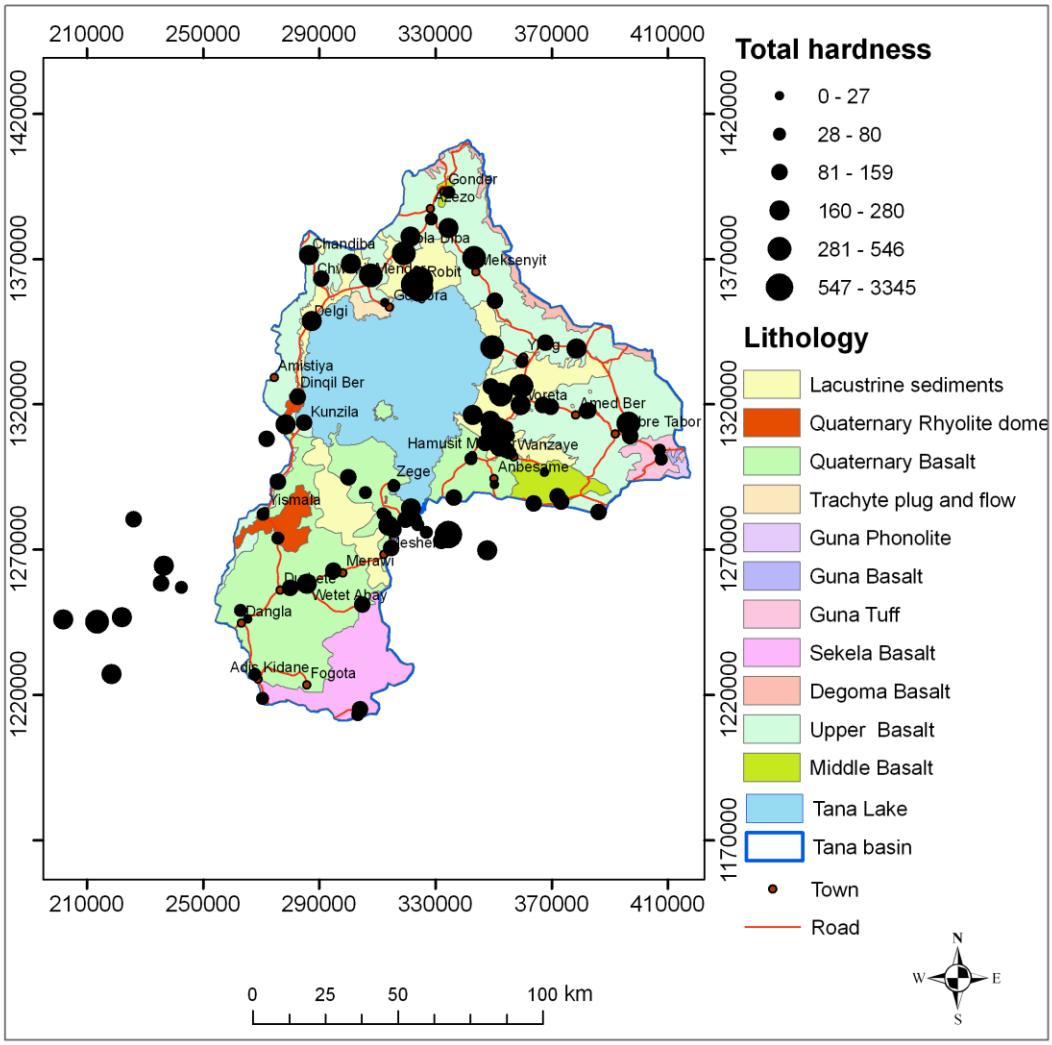

Figure 9.5. Spatial distribution of total hardness (mg/l).

9.3.2. Major ions

A. Calcium and Magnesium

Ca^{2+} varies from about 0.01 for GW32 in eastern area to 680 mg/l for GW4 in northern area. Most groundwater samples have less than 46 mg/l (Fig. 9.6).

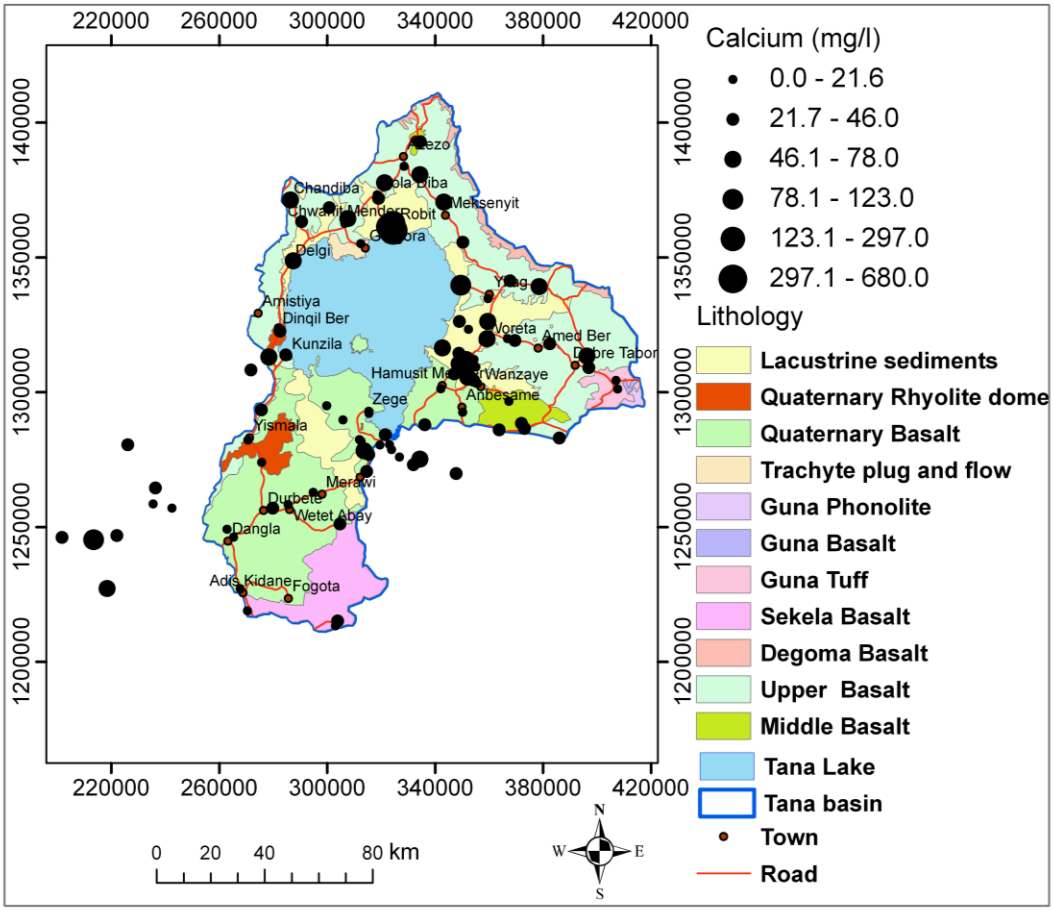

Figure 9.6. Spatial distribution of Ca^{2+}.

Groundwater in the southwestern area has low Ca^{2+} when compared to other parts of the area. Relatively high values are seen in GW4, 24 and 75, which are found within the lacustrine sediments in the northern area (see Section 9.5).

Ca^{2+} decreases along groundwater flow direction although locally high and low values are found due to variation in depth of boreholes, geochemical reaction, ion exchange and presence of deep groundwater system (Fig. 9.6).

Mg^{2+} values of groundwater range from 0.1 for GW21 in the eastern area to 400 mg/l for GW21 in the northern area. Most of the groundwater samples in the basin have Mg^{2+} below 19.3 mg/l. GW27 in the eastern area, and GW4, 75 and 24 in the northern area have exceptionally high Mg^{2+} content (100-400 mg/l).

Low Mg^{2+} content is seen in the southwestern area than the rest areas. Mg^{2+} decreases along groundwater flow direction in southwestern and eastern areas while increases in the northern area although there are some groundwater points with high and low values (Fig. 9.7).

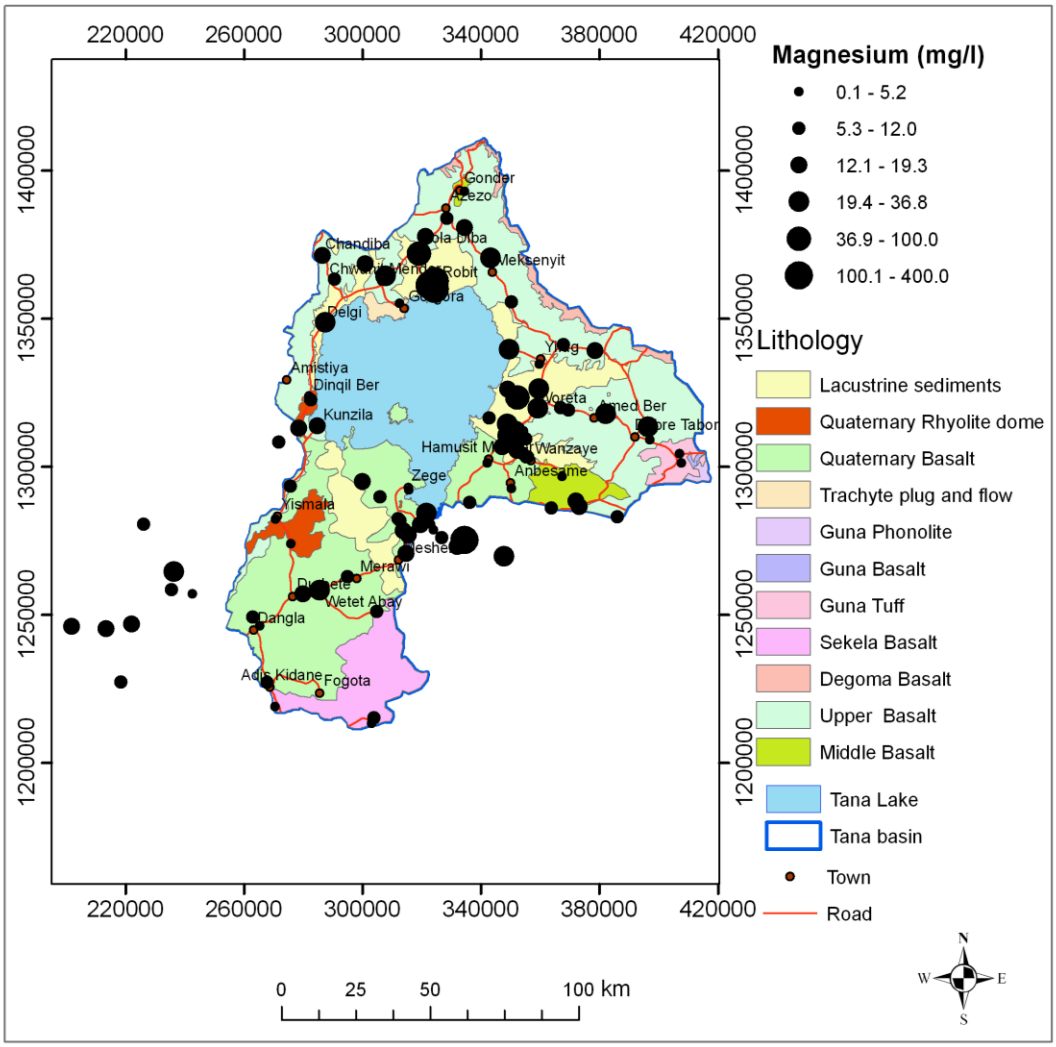

Figure 9.7. Spatial distribution of Mg^{2+}.

B. Sodium

The minimum and maximum values of Na^+ are 2.05 and 3700 mg/l, which are for GW43 in southwestern area and GW32 in eastern area. Most of the groundwater samples have Na^+ less than 35.3 mg/l. Relatively high value of 504 mg/l has also been seen for sample GW9 in volcanic rocks of eastern area. GW75 and GW4 in northern area, which are found in lacustrine sediments, showed Na^+ concentration of 625 to 877 mg/l.

Na^+ concentration is lower in southwestern area than the eastern and northern area. Spatial distribution of Na^+ is complicated by high and low values of groundwater points along groundwater flow direction, which is due to variation in depth. Generally, Na^+ tends to increases along groundwater flow direction although complicated by variation in borehole depth, local dissolution of evaporites in lacustrine sediments and short circuts of deep ground waters as in the eastern area (GW9 and 32), see Fig. 9.8.

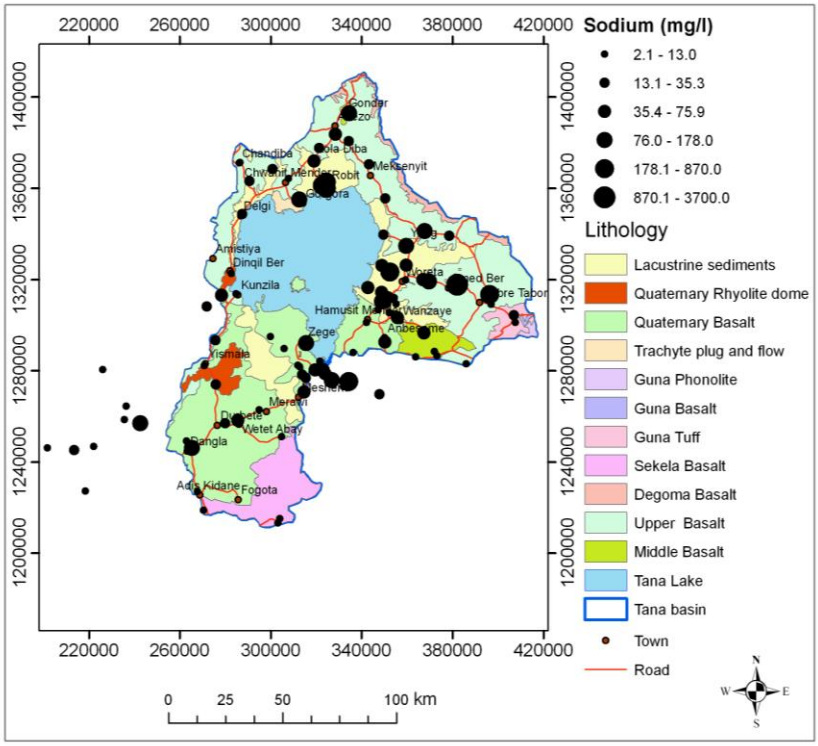

Figure 9.8. Spatial distribution of Na^+.

C. Bicarbonate

Bicarbonate ion varies from 27 mg/l for hot spring GW46 to 7893 mg/l for GW32 (Serba Maryiam salty oozing spring) in eastern area. Most samples show $HCO3^-$ content less than 281 mg/l. GW24, 75, 4, 9 and 27 have relatively high $HCO3^-$ values (Fig. 9.9).

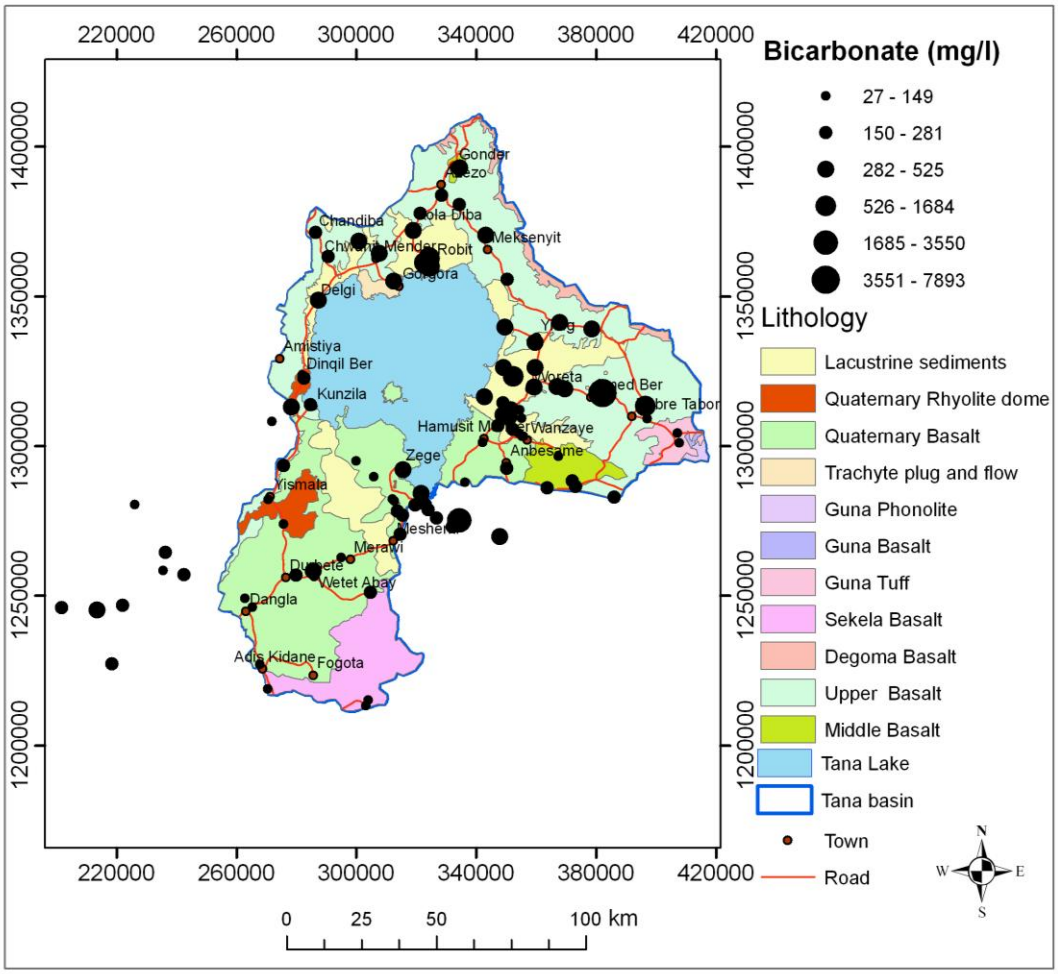

Figure 9.9. Spatial distribution of HCO_3^-.

The southwestern area has relatively lower concentration than other parts of the area. Presence of groundwater points with high and low HCO_3^- complicate the trend along the groundwater flow direction. In the southwest and northern areas HCO_3^- increases along groundwater flow direction.

D. Chloride

Some groundwater samples showed the minimum Cl^- content of 1 mg/l, which are found in lacustrine sediments, Quaternary and Upper basalts aquifers. Hand dug well GW75 in lacustrine sediments of northern area shows the maximum value of 1872 mg/l. Most samples have Cl^- content below 18 mg/l. Relatively high values of 1071 mg/l (GW32) and 580 mg/l (GW27) in the eastern area, and 1 489 (GW4) and 876 mg/l (GW24) in northern area have been observed.

Groundwater in southwestern area have very low Cl^- content, which is less than 15 mg/l and slightly increases along groundwater flow direction. Cl^- increases along groundwater flow direction in the northern area as well. Cl^- content also tends to increase along groundwater flow direction in the eastern area although complicated by high and low values at different places due to variation in borehole depth, local dissolution of evaporites and short circuits of deep ground waters (e.g. GW32), see Fig.9.10.

E. Sulfate

GW90 and GW4 have the minimum and maximum $SO4^{2-}$ content of 0.14 and 2297 mg/l, respectively. Most samples have less than 19.1 mg/l. Some high values of $SO4^{2-}$ are seen in GW75 (779 mg/l) and GW24 (876 mg/l), see Section 9.5.

Sulfate concentration in the southwestern area is very low (<7.7 mg/l), except one sample with 26.7 mg/l, when compared to other parts of the area. There is no clear trend along groundwater flow direction in this area. Sulfate tends to increase along groundwater flow directions in the eastern and northern areas although there are some high and low spots (Fig. 9.11).

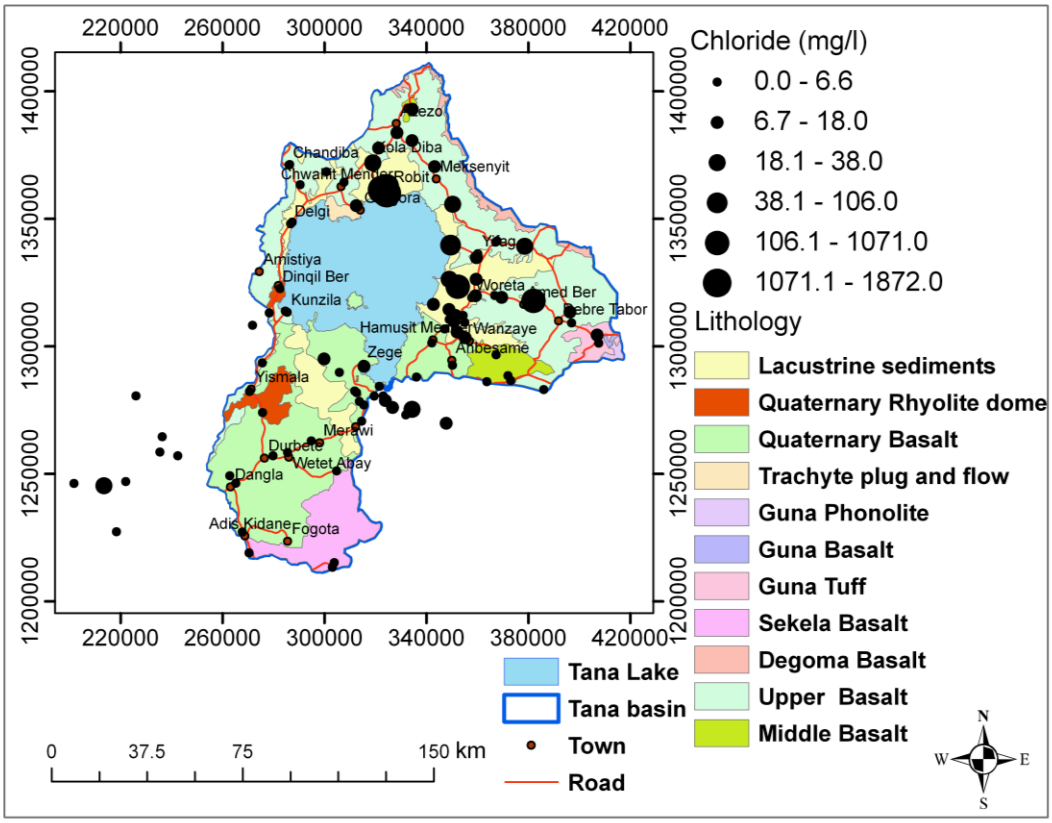

Figure 9.10. Spatial distribution of chloride.

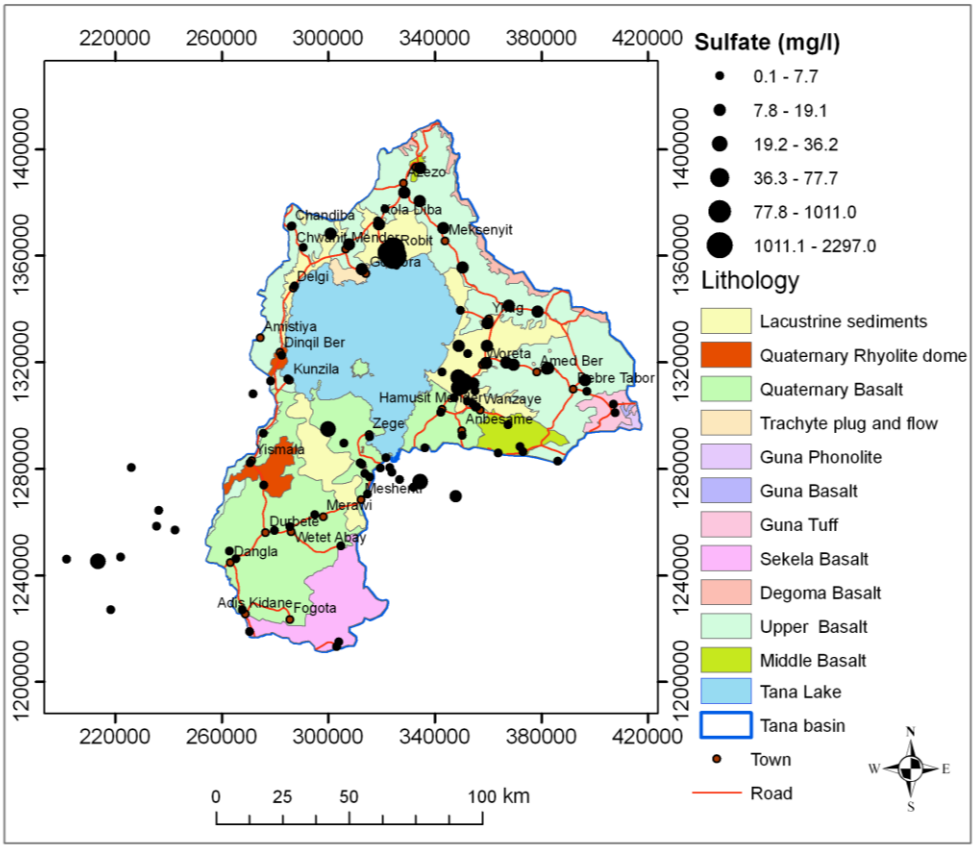

Figure 9.11. Spatial distribution of sulfate.

F. Fluoride

The minimum (0.06 mg/l) and maximum (5.5 mg/l) values of F^- are seen for GW4 and GW32. Fluoride is often less than 1.5 mg/l. Relatively higher value has been observed at GW9 (2.8 mg/l), which is in Upper Basalt aquifer in the eastern area. This borehole and GW32 seem to tap intermediate and deep groundwater systems, respectively (see Section 9.5).

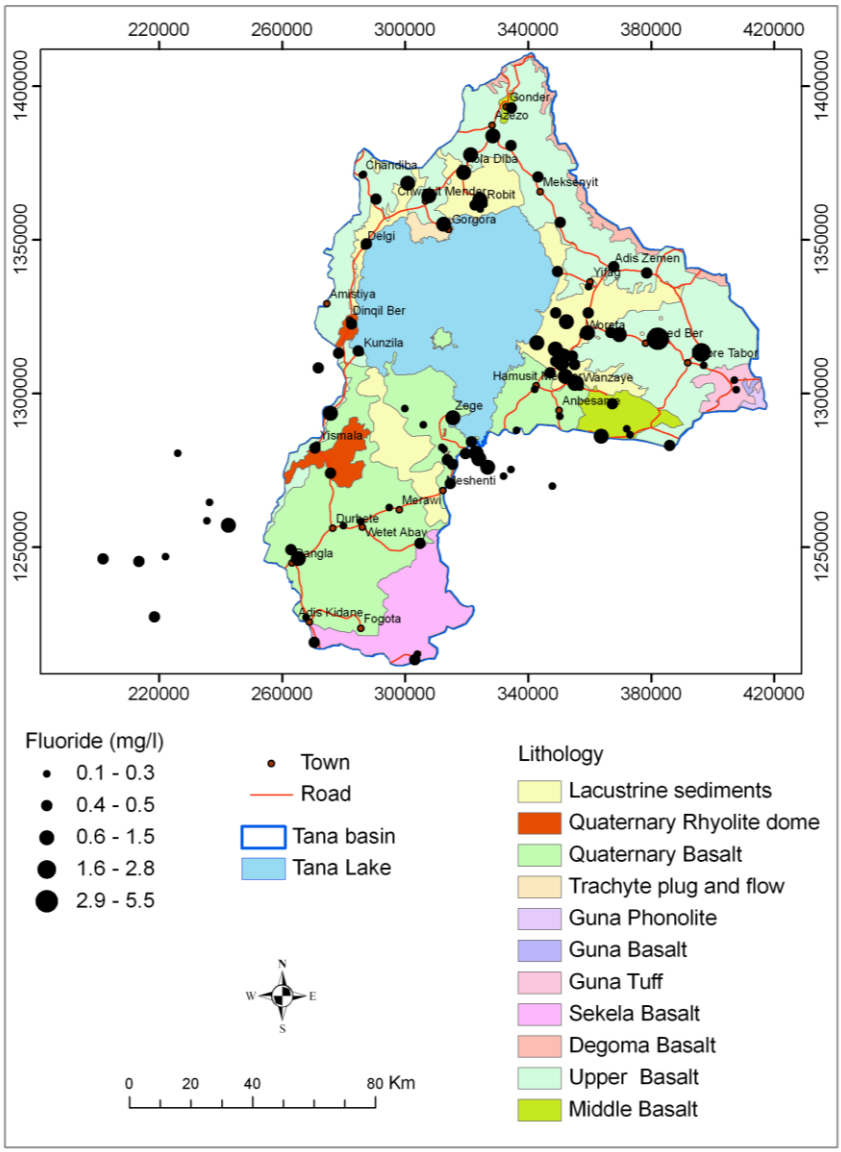

Figure 9.12. Spatial distribution of fluoride.

9.4. Multivariate Analysis and Hydrochemical Facies

The spatial variability observed in the composition of natural tracers can provide in sight into aquifer heterogeneity and connectivity, flow paths, as well as the physical and chemical processes controlling the water chemistry (Güler et al., 2002).

Classification or partitioning of water chemistry samples in to homogenous groups each representing hydrochemical facies is an important tool for successful characterization of hydrogeologic system (Güler et al., 2002; 2003; Hershey et al., 2010). Multivariate statistical method is more robust and objective approach to classify or group water chemistry data in to distinct population, which have similar physical and chemical characteristics that may be significant in geologic and geographic context.

Q-mode hierarchical cluster analysis (HCA) using portable Statistica 8 has been used here. In this classification, the Euclidean distance measure for the observations and Ward's method for the linkage rule were used. Ward's (1963) method uses an analysis of variance approach to evaluate the distance between clusters, and is distinct from other linkage rules. Ward's method calculates the sum of the distances from each individual to the center of its parent group and forms smaller distinct clusters than those formed by other methods (Stat Soft, INC, 1995). Euclidian distance (straight line distance) between two points in a C-dimensional space defined by C-variables is used as a similarity measurement together with Ward's method for linkage. Among the various choices for distance measure and linkage rule that can be used in HCA, this combination has been shown to yield the most distinctive groups for hydrogeochemical data (Güler et al., 2002; Hershey et al., 2010). Each member in the group is more similar to its fellow members than any member from outside the group. The result of HCA can be presented in a familiar diagram called dendogram.

Eleven parameters (EC, pH, Na^{+}, K^{+}, Ca^{2+}, Mg^{2+}, HCO_3^{2-}, Cl^{2-}, SO_4^{2-}, F^{-} and SiO_2) have been chosen and log transformed by taking the base-10 log to provide symmetric input. Then, all the parameters were standardized by calculating their standard scores (Z-scores) as follows to make each variable has equal weight into statistical analysis (Güler et al., 2002; Hershey et al., 2010).

$$Z_i = (X_i - X)/s \qquad (18)$$

Where, Z_i is the standard score of sample i, X_i is value of sample i, X is mean, and s is the standard deviation.

Q-mode classification (HCA) has given 3 sub groups (Subgroups1, 2 and 3). Subgroup1 belongs to Group1 while subgroups 2 and 3 belong to Group 2 (Fig. 9.13)

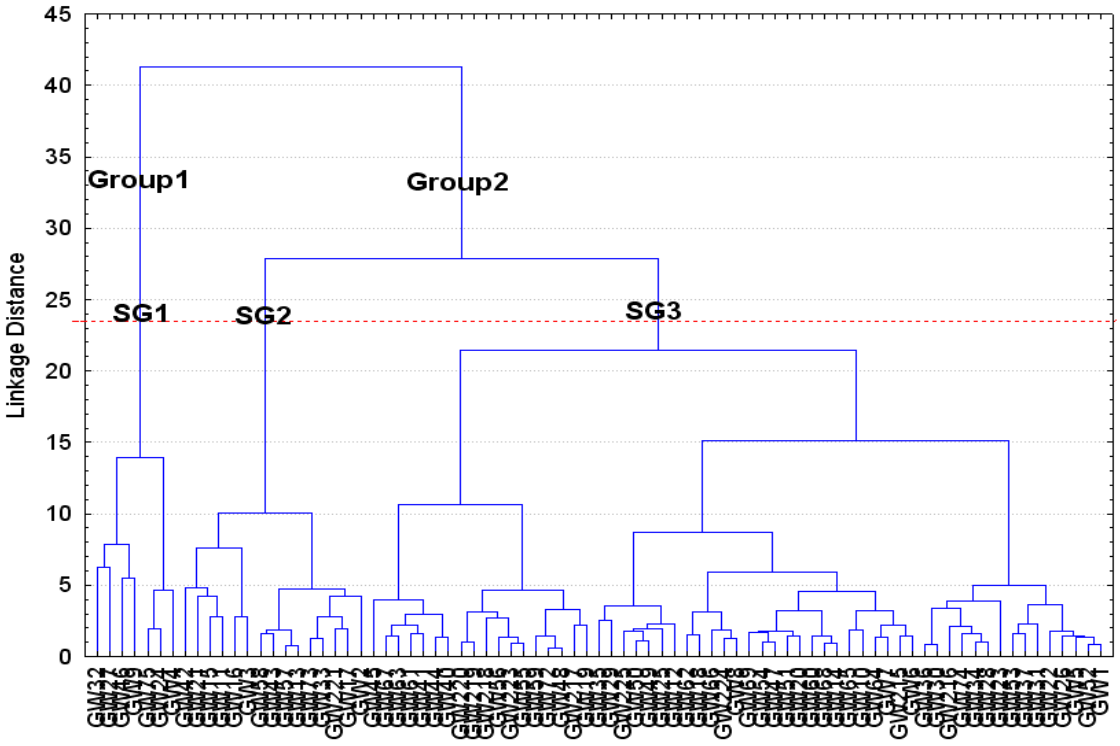

Figure 9.13. Dendogram showing clusters or subgroups (SG) of ground waters. Dashed red line is the phenon line. Labels of X axis are sample numbers (see Appendix 4).

To further test the robustness of clustering and to see overlap of clusters based on the two methods, principal component analysis (PCA) was applied. PCA is a mathematical manipulation that may provide a certain amount of insight into the structure of the data matrix by reducing the dimension of the data matrix (Davis, 2002).

This technique reduces the number of dimensions present in the data. The PCA defined new variables can then be displayed in a scatter diagram, presenting the water samples as a points in 2D space.

The loadings of the principal components are shown in Table 9.2 along with their percentage of variance for which they account. About 95% of the variance is contributed by the first 7 principal components. Principal components 1 and 2 account to 61 % of the variances. PC1 is dominated by EC, HCO_3^-, Na^+, Cl^-, SO_4^{2-} and Mg^{2+}. Ca^{2+}, pH, F^- and Mg^{2+} are major contributors to PC2 while SiO2 and K^+ are major contributors of PC3. pH and to a lesser extent Ca^{2+} and K^+ are major contributors to PC5. PC6 is mainly contributed by $SO4^{2-}$ and Mg^{2+} while PC7 is by F^- and Ca^{2+}.

PCA helped to verify and make smooth the Q-mode classification. A plot of scores of PC2 versus scores of PC1 is shown in Figure9.13.

Table 9.2. Variance and loadings of variables to principal components.

	Factor 1	Factor 2	Factor 3	Factor 4	Factor 5	Factor 6	Factor 7	Factor 8	Factor 9	Fact.10	Fact.11
Total variance	41.51	19.21	13.00	8.18	5.26	4.14	3.82	2.36	1.58	0.67	0.26
Na	-0.89	0.31	-0.10	-0.04	0.09	0.06	0.00	-0.18	-0.15	0.18	0.03
K	-0.32	0.20	0.57	0.63	0.30	0.04	0.11	0.16	0.00	0.01	-0.01
Ca	-0.07	-0.85	-0.02	0.04	0.34	-0.04	-0.38	-0.04	0.11	0.05	0.00
Mg	-0.65	-0.52	0.10	-0.17	-0.27	0.31	0.03	0.30	0.01	0.06	0.02
HCO3	-0.90	-0.01	0.27	-0.07	0.04	0.21	-0.10	-0.16	-0.02	-0.16	0.07
Cl	-0.86	-0.01	-0.24	0.07	-0.05	-0.23	0.23	-0.03	0.29	0.02	0.04
F	-0.41	0.63	0.36	-0.04	-0.27	-0.24	-0.40	0.10	0.05	0.02	0.00
SO4	-0.74	-0.30	-0.38	0.01	0.09	-0.36	0.01	0.17	-0.21	-0.07	0.01
SiO2	0.06	-0.15	0.72	-0.59	0.20	-0.20	0.18	0.01	-0.01	0.02	0.00
pH	-0.13	0.68	-0.40	-0.33	0.41	0.17	-0.06	0.19	0.08	-0.02	-0.01
EC	-0.98	-0.06	0.03	-0.05	-0.02	0.07	0.03	-0.10	0.02	-0.03	-0.14

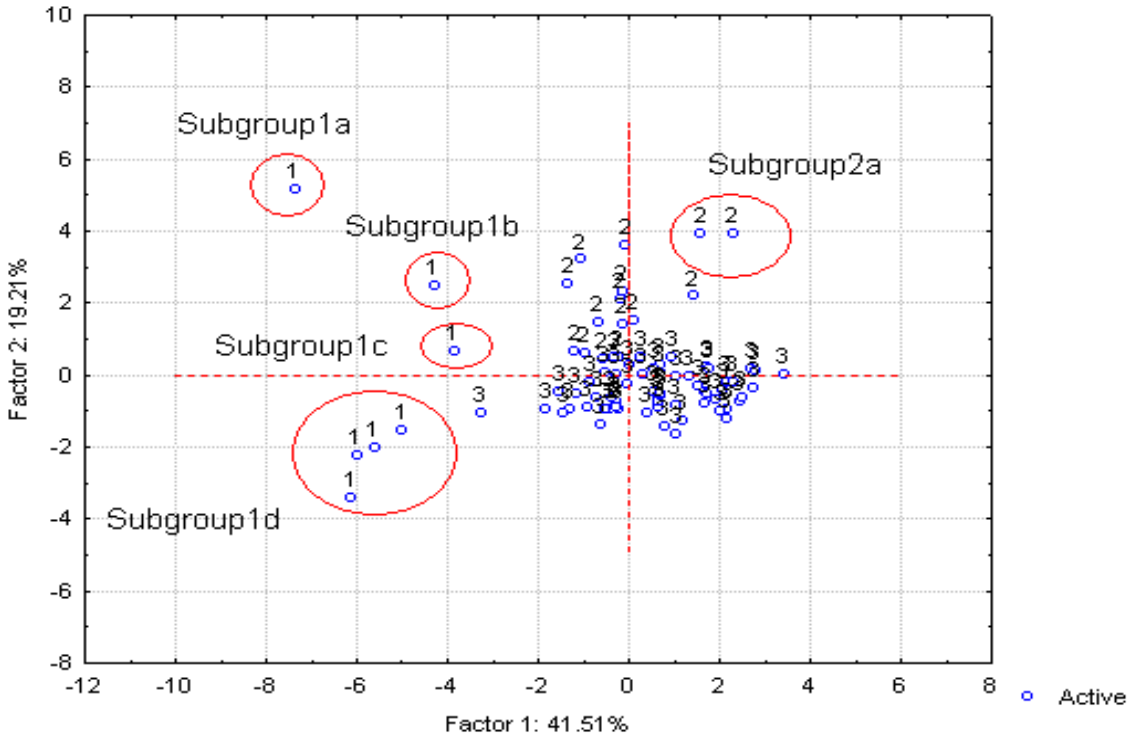

Figure 9.14. Further classification by PCA. Numbers indicate subgroups based on HCA classification.

Further clustering of the subgroups made by Q-mode classification has been observed in Figure 9.14. Accordingly, Subgroup1 is further subdivided into Subgroups 1a, 1b , 1c and 1d. Subgroup2 is partitioned into subgroup 2a, which represent hot springs, and as Subgroup2 proper. Subgroup3 is maintained as obtained by HCA.

Mean values of variables of each cluster has been estimated from member samples (Table 9.3). In this Table GW46 has been treated separately from subgroup1d for better visualization. PCO_2 has also been estimated for each subgroup based on the following formula (StatSoft.Inc, 2007).

$$PCO_2 = 10^{1.468} \times \alpha CO_2(aq) \quad \text{.....(19)}$$

Where, PCO_2 *is* partial pressure of carbon dioxide, $\alpha CO_2(aq)$ represents activity of aqueous carbon dioxide and $10^{1.468}$ is Henry's law constant

The average hydrochemical data of ground waters, which belong to each subgroup has been plotted into Piper diagram (Fig. 9.15). Size of symbol increase with increase in total dissolved solids. Average values of surface waters and rainfall chemistry data have also been plotted in this diagram.

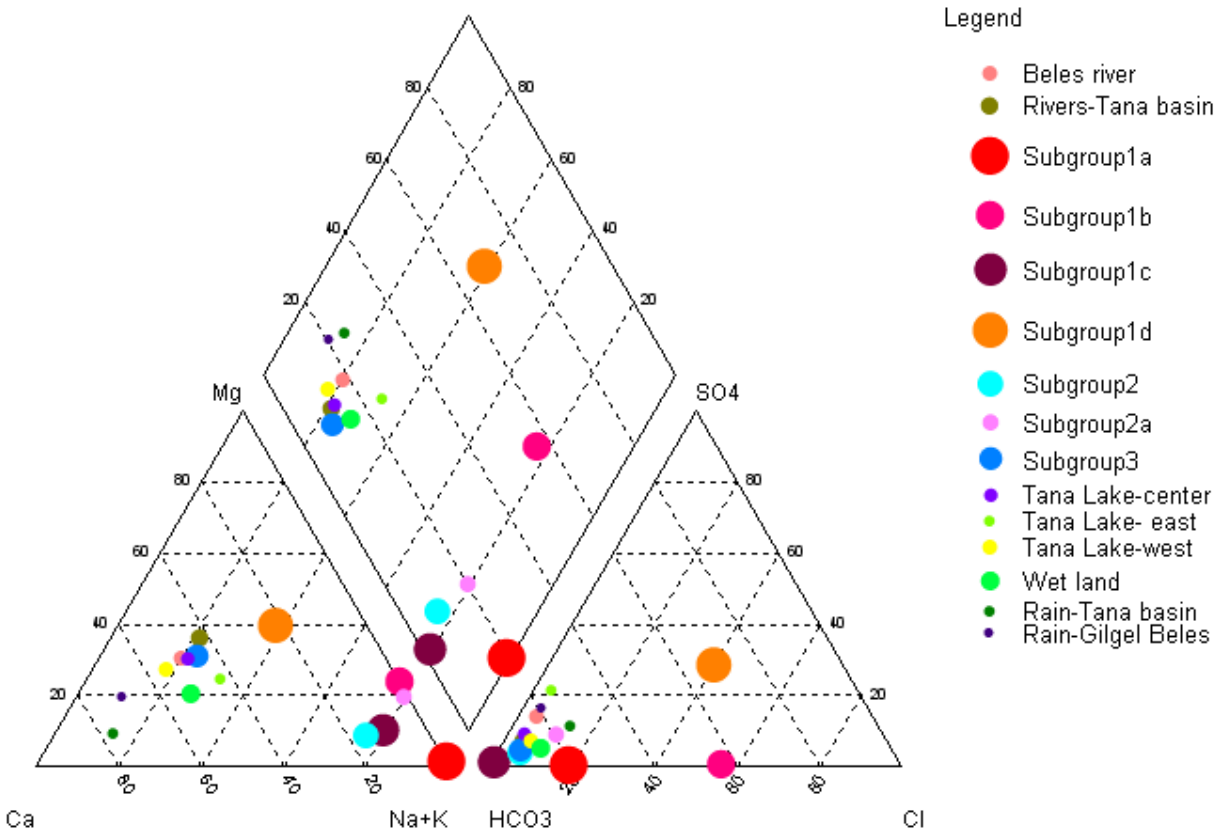

Figure 9.15. Piper diagram of groundwater subgroups, surface waters and rainfall. Size of symbols is proportional to their total dissolved solids content.

Table 9.3a. Mean values of ions and hydrochemical parameters for groundwater clusters or subgroups (mg/l).

SampleID	Na	K	Ca	Mg	HCO_3	CO_3	Cl	F	SO_4	NO_3	SiO_2	Br	TDS	pH	PCO_2(atm)	EC (µS/cm)
subgroup1a	3700.00	88.00	0.01	25.00	7893.00	0.00	1071.00	5.50	9.64	1.00	47.00	0.1	12840.25	7.50	23.84	14030.00
subgroup1b	625.00	1.00	0.10	100.00	780.00	0.00	580.00	1.10	6.77	7.00	23.00	9.2	2133.17	7.55	0.024	3980.00
subgroup1c	504.02	14.92	61.00	33.50	1684.00	0.00	8.40	2.80	8.38	0.00	24.00	0.23	2341.25	6.47	0.628	2390.00
subgroup1d	640.00	1.22	402.33	325.00	744.67	0.00	1412.33	0.29	1362.33	12.93	25.33	13.98	4940.41	7.42	0.027	6610.00
subgroup2a	39.03	0.49	0.53	5.15	41.50	35.00	3.50	0.66	3.60	0.40	49.30	0.18	179.33	9.53	9.52×10^{-6}	195.00
subgroup2	85.36	2.20	15.62	5.01	273.46	4.00	9.68	0.55	8.07	2.25	32.46	0.62	439.28	8.25	2.26×10^{-10}	459.54
Subgroup3	21.00	2.00	37.00	15.00	223.00	0.00	8.00	0.30	8.00	12.00	49.00	0.59	375.90	7.00	0.027	402.00
GW46	543	10.65	56	364	3550	0	30	0.25	36.2	0.4	107	2	4699.5	7.19	0.228	4410
GW226	188.5	14.6	39.5	49.25	824	0	13.12	0.39	0.39	1.77	83.89	-	1215.4	7.08	2.798	1247

Table 9.3b. Mean values of ions and hydrochemical parameters for surface waters and rainfall (mg/l).

SampleID	Na	K	Ca	Mg	HCO_3	CO_3	Cl	F	SO_4	NO_3	SiO_2	Br	TDS	pH	PCO_2 (atm)	EC (µS/cm)
Wet land	15.0	1.7	26.5	6.3	137.5	0.0	9.5	0.8	6.2	1.7	6.5	0.08	211.7	6.8		253.0
Tana Lake-east	11.5	1.7	14.4	5.0	79.3	0.0	2.8	0.5	17.8	0.4	9.1	2.19	142.3	7.5		157.3
Tana Lake-west	5.8	2.1	19.2	5.8	92.7	0.0	3.9	0.4	6.0	0.4	7.2	0.5	143.5	7.6		159.7
Tana Lake-center	6.2	2.3	14.8	5.6	87.3	0.0	2.3	0.5	7.2	0.4	8.0	0.6	134.7	7.8		162.0
Rivers-Tana basin	9.8	2.5	19.4	10.0	121.9	1.6	3.8	0.2	7.6	3.3	20.2	0.52	200.3	8.0		228.4
Beles river	6.4	2.1	16.7	6.1	89.0	0.0	2.7	0.3	12.2	0.4	4.9	0.4	140.4	7.3		160.0
Rain-Tana basin	0.61	0.44	4.16	0.32	11.07	0.00	1.20	0.10	1.36	3.32	0.25	0.2325	23.06	6.81375	0.096	32.625
Rain-Gilgel Beles	0.70	0.18	4.25	0.72	14.00	0	0.50	0.14	2.22	2.66	1.00	0.26	26.63	6.66		33.00

Water type classification by Aquachem software is based on the dominancy of ions but it has no means to indicate whether the relative percentage of the ions is high or low. A better classification approach is used here based on the percentage milli equivalent method as follows, which groups hydrochemical facies as basic, transitional and mixed types.

Basic: the contents of cation and anion exceeds 50% meq
Transitional: the contents of cation and anion range between 34 and 50 meq or exceeds 50% meq only for one ion.
Mixed: the contents of the cation and anion are less than 34% meq or exceed 34 % meq only for one ion.
The second and third dominant ions may be considered in the naming.

On the basis of the above classification, the groundwater subgroups and surface and rain waters have the following hydrochemical facies (Table 9.4).

Spatial distributions of groundwater subgroups and hydrochemical facies have been shown in Figures 9.16 and 17. Subgroup 3 has less TDS (376 mg/l) than subgroup2 (439 mg/l). Subgroup2a has the least TDS (179 mg/l). Subgroup1a has the highest TDS (12840 mg/l). Subgroups 1b, 1c and 1d have TDS of 2 133, 2341 and 4880 mg/l, respectively.

Table 9.4. Hydrochemical facies associated with ground waters subgroups, surface and rain waters.

Water body	Hydrochemical facies
Subgroup1a	Na-HCO_3 (basic)
Subgroup1b	Na-Mg-Cl- HCO_3 (basic)
Subgroup1c	Na- HCO_3 (basic)
Subgroup1d	Na-Mg-Ca-Cl-SO_4 (transitional)
GW46	Mg-Na- HCO_3 (basic)
Subgroup2a	Na-Mg- HCO_3(basic)
Subgroup2	Na- HCO_3 (basic)
Subgroup3	Ca-Mg-Na- HCO_3 (transitional)
GW226	Na-Mg-Ca-HCO3 (basic)
Rain-Tana basin	Ca- HCO_3 (basic)
Rain-Gilgel Beles	Ca- HCO_3 (basic)
River-Tana basin	Ca-Mg-Na- HCO_3(transitional)
Beles river	Ca-Mg-Na- HCO_3 (basic)
Wet land	Ca-Na-Mg- HCO_3 (basic)
Tana Lake(east and north)	Ca-Na-Mg- HCO_3-SO_4 (transitional)
Tana Lake (west)	Ca-Mg-Na- HCO_3 (basic)
Tana Lake (center)	Ca-Mg-Na- HCO_3 (transitional)

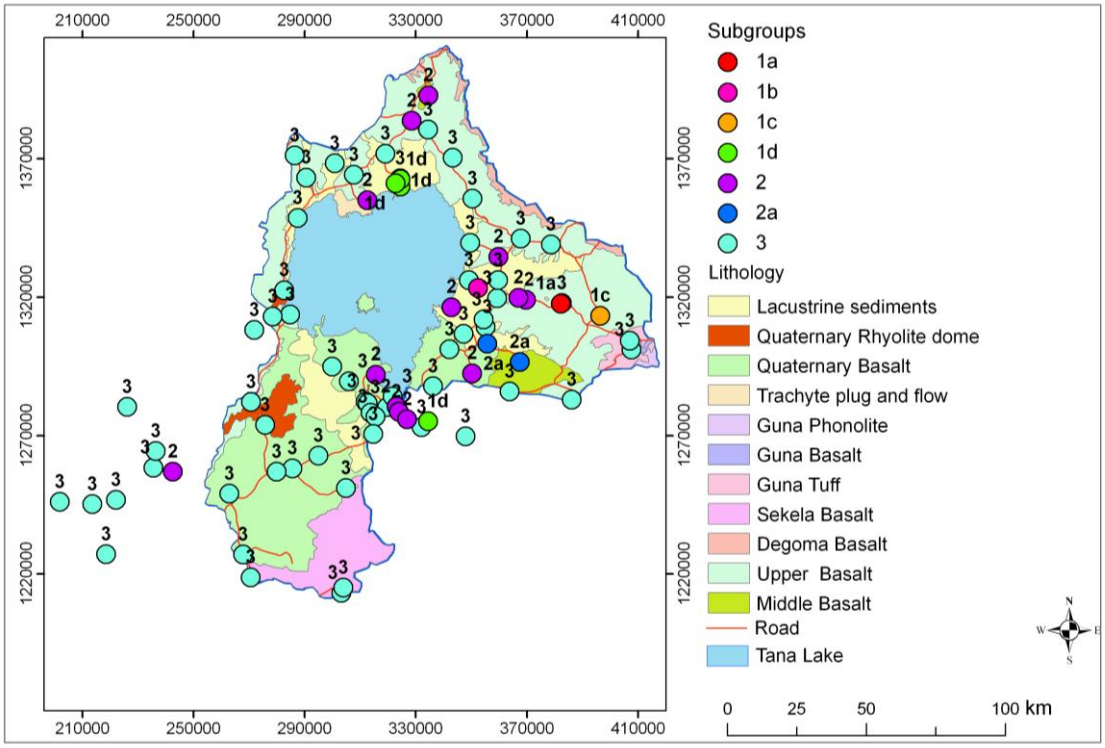

Figure 9.16. Spatial distributions of groundwater subgroups.

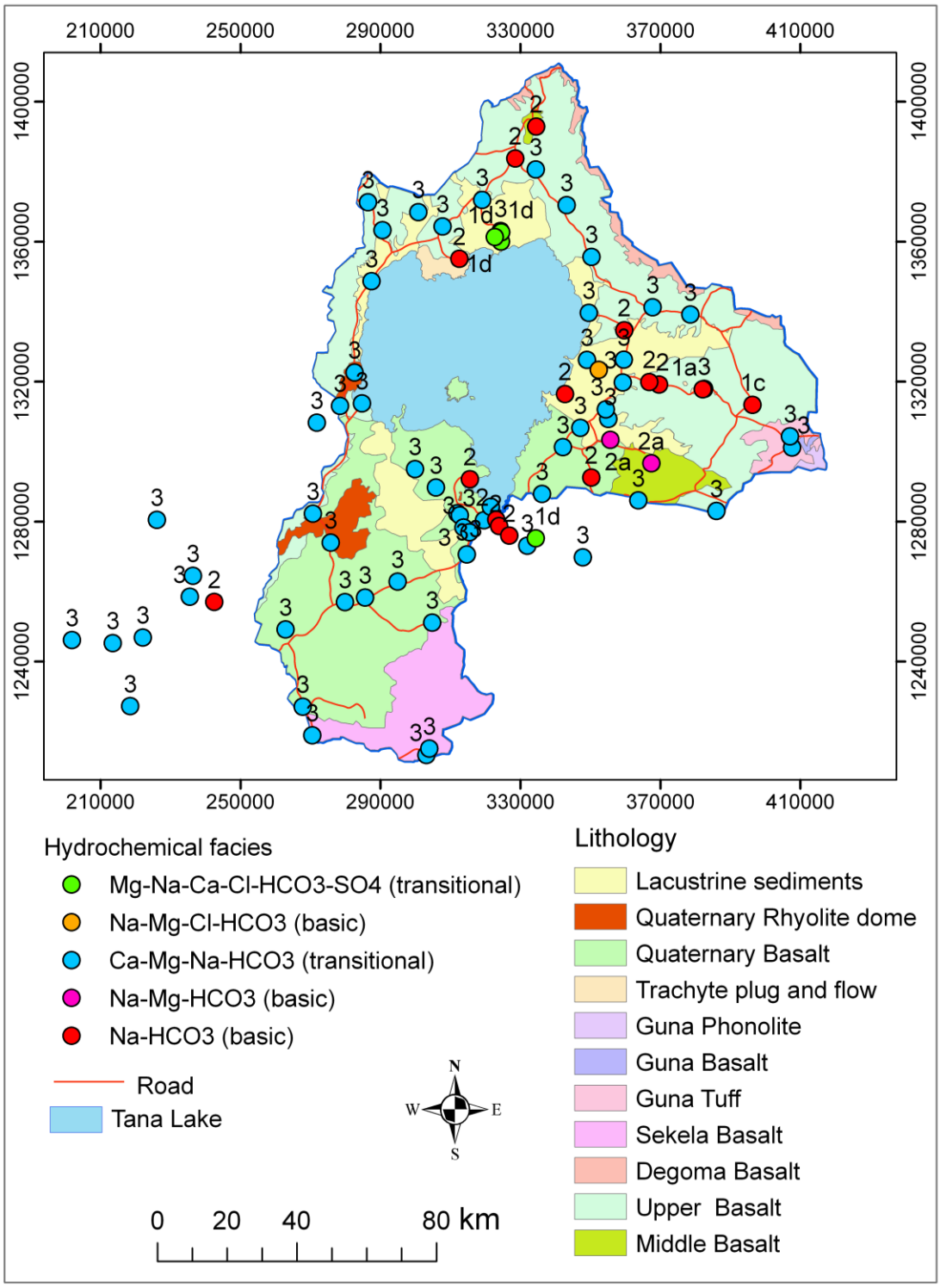

Figure 9.17. Spatial distributions of hydrochemical facies. Number indicates subgroup to which the groundwater sample belongs.

The southwestern area contains Subgroup3 except borehole GW43, which is located near the lake and belongs to Subgroup2. Deep (500m) test well drilled in this area near by the lake (GW226) also has Na-Mg-Ca-HCO3 (basic) water type and has TDS of 1215mg/l. Western escarpment also consists of Subgroup3 while the northern area consists of often Subgroup3. Borehole in Middle Basalt aquifer (GW20) and the deep borehole (301m) that intersect the Upper, Middle and Lower basalts aquifers (GW3) belong to Subgroup2 in northern area. Subgroup1d is found in hand dug wells within the lacustrine sediments aquifer in this area. In the eastern part of the area, subgroups1a, 1b, 1c, 2a, 2 and 3 have been observed.

No clear geographic differentiation was observed among each groundwater subgroups, which seems to be due to different depths of the boreholes. Figure 9.18 shows variation of borehole depth for subgroups 3, 2 and 1c. Subgroup1a is uprising salty cold spring from deep/lower confined aquifer system via lineament while 1c is from intermediate aquifer system (see Section 11.1). Both are found in the Upper Basalt aquifer in the eastern area. Subgroup1b and 1d from hand dug wells in lacustrine sediments (see Section 9.5 and 11.1 and 11.5). Subgroup2a is thermal springs.

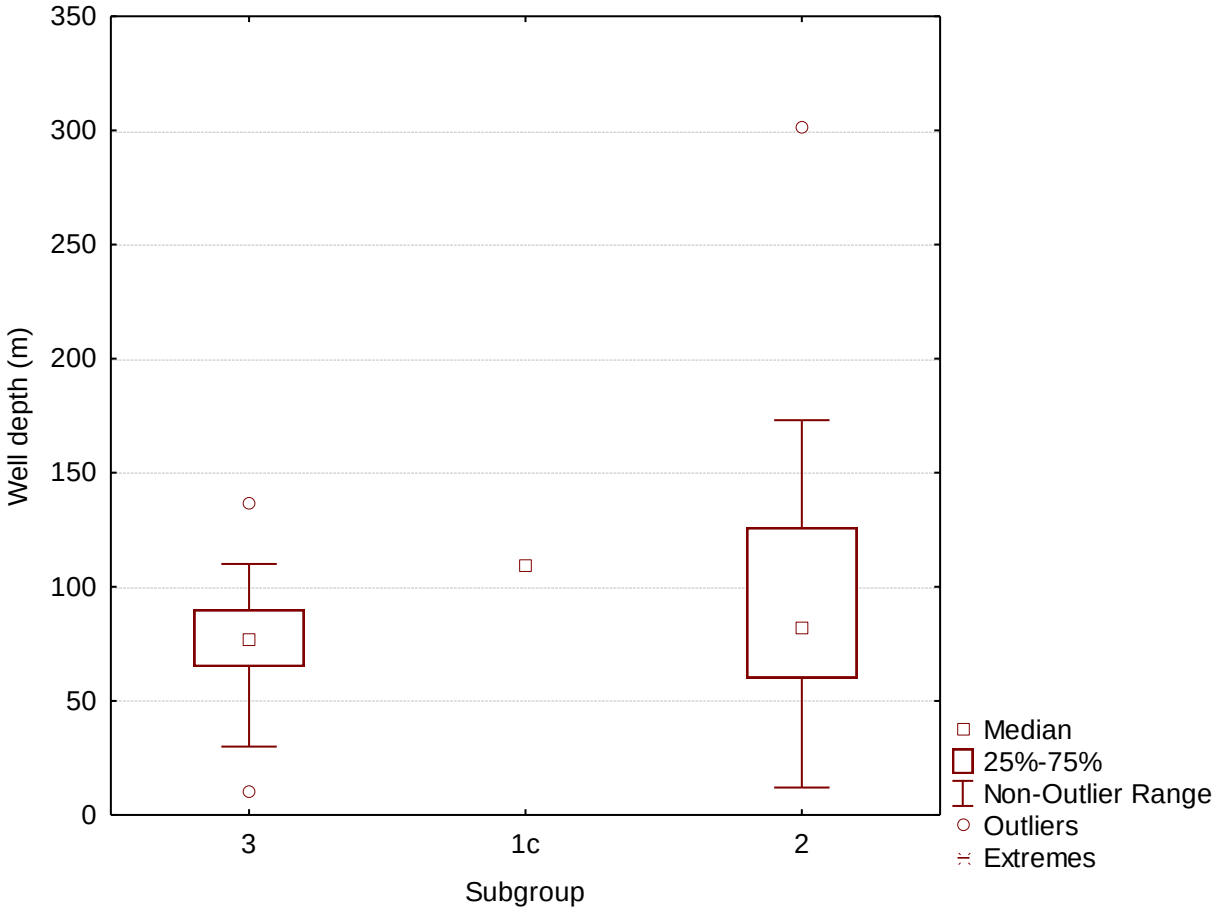

Figure 9.18. Box plot showing variation of borehole depth for groundwater subgroups.

Boreholes in Tis Abay area near down stream south of the lake have shown groundwater, which belong to Subgroup2 (Na-HCO3, basic type), and the average pH is high (8.4) unlike the surrounding ground waters, which belong to Subgroup3 (Ca-Mg-Na-HCO_3, transitional) and pH less than 8. This suggests that the upland deep groundwater in Tana basin (Subgroup2) converges beneath lake area and underflows to Tis Abay area via volcanic rocks underlying the lake bed sediments.

Andesa cold oozing spring (GW46) in Tis Abay area belongs to Subgroup1d and seems to be mixture upland ground waters in Tana basin and modern local water in the area. It has high TDS (4700 mg/l) and Mg-Na-HCO_3 (basic) hydrochemical facies.

Most ground waters in Beles basin belong to Subgroup3. However, one borehole (GW221) is of Subgroup2 and is relatively depleted in deuterium and oxygen-18 (Section 10.2) than other groundwater points in the area. This may suggest that it is evolved local groundwater from the divide area with little leakage water input. Leakage contribution from Tana Lake to this area (see Section 10.2 and 11.4.2.2.) seems to dilute such ground waters in the area.

The hydrochemical facies of Tana Lake seem to be attained due to some groundwater input to the lake from all sides. Wetland hydrochemical facies also shows some groundwater input besides the inundated Lake and rivers flood waters.

9.5. Origin of Groundwater Salinity, Hydrogeochemical Evolution and Inverse Hydrogeochemical Modeling

9.5.1. Origin of salinity and hydrogeochemical evolution

Different plots (meq/l) have been prepared to understand source of ions and salinity and hydrogeochemical processes. Plot of Na^+ versus Cl^- (Fig. 9.19) showed that Subgroup1b and 1d plot close to halite dissolution line indicating that source of Na^+ and Cl^- is halite dissolution in lacustrine sediments aquifer. Subgroups 2, 2a, 1c and 1a lie above the halite dissolution line, which show relatively Na^+ excess to Cl^-. This may suggest additional source of Na^+ than contribution by halite dissolution or other non-halite source of Na^+ such as albite dissolution and cation exchange.

Plot of Na^+ versus HCO_3^- (Fig. 9.20) shows that all subgroups are affected by albite dissolution, except Subgroup3, which is a little evolved. Ca^{2+} versus HCO_3^- plot indicates that Subgroup1d has relatively excess Ca^{2+} than HCO_3^- (Fig. 9.21) than that can be

contributed by calcite and dolomite dissolution. This can be due to dissolution of gypsum and anorthite. Plot of Ca^{2+} versus SO_4^{2-} (Fig. 9.22) reveals gypsum dissolution for Subgroup1d. Calcite and dolomite are oversaturated in this groundwater subgroup and seem to precipitate. Subgroups 3, 2, 2a, 1a, 1b, 1c and GW46 show deficiency of Ca^{2+}. Sources of Ca^{2+} in these subgroups seem to be anorthite and deficiency in Ca^{2+} comes due to cation exchange, fixation of Ca^{2+} and libration of Mg^{2+} and/or Na^{+}. Carbonate and evaporites dissolution in subgroups 3, 2, 2a and 1c and 1a seems to be unlikely.

Plot of $(Ca^{2+} + Mg^{2+})$-$(HCO_3^- + SO_4^{2-})$ versus $(Na^+ + K^+ - Cl^-)$ (Fig. 9.23) in meq/l proves ion exchange processes. In the absence of ion exchange all data plot close to the origin (Kamel et al., 2005). On the other hand, albite dissolution can also give excess Na^+ relative to Ca^{2+}+Mg^{2+}. Subgroups 1c and 1a, and GW46 show increase of Na^++K^+ related to decrease of Ca^{2+}+Mg^{2+}. This can be attributed to dissolution of albite and fixation of Ca^{2+} and libration of Na^+. Subgroup1d shows increase of Ca^{2+}+Mg^{2+} relative to Na^++K^+. This could be due to fixation Na^{2+} and libration of Mg^{2+} and dissolution of gypsum and anorthite (see Section 9.5.2). Subgroups3, 2 and 2a plot near to the origin and are not affected by cation exchange processes.

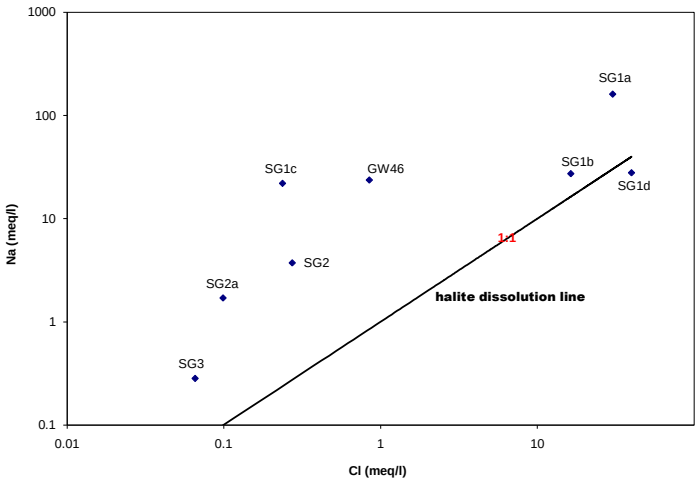

Figure 9.19. Plot of Na^+ versus Cl^-; SG stands for subgroup.

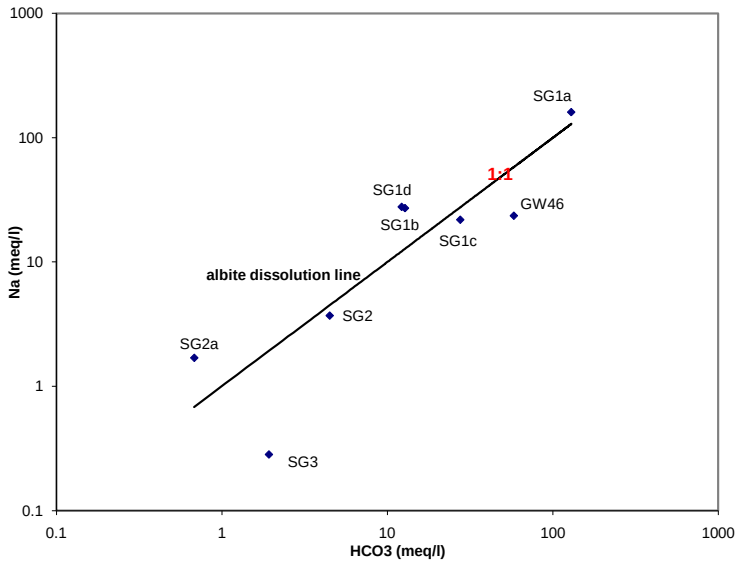

Figure 9.20. Plot of Na^{+} versus HCO_3^{-}.

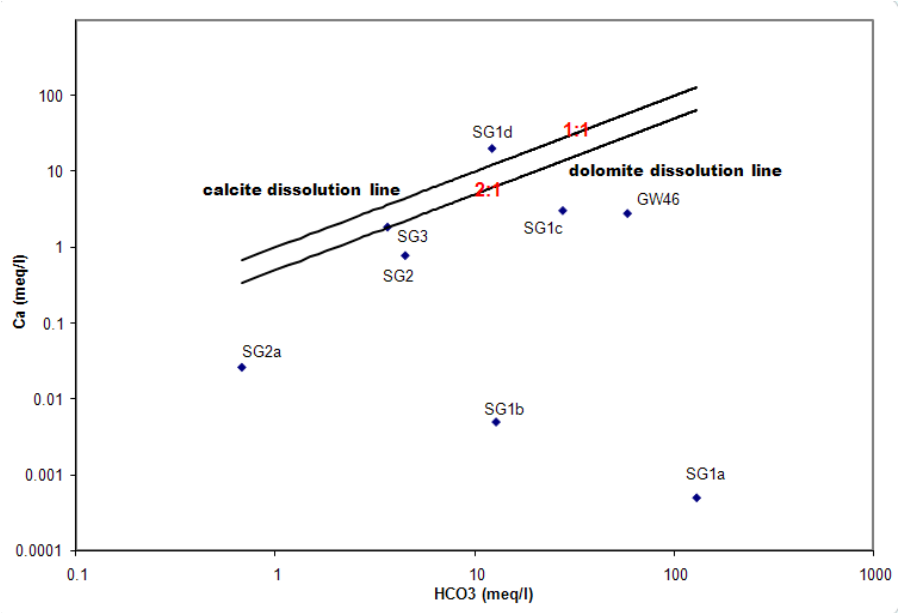

Figure 9.21. Plot of Ca^{2+} versus HCO_3^{-}.

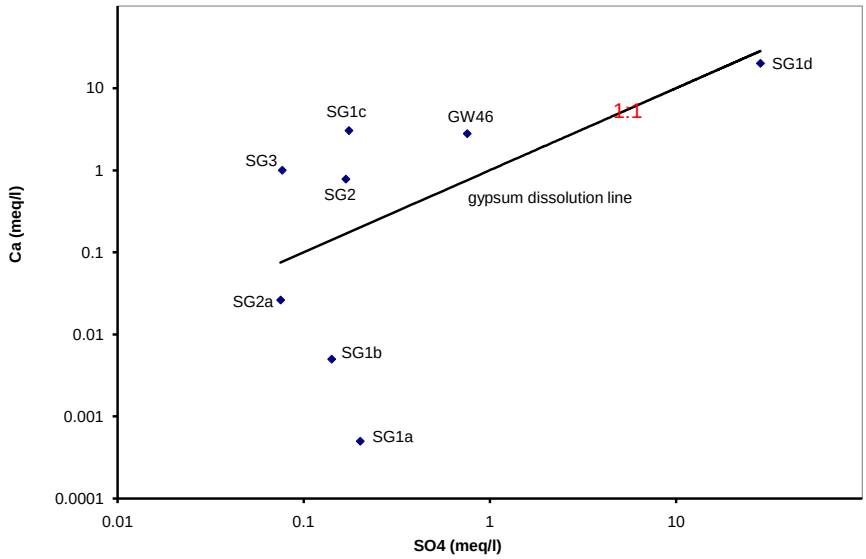

Figure 9.22. Plot of Ca^{2+} versus SO_4^{2-}.

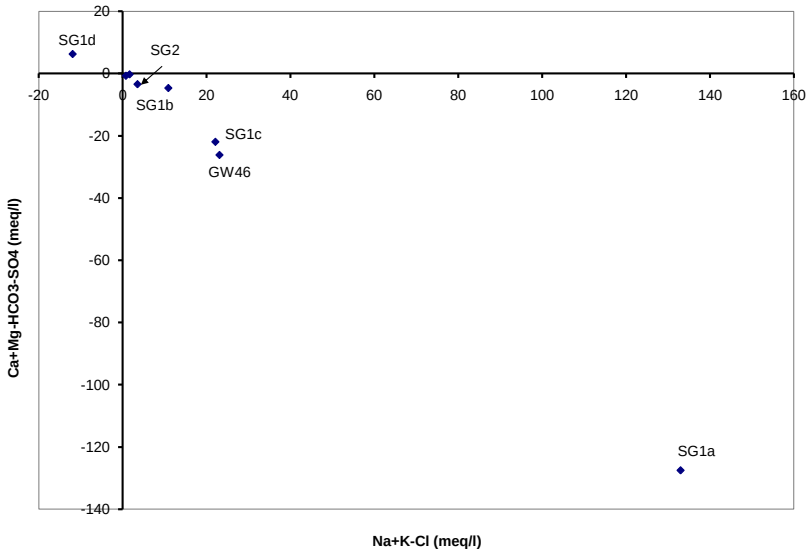

Figure 9.23. Plot of $(Ca^{2+} + Mg^{2+})$-$(HCO_3^- + SO_4^{2-})$ versus $(Na^+ + K^+ - Cl^-)$.

To understand the hydrogeochemical evolution of the groundwater, different bivarient plots have been prepared using the groundwater subgroups formed based on HCA and PCA classification. Plots of Cl^-, HCO_3^-, Na^+ and Ca^{2+} versus TDS (Figs. 9.24-27) showed that subgroups 3 and 2 form one cluster suggesting that they are interrelated. Subgroup3 is less evolved while Subgroup2 is evolved. Subgroup3 has open system in the unconfined aquifer with PCO_2 a little lower than that of the rain in Tana basin. Subgroup2 has a closed system, which has high pH and very low PCO_2 (Table 9.3a&b), see Section11.1. This suggests that Subgroup3 evolves with depth to Subgroup2, which occur in the deep (semi)confined aquifer(s) (Figure11.1).

Under closed system, the supply of CO_2 decrease and consumed so that the rate of dissolution and weathering of silicate minerals decreases as pH highly increases while both dissolved ions and pH increase in open system (Appelo and Postma, 1994), see Figure11.1.

Subgroup2a is different from those of subgroups 3 and 2. It consists of thermal springs and has low concentration but hyper alkaline (pH = 9.53) when compared to subgroups 3 and 2. It has very low PCO_2, which shows a closed system (Figure11.1).

Subgroup1a, 1b, 1c and 1d have relatively high salinity and are scattered in the diagrams indicating their different source of ions and different evolution. Subgroups 1a and 1c have lower pH than subgroups2 and 2a, and consist of dissolved (bubbling) CO_2 from deep source with PCO_2 much higher than the atmosphere and those of subgroups2 and 2a. Besides, the PCO_2 of subgroups1a and 1c is much higher than those of subgroups1b and 1d although all have open system. However, subgroups1b and 1d have PCO_2 a little lower than the rain and nearly similar with that of Subgroup3 (Tables 9.3a&b, Figure11.1). This suggests that subgroups1a and 1c belong to different deep evolved confined aquifer systems than subgroups 3, 2, 2a, 1b and 1d, which seem to exist beneath Subgroup2 under open system to deep CO_2 source. On the other hand, subgroups 1b and 1d evolve locally at shallow depth in unconfined lacustrine sediments aquifer from

Subgroup 3 as a result of evaporites dissolution and cation exchange under open system to atmospheric CO_2, which have given relatively higher salinity.

Concentration of ions and chemical parameters versus subgroups are shown in Figure 9.28. Saturation indices of the common mineral phases of each groundwater subgroup are deduced by PhreeqC software. Subgroup2 is characterized by increased value of pH, TDS, HCO_3^-, Cl^-, SO_4^{2-}, K^+, F^- and decreased values in SiO_2, Ca^{2+}, Mg^{2+} than Subgroup3, which suggest that Subgroup3 evolves to Subgroup2, see also Section 11.5. In Subgroup3, chalcedony is oversaturated while others (halite, gypsum, calcite and dolomite) are under saturated. Calcite and dolomite are oversaturated while others are under saturated in Subgroup2. Therefore, the decrease in Ca^{2+} and Mg^{2+} is attributed to precipitation of calcite and dolomite when the groundwater evolves from Subgroup3 to Subgroup2.

All common minerals are under saturated in Subgroup2a. In Subgroup1d, calcite and dolomite are oversaturated, but other mineral phases are under saturated. Subgroups 1a, 1b and 1c show that all common mineral phases are under saturated. Chalcedony is slightly oversaturated in Subgroup1a. Presence of CO_2 from deep source keeps these deep evolved highly saline groundwater systems (subgroups1a &1c) to be under saturated for most common mineral phases underneath to the closed system of Subgroup2.

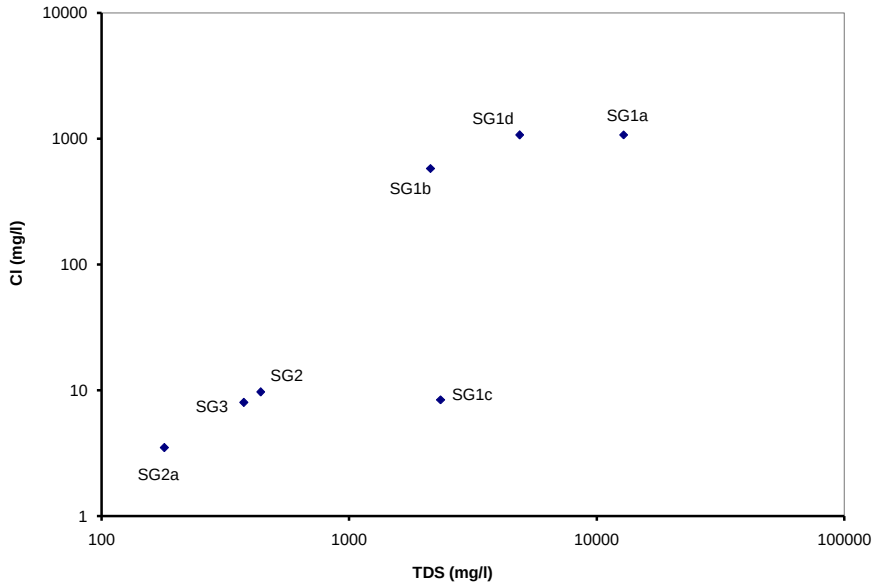

Figure 9.24. Plot of Cl^- versus TDS.

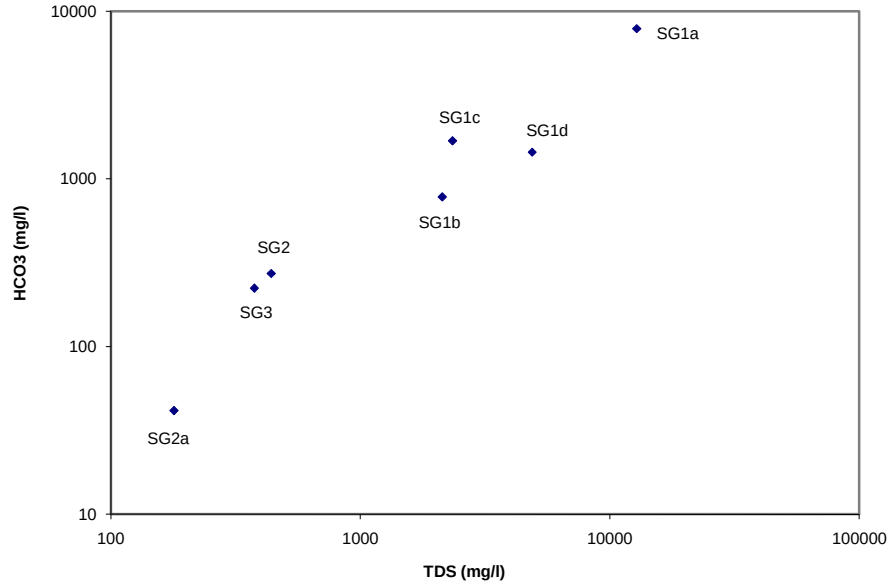

Figure 9.25. Plot of HCO_3^- versus TDS.

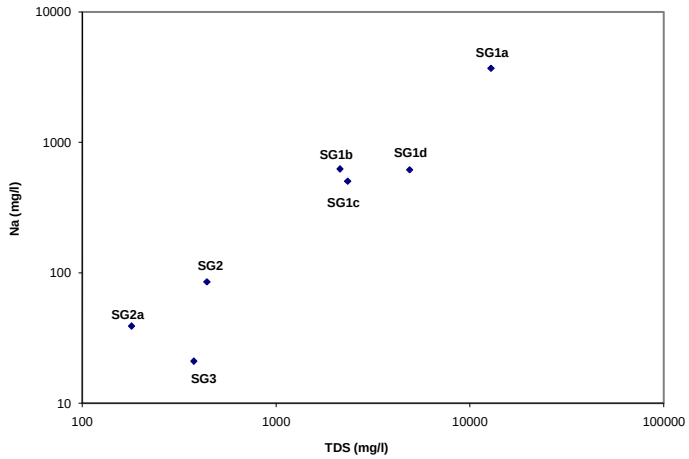

Figure 9.26. Plot of Na^{+} versus TDS.

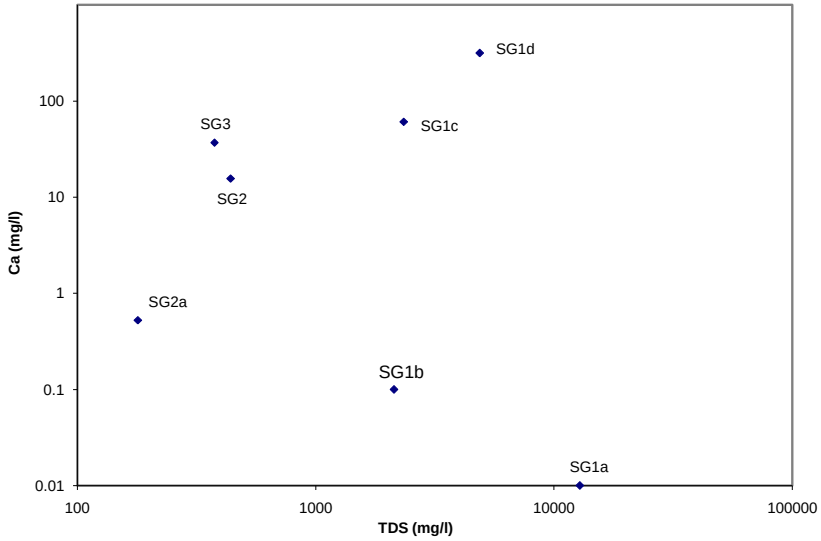

Figure 9.27. Plot of Ca^{2+} versus TDS.

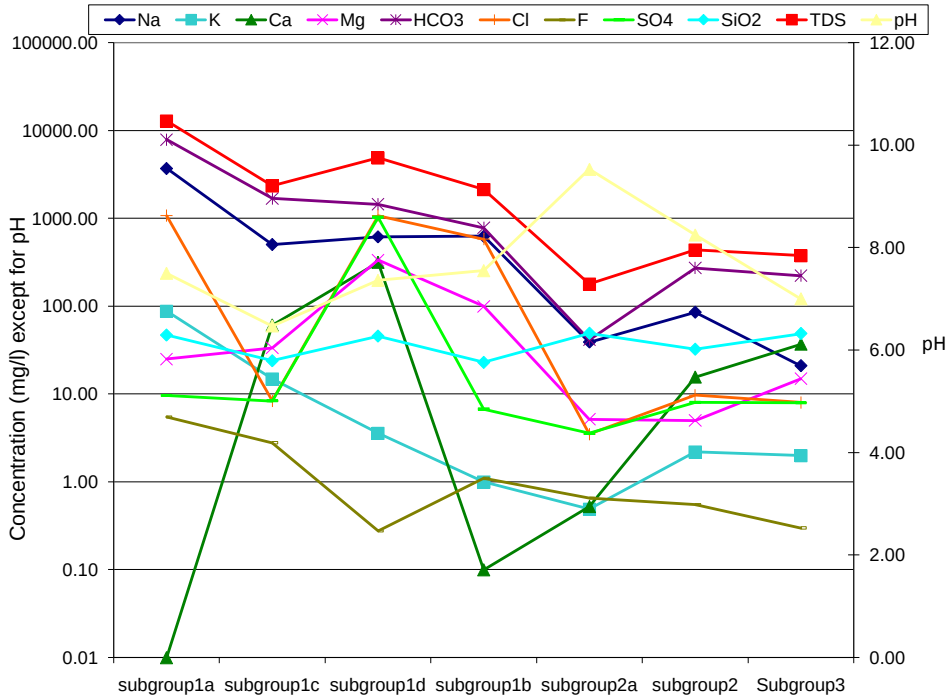

Figure 9.28. Plot of concentrations of ions and chemical parameters versus groundwater subgroups.

Bromide and chloride are conservative elements that do not share in oxidizing or reducing reactions and do not form insoluble precipitation. During evaporation and mixing with fresh water, Br/Cl ratio (molar) remains constant (Hsissou et al., 1999).

Br^-/Cl^- ratio in groundwater is primarily controlled by the initial ratio found in precipitation (Stimson et al., 1993). Impoverishment or enrichment in Br^- can be used as indicator of contribution of either Br-poor evaporite and fertilizers or of Br-rich organic sediments.

Br^-/Cl^- ratio of rain in Tana basin is 86.2 ‰, which is much higher than sea water (1.5 to 1.7 ‰). This may be attributed to the effect of biomass and fossil fuel combustion during vapor transportation.

Plot of Br^- versus Cl^- (mmol/l) shows that Br^- and Cl^- increase from rain water and evolve to Subgroup3, and then to Subgroup2, 1b and 1d (Fig. 9.29), which represent that these subgroups belong to one aquifer system (see Section 11.1). Source of Br^- could be organic sediments like coal and biomass that present in the area, and Cl^- may originates from impurities in minerals like hornblende, mica, solid solution in volcanic glass and halite dissolution.

On the other hand, another trend is seen from mean rain in Tana basin through Subgroup2a to 1c and 1a, which shows decrease of Br^- as Cl^- increases. These subgroups are found in volcanic rocks like those of subgroups3 and 2. However, they are of different sources. Subgroup1c is from the intermediate confined groundwater (aquifer) system while Subgroup1a represents deep seated confined paleo groundwater (Lower aquifer system), see Section11.1. Br^- of these groundwater subgroups is less than the modern rain in the basin suggesting their source is previous episodes of recharges.

Br^-/Cl^- versus Cl^- (mmol/l) plot also shows decrease of Br^-/Cl^- ratio as Cl^- increases. The two trends described above are also seen in this graph (Fig. 9.30).

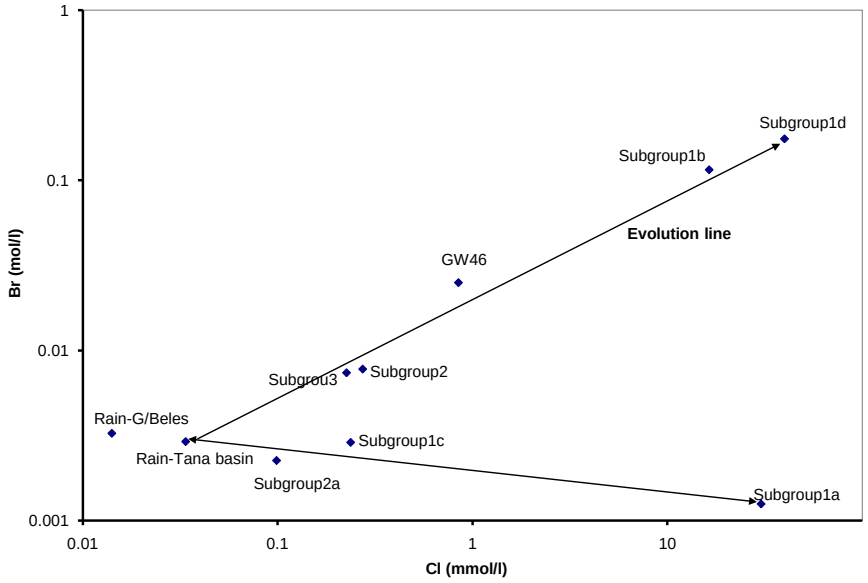

Figure 9.29. Plot of Br^- versus Cl^-.

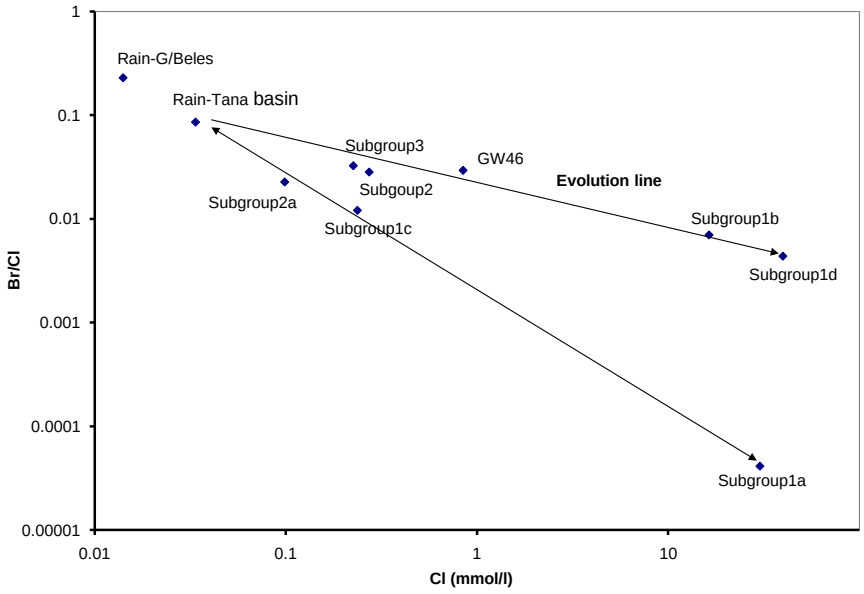

Figure 9.30. Plot of Br^-/Cl^- versus Cl^-.

Plot of delta^{18}O (‰) versus electric conductivity (µS/cm) (Fig. 9.31a&b) also reveal that the main sources of salinity is rock/soil and water interaction. Subgroups 1a and 1c have relatively highly depleted delta ^{18}O values and high salinity, which indicate separate evolved groundwater systems that belong to deeper aquifer systems (Section11.1).

Ground waters subgroups (subgroups 3, 2 and 2a) form one cluster with depleted to slightly enriched delta ^{18}O and low salinity indicating that they are interrelated and belong to the same one aquifer system, but Subgroup2 have generally increased salinity and depleted than most of Subgroup3 suggesting that the latter evolves to the former. Subgroups1b and 1d have simalr delta ^{18}O with these subgroups, but these subgroups and some members of Subgroup3 have relatively high salinity in lacustrine sediments, which suggest that they as mentioned underwent further evolution due to dissolution processes of trace evaporites and carbonates from Subgroup3 in this aquifer system. During the process of leaching of salt formations or mineral dissolutions, the stable isotopes content of the water is not affected while the salinity of the water increases (Yurtsever Y., 1997).

Some ground waters with slightly enriched δ^{18}O show sign of evaporation. However, surface waters (Tana Lake, rivers and wet land) show major evaporation processes.

Besides, plot of electric conductivity versus altitude (Fig. 9.32a&b) also shows that groundwater salinity increases from the uplands to the lowlands along the groundwater flow direction for subgroups 3, 2, 1b and 1d which indicate that they belong to one the above mentioned aquifer system. Some members of Subgroup3 and especially subgroups1b and 1d have relatively high electric conductivity at lower altitude than others subgroups3 and 2 in the eastern and northern plain and volcanic areas due to the mentioned dissolution of evaporites and carbonates and cation exchanges in lacustrine sediments

(a)

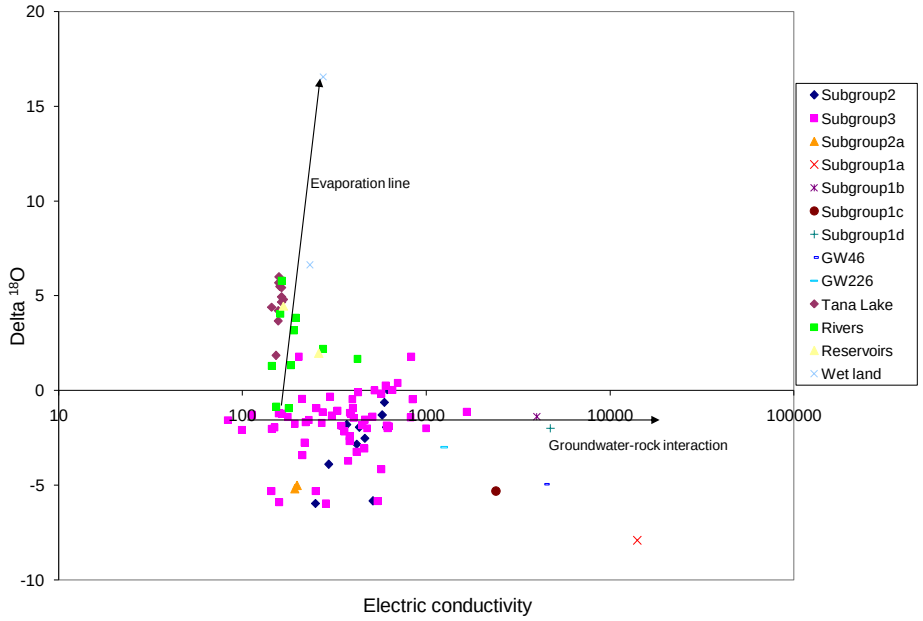

(b)

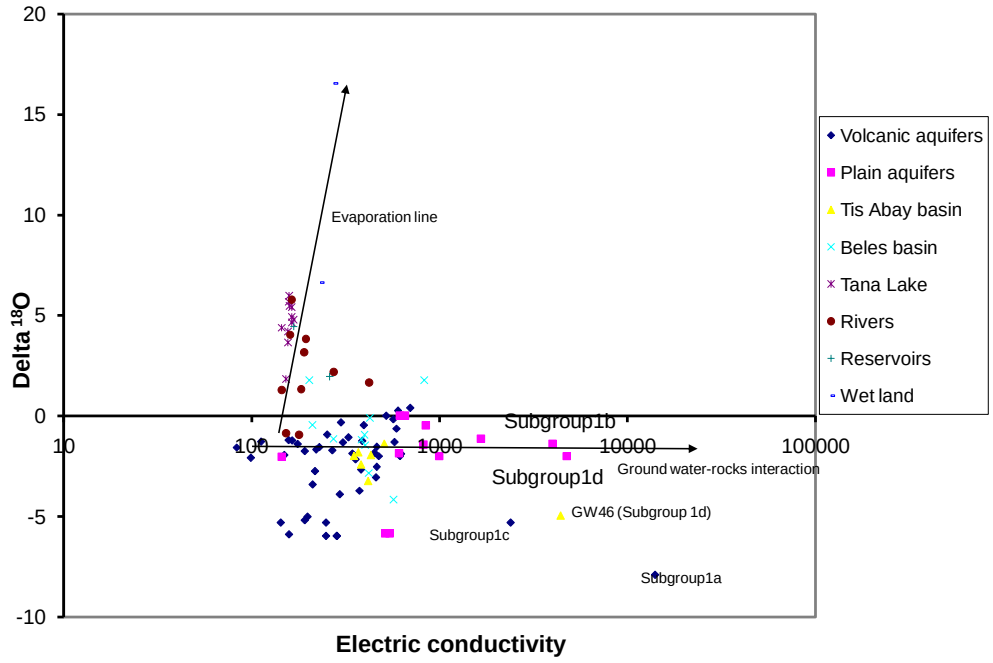

Figure 9.31. Plot of $\delta^{18}O$ (‰) versus electric conductivity (µS/cm). a) samples are grouped by subgroups b) grouped by aquifers.

Very high salinity (salty) groundwater at mid altitude of Subgroup1a indicates more evolved system from very deep aquifer. Similarly, moderate saline (brackish) groundwater at higher altitude (Subgroup1c) indicates moderately evolved groundwater from intermediate aquifer system.

(a)

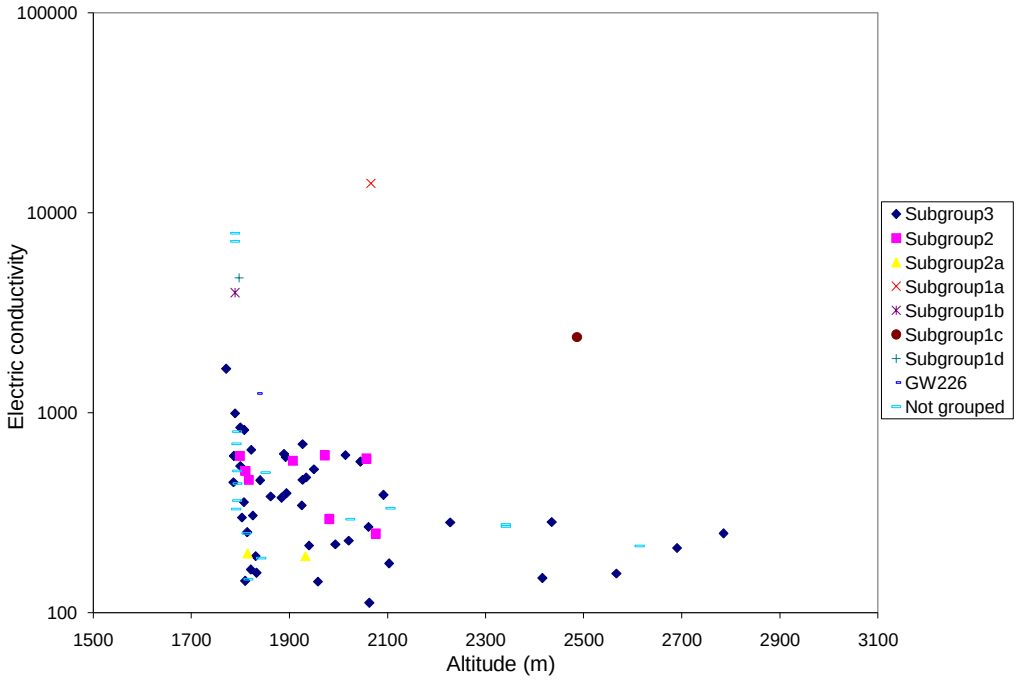

(b)

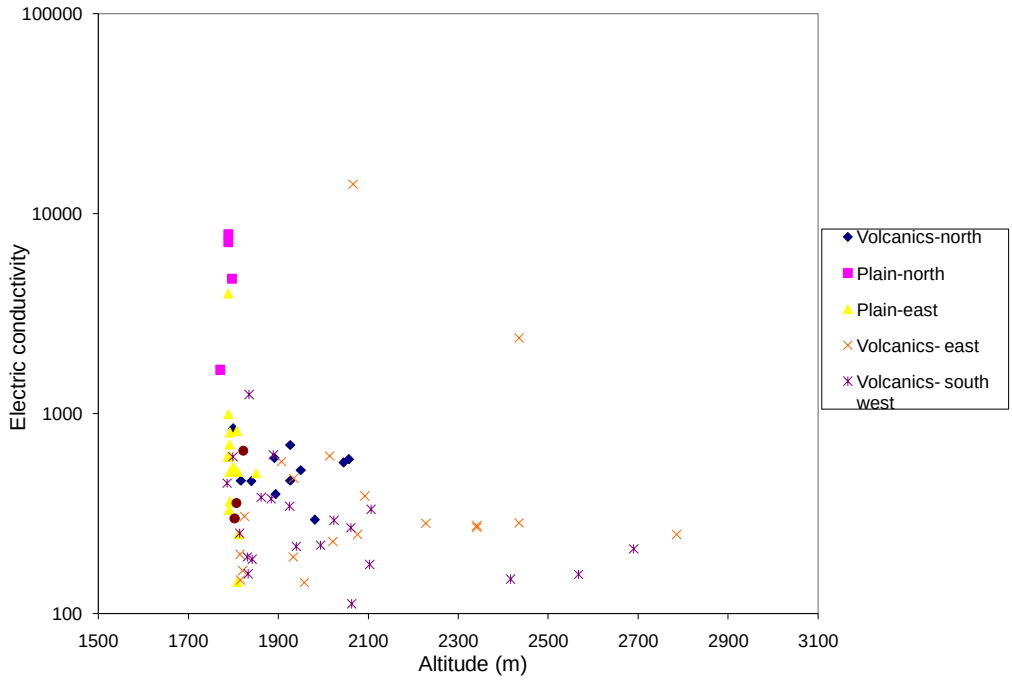

Figure 9.32. Plots of electric conductivity (µS/cm) versus altitude. a) grouped by groundwater subgroups, b) grouped by aquifers.

Residual carbonate alkalinity (RCA) is an important parameter to indicate evolution of the groundwater. RCA used to increase along the groundwater flow direction and age as Ca^{2+} and/or Mg^{2+} stabilize due to precipitation and exchange with Na^{+}. Decrease in RCA in the down groundwater flow direction indicates local sources of $Ca^{2+}$and Mg^{2+}. RCA of the subgroups have been calculated using the following equation (Raghunath,1996).

$$RCA = HCO_3^- + CO_3^{2-} - Ca^{2+} + Mg^{2+}, \text{ in meq/l} \quad \ldots\ldots(20)$$

Subgroup1a shows the highest RCA, Na^+ and K^+ content. Na/Ca, Na/Mg and Na/Cl ratios are also very high. This indicates Subgroup1a is separate old deep evolved groundwater (see Section 11.1) than the other subgroups and silicate hydrolysis and cation exchange (fixation of Ca^{2+} and/or $Mg^{2+}$and libration of Na^+) are the main sources of salinity. Subgroup1c also has moderately high RCA, Na^+ and K^+, Na/Ca and Na/Mg ratios, and very high Na/Cl ratio. This suggests that this groundwater belongs to the intermediate system and the main source of ions is silicate hydrolysis and may also cation exchange (fixation of Ca^{2+} and Mg^{2+}, and libration of Na^+).

Subgroups3 and 2 generally have low RCA, Na^+ and K^+ values. However, these values and Na/Cl, Na/Ca and Na/Mg increase while the groundwater evolves from the Subgroup3 to 2 due to dissolution of albite and precipitation of calcite and dolomite. Subgroup2a shows the lowest RCA and low Na^+ and K^+ values while Na/Cl and Na/Ca ratios are relatively higher than Subgroup2. These subgroups in general are less evolved than Subgroup1a and 1c, see further explanation in Section11.1. Source of groundwater salinity is silicate hydrolysis.

Subgroup1b has low RCA and moderate Na^+ values. Na/Cl ratio is close to one while Na/Ca and Na/Mg ratios are high and low, respectively. This suggests that anorthite and halite dissolution and cation exchange (fixation of Ca^{2+} and libration of Mg^{2+}) in lacustrine sediments aquifer are the main source of groundwater salinity. A little rise from one in Na/Cl ratio indicates additional source of Na^+ from albite dissolution (see Section 9.5.2).

Subgroup1d shows negative RCA and moderate Na^+ values and Na/Cl ratio is close to one. Na/Ca and Na/Mg ratios are low. This proves addition of Ca^{2+} and Mg^{2+} locally in lacustrine sediments due to dissolution of anorthite, gypsum and libration of Mg^{2+} and fixation of Na^+(see Section 9.5.2). Sources of Na^+ are halite and albite dissolution. A little decrease of Na/Cl ratio from one indicates the mentioned cation exchange process.

Table 9.5. RCA and selected ions and ionic ratios.

	RCA	Na (meq/l)	K (meq/l)	Na/Cl	Na/Ca	Na/Mg
Subgroup1a	127.30	160.94	2.25	5.33	322509.87	78.23
Subgroup1b	4.55	27.19	0.03	1.66	5447.80	3.30
Subgroup1c	21.80	21.92	0.38	92.53	7.20	7.95
Subgroup1d	-19.60	26.78	0.09	0.89	1.70	0.97
Subgroup2	3.29	3.71	0.06	13.60	4.76	9.01
Subgroup2a	0.23	1.70	0.01	17.19	64.79	4.01
Subgroup3	0.57	0.91	0.05	4.05	0.49	0.74

9.5.2. Inverse hydrogeochemical modeling

Inverse hydrogeochemical modeling has been done to understand the major geochemical processes and mole transfer when the groundwater evolves from Subgroup 3 to 1b and 1d in the eastern and northern areas, respectively, which represent pockets of brackish ground waters in unconfined lacustrine sediments aquifer. Sources of salinity for other subgroups (3, 2 and 2a) are mainly silicate minerals hydrolysis. Subgroup 1a and 1c are older episode of recharges, which is not possible to do inverse geochemical modeling. However, the major sources of ions for theses groundwater systems are silicate hydrolysis and cation exchange.

Mineral phases have been chosen and the inverse modeling is constrained based on the information on mineralogy of rocks and soils, saturation indices and the general pattern of the hydrogeochemical evolution along the groundwater flow path. The groundwater is let to evaporate in the models as the shallow unconfined ground waters in lacustrine sediments seem to have been affected by evaporation. Phases and thermodynamic data are from PhreeqC and its data base.

Inverse modeling solutions with reasonable combinations of reactants and products that represent the processes undergone and that accounts for the change in water chemistry from initial to final waters have been selected (Table9.5).

Table 9.6. Saturation indices (SI) and selected mass transfer model solutions (mmol/kg of water) when Subgroup3 evolves to subgroups 1b and 1d.

Mineral phases	SI (Subgroup1b)	Mass transfer (Subgroup1b)	SI (Subgroup1d)	Mass transfer (Subgroup1d)
Albite		0.045		1.1
Anorthite		0.36		1.7
Calcite	-2.14		1.07	-3.5
Gypsum	-5.93		-0.42	3.3
Halite	-5.09	10.032	-4.76	9.3
Sylvite	-6.54	0.131	-6.15	
CaX2		-1.941		
MgX2		1.941		2
NaX				-0.004
H2O		-20247.78		-41162.8
Illite		-0.332		-0.008
Ca-Montimorillon				-1.933

The reactions for model solutions of Subgroups 1b and 1d can be given as follows.

Model solution for Subgroup1b:

Ca-Mg-Na-HCO_3 water (Subgroup3 in the eastern area) + albite + anorthite + halite + sylvite + Mg^{2+} (from ion exchange) + CO_2(g) $\longrightarrow$ Na-Mg-Cl-HCO_3 water (Subgroup1b) + illite + Ca^{2+} (loss to ion exchange) + groundwater evaporation

Model solution for Subgroup1d:

Ca-Mg-Na-HCO_3 water (Subgroup3 in the northern area) + albite + anorthite + halite + gypsum + Mg^{2+} (from ion exchange) + CO_2(g) $\longrightarrow$ Na-Mg-Ca-Cl-SO_4 water (Subgroup1d) + Ca-Montimorillon + illite + Calcite (precipitation) + Na (loss to ion exchange) + groundwater evaporation

The reactions and mole transfers show that the major processes for relatively high salinity of pockets of ground waters in lacustrine sediments are dissolution of evaporites (halite, gypsum and sylvite) and cation exchanges. Silicate minerals hydrolysis also contributes to the salinity. Clay minerals of illite and Ca-Montimorillon form as end products of the reaction.

10. ENVIRONMENTAL ISOTOPES HYDROLOGY

10.1. General

Investigation of the origin, proper characterization of the flow pattern, mixing of water from different sources and to identify water that has undergone evaporation requires the use of several hydrochemical and isotopic tools.

Classically, groundwater flow patterns are deduced from indirect investigations. For instance, flow directions are deduced from water potentials. In all hydrogeological studies the basic assumption is that water continuity is respected within the aquifer but not direct identifications can be obtained on the water itself. Isotope hydrology partially fills the gap by providing information on type, origin and age of the water (Fontes, 1980). Constitutive isotopes of the water molecules (^{18}O, ^{2}H and ^{3}H) are often used for this purpose.

Some general rules can be recognized for the distribution of these isotopes in ground waters. If the isotope content does not change within the aquifer, it will reflect the origin (location, period and process of the recharge) of the groundwater. If the isotopic content

changes along groundwater paths, it will reflect the history of the water (mixing, salinization and discharge processes). Evaporation increases the isotope concentration while transpiration does not affect or little affect isotope concentration.

Environmental isotope techniques allow tackling any hydrological problem with practically no limit to the spatial and temporal scale. Although isotope techniques can be used as independent approach to solve hydrogeological problem, studies including combined hydrogeological, hydrochemical and isotopic data will give more detailed and in some cases safer conclusions.

Investigations of environmental isotopes (deuterium, oxygen-18 and tritium) have been done in Tana basin and the surrounding areas in combination with hydrogeological and hydrogeochemical studies. Isotopic data are given in Appendix3.

The isotopes together with the hydrogeological and hydrogeochemical results helped and used here to identify and analyze aquifer systems and groundwater flow systems or dynamics, paleo groundwater, origin of groundwater, mixing among ground waters and surface waters (Tana Lake, reservoirs and rivers), trace the basin groundwater outflow area and leakage paths from Tana Lake and estimating mixing rate, and decipher evaporation processes.

10.2. Deuterium and Oxygen-18

10.2.1. Local meteoric water line (LMWL)

Rainfall samples were collected for one hydrological year (2012) from five meteorological stations. Four of these stations are within the Tana basin while one is in the adjacent low lying Beles basin.

Delta deuterium and oxygen-18 data of these rainfall samples have been plotted on scatter diagram. The density of points fitted with best fit has given a regression line

called the local meteoric water line with the following equation and regression coefficient of R^2=0.97 (Fig.10.1).

$$\delta^{2}H = 7.96\delta^{18}O + 21.4 \quad \text{.....(21)}$$

Besides, the local meteoric water line has been established for Addis Ababa GNIP station using monthly $\delta^{2}H$ and $\delta^{18}O$ data from 1990 to 2009. Summer Monsoon rainfall (June-September) data have been used to establish this meteoric water line for comparison with the Tana area LMWL. This has given LMWL with the following equation with R^2 =0.96.

$$\delta^{2}H = 8.0\,\delta^{18}O + 14.5 \quad \text{.....(22)}$$

The local meteoric water line for Tana area has intercept greater than the Addis Ababa and the world meteoric water line (Craig, 1961). This is assumed to be due to recycling of moisture in the area associated with the Tana Lake.

The similarity or departure from the LMWL has been interpreted in terms of hydrological processes such as recharge source and time, recharge mechanism, evaporation, mixing between different waters, isotope exchange, etc.

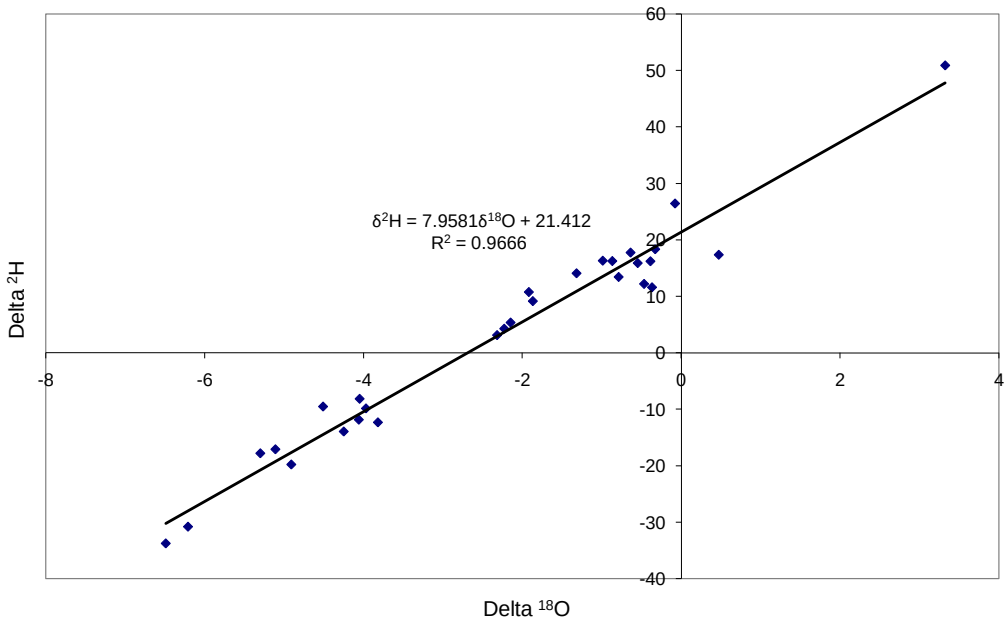

Figure 10.1. Local meteoric water line for Tana and surrounding areas (data in ‰).

10.2.2. Altitude effect

When the rain forming vapor rises from low land to high lands the vapor and as a result the rain water get depleted in delta ^{18}O and ^{2}H. Thus, the isotopic content of the rainfall is depleted with altitude as the temperature decreases with altitude, which is known as the altitude effect. This help to understand the recharge altitude of the groundwater with specified delta deuterium and oxygen-18.

The weighted mean delta ^{18}O and ^{2}H values have been calculated from the monthly values for each station. Tables10.1a&b show the location and weighted mean values for each station. $\delta^{18}O$ varies from -4.41 (Sekela station) to -3.36 ‰ (Gilgel Beles station). $\delta^{2}H$ values vary from -14.76 (Sekela station) to -5.23 ‰ (Gilgel Beles station). Then, these weighted mean values of the five stations are plotted against their respective

altitude of the stations (Figs.10.2a&b). This gave an altitude effect of -0.06 and -0.42 ‰ per 100 m for oxygen-18 and deuterium, respectively.

(a)

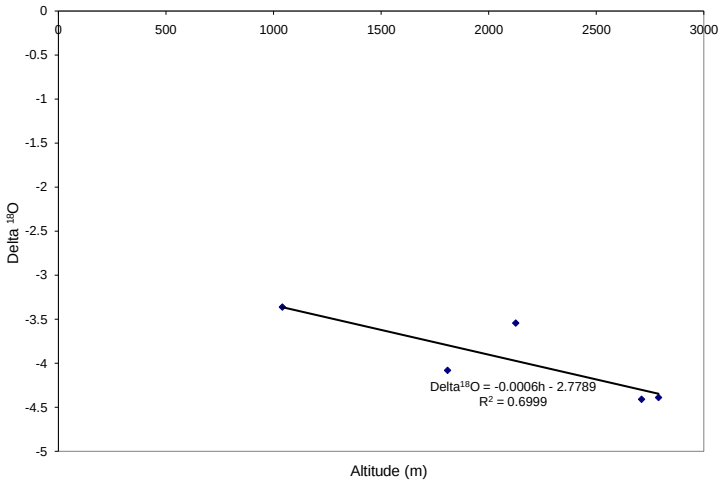

(b)

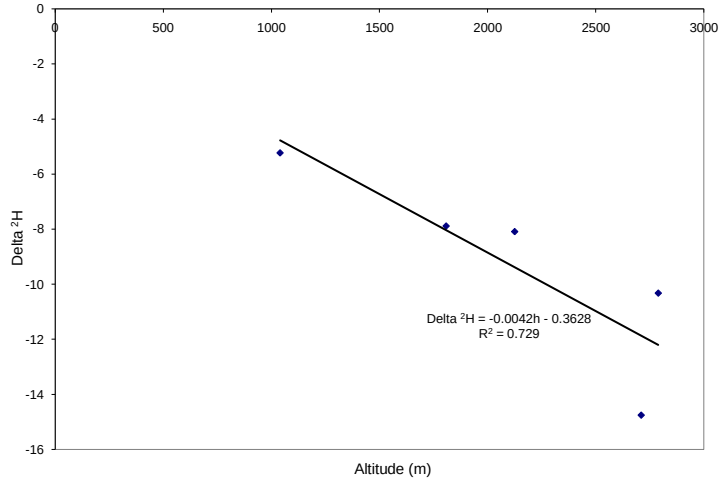

Figure 10.2. Altitude effect a) based on delta ^{18}O (‰), b) based on delta ^{2}H (‰).

Seifu Kebede et al., (2005) established an altitude effect of 0.1 ‰ per 100 m, using ground waters $\delta^{18}O$ and altitude relationships, which is comparable with the present result.

According to Clarck (1997), altitude effect based on delta ^{18}O and delta ^{2}H ranges as follows.

Delta ^{18}O = -0.15 to -0.5 ‰ per 100 m
Delta ^{2}H =-1 to -4 ‰ per 100 m

Altitude effect for Tana basin based on $\delta^{18}O$ and $\delta^{2}H$ is a little lower than this range, which may indicate fast fractionation in the area.

Recharge area of ground waters have been assessed using the local altitude effect. Ground waters with tritium less than 1 TU (predominantly pre 1952 and paleo groundwater) and some mixed ground waters show recharge altitude that cannot be justified by this relationship. They are of previous episodes of recharges. This suggests that the area was humid prior to 1952 and the temperature has subsequently increased due to devastation of vegetations. Subgroup1a seems paleo (Early Holocene) groundwater (see Section10.3).

Table 10.1. Meteorological stations where rainfall samples collected.

Station	X	Y	Altitude (m)
Bahir Dar	321196	1282803	1808
Gonder (Fasiledes)	332613	1395124	2125
Sekela	304802	1215226	2710
Gassay	406941	1304349	2789
Gilgel Beles	209521	1235107	1040
Addis Ababa	470415	994980	2360

Table 10.2. Weighted (by precipitation) mean delta deuterium and oxygen-18 value of the rainfall at the stations.

	Bahir Dar	Gassay	Gonder	Sekela	Gilgel Beles	Addis Ababa (1990-2009)
Delta ^{18}O (‰)	-4.08	-4.39	-3.54	-4.41	-3.36	-2.58
Delta ^{2}H (‰)	-7.88	-10.32	-8.09	-14.76	-5.23	-6.09

10.2.3. Deuterium and Oxygen-18 data evaluation

Spatial plot of delta ^{18}O of groundwater samples is shown in Figure 10.3. In Gilgel Abay sub-basin (southwestern area), delta ^{18}O generally range between -2.3 and -1.7 ‰ except 2 hand dug wells that are enriched, and 3 boreholes of relatively locally depleted values. In escarpment area, delta ^{18}O has value of -0.8 to -0.4 ‰. Most groundwater points in northern area have delta ^{18}O between -0.8 to -0.4 ‰. One hand dug well in lacustrine sediments aquifer (Subgroup1d) here has relatively depleted value, which may contain deep groundwater component. Moreover, deep borehole (301m depth, GW3) that belong to Subgroup2 showed depleted $\delta^{18}O$ value (-3.9 ‰), which is also due to deep (pre-1952) groundwater component. Angereb borehole (GW21), which also belongs to Subgroup2, shows enriched $\delta^{18}O$ value of -0.62 ‰. This seems to be due to mixing of leakage water from Angereb reservoir.

Groundwater points in the eastern volcanic area have relatively depleted $\delta^{18}O$ values than other areas, which consists of modern and pre-1952 episodes of recharges that belong to Subgroups2 and 3. Delta ^{18}O varies from -1.24 to -5.96 ‰, but often greater than -5.01 ‰. This seems to be due to the highest altitude in this area than the rest. Especially Subgroup1a is highly depleted (-7.9 ‰), which suggests paleo groundwater. Plot of $\delta^{18}O$ versus altitude (Fig. 10.5b) shows often relatively depleted values in the upland, mid and

low altitudes of the eastern area when compared to the southwestern, northern and western escarpment areas, which is due to fractionation related to the higher altitude or altitude effect in this area.

In plain lacustrine sediments aquifer, ground waters have generally slightly enriched values, which seems to be due to recharge of evaporated water from Tana Lake water inundation and rivers flood pools and/or evaporation at shallow depths, and due to influent rivers.

One borehole from Subgroup3 (Wereta borehole, GW29) with depth of 76 m in the plain is depleted indicating its upland recharge. It means upland groundwater underflows to the lacustrine sediments aquifer surrounding the Tana Lake.

Tana Lake also shows relatively depleted values at some places especially in the east suggesting some groundwater inflow to the lake. Minor groundwater inflow seems also to occur via other lake margins, but as is mentioned in Chapter7, the groundwater inflow to the lake is low for quantitative purposes.

Plots of delta deuterium versus delta ^{18}O are given in Figure 10.4a, b&c. Most ground waters from volcanic aquifers (subgroups 3 and 2) in the eastern, northern and southwestern parts of the area plot close to the mean summer rainfall values suggesting diffuse recharge through soil and weathered mantle of the rocks. Some ground waters with tritium less than 1 TU from the eastern and northern areas (subgroups 3, 2, 2a and 1c, Section 10.3) plot at the lower side of the mean summer rainfall values, which show dominantly pre-1952 episode of recharge (see Section 10.3). Subgroup1a plots at the lower end of the LMWL suggesting that it is paleo groundwater.

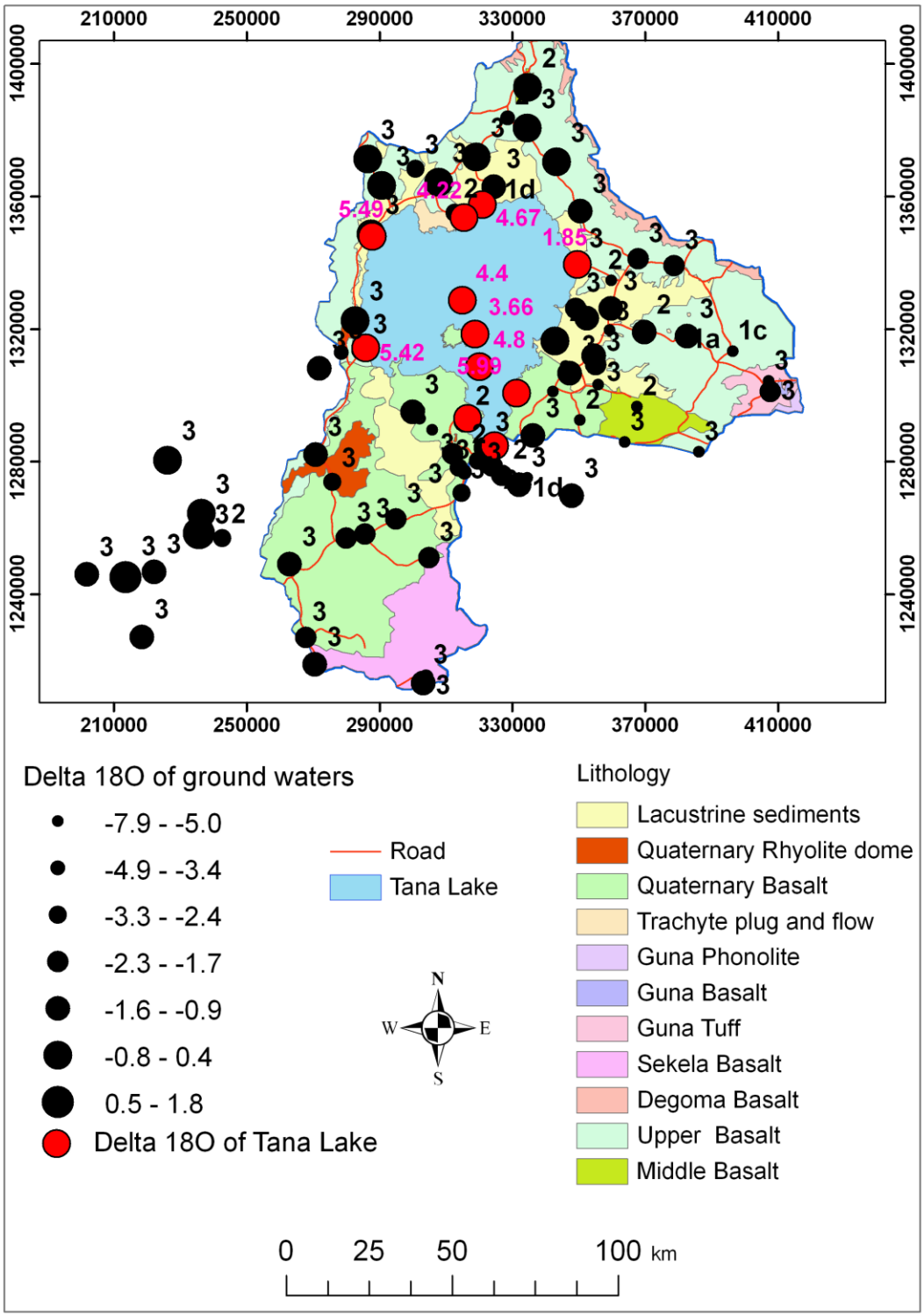

Figure 10.3. Spatial distribution of delta ^{18}O (‰).

Ground waters (subgroups 3, 2, 1b and 1d) in the plain lacustrine sediments aquifer, Tis Abay and Beles areas, and groundwater samples from volcanic aquifers that are taken from tap, and hand dug wells and small springs are relatively slightly enriched than the mean summer rain falls in the area, which seem to be due to evaporation. Tana Lake, reservoirs, rivers and wet land waters are evaporated and lie in the evaporation line.

Plot of delta Oxygen-18 versus altitude for the different subgroups (Fig.10.5a) shows that Subgroup3 has wide scatter from slightly enriched to depleted in uplands and relatively enriched in low lands and depleted for a few mentioned groundwater members here. Subgroup2 indicates from relatively slightly enriched in lowlands to depleted values. Subgroup2a and 1c, and especially 1a have relatively highly depleted values at upland and mid altitudes, respectively. Relatively depleted values at lower altitude such as some members of Subgroups3, 2 and 2a suggest up flow of deep regional baseflow that have recharge in uplands, while some are pre-1952 episodes of recharge, and Subgroup1a is paleo groundwater as mentioned above. Slightly enriched values of subgroups at lower altitude or in the plain lacustrine sediments aquifer are also found for the reasons given above.

Ground waters in Beles basin have generally enriched value except one borehole (GW221) which is depleted (Fig. 10.3). Groundwater in Beles escarpment around the divide with Tana basin (GW225) has relatively depleted value than these low lying areas. This borehole has depth above the Tana Lake level. This suggests that there is leakage underflow from Tana Lake to the low lying Beles area with relatively enriched values.

Groundwater samples taken during rainy season in Beles basin (Sogreah, 2012) plot close to the local meteoric water line and are depleted, which show dilution of the groundwater by the local rainfall that mask the mixing effect of the lake. Ali spring (GW217) has tritium value of 5.96 TU in this wet season while has 1.23 TU in dry period for the same reason. Samples taken during dry period from this area have enriched delta ^{18}O and ^{2}H values, which indicate that mixing of leakage water from the Tana Lake with the local groundwater flow is enhanced that otherwise is used to be depleted (Fig.10.4a).

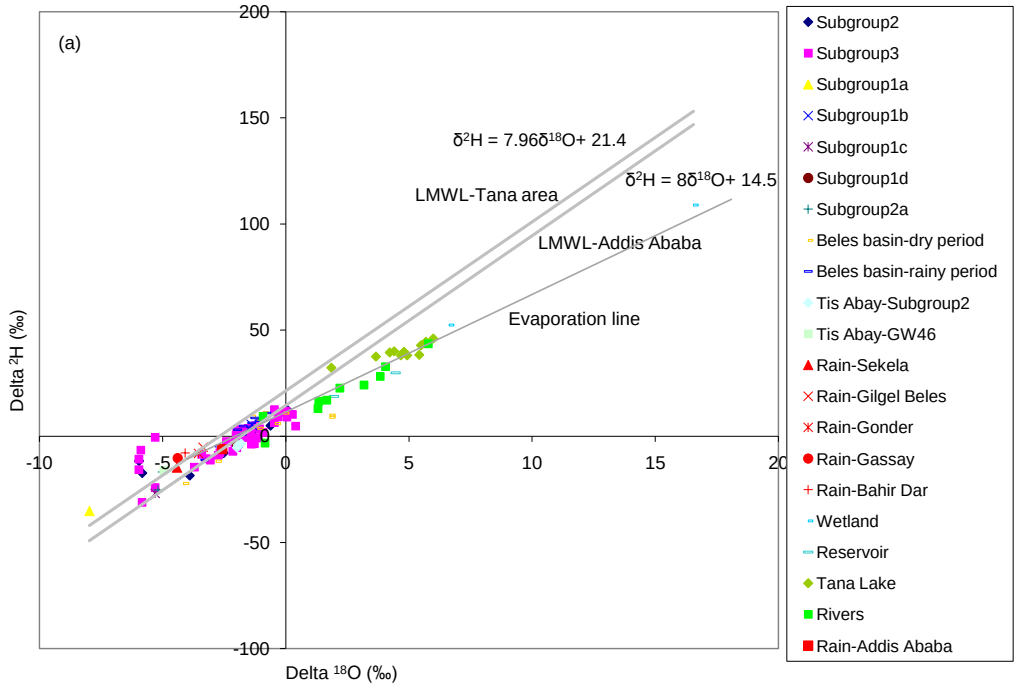
(a)
200
150
100
50
0
-50
-100
-10
-5
0
5
10
15
20
Delta ²H (‰)
Delta ¹⁸O (‰)
δ²H = 7.96δ¹⁸O+ 21.4
δ²H = 8δ¹⁸O+ 14.5
LMWL-Tana area
LMWL-Addis Ababa
Evaporation line
Subgroup2
Subgroup3
Subgroup1a
Subgroup1b
Subgroup1c
Subgroup1d
Subgroup2a
Beles basin-dry period
Beles basin-rainy period
Tis Abay-Subgroup2
Tis Abay-GW46
Rain-Sekela
Rain-Gilgel Beles
Rain-Gonder
Rain-Gassay
Rain-Bahir Dar
Wetland
Reservoir
Tana Lake
Rivers
Rain-Addis Ababa

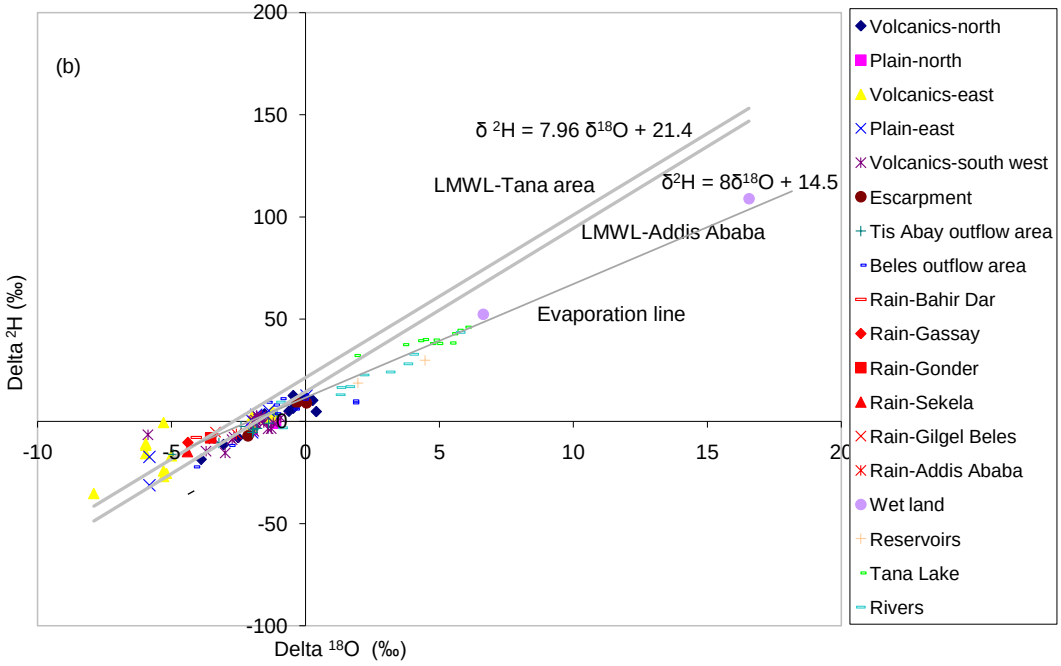
(b)
δ ²H = 7.96 δ¹⁸O + 21.4
LMWL-Tana area
δ²H = 8δ¹⁸O + 14.5
LMWL-Addis Ababa
Evaporation line
Delta ²H (‰)
Delta ¹⁸O (‰)
200
150
100
50
0
-50
-100
-10
-5
0
5
10
15
20
Volcanics-north
Plain-north
Volcanics-east
Plain-east
Volcanics-south west
Escarpment
Tis Abay outflow area
Beles outflow area
Rain-Bahir Dar
Rain-Gassay
Rain-Gonder
Rain-Sekela
Rain-Gilgel Beles
Rain-Addis Ababa
Wet land
Reservoirs
Tana Lake
Rivers

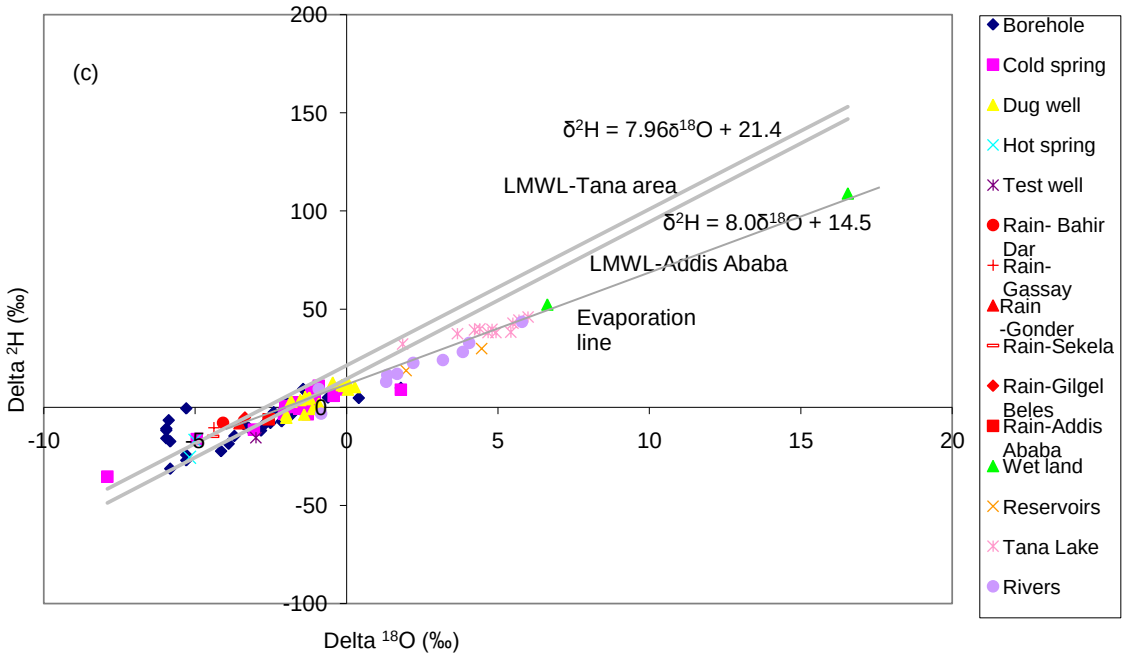

Figure 10.4. Plot of delta deuterium versus oxygen-18 (‰). a) grouped by groundwater subgroups, b) grouped by aquifers, c) grouped by type of schemes.

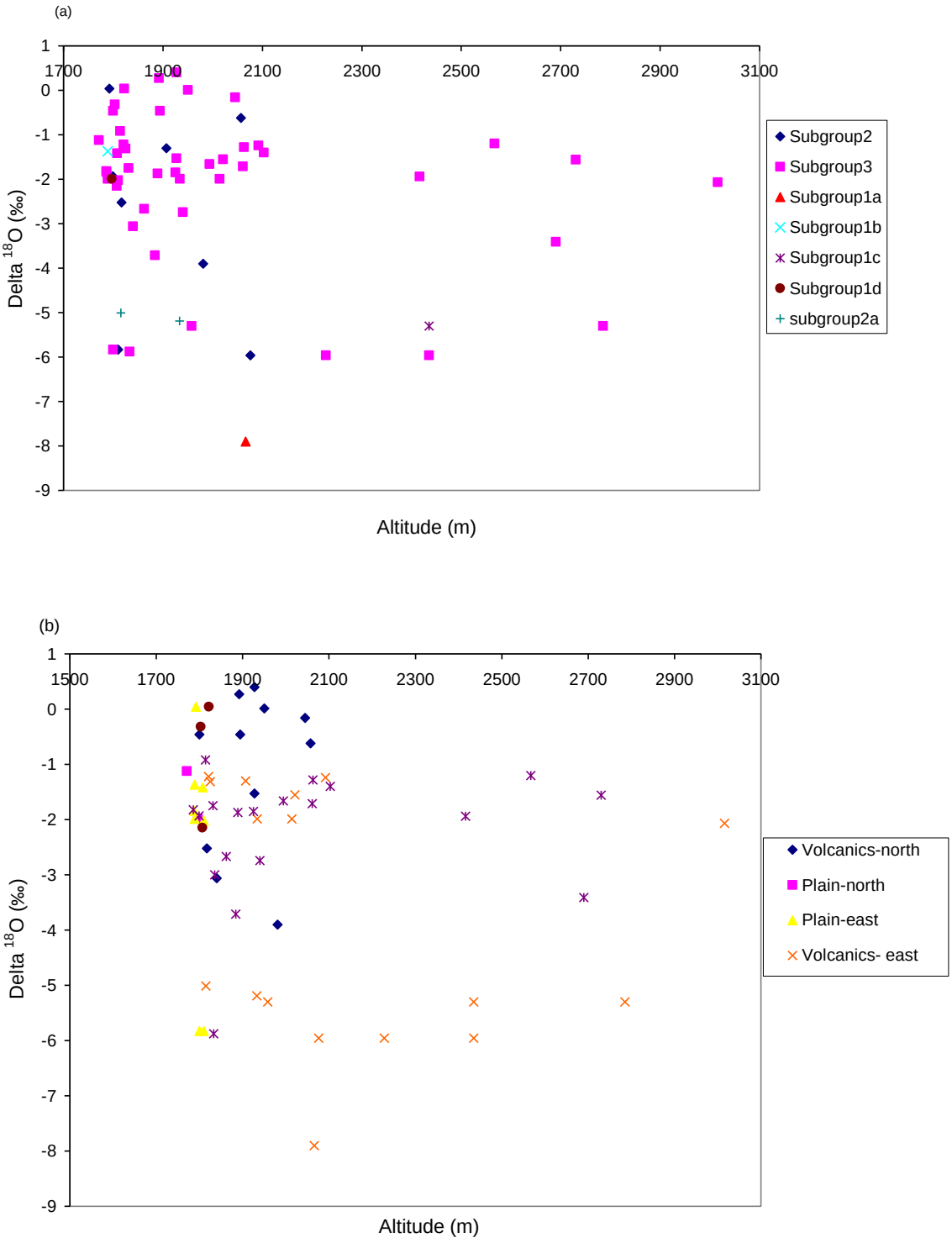

Figure 10.5. Plot of delta Oxygen-18 versus altitude a) grouped by groundwater subgroups and b) grouped by sub-areas.

Mixing rate of Tana Lake (SW15) with Ali spring (GW217) in Beles basin has been estimated as follows. Salini borehole (GW225), which is at the divide between Tana and Beles basins and represents groundwater in the Beles upland areas, are used as groundwater end member (see Figs. 8.1 and 11.5).

$$aX + bY = Z \quad \text{.....(23)}$$

Where, a + b = 1

X, *Y*, and *Z* represent isotopic values for Tana Lake, Salini Borehole and Ali spring, respectively

These waters have the following contents.

Ali spring (GW217): Delta ^{18}O= 1.79 ‰, delta ^{2}H= 8.98 ‰
GW225: delta ^{18}O=-4.15 ‰, delta ^{2}H= -22.27 ‰
Tana Lake at Kunzila (SW15): delta ^{18}O= 5.42 ‰, delta ^{2}H= 38.36 ‰

Substituting these values in Equation 23, has given 62% and 52% contribution or mixing rates of Tana Lake to Ali spring based on delta ^{18}O and deuterium, respectively. The average Tana Lake contribution to Ali spring is 57%. The local groundwater recharge accounts to 43% of Ali spring discharge. Ali spring has tritium content of 1.23 TU, which shows mixed groundwater. Because of variation in depth of boreholes, the mixing rate from Tana Lake varies spatially in Beles basin, and mixing rate with Ali spring shows the maximum lake contribution to the area.

Depleted delta deuterium and oxygen-18 values for borehole GW221 in Beles basin, which belong to Subgroup2 may suggest evolved local groundwater from the escarpment area, with relatively little leakage water mixing. GW216 in Beles basin shows relatively highly enriched delta ^{2}H and ^{18}O values and relatively high TDS but has tritium content of 5.13 TU, which indicates modern groundwater. This is attributed to be due to

evaporation of locally influent stream. This borehole is in stream course and the groundwater level is below the stream bed.

Boreholes GW13, 57, 58 in the adjacent low lying Tis Abay area, south of the Tana Lake, have delta ^{18}O values between -2.3 and -1.7 ‰, which are relatively enriched than other boreholes in the peripheral areas and depleted than the springs at the nearby downstream areas. The fact that these boreholes have enriched values than other ground waters in Tana basin (Subgoup2 excepting the plain areas, 2a, 1a and 1c) and in Tis Abay area (Subgroup3) suggest minor leakage water mixing from Tana Lake to this Tana basin groundwater outflow area. Andesa spring (GW46) has relatively very low delta ^{18}O (-4.95 ‰) and ^{2}H (-16.13 ‰) and high TDS (4700 mg/l) when compared to the above mentioned nearby boreholes and springs. It seems to be mixed depleted upland ground waters (Subgroups1a and 1c) and Subgroup2 of Tana basin, and Subgroup3 of the local groundwater (Figs. 10.3 and 10.4a).

The wetland waters are generally highly enriched than the Tana Lake, which is due to shallow water evaporation. This may suggest that the main part of this water is from inundated lake water during summer and river floods, with shallow groundwater underneath. On the other hand, this suggests that the major process for this enrichment is evaporation than transpiration.

Average delta deuterium, delta oxygen-18 and tritium values of groundwater subgroups in Tana basin, Tis Abay area and Beles leakage water mixing area are given in Table 10.3.

Table 10.3. Summary statistics for environmental isotopes data.

Subgroup	$\delta^{18}O$ (‰)				$\delta^{2}H$ (‰)				Tritium (TU)			
	Minimum	Maximum	mean	count	Minimum	Maximum	mean	count	Minimum	Maximum	mean	count
Subgroup3	-5.96	0.4	-2.06	45	-31.21	12.61	-1.2	45	0.37	6.41	3.63	26
Subgroup2	-5.96	0.04	-2.75	8	-18.52	12.66	-4.99	8	0.5	3.14	1.82	6
Subgroup2a	-5.19	-5.01	-5.1	2	-25.4	-16.83	-21.1	2	0.67	0.82	0.74	2
Subgroup1a	-7.9			1	-35.27			1	0.43			1
Subgroup1b	-1.37			1	5.31			1	3.34			1
Subgroup1c	-5.3			1	-26.95			1	0.51			1
Subgroup1d	-1.99			1	-3.78			1	0.92			1
GW46	-4.95			1	-16.13			1	3.0			1
GW226	-3.0			1	-15.45			1	2.25			1

10.3. Tritium

Tritium with a radioactive decay half life of 12.43 years is part of the water molecule and can be used to date the water often qualitatively. Natural tritium is produced by the impact of cosmic neutron on nitrogen nuclei in the upper atmosphere resulting in steady state concentration of less than or equal to 20 TU in precipitation (Fontes, 1980).

Tritium is used for the definition of modern groundwater. The era of thermonuclear bomb testing in the atmosphere, from May 1951 to 1976, provided enormous amount of man made tritium, which is used as the tritium input signal that defines modern water. Tritium free ground waters are considered to be sub-modern (Pre 1952) or older due to its natural decay (Clarck, 1997).

Tritium input function for continental regions has been deduced for the year 2013 from Clarck (1997) using the following equation.

$$a_t = a_o e^{-\lambda t} \quad \text{.....(24)}$$

Where, a_o is initial activity in 1997, a_t is activity after time t (16 years), λ is decay constant = $\ln 2/t_{1/2}$, $t_{1/2}$ is half life of tritium

Consequently, the following tritium input functions can be considered in qualitative groundwater age dating using tritium.

< 0.3 TU – sub-modern (pre 1952) or older
0.3-5 TU – mixture of sub-modern or older groundwater and recent recharge
5-15 TU – modern (<5 to 10 years)
>10.8 TU- some 1960s or 1970s mixture present

Bomb period tritium inputs currently have similar values with modern groundwater and are misleading.

Spatial variation of tritium is depicted in Figure 10.6. No systematic variation is seen in this map along groundwater flow direction, which is due to variation of depths of boreholes and mixing with modern groundwater.

In general, Subgroup3 has relatively higher tritium content (mixed and modern ground waters) while some groundwater of this subgroup in the eastern area with depleted stable isotopes have less than 1TU (GW29, GW10) indicating more dominant pre1952 ground water recharge. Subgroup2 especially deeper boreholes in the northern area show less than 1 TU (GW2, GW3), which is due to more dominant component of old pre-1952 groundwater recharge. Others are mixed between modern and pre 1952 ground waters (1-5 TU).

Subgroup2a has also tritium less than 1TU suggesting older (pre 1952) groundwater component. Subgroups1a and 1c have also tritium less than 1 TU, indicating older ground waters. The former is highly depleted in delta ^{18}O and seems to be paleo groundwater (Early Holocene). Subgoup1d has also less than 1 TU, which indicates old deeper groundwater component. Subgoup1b has tritium value of 3.34 TU, which is mixed groundwater between modern and pre-1952 ground waters.

Ali spring (GW217) in Beles basin where leakage water from Tana Lake mixes with the local groundwater has tritium value of 1.23 TU while groundwater at Tis Abay basin groundwater outflow area (GW13) has 2.06 TU. Andesa up rising cold spring (GW46) has tritium content of 3 TU, which is mixed between ground waters underflow from Tana basin (Subgroups2 and 1a) and modern (Subgroup3) local groundwater. It has depleted stable isotopes.

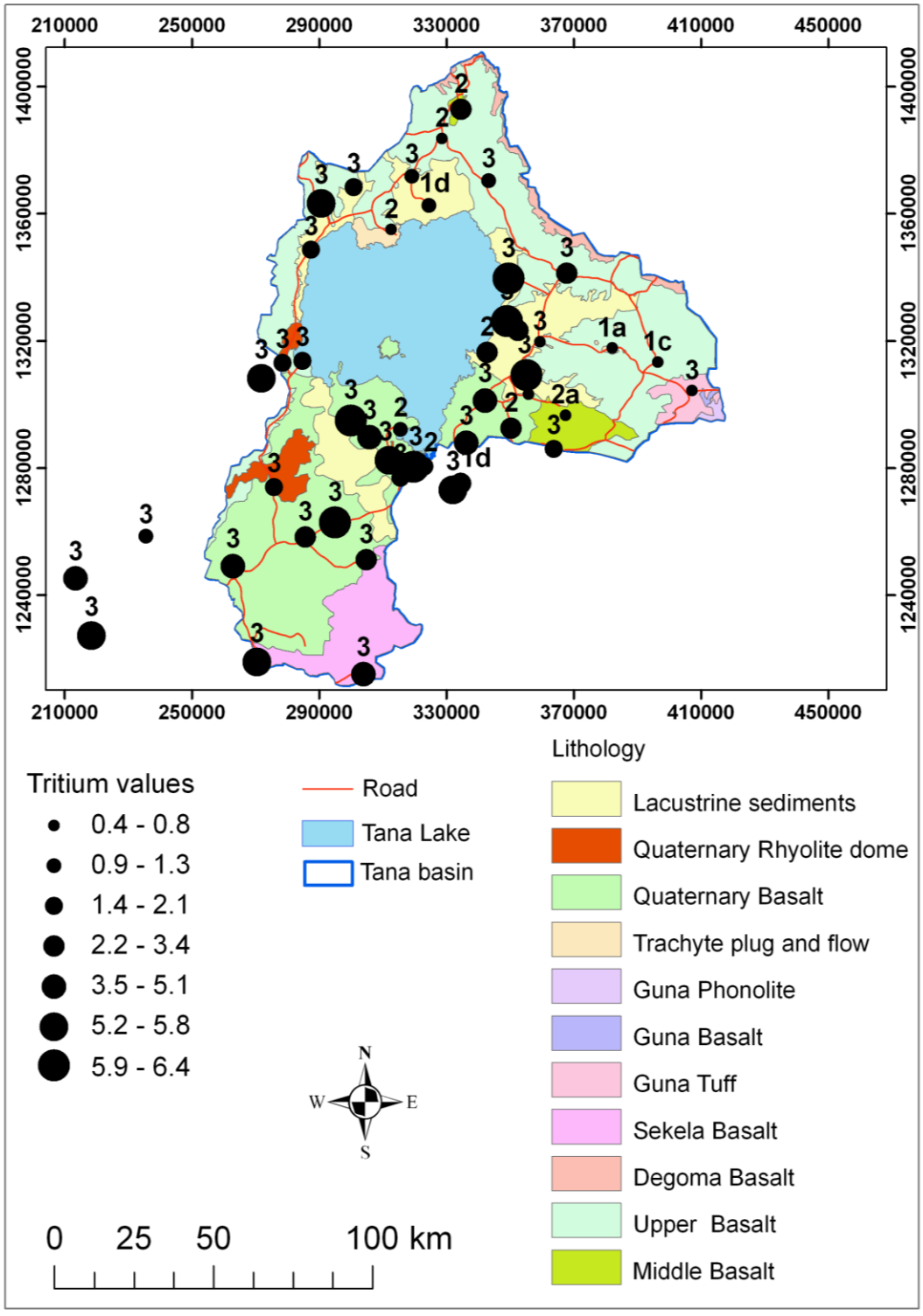

Figure 10.6. Spatial distribution of tritium (in TU).

Plot of tritium versus altitude (Figure 10.7) depicts that one upland groundwater member of Subgroup3 (GW10) and Subgroup1c (GW9) have tritium less than 1 TU, while some other groundwater members of Subgroup3 show mixed and modern water in the upland. Subgroup1a (GW32) and one groundwater member from Subgroup2 (GW3) and 2a (GW42) have tritium less than 1 TU or more of older ground water components at the mid altitude. On the lower altitude, few ground waters from subgroup2 (GW2), 2a (GW16), 3 (GW29) and 1d (GW24) have tritium less than 1 TU, indicating old ground waters components. Other ground waters from subgroup2 and 3 show mixed ground waters (1-5 TU) and some members of Subgroup3 are modern ground waters (> 5TU) at lower altitude.

Plot of tritium versus delta ^{18}O is given in Figure 10.8. Wide scattering have been seen for Subgroup3. Most groundwater points show relatively enriched delta ^{18}O with relatively increased tritium content (modern groundwater) while some with modest tritium (mixed) and depleted oxygen-18, and few with tritium less than 1 TU and depleted in ^{18}O values (GW10: -5.3 ‰ and 0.37 TU, GW29: -5.83 ‰ and 0.63 TU) are observed. Some members of Subgroup2 have relatively slightly enriched delta ^{18}O (0 to -2 ‰) and moderate tritium (1-3 TU) or mixed groundwater. Others have moderate delta ^{18}O content (-2 to -4 ‰) and tritium less than 1 TU (GW2: 0.5 TU, GW3: 0.52). These ground waters are found in the northern part of the Tana basin, which represent stratified and deep volcanic aquifers. GW11 of Subgroup2 in the eastern part of the area has tritium of 3.14 TU that shows mixed groundwater and depleted delta ^{18}O value (-5.96 ‰).

Subgroup2a has depleted delta ^{18}O (-5.1 ‰) and less than 0.74 TU. Subgroup1c has depleted delta ^{18}O (-5.3 ‰) and tritium content of 0.51 TU. Subgroup1a shows the most depleted $\delta^{18}O$ (-7.9 ‰) with tritium of 0.43 TU. Ground waters with depleted $\delta^{18}O$ and tritium less than 1TU are older ground waters, at least the dominant component is pre-1952 ground waters recharge, and paleo (Early Holocene) groundwater for Subgroup1a. Average tritium content of each subgroup is given in Table 10.3.

The fact that Sbgroup3 has enriched delta ^{18}O and ^{2}H and modern groundwater in the upland and low altitudes in the area suggests that the aquifer is unconfined with recharge every where. Relatively depleted and pre-1952 ground waters in the upland and low altitudes in the eastern area also proves older groundwater with depth in this aquifer that flow from the upland to the low lying area or to the Tana Lake.

Subgroup2 generally are older groundwater (pre-1952) with depleted delta ^{18}O and ^{2}H values, which is at places mixed with modern groundwater. This suggests that this groundwater occurs beneath and interacts with the overlying unconfined aquifer. Hydrogeological evidences indicated that the deeper aquifers beneath the top unconfined aquifer is in (semi) confined conditions. Subgroup2a has depleted and tritium less than 1 TU (pre-1952) both in the upland and mid altitude of the eastern area suggesting older groundwater.

Subgroup1c has depleted and tritium less than 1 TU in the upland and Subgroup1a has the lowest delta ^{18}O and ^{2}H values and tritium less than 1 TU as well as high TDS in the eastern area. These ground waters belong to the intermediate and deeper groundwater systems that rose to near surface (Subgroup1c) and emerges at the surface as cold spring (Subgroup1a) due to short circuits of groundwater flow systems by deep fault and lineament, respectively (see Section 11.1).

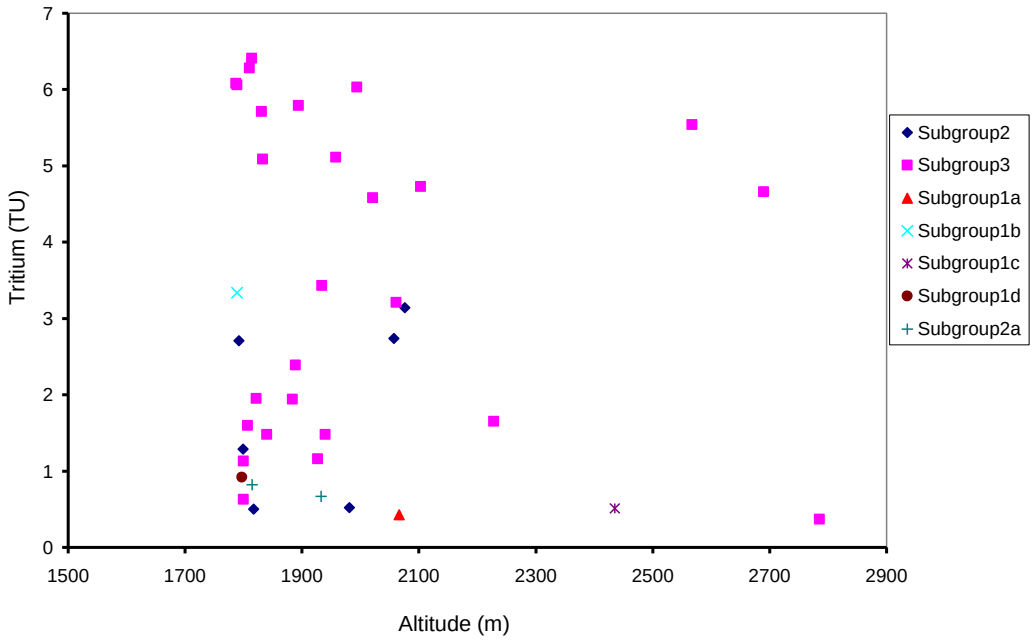

Figure 10.7. Plot of tritium versus altitude.

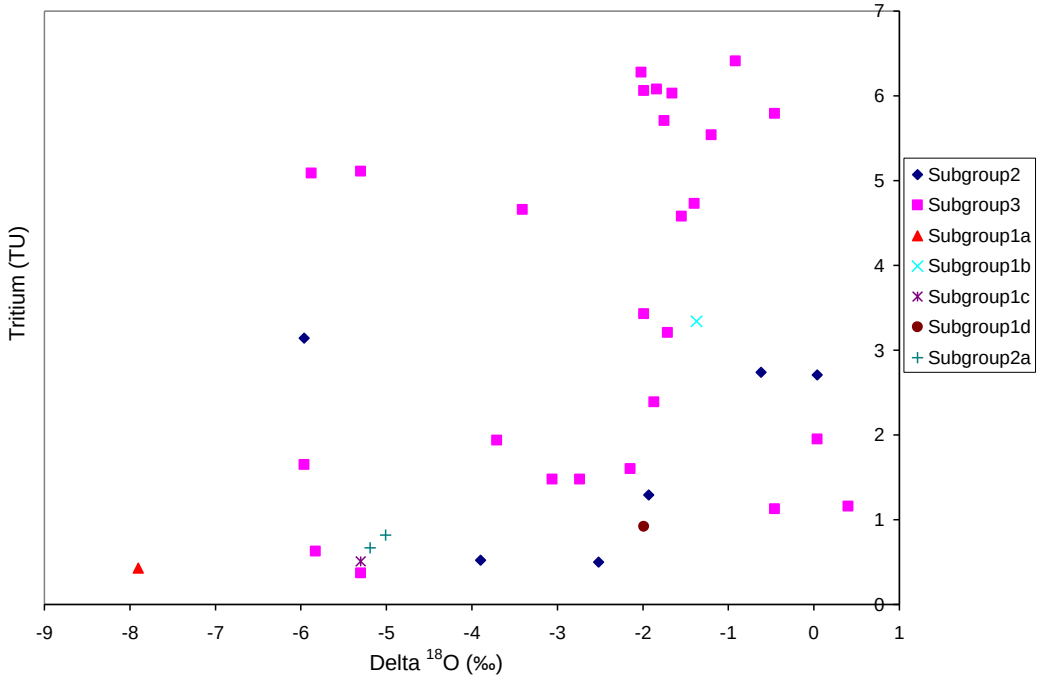

Figure 10.8. Plot of tritium versus delta ^{18}O.

11. SYNTHESIS

11.1. Analysis of Aquifers, Aquifer Systems and Groundwater Flow Regime

Cronostratigraphic units that exist in Tana basin have been converted into hydrostratigraphic aquifers and confining units, which include fracture and intergranular media. Productivity of each hydrostratigraphic aquifer unit has been ranked from low to moderate to high based on their field hydraulic properties, transsmissivity values and topographic setting (Fig. 5.2). Most of existing water supply boreholes in volcanic rocks have depth less than 150 m and penetrate one hydrostratigraphic unit, which has often given low productivity. However, the recently drilled test well in the southwestern part (500 m) and boreholes for Gonder town water supply in the northern area (300-400 m) penetrated the most parts of the Tertiary volcanic formations (Upper, Middle and Lower basalts aquifers). These boreholes showed high productivities (transsmissivity of 69 to 108 m^2/d) suggesting that groundwater potential increases and becomes high with depth of penetration of these stratified volcanic aquifers.

Groundwater has been stricken at different depths in these hydrostratigarphic units. This indicates that multi layered aquifers exist in the volcanic rocks. Each hydrostratigraphic unit intersected has been found to consist of two or more aquifer zones separated by less fractured aquitards (Figs. 5.9a&b). There are no major regional confining units between these hydrostratigarphic units in the northern and southwestern areas except reddish silty clay paleosols of often up to 0.5 m and rarely up to 2 m thick. Regional extensions of the aquifers and confining zones in each hydrostratigraphic unit can not be traced due to lack of enough deep boreholes penetrating the multi layers volcanic rocks.

In volcanic terrain, the interflow zones, and the upper and lower part of the lava generally have greater permeability than the hard dense interior part. The zones of dense basalt at the middle of each flow may have low hydraulic conductivity and effective porosity, but generally capable to transmit considerable water. Permeability can be attained due to columnar joints and secondary joints and faults at the middle of the flow. However, some

zones that are totally dense and unfractured act as regional aquitards (Freez and Cherry, 1979)

Aquifer system can be of two types as given below (Sun and Johnston, 1994).

Type I

An aquifer system comprised of an extensive set of aquifers and confining units that may be discontinuous locally, but which act hydrologically as a single system on a regional scale. This aquifer system may contain several geological formations and chronostratigarphic units as several regional aquifers and confining units. Hydraulic continuity exists to the extent that a flow system can be defined for the entire aquifer system (Johnston, 1999). Potentiometric surfaces can be mapped for the aquifer system or its components if sufficient water level data exist.

Type II

It is a system consisting of a set of independent aquifers that share many common hydrologic characteristics. According to Johnston (1999), this aquifer system contains numerous isolated flow systems and cannot be simulated as a single hydrologic unit. Hydrologic changes in one aquifer have no effect on other aquifers.

Three aquifer systems have been recognized in the Tana basin, which are termed as the Upper, Intermediate and Lower Aquifer Systems based on the results of hydrogeology, hydrogeochemistry and isotope hydrology.

The Upper Aquifer System (UAS)

This aquifer system consists of the Quaternary and Tertiary basalts and the overlying lacustrine sediments aquifers that form vertically multi layers stratified aquifers, which are interacting. Deep boreholes in the northern and southwestern areas revealed that the upper aquifer is in unconfined condition while the deeper ones are in (semi) confined aquifer conditions.

Groundwater level rise or drop have been observed at different boreholes when the deeper aquifers are penetrated, and pumping test data analysis showed storativity values typical of confined aquifers (Figs. 5.7& 5.11). These aquifers are interacting via deep faults and gets recharge where they are exposed and through faults and pervasive lineaments. Double porosity fracture aquifer is anticipated in this aquifer system where groundwater flows both in the rock matrix and fractures. There are no deep boreholes in the eastern area, which show the nature of the aquifer system in this area.

Laterally, the Upper Aquifer System consists of independent sets of aquifers that share many common hydrologic characteristics (hydraulic properties that control recharge and discharge rates, nature of aquifers, climate, lithology and soil), with isolated groundwater flow systems in the southwestern, eastern, northern and western parts of the basin. Analysis of hydrogeochemistry and isotopes data revealed that this aquifer system is characterized by shallow deep groundwater flow systems in unconfined and (semi) confined aquifer, respectively.

This aquifer system seems to be similar with Type II aquifer system. Because of related lithology, soil, climate, hydraulic properties and nature of aquifers, this system exhibit closely related hydrogeochemical processes and hydrochemical facies in the different parts of the basin.

The Upper Aquifer System is found to be characterized by or consists of groundwater subgroups 3, 2, 1b, 1d and 2a. The shallow unconfined aquifer is represented or characterized by subgroups 3, 1b and 1d, which are under open system. On the other hand, the deep aquifers of the UAS, which are often in (semi) confined conditions, are represented by Subgroup2 that is under a closed system.

Plot of delta^{18}O (‰) versus electric conductivity (µS/cm) (Fig 9.31) reveals that subgroups 3, 2, 2a, 1b and 1d form one cluster indicating that they are interrelated and belong to one or the Upper Aquifer System. Plot of tritium versus electric conductivity (Figs.11.1a&b) also reveal that subgroups 3, 2 and 2a have similar clustering, from all

parts of the area, with electric conductivity less than 1000 µS/cm for modern, mixed and pre-1952 ground waters suggesting the same aquifer system.

Besides, plot of electric conductivity versus altitude (Fig. 9.32a&b) also shows that groundwater salinity increases from the uplands to the lowlands along the groundwater flow direction for subgroups 3, 2, 1b and 1d which indicate that they belong to one aquifer system.

Some members of Subgroup3 and especially subgroups1b and 1d with mixed ground waters have relatively high electric conductivity at lower altitude than others subgroups 3 and 2 in the eastern and northern plain and volcanic areas due to further evolution by dissolution of evaporites and carbonates and cation exchanges in lacusterine sediments.

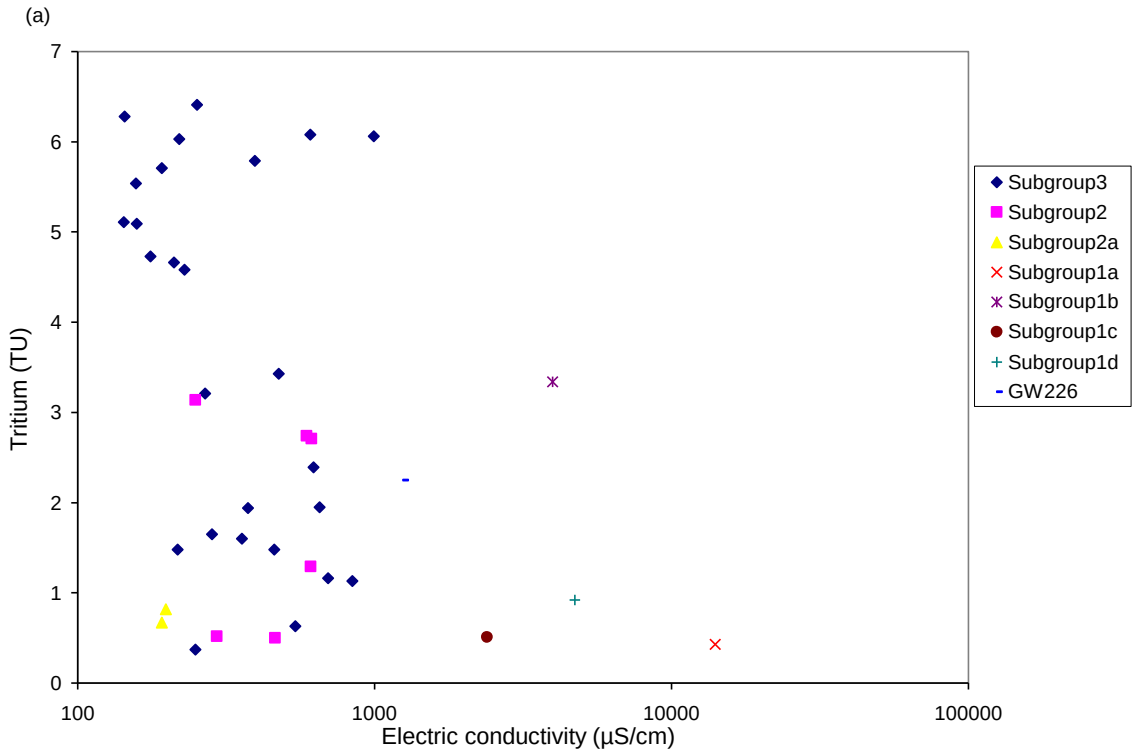

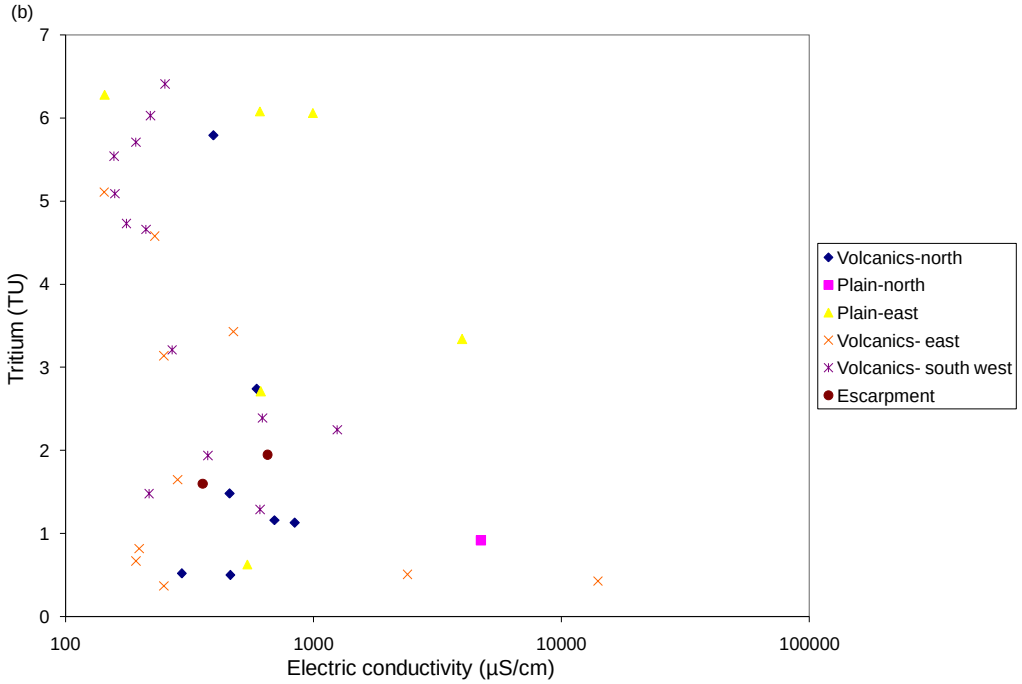

Figure 11.1. Plot of tritium versus electric conductivity. a) grouped by groundwater subgroups, b) grouped by aquifers.

Bivarient plots (Figs.9.24 to 9.27) also show that subgroups 3 and 2 are interrelated ground waters. Subgroup3 represents the shallow unconfined ground waters in the basin that did not under go much rock-water interaction and interacts with rivers and the Tana Lake. Subgroup3 has Ca-Mg-Na-HCO_3 (transitional) type of hydrochemical facies and TDS of 376 mg/l. Modern groundwater with depleted and relatively enriched stable isotopes, and some depleted pre-1952 groundwater members (GW10 and GW29) are found for Subgeroup3 in the eastern area, while it consists of modern and mixed ground waters with modest stable isotopes values in the southwestern, western and northern areas (Table 10.3 and Fig.10.3). Subgroup3 has closely similar but a little lower PCO_2 (0.027 atm) than that of the rainfall (0.096 atm) in Tana basin, and with low pH and HOC_3 that indicates open system to atmospheric CO_2 (Fig.11.2).

Subgroups 1b and 1d belong to the Upper Aquifer System, but highly evolved from Subgroup3 and attained relatively high salinity (brackish groundwater) due to local dissolution of evaporites and cation exchange in shallow unconfined lacustrine sediments. They have Na-Mg-Cl-HCO_3 (basic) and Na-Mg-Ca-Cl-SO_4 (transitional) type of hydrochemical facies, respectively. Subgroups 1b and 1d also have nearly similar PCO_2 (0.024 and 0.027 atm, respectively) with that of Subgroup3, and low pH but increased HCO_3, which show that Subgroup3 evolves to Subgroups1b and 1d under open system to atmospheric CO_2 locally in the unconfined lacustrine sediments aquifer (Fig.11.2).

They have mixed groundwater and δ^2H and $\delta^{18}O$ similar with the surrounding members of Subgroups 3. Moreover, some other groundwater samples of Subgroup3 in lacustrine sediments aquifer also showed relatively increased salinity than ground waters in volcanic aquifers that belong to subgroups 3 and 2 suggesting leaching of salt deposits here (Fig. 9.31b).

Subgroup2 has Na-HCO_3 (basic) type of hydrochemical facies. TDS (439 mg/l), pH (8.25) and most ions are higher than Subgroup3. However, Ca^{2+} and Mg^{2+} tend to decrease due to precipitation of calcite and dolomite during this process, which are oversaturated in ground waters of Subgroup2. It has relatively higher HCO_3 than Subgroup3 and high pH and very low PCO_2 (2.26×10^{-10} atm) than Subgroup3 and the rainfall (Fig.11.2). This indicates that Subgroup3 evolves to Subgroup2, and that Subgroup2 is under closed system to any CO_2 sources.

Groundwater samples from Subgroup2 showed mixed and pre-1952 groundwater in all parts of the area, which are often relatively depleted than Subgroup3, except where they are affected by evaporation (Table10.3 and Fig.10.3). Ground waters from deep boreholes in this aquifer system belong to Subgroup2 and aquifers are in semi (confined) conditions in northern and southwestern areas. Nature of aquifers in the eastern part of the area is unknown as there are no deep boreholes. However, it is expected to be similar to that of the northern and southwestern areas.

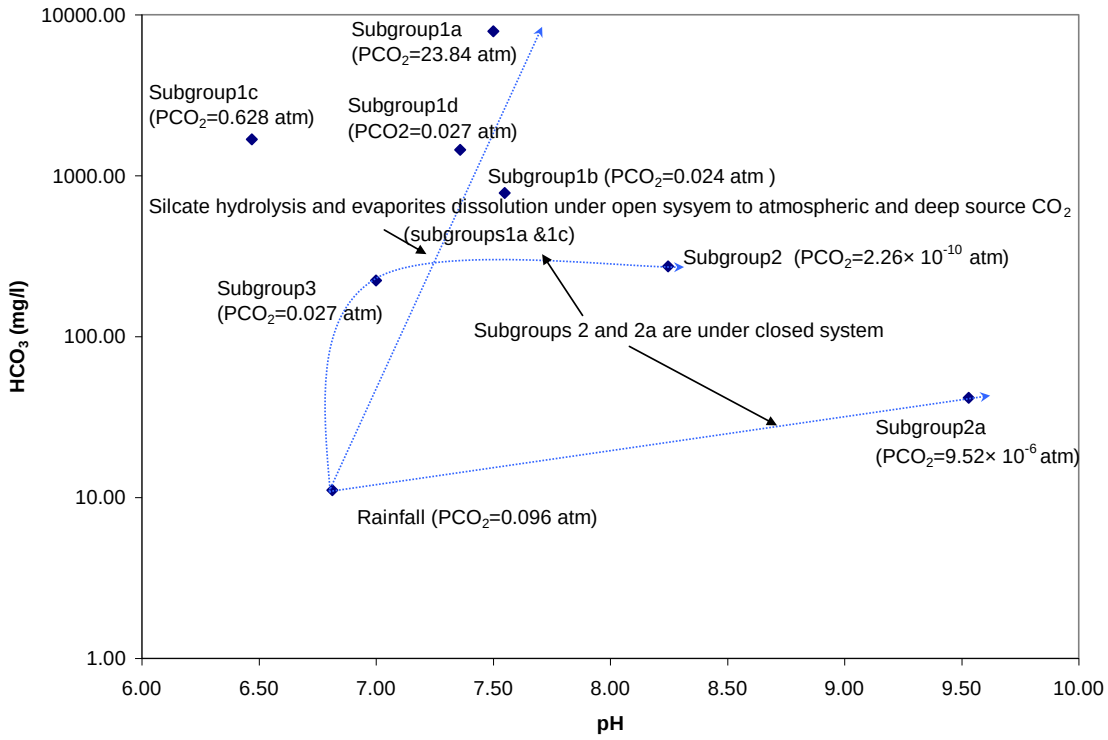

Figure 11.2. Plot of HCO_3^- versus pH showing open and closed systems in the area.

Thermal springs emerging associated with faults in the eastern part of the area are represented by Subgroup2a, which belongs to the Upper Aquifer System. This groundwater has relatively higher concentrations of Na^+, Cl^-, F^-, SO_4^{2-}, SiO_2 and hyper alkaline pH (9.5) , but lower concentrations of K^+, Ca^{2+}, Mg^{2+}, HCO_3^- and TDS (179 mg/l) than the shallow groundwater (Subgroup3: GW6 and 7) in the upstream area, which consist of mixed groundwater that belong to the Upper Aquifer System. This can be due to precipitation of K^+, Mg^{2+} and Ca^{2+} clay products as a result of silicate hydrolysis. It has Na-Mg-HCO_3 (basic) type of hydrochemicasl facies.

Subgroup2a has PCO_2 (9.52 $\times 10^{-6}$ atm) much lower than that of Subgroup3 and the rainfall suggesting a closed system. It is relatively depleted and plots lower than the mean values of modern rains on graph of δ^2H versus $\delta^{18}O$ (Fig.10.4a and Table10.3a). It has low mean tritium content (0.74 TU) and the δ^2H and $\delta^{18}O$ altitude relationship for the

area can not justify the recharge altitude of this groundwater suggesting mainly pre-1952 episode of recharge. It seems that this groundwater might probably have been locally warmed within the fault planes by heat convection associated with the recent magmatic activity in the area. Such thermal groundwater springs with low TDS and high pH values are not uncommon in volcanic aquifers within Ethiopia and else where in the world.

Deep test well (GW226) drilled in the southwestern area intersected the Precambrian granite (356-500 m) below the Quaternary and Tertiary volcanic aquifers. Groundwater from this borehole has high TDS of 1215.4 mg/l when compared with other ground waters in volcanic aquifers of the UAS, and has Na-Mg-Ca-HCO_3 (basic) type of hydrochemical facies. PCO_2 (2.8 atm) of this groundwater is higher than that of the rain in the area suggesting a contribution from other deeper aquifer system below the aquifers of Subgroup2 (UAS), which are in closed system. This shows groundwater at depth with head below the UAS and under open system with deep source of CO_2 and with relatively higher salinity. The test well has modest $\delta^{18}O$ (-3.0 ‰) and $\delta^{2}H$ (-15.45 ‰) values and the tritium content is 2.25 TU, which shows mixed groundwater.

Intermediate Aquifer System (IAS)

Subgroup1c is found in the higher altitude and represents intermediate groundwater system between the upper and lower aquifer systems in the eastern area. It has Na-HCO_3 (basic) type of hydrochemical facies, and brackish groundwater with relatively high TDS (2341 mg/l) and for most of the ions including F^- (2.8 mg/l) in the upland (Fig. 9.32), and lower pH (6.47) than groundwater subgroups in the Upper Aquifer System and in the Lower Aquifer System (Table 9.3). It has dissolved CO_2 and its PCO_2 (0.628 atm) is higher than those of the UAS and the rainfall in the area (Fig.11.2), which indicates open system at deeper depth below the UAS. Sources of CO_2 can be due to deep decarbonation of the underlying Mesozoic carbonate rocks due to heating by the recent magmatic chamber in the area or from the mantle.

The source borehole (GW9) is in the upland of the eastern area, and has depth of 109 m and was drilled on the fault. The aquifer is basalt inter bedded by tuff and ignimbrite that

form a confined aquifers (Fig. 8.9b). Ground waters collected from four boreholes in the relay station in the near by area, which are not affected by the fault, have mean electric conductivity of 256 mg/l, which belong to the Upper Aquifer System. This suggests that Subgroup1c seems to represent groundwater that ascends through the fault from intermediate volcanic aquifer system with head above the UAS. It seems unlikely to be a mixture of ground waters of the upper and lower aquifer systems because of its lower Cl^- and SiO_2 values than the ground waters from both the lower and upper aquifer systems.

Subgroup1c is depleted in $\delta^{18}O$ (-5.3 ‰) and $\delta^{2}H$ (-26.95 ‰) and plots lower than the mean modern rain values (Fig.10.4a). It has low tritium value (T= 0.51 TU) indicating more of older groundwater component. Delta Deuterium and oxygen-18 altitude relationship for the area suggests that Subgroup1c is pre-1952 or older episode of recharge, which is during more humid condition than the present. Subgroup1c has higher TDS and low tritium values at the higher altitude than other ground waters of pre-1952 episodes of recharge that belong to Subgroups3, 2 and 2a in the area (Figs.9.31a, 9.32a and 11.1a). This aquifer system is not intersected at any other place as there are no deep boreholes but seems to exist below the Upper Aquifer System in the eastern area.

The Lower Aquifer System (LAS)

The Lower Aquifer System is ascertained to exist in the eastern part of the area, which underlies the above mentioned aquifer systems (UAS and IAS), with groundwater head above them. It is in confined condition. It is represented by Subgroup1a, which is uprising salty cold spring through lineament at mid altitude in the eastern area. It has dissolved CO_2 with very high PCO_2 (23.84 atm) when compared with the rain, UAS and IAS, and high ions concentration and TDS (12840 mg/l), see Figure 9.32. Subgroup1a has relatively low pH than Subgroup2 of the Upper Aquifer System but higher than Subgroup1c of the Intermediate Aquifer System (Table 9.3). All common mineral phases of carbonates and evaporites are under saturated. This indicates open system at deeper depths of volcanic aquifers due to the presence of CO_2 from deep source (Fig.11.2).

It is highly depleted in stable isotopes of delta ^{18}O (-7.9 ‰) and ^{2}H (-35.27 ‰), and plot at the lower end of the LMWL on $\delta^{2}H$ versus $\delta^{18}O$ plot (Fig. 10.4a-c). Furthermore, it has low tritium value (0.43 TU). Plots of $\delta^{18}O$ and tritium versus altitude (Figs.10.5 and 10.7), $\delta^{18}O$ versus electric conductivity, electric conductivity versus altitude, tritium versus $\delta^{18}O$ and tritium versus electric conductivity (Figs. 9.31a, 9.32a, , 10.8 and 11.1a) show its highly depleted $\delta^{18}O$ value, low tritium and high salinity than other ground waters subgroups in the upland, mid and lower altitudes of the area. Recharge altitude of Subgroup1a cannot be justified by the present delta deuterium and oxygen-18 altitude relationship for the area. This suggests that this groundwater is paleo groundwater (Early Holocene recharge through deep faults and lineaments), and has no current recharge and ascends through deep lineament.

This groundwater has high fluoride (5.5 mg/l), Cl and TDS, which may indicate that the reservoir aquifer(s) are the lower part of the Tertiary volcanic rocks that may be in hydraulic continuity with the underlying Mesozoic sedimentary rocks. The depth to this Lower Aquifer System is not known as there are no deep boreholes drilled in this area. However, previous geophysical studies using magneto telluric imaging (Hautot et al., 2006) and magnetic (Tadesse Meselu, 2009) techniques anticipated Mesozoic sedimentary rocks below thick volcanic rocks in the eastern area.

There is lack of potentiometeric data to decipher the groundwater flow regime of this system. However, Andesa uprising cold spring (GW46) in Tis Abay area, which has high TDS (4700 mg/l), dissolved CO_2 with PCO_2 (0.228) higher than those of the UAS and lower than IAS and LAS, and depleted stable isotopes ($\delta^{18}O$ = -4.95 ‰ and $\delta^{2}H$ = -16.13 ‰) that can not be justified by the local altitude, seem to be mixture of ground waters from LAS, IAS and the UAS of Tana basin and the local groundwater. Tritium value is 3 TU, which proves mixing of these ground waters.

However, the Lower Aquifer System is missing in the southwestern part of the area. Deep test well (GW226) drilled here and that intersected the Precambrian granite (356-500m) below the Quaternary and Tertiary volcanic aquifers did not show this groundwater.

Presence of the lower aquifer system in the northern part of the Tana basin is not ascertained. Deep boreholes drilled up to 400 m penetrated the Tertiary volcanic rocks that formed the multi layered Upper Aquifer System. However, additional very deep boreholes that penetrate the whole thickness of volcanic aquifers and some depth to the aquifer underneath are necessary to understand the presence or absence of the Lower Aquifer System in this area.

The Upper Aquifer System has isolated groundwater flow systems in the southwestern, eastern, northern and western parts of the basin. However, ground waters from all sides move to the Tana Lake, which is the ground waters confluence area. Plot of electric conductivity versus altitude (Fig. 9.32a) shows that groundwater salinity increases from the uplands to the low lands surrounding the lake for subgroups 3 and 2, 2a, 1b and 1d, which proves the groundwater flow direction of the UAS.

The shallow unconfined groundwater (Subgroup3) discharges to the lake and streams while the deeper (semi)confined groundwater (Subgoup2) converges under the lake bed sediments to the south low lying Tis Abay area, which is ascertained to be the Tana basin groundwater outflow area (see Section 11.3). The groundwater level contour map, which is a composite head map for the different intersected hydrostratigraphic aquifers in the UAS (Fig. 8.2) represents the groundwater flow systems in the northern, eastern and southwestern parts of this aquifer system.

Different ground waters exist in the eastern part of the basin associated with the upper, intermediate and lower aquifer systems. The geometry and groundwater flow regime of the intermediate and lower aquifer systems is difficult to be ascertained at present as there are no deep boreholes penetrating these aquifer systems. However, intense faults and lineaments make short circuits among these different ground water systems to appear at the surface and to shallow depth in this area.

11.2. Groundwater Recharge Estimates

Different methods have been employed to estimate groundwater recharge rate in the area. Previous attempts mainly used hydrograph separation methods and only one have used chloride mass balance method, which did not take into account the surface runoff. Recharge rate of 184.3, 161.7, 70-120, 142.7 mm/year have been estimated by Sogreah (2012), Getachew Zewde (2010), Getachew Hadush (2008) and BECOM (1998), respectively.

However, the area is known to have shallow groundwater circulation in unconfined aquifer and deep baseflow in confined aquifer. These aquifers are interacting through fractures. The confined aquifers are exposed at some places and get recharge here and through deep faults and lineaments. The shallow groundwater interacts with the streams and Tana Lake. Hence, groundwater recharge estimation based on only river hydrograph separation does not give the real recharge rate taking place. It under estimates the recharge by the amount equal to the riparian evapotranspiration, consumptive uses in upstream areas, groundwater discharges as spring and other surface waters, and deep groundwater recharge.

Recharge rate has been estimated in this study using baseflow separation, soil water balance and chloride mass balance methods. Baseflow analysis gave mean recharge of 195.6 mm/year (Section 6.2). The result is in agreement with the results of Sogreah (2012) and Getachew Zewde (2010). Other previous studies underestimate the groundwater baseflow to streams.

Baseflow separation method shows recharge to shallow aquifer that returns to and sustains the rivers flows as groundwater discharge or baseflow. Most of the streams and major rivers are perennial and there are frequent springs and shallow hand dug wells with groundwater head above the streams' water level suggesting that the streams are fed by the groundwater.

Soil water balance and chloride mass balance on the other hand have given net recharge rates of 285.4and 284 mm/year, respectively (Sections 6.3&4). The results of these two methods are reasonable and nearly similar despite the fact that the methods are different. This is because the effect of interflow and seepage on the estimated recharge from soil water balance is negligible or low. Interflow component of the river hydrograph has been incorporated in the direct runoff that was used in the soil water balance computation (Table 6.2). Furthermore, the recharge is not a preferential flow via fractures but has passed through soil and weathered zones of volcanic aquifers where the recharge water has got time to evaporate before reaching the water table so that the CMB method does not over estimate the recharge. Diffuse recharge through the soil and weathered zone of the volcanic aquifers has been revealed to take place by isotopic data.

The mean recharge of the basin, which includes the shallow and deep ground waters recharge, can then be taken as the average of recharge estimates by soil water balance and chloride mass balance methods, which is equal to 284.7 mm/year. It accounts to 20.1 % of the basin precipitation.

The groundwater baseflow to streams is about 68.7 % of the mean basin recharge. The rest 31.3% (89.1 mm/year) is deep recharge that does not return to streams, and contributes to regional groundwater flow under the stream beds and minor contribution to the lake. Hydrogeochemical and isotopic data showed that there is upland deep groundwater flow toward the lake from all sides, which supports the above conclusion.

The fact that most of the recharge contributes to streams has great implication to the groundwater management. The Government has an attempt to develop the groundwater and rivers for irrigation use. Therefore, medium and large scale development of groundwater will reduce the flow of streams and rivers that is fed by the groundwater and dewater the groundwater reserve, which adversely affect the existing and proposed irrigation schemes using surface waters and prior and proposed groundwater uses for urban, rural and industrial supply and on environment. It is therefore better to develop surface waters for irrigation and keep the groundwater resource for other domestic and

industrial uses. Groundwater development for irrigation may be considered in sub-catchments where there is no intensive rivers and groundwater developments and where that it does not cause lowering of the regional water table.

11.3. Inter Basin Groundwater Outflow Rate and Deciphering Outflow Area

There was no any attempt done to determine whether or not groundwater outflow occurs from Tana basin to the adjacent basins except the conceptual model of WWDSE (2007) that speculated leakage from Tana Lake to northern adjacent Chilga basin and to deep groundwater in the eastern part of the area through its floor. Other previous studies concluded that the Tana basin and the Lake to be a closed system in terms of groundwater outflow.

Basin water balance evaluation has been done here (Chapter 7) and gave inter basin groundwater outflow of 3333.5 hm3/year. This value is a comprehensive of the leakage rate from the lake.

Groundwater samples in the low lying downstream southern area of the Tana Lake**,** Tis Abay area, has Na-HCO3 (basic) type of hydrochemical facies and high average pH (8.4) and belong to Subgroup 2 (Figs. 9.16 and 9.17) like the evolved deep upland groundwater in Tana basin (Subgroup 2) of the Upper Aquifer System. Local ground waters (Subgroup 3) in Tis Abay area have Ca-Mg-Na-HCO_3 (transitional) water type (Figs. 9.16 & 9.17). Besides, this groundwater has lower tritium values than Subgroup3 in Tis Abay area (Fig. 10.7).

This indicates that the Tis Abay area is inter basin groundwater outflow area for the deep part of groundwater (Subgroup 2) of the Upper Aquifer System in Tana basin (Figs.9.16 and 9.17). Besides, Andesa uprising spring (GW46) in this area seems to be a mixture of ground waters from Tana basin (Subgroup 2 of the Upper Aquifer System and ground waters from the Intermediate and the Lower Aquifer System) and recent local ground waters in Tis Abay area. It has Mg-Na-HCO_3 (basic) hydrochemical facies and depleted

delta ^{2}H (-16.13 ‰) and ^{18}O (-4.95 ‰), which can not be explained by local recharge altitude. Its tritium value is 3 TU, which indicate mixed groundwater. This suggests that ground waters of the IAS and LAS also underflow from Tana basin at deeper depths to Tis Abay area.

Inter basin groundwater underflow is via the volcanic rocks underlying the Tana Lake bed sediments (Fig.11.3 and 11.4). There seems to be no groundwater flow through the lake bed lacustrine sediments, which are massive and compacted clay. Drilling of 97 m borehole within the lake (5 km south of Gorgora) has proved no groundwater in the whole depth, which is in the lacustrine sediments (oral communication). This supports the above conclusion.

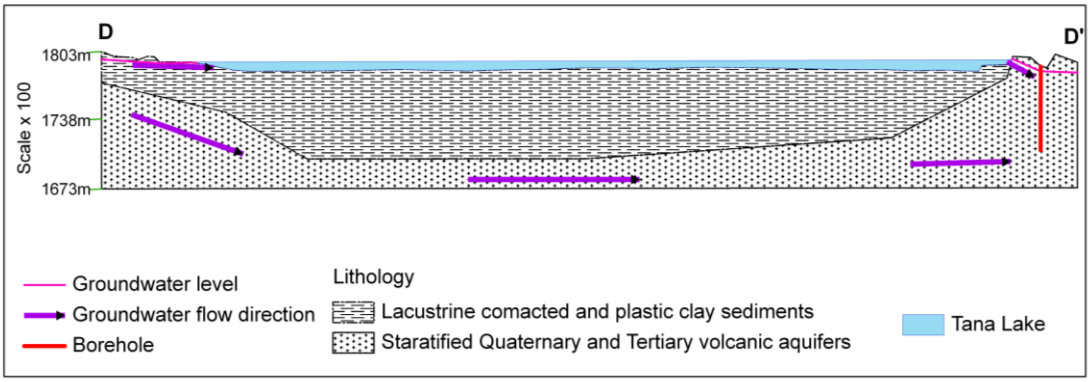

Figure 11.3. Cross section along D-D' depicting inter basin groundwater outflow from Tana basin to Tis Abay area. Vertical scale is exaggerated 100 times. Cross section line is shown in Figure 5.2.

11.4. Groundwater and Surface Waters Interaction

11.4.1. Groundwater- streams interaction

Most streams are perennial indicating groundwater contribution during dry period. Base flow analysis showed that about 68.7 % of the basin recharge feeds the streams. Besides,

water type of the shallow groundwater (Subgroup3) and streams is similar (Ca-Mg-Na-HCO3, transitional) suggesting their interaction.

Enriched isotopic groundwater data revealed that rivers flood pools, ponds due to inundation by the lake during high water level in summer and influent streams seem to recharge the groundwater in lacustrine aquifers surrounding the lake.

11.4.2. Groundwater-Tana Lake interaction

11.4.2.1. Groundwater inflow to the lake

The lake is surrounded by lacustrine clayey sediments and volcanic rocks. Groundwater level contour map, which is depicted in Figure 5.2, shows groundwater flow from all sides to the lake in the Upper Aquifer System.

The lake has Ca-Na-Mg-HCO_3-SO_4 (transitional) in the eastern and northern shores suggesting groundwater inflow. It has Ca-Mg-Na-HCO_3 (transitional) water type in the central part and Ca-Mg-Na-HCO_3 (basic) in the western shore. Isotopic data showed often enriched values (δ^2H: 32.3 to 4 6.03 ‰ and $\delta^{18}O$: 1.85 to 5.99 ‰) at the lake shore and central parts. However, relatively depleted value (1.85 ‰) was seen in the northern shore. Besides, previous $\delta^{18}O$ data (Seifu Kebede et al., 2005) showed relatively depleted values in the southwest and northern shores.

Moreover, groundwater issue as springs and forms perennial streams in volcanic aquifers close to the lake in the southwest, west and east, and groundwater table was seen to be close to the lake level in lacustrine sediments at the eastern and northern areas. Therefore, some groundwater inflows occur through the east, north, west and southwest margins although the dynamic lake depth is not known.

However, lake balance evaluation (Chapter 8) has given negative groundwater inflow rate (-93.1 hm^3/year) to the lake. The result suggests that there is no major groundwater inflow directly entering to the lake from the surrounding areas (i.e., it is within the bound

of uncertainty or error related to data measurement) although hydrogeological and hydrogeochemical evidences indicated some groundwater contribution.

This agrees with most of the previous authors' conclusion that the groundwater inflow to the lake is negligible (Geatchew Hadush, 2008; Seifu Kebede et al., 2012; 2005; SMEC, 2007). The low groundwater contribution seems to be due to the clayey nature or low permeability of the lacustrine sediments around the lake margin and beneath the lake. The floor of the lake seems to be water tight and contribution of the groundwater to the lake through its floor is negligible.

11.4.2.2. Leakage rate of Tana Lake and tracing of leakage path

Previous studies concluded that the Tana Lake is a closed system in terms of groundwater outflow except WWDSE (2007) that speculated leakage from Tana Lake to northern adjacent Chilga basin and to deep groundwater in the eastern part of the area through its floor.

Lake balance evaluation has given leakage rate of 954.8 hm3/year from Tana Lake. Leakage is ascertained to be via deep regional lineaments at the western lake margin to the adjacent low lying Beles river basin (Fig. 11.4). Boreholes and Ali spring in this area has enriched deuterium and oxygen-18 values than the un-affected ground waters (boreholes and springs) in the peripheral areas suggesting mixing of lake water to these ground waters.

Groundwater samples taken from the Beles basin during rainy period are relatively depleted than those of the dry period samples due to dilution by the local rain (Fig.10.4a). Besides, this spring shows triutm of 5.96 TU during rainy and 1.23 TU in dry periods, respectively. This reveals that the local rains are relatively depleted than the groundwater during dry season suggesting leakage mixing is the cause of enrichment during this time. Furthermore, during dry period the groundwater should have been depleted regional

baseflow from the Beles escarpment or upland areas had it not been for mixing from evaporated lake water.

Hydrograph analysis of the main Beles river showed groundwater baseflow of 707.2 hm^3/year, and Ali spring (GW217) with discharge of about 200 l/s exist in the area.

The local recharge upstream of the Beles hydrological station may be taken as about 10 % of the annual precipitation in the area. This gives groundwater resource of 474.6 hm^3/year from the local recharge. Therefore, the available groundwater resource, which is above the local recharge, proves leakage underflow from the Lake Tana to this area.

Furthermore, drillings of up to 150 m depths , which are close upstream areas from the Beles hydrological station, showed high borehole yield (up to 30 l/s) that may support presence of regional groundwater baseflow beneath the river bed (oral communication).

Mixing rates or contribution of the Tana Lake to Ali spring has been estimated to be 62 % and 52 % based on delta ^{18}O and deuterium, respectively. The average Tana lake contribution to Ali spring is 57 % (Section 10.2.3). The local groundwater recharge accounts to 43 % of the discharge of Ali spring. Because of variation in depth of boreholes, the mixing rates from Tana Lake vary spatially in Beles basin.

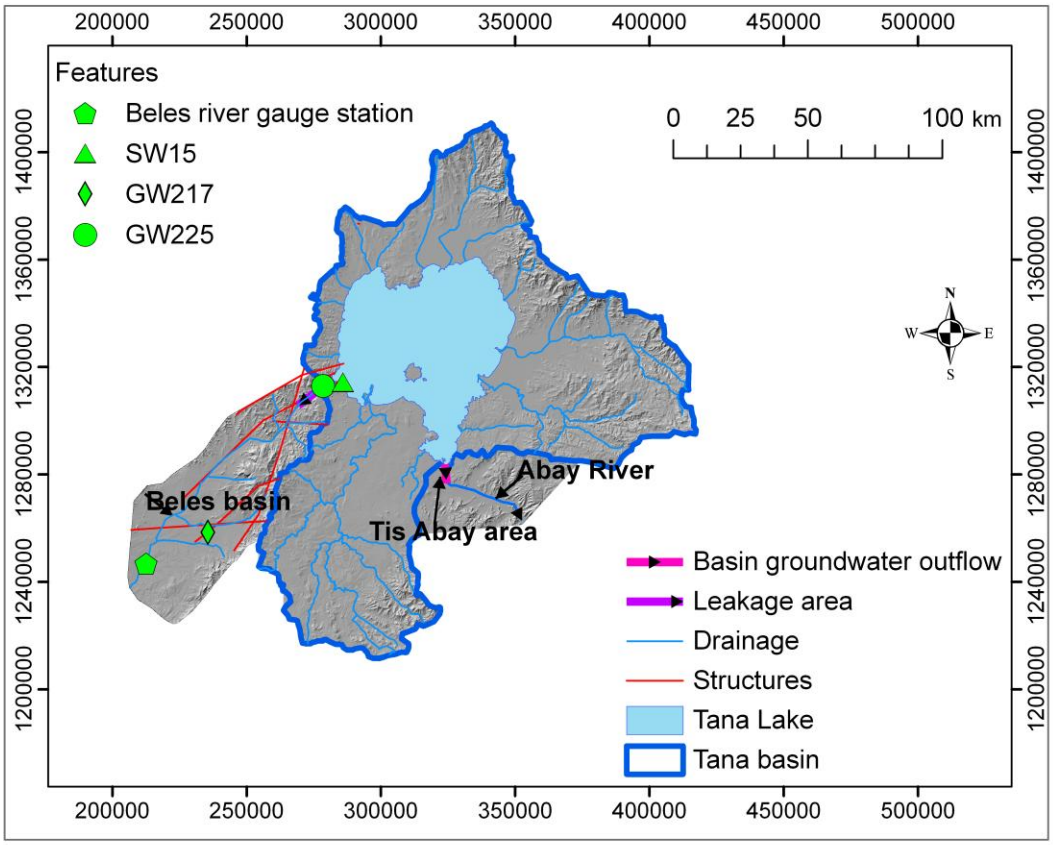

Figure 11.4. Map showing the groundwater outflow area from Tana basin and leakage area from Tana Lake.

Groundwater samples from boreholes (Subgroup 2) in the Tis Abay inter basin groundwater outflow area have enriched delta deuterium and oxygen-18 values and less EC than boreholes of the Subgroup 2 in Tana basin, excepting those in the lacustrine sediments, and subgroup 3 in Tis Abay area suggesting minor leakage outflow from the lake via the southern margin. There is no vertical leakage from the lake through the floor as there is no major enriched isotopic contribution to the inter basin groundwater outflow beneath the lake bed sediments. Besides, no leakage is deciphered to northern adjacent Chilga area as the groundwater flow is from north towards the lake in this area.

11.5. Origin of Groundwater Salinity

Groundwater subgroups 3, 2,1b, 1d and 2a are ascertained to belong to the Upper Aquifer System, while Subgroup1a and 1c are of the lower and intermediate aquifer systems, respectively.

Subgroup 1a and 1c have no indications of carbonates and evaporites dissolution. All common carbonates and evaporites mineral phases are under saturated. Sources of ions are mainly from dissolution of silicate minerals under open system at deeper depths due to deep source CO_2, and cation exchange. Source of salinity for Subgroup2a is also silicate hydrolysis. It has a closed condition.

Subgroup3 is shallow circulating groundwater in the unconfined aquifer that underwent little rock-water interaction in open system to atmospheric CO_2. Subgroup2 is groundwater evolved from Subgroup3 in the deeper (semi)confined aquifer(s) and has a closed system. Both have low salinity (TDS<500 mg/l). Silicates hydrolysis is the main process of groundwater salinization in these ground waters. Subgroups 3 and 2 have water types of Ca-Mg-Na-HCO_3 (transitional) and Na-HCO_3 (basic), respectively.

On the other hand, subgroups1b and 1d (excluding GW46) in the shallow unconfined lacustrine sediments aquifer have relatively high ions concentrations and TDS (2133 and 4952 mg/l, respectively) than Subgroups 3 and 2. They have Na-Mg-Cl-HCO_3 (basic) and Na-Mg-Ca-Cl-SO_4 (transitional) type of hydrochemical facies, respectively. Besides, ground waters that belong to Subgroup3 with high chemical concentrations relative to the near by ground waters (Subgroups3 and 2) also exist in some localized spots within the lacustrine sediments (Fig 9.31) aquifers. However, the delta ^{2}H and ^{18}O and tritium data suggest that these ground waters with relatively high salinity are similar with the surrounding low salinity ground water points.

Bivarient plots (Figs.9.19 to 9.23) and inverse hydrogeochemical modeling revealed that the high chemical concentrations for such localized ground waters is attributed mainly to

the dissolution of trace evaporites (halite, gypsum and sylvite) and cation exchange (fixation of Ca^{2+} and Na^{+} and libration of Mg^{2+}) in addition to silicate hydroloysis (Section 9.5), which have evolved from initial Subgroup3 under open system to atmospheric CO_2. Carbonates mineral phases might have also dissolved as such minerals can exist where evaporites form. Subgroup1d is oversaturated in calcite and dolomite

Plots of delta ^{18}O versus electric conductivity (Fig. 9.31a&b) reveal that the major source of salinity for Subgroup3, 2, 2a, 1b and 1d, which are found in the Upper Aquifer System is rock-water interaction (silicates hydroloysis) and leaching of salts, with slight effect of evaporation in plain areas of lacustrine sediments and shallow ground waters in volcanic aquifers. Bromide contents of Subgroup1b and 1d are relatively high like that of chloride when compared to other ground waters (Table 9.3) within the lacustrine sediments and else where in the basin. This indicates that Br^{-} and Cl^{-} are selectively concentrated or retained by clay membrane effect in addition to dissolution of evaporites. According to Hem (1985), Cl^{-} and Br^{-} can be preferentially retained in clay sediments while the water molecules pass. Cations also concentrate in these sediments due to cation exchange processes.

Non-marine evaporite deposits including halite, gypsum and anhydrite form when the net evaporation rate exceeds the water input in surface water (e.g. Lake) and groundwater so that the remaining water is enriched with salts and precipitation of salts occurs when the water becomes supersaturated. The inflow should be in closed basin or one with restricted outflow so that the sediments have time to pool and form in a lake or other standing water body. Such deposits could be formed in graben or half graben areas within continental environments feed by limited riverine drainage, usually in subtropical or tropical environments (Wikimedia Foundation Inc, 2014).

According to Lamb et al. (2007), Tana Lake was closed and completely dried at around 18700 to 15100 years before present, and the lake area was in arid condition at some time. Evaporation during this time has been reported to cause the lake to have been relatively saline (EC ≈ 900 μS/cm). Therefore, trace evaporite deposits might have been

deposited during this arid, closed and relatively saline lake condition, which have been dissolved to give localized relatively highly saline (brackish) ground waters in lacustrine sediments surrounding the lake.

Evaporation from shallow groundwater in the lacustrine sediments seems to have minor effect on groundwater salinity.

11.6. Origin of Wetlands

Perennial and seasonal wet lands exist in the area. The perennial wet land persists through out the year. The seasonal marsh only occurs between August and November because of river food pools and inundation by the lake water during summer, and is dry during the rest seasons. The groundwater table in the perennial marsh is close to the surface. The perennial marsh has Ca-Na-Mg-HCO_3 (basic) type of hydrochemical facies, which seems to indicate groundwater input to the surface waters (river flood pool and inundated lake water). The groundwater input seems to help the wet land to exist through out the year. Stable isotopes (δ^2H & $\delta^{18}O$) data show relatively highly evaporated water in the perennial wet land than the lake because of shallow water depth. The conclusion reached here is agreeable to Seifu Kebede et al. (2012).

12. CONCLUSIONS AND RECOMMENDATIONS

Interpretation and analysis of the hydrogeological, hydrogeochemical and isotopic data revealed that three aquifer systems exist in the area, which are the upper, intermediate and lower aquifer systems.

Independent set of aquifers in the northern, eastern, southwestern and western escarpment areas constitute the Upper Aquifer System. The Upper Aquifer System has isolated groundwater flow systems (shallow and deep) from each side, which flow toward the lake. This aquifer system contains the shallow unconfined aquifer that interacts and

contributes to the streams and the Tana Lake, and deeper (semi)confined aquifers, which has regional outflow or underflows from Tana basin to Tis Abay area.

The intermediate and lower aquifer system are ascertained to exist underlying the UAS in the eastern area and have regional outflow from the basin to Tis Abay area.

On the basis of basin water balance evaluation, the inter basin groundwater outflow is estimated to be 3333.5 hm^3/year. The major part of this value is regional groundwater outflow from Tana basin to Tis Abay area. Groundwater underflow to this area is via the Quaternary and Tertiary basalts aquifer(s), which are found beneath the Tana Lake bed sediments. There is no groundwater flow through the lake bed sediments.

Some of the inter basin groundwater outflow rate occur as leakage outflow from the Tana Lake. Lake balance study revealed leakage rate of 954.8 hm^3/year, which is deciphered to mainly underflows and mixes with the local groundwater in the adjacent low lying Beles basin and to certain extent to Tis Abay area based on isotopic data. On the other hand, groundwater inflow directly to the lake has been found to be minor. The lake is tight at the floor and does not interact with the underlying groundwater.

In this study, recharge estimation was done based on baseflow separation, soil water balance and chloride mass balance methods. Recharge evaluation using baseflow analysis gave the shallow groundwater recharge rate of 195.6 mm/year, which forms the groundwater discharge as baseflow to streams. On the other hand, soil water balance and chloride mass balance methods although are different approaches have given comparable recharge rates of 285.4 and 284.0 mm/year. Average groundwater recharge of the basin has been estimated to be 284.7 mm/year based on the results of the two methods.

Origin of salinity for groundwater subgroups 1a, 1c, 2a, 2 and 3 is due to silicate hydrolysis. Subgroups 1a and 1c evolves at deeper depths under open system to deep CO_2 source while Subgroup 3 evolved at shallow depth under open system to atmospheric CO_2. Subgroups 2 and 2a have closed system to CO_2 sources. Subgroup 3 evolves with

depth to Subgroup 2. Subgroups 1b and 1d and some members of Subgroup 3 in the shallow unconfined lacustrine sediments aquifer attain relatively high salinity because of dissolution of trace evaporite salts (halite, gypsum and sylvite) and cation exchange under open system to atmospheric CO_2. Subgroups 1b and 1d evolve from Subgroup 3.

Further research study is recommended to understand the mode of origin and occurrence of these evaporite deposits in the area.

Carbon-13&14 investigation may be recommended for pre-1952 ground waters (with tritium less 1 TU) of Subgroup 3 (GW10 & 29), Subgroup 2 (GW2 & 3), Subgroup 2a (GW16 & 42), Subgroup 1c (GW9), Subgroup 1d (GW24) and Subgroup 1a (GW32). However, subgroups 3, and 1a and 1c have open system to the atmospheric and deep dead CO_2 sources, respectively, which make ^{14}C correction difficult.

REFERENCES

Abeyou Wale (2008). Hydrological balance of Lake Tana, upper Blue Nile Basin, Ethiopia. MSc. thesis, International Institute for Geo-information Science and Earth Observation, The Netherlands.

Addis Hailu (2011). Groundwater-surface water interaction and groundwater recharge estimation using hydrogeochemistry and isotope hydrology; Blue Nile basin, Ethiopia. MSc thesis, Department of Earth Sciences, Addis Ababa University.

Adise Mekonnen (2006). Geology and geochemistry of Guna volcanic massif, north western Ethiopian Plateau. MSc thesis, Department of Earth Sciences, Addis Ababa University.

Allen, R.G, Pereira, L.S., Raes, D. and Smith, M. (1998). Crop evaporation-guidelines for computing crop water requirements-FAO irrigation and drainage paper 56. Food and Agriculture Organization of the United Nations, Rome, Italy.

Amhara Design and Supervision Works Enterpris (2009) Groundwater resources investigation for Gonder Malt factory, Bahir Dar

Andarge Mekonen (2010). Hydrogeological and hydrochemical maps of Harar NC38-9

and NC38-10 (Sima, J., ed.). Geological Survey of Ethiopia.

Andreson, M.P. and Woessner, W.W. (1991). *Applied groundwater modeling, simulation of flow and advective transport*. Academic press, New York.

Appelo, C.A.J and Postma, D. (1994). *Geochemistry, groundwater and pollution*, A.A. BALKEMA/ROTTERDAM/BROOKFIELD.

Bayissa Asfaw (2003). Regional hydrogeological investigation of northern Ethiopia. Geological Survey of Ethiopia

BCEOM (1998). Abbay River integrated development master plan project (phase 2), data collection-site investigation, survey and analysis, section IV, water resources, part 3, hydrogeology. Ministry of Water, Irrigation and Energy.

Beekman, H.E. and Xu, Y. (2003). Review of groundwater recharge estimation in arid and semi arid Southern Africa. In: *groundwater recharge estimation in Southern Africa* (Y. Xu and H.E. Beekman, eds). UNESCO IHP series No. 64.

Begosew Abate, Koeberl, C., Buchanan, P.C. and Korner W. (1998). Petrography and geochemistry of basaltic and rhyiodacitic rocks from lake Tana and Gimjabet-Kosober areas (north central Ethiopia). *Journal of African Earth Sciences* **26(**1), pp119-134.

Beruke Abel (2009). Groundwater resource evaluation and management practices in Gilgel Abay catchment, Tana basin. MSc thesis, Department of Earth Sciences, Addis Ababa University.

Berhe, S.M., Desta, B., Nicoletti, M. and Teferra, M. (1987). Geology, geochronology and geodynamic implications of the Cenozoic magmatic province in W and SE Ethiopia. *Journal of the Geological Society*, London **144**, pp213-226.

Bruin, H.A.R. (1988). Evaporation in arid and semi arid regions. In: *Estimation of natural groundwater recharge* (Simmers, I., ed.). NATO ASI Series, Series C, mathematical and physical sciences **22**(D), pp73-88, Reidel Publishing Company, Tokyo.

Chorowicz, J., Collet, B., Bonavia, F.F., Mohor, P., Parrot, J.F. and Tesfaye Korme (1998). The Tana basin, Ethiopia: intra-plateau uplift, rifting and subsidence. *Tectonophysics* **295**, pp351-367, ELSEVIER.

Clark, I.D. and Fritz, P. (1996). *Environmental isotopes in hydrogeology*, Lewis

Publishers, New York.

Craig, H. (1961). Isotopic variations in meteoric waters, *Science* 133, 1702-1703

Daniel Gamatchu (1997). *Aspects and water budget in Ethiopia*, Addis Ababa University Press, Ethiopia

Davis, J.C. (2002). *Statistics and data analysis in geology*, 3rd edition. John Wiley and Sons, New York.

Dejene H/Mariam, Aman Yismaw, Mathios Agonafir, Basalfew Zenebe, Melkamu Sewnet, Muhammed Edris, Getachew Burussa, Ezra Yehualaeshet and Shimeles Ashenafi (2012). Geology, geochemistry and gravity survey of Yifag area (memoir no.32). Geological Survey of Ethiopia.

Efrem Beshawered, Shimeles Ashenafi, Mohamed Edris, Getachew Burusa, Teferie Zewede, Yibeltal Tesfaye, Henok Bekele, Melese Tadesse and Meran Wendant (2010). Geology, geochemistry and gravity survey of the Bahir Dar area, memoir 30. Geolological Survey of Ethiopia.

Eriksson, E. and Khunakasem, V. (1969). Chloride concentration in groundwater, recharge rate and rate of deposition of chloride in Israel Coastal Plain. *J. Hydrol*.**7**, 178-197.

Fetter, C.W. (2001). *Applied hydrogeology*, 4th edition, Prentice-Hall, Inc, New Jersey.

Fontes J.C (1998) Environmental isotopes in groundwater hydrology. Chapter3 In:. *Hand book of environmental isotope geochemistry*, vol.1, pp75-140 (Fritz, P. and Fontes, J.C., eds). Elsevier, Amster Dam

Food and Agriculture Organization (1997). Global soil and terrain data base.

Food and Agriculture Organization (2009). Cropwat manual. http://www.fao.org/nr/water/inforces_database_cropwat.html.

Freeze, R.A. and Cherry, J.A. (1979). *Groundwater*. Prentice-Hall, Inc., New Jersy 07632.

Geoffrey, W.F. and Gall, E.C. (1991). Regional aquifer system analysis- Upper Colorado river basin, excluding San Juan basin. U.S. Geological Survey professional paper 1411-c, Washington.

Getachew Hadush (2008). Groundwater contribution and recharge estimation in the

upper Blue Nile flows, Ethiopia. MSc thesis, International Institute for Geo-information Science and Earth Observation, The Netherlands.

Getachew Zewde (2010). Base flow analysis of rivers in Lake Tana sub-basin. MSc thesis, Department of Earth Sciences, Addis Ababa University, Ethiopia.

Girum Admasu (2010). Groundwater and surface water interaction in Lake Tana sub-basin using isotope and geochemical approach. MSc thesis, Department of Earth Sciences, Addis Ababa University, Ethiopia

Gozálbez, J. and Cebrián, D. (2006). *Touching Ethiopia*, 2nd English edition. Shama Publisher.

Güler, C. and Thyne, G.D. (2003). Hydrologic and geologic factors controlling surface and groundwater chemistry in Indian Wells-Owens valley area, southeastern California, USA. *Journal of Hydrology*, Elsevier.

Güler, C., Thyne, G.D., McCray, J.E. and Turner, A.K. (2002). Evaluation of graphical and multivariate statistical methods for classification of water chemistry data. *Hydrogeology Journal* **10**, pp455-474.

Hautot, S., Whaler, K., Workneh Gebru, Mohammednur Desissa (2006). The structure of Mesozoic basin beneath the Lake Tana area, Ethiopia, revealed by magneto telluric imaging. *Journal of African Earth Sciences*, Elsevier.

Hem, J.D. (1985). Study and interpretation of the chemical characteristics of natural water, 3rd edition. U.S. Geological Survey water-supply paper 2254.

Hershey, R.L., Mizeel, S.A. and Earman, S. (2010). Chemical and physical characteristics of springs discharging from regional flow systems of the carbonate-rock province of the Great Basin, western United States. *Hydrogeology Journal* **18** (4), pp1007-1027.

Hofmann, C., Courtillot, V., Feraud, G., Rochette, P., Yirgu, G., Ketefo, E. and Pik, R. (1997). Timing of the Ethiopian flood basalt event and implications for the plume birth and global change, *Nature* **389**, pp338-341.

Hsissou, Y., Mudry, J., Mania, J., Bouchaou, L. and Chauve, P. (1999). Use of the Br/Cl ratio to determine the origin of the salinity of groundwater: an example from the Souss plain (Morocco). *Earth and Planetary Sciences* **328**, pp381-386.

Johnston, R.H. (1999). Hydrologic budgets of regional aquifer systems of the United

States for pre development and development conditions. U.S. Geological Survey professional paper 1425.

Kamel, S., Dassi, L., Zouari, K. and Abidi, B. (2005). Geochemical and isotopic investigation of the aquifer system in the Djerid-Nefzaoua basin, southern Tunisia. *Environ Geol* **49**, pp159-70

Kieffer, B., Arndt, N., Lapierre, H., Bastien, F., Bosch, D., Pecher, A., Gezahegn Yiergu, Dereje Ayalew, Weis, D., Jerram, D.A., Keller, F. and Meugniot, C. (2004). Flood and Shield basalts from Ethiopia: Magmas from the African super swell. *Journal of Petrology* **45** (4), pp793-834.

Kuzmin, P.P., Vikulina, Z.A., Nezhikhovski, R.A., Babkin, V.I., Popov, O.V., Bochkov, A.P., Fedorov, S.F., Kharchenko, S.I., Subbotin, A.S., Bavina, L.G., Plitkin, G.A., Sorochan, O.G., Krenke, A.N. and Khodakov, V.G. (1974). Methods for water balance computations, an international guide for research practice (A.A. Sokolov and T.G. Chapman, ,eds). The UNESCO press, Paris, France.

Lamb, H.F., Bates, C.R., Coombes, P.V., Marshall, M.H., Mohammod Umer, Davies, S.J. and Eshete Dejen (2007). Late Pleistocene desiccation of lake Tana, source of the Blue Nile. *Quaternary Science Reviews* **26**, pp287-299, ELSEVIER.

Marsh, N.A., Stewardson, M.J. and Kennard, M.J. (2003). River analysis package, cooperative research centre for catchment hydrology. Monash University Melbourne, Australia.

Matebie Meten (2009). Hydrogeology of Chemoga-Jedeb catchment, Debre Markos area, north west Ethiopia. MSc thesis, Department of Earth Sciences, Addis Ababa University

Mengesha Tefera, Tadiwos Chernet and Workineh Haro (1996). Geological map of Ethiopia. Geological Survey of Ethiopia.

Molla Fetene (2004). Water resources potential evaluation of Ribb river basin, northwest Ethiopia, south Gonder. MSc thesis, Department of Earth Sciences, Addis Ababa University

Nigussie Ayele (2010). Numerical groundwater flow modeling of the northern river catchment of the Lake Tana. MSc thesis, Department of Earth Sciences, Addis

Ababa University

NMSA (1996). Assessment of drought in Ethiopia, meteorological research reports series no.2, Ethiopia

Nyagwambo, N.L. (2002). Groundwater recharge estimation and water resources assessment in a tropical crystalline basement aquifer. PhD thesis, Delft University of Technology, the Netherlands.

Pietrangeli, S. (1990). Geological report, Ministry of Water, Irrigation and Energy

Raghunath, H.M. (1996). Groundwater 2nd ed., New Age International Publisher, New Delhi.

Rozanski, K., Froehlich, K. and Mook, W.G. (2001) Environmental isotopes in hydrologic cycle, Vol. III In: *Surface water* (Mook, W.G., ed.). UNESCO, Paris, France.

Rutledge, A.T. and Mesko, T.O. (1996). Estimated hydrologic characteristics of Shallow aquifer systems in the Valley and Ridge, Blue Ridge, and the Piedmont Physiographic Provinces based on analysis of stream flow recession and base flow. U.S. Geological Survey professional paper 1422-B, United States Government Printing Office, Washington, USA.

Sacks, L.A., Swancar, A. and Lee, T.M. (1998). Estimating groundwater exchange with lakes using water budget and chemical mass balance approaches for ten lakes in Ridge areas of Polk and highlands counties, Florida. United States Geological Survey, water resources investigations report, 9804133, USA.

Samson Mengistu (2010). Numerical groundwater flow modeling of the Lake Tana basin, upper Nile, Ethiopia. MSc. thesis, Department of Earth Sciences, Addis Ababa University

Scanlon, B.R., Healy, R.W. and Cook, P.G. (2002). Choosing appropriate techniques for quantifying groundwater recharge. *Hydrogeology Journal* **10,** pp18-39.

Seifu Kebede, Girum Admasu and Travi, Y. (2012). Estimating un-gauged catchments flows from Lake Tana flood plains, Ethiopia: isotope hydrological approach. *Isotopes in Environmental and Health Studies* **47** (1), pp71-86.

Seifu Kebede, Travi, Y., Tamiru Alemayehu and Marc, V. (2005). Water balance of

Lake Tana and its sensitivity to fluctuations in rain fall, Blue Nile Basin, Ethiopia. *J. Hydrol.* **316**, pp233-243.

Seifu Kebede, Travi, Y., Tamiru Alemayehu and Tenalem Ayenew (2005). Groundwater recharge, circulation and geochemical evolution in the source of the Blue Nile River, Ethiopia. *Applied Geochemistry* **20**, pp1658-1676, Elsevier.

Seifu Kebede (2004). Environmental isotopes and geochemistry in investigating groundwater and lake hydrology: case from the Blue Nile basin and the Ethiopian Rift (Ethiopia). PhD thesis, University of Avignon, France.

Shaw, E.M. (1994). *Hydrology in practice*, 3rd edition. Chapman and Hall, London, UK.

SMEC (2007). Hydrological study of the Tana- Beles sub basins, groundwater investigation. Ministry of Water Resources and Energy

Sogreah (2012). Consulting service for detailed groundwater investigation and monitoring in Tana and Beles sub-basins, Stage 1 final report, Vol. II, Part 5: hydrological survey. Ministry of Water, Irrigation and Energy, Ethiopia.

Subramanya, K. (2004). *Engineering hydrology*, 2nd edition. Tata McGraw-Hill Publishing Company Limited, New Delhi, India.

Sun, R.J. and Johnston, R.J. (1994). Regional aquifer system analysis program of the U.S. Geological Survey, circular 1099.

StatSoft.Inc. (2007). Statistica version 8.0 manual. www.statsoft.com

Stimson, J., Rudolph, D., Farvolden, F., Frape, S. and Drimmie, S. (1993). Causes of groundwater salinization in low lying area of Cochabamba valley, Bolivia. **In**: *Isotope techniques in the study of past and current environmental changes in the hydrosphere and the atmosphere*. International Atomic Energy Agency,Vienna

Tadesse Meselu (2009). Delineating the Debre-Tabor sedimentary basin using gravity Method. MSc thesis, Department of Earth Sciences, Addis Ababa University

Tenalem Ayenew and Tamiru Alemayehu (2001). *Principles of hydrogeology*. Department of Geology and Geophysics, Addis Ababa University, Ethiopia.

Tenalem Ayenew (1998). The hydrogeological system of the Lake District Basin, Central main Ethiopian rift. PhD thesis, ITC publication number 64, The Netherlands.

Tesfaye Cherenet (1993). Hydrogeological map of Ethiopia. Geological Survey of Ethiopia

Thornthwaite, C.W. and Mather, J.R. (1957). Instructions and tables for computing potential evapotranspiration and the water balance, Laboratory of Climatology, Drexel Institute of Technology, New Jersey, USA. *Publication in Climatology* **10**(3), pp185-311.

Water Works Design and Supervision Enterprise (2007). Groundwater resources in Lake Tana sub-basin and adjacent areas, rapid assessment. Ministry of Water, Irrigation and Energy.

Weight, W.D. (2008). *Hydrogeology*, field manual, 2nd edition, McGraw Hill, New York.

Wikimedia Foundation, Inc (2014). http://en.wikimedia.org/w/index.php?title=Evaporite & oldid=596728500

Wilson, J.L. and Guan, H. (2004). Mountain block hydrology and mountain front recharge. New Mexico Institute of Mining and Technology, Socorro, USA.

Workineh Haro, Thomas Kassahun, Yibeltal Tesfaye, Teferi Zewde, Gemechu Shimeles, Muhammed Edris, Getachew Burussa, Ezra Yehualaeshet and Shimeles Ashenafi (2011). Geology, geochemistry and gravity of Gonder and west Gonder map sheets (memoir 33). Geological Survey of Ethiopia.

Workineh Haro, Dejene Hailemariam, Iyasu Getachew, Thomas Kassahun, Shimeles Ashenafi, Getachew Burisa and Mohamed Edris (2010). Geology, geochemistry and gravity survey of the Debre Tabore area (memoir 29). Geological Survey of Ethiopia.

Yurtsever, Y. (1997). Role and contribution of environmental tracers for study of sources and processes of groundwater salinization. In: *Hydochemistry, Proceedings of the Rabat Symposium*, (N.E. Peters and A.C. Ribstein, eds.). IAHS Publ. no.244, pp 3-12.

Zanettin, B. Gregnanin, A., Visentin, E.J., Mezzacasa, G. and Piccirillo, E.M. (1974). Petrchemistry of the volcanic series of the central eastern Ethiopian Plateau and relationship between tectonics and magmatology.

Zelalem Leyew (2009) Groundwater potential assessment of Gumara river catchment,

northwest Ethiopia. MSc thesis, Department of Earth Sciences, Addis Ababa University.

Zenaw Tessema (2011). Hydrogeology report, Megech (Serba) irrigation and drainage project, vol. II: water resources and irrigation. Ministry of Water, Irrigation and Energy

Zenaw Tessema (2011). Hydrogeology report, Rib irrigation and drainage project, vol. II: water resources and irrigation. Ministry of Water, Irrigation and Energy

.

APPENDICES

Appendix 1. Groundwater inventory data.

ID	Site	X	Y	Type	E	D (m)	WS	SWL	Q(l/s)	s	S.C (l/s/m)	T (m^2/d)	Source
GW1	Maksegniet town supply	343291	1370434	borehole	1927			4.7	2				This study
GW2	Gorgora town supply/Kes Mender	312606	1355049	borehole	1817	121		2.68	5			10.4	This study
GW3	Dashen brewery borehole 1B/Lashka	328564	1383745	borehole	1981	301	25.1,99.3,149.9,168.2,195.6,,227.8,237.4	98	18	17.34	1.04	69	This study
GW4		324513	1359981	dug well	1789								Getachew, 2008
GW5	Teda town	334446	1380606	dug well	1950								This study
GW6	Arb Gebeya town supply	363781	1285984	borehole	2228	95.6	5,80	59.02	4.6	36.52	0.12	12.7	This study
GW7	Jib Asra town supply	386114	1282962	borehole	2435	90	21,30,40,55,65,78	8	10				This study
GW8	Kunzila town supply	284766	1313751	borehole	1807	70		5.47	2.2	9.23	0.24	25.3	This study
GW9	Debretabore town supply/Gafat No.10	396407	1313342	borehole	2486	109	35,76	15.55	6.5	14.59		28.8	This study
GW10	Gasay town supply	407117	1304322	borehole	2785	42	12,30	0.9	3.1	0.13	13.7		This study
GW11	Anbesame town supply	350291	1292521	borehole	2076	62.8	5,6,37,58	2.28	3.7	0.19	20		This study
GW12	Wetete Abay town supply	285626	1258237	borehole	1889	38		4.9		13.98			This study
GW13	AWWCE borehole	323134	1280503	borehole	1798	82		4.5	6.7			58268	This study
GW14	Dudu/Amhara PVC factory	319628	1280330	borehole	1822	80		31.13	12				This study
GW15	Yifag town supply	359714	1334645	borehole	1810	60	22,50	3.72	6	18.25	0.33	34.8	Bayisa (2003)
GW16	Wonzaye	355780	1303277	hot spring	1815								This study
GW17	Wagtera school	342822	1316411	dug well	1972								This study
GW18	Mesno clinic	354487	1312034	dug well	1821								This study
GW19	Tanku Gebriel/Medehaniealem tsebel	355164	1309272	cold spring	1810								This study
GW20	Zarak/Showble school	347199	1306740	dug well	1825								This study
GW21	Angereb 6/NW5	334578	1392871	borehole	2057	173?							This study
GW22	Kola diba town borehole/Wonfela	319108	1371888	borehole	1800	286/64-75?		12					This study
GW23	Robit village supply	324386	1362994	dug well	1771								This study
GW24	Robit Medihanealem tsebel	324540	1362647	dug well	1797								This study
GW25	Gurehae/Beles	300883	1368388	cold spring	1840								This study
GW26	Chewayit supply	307771	1364312	dug well	1892								This study

ID	Site	X	Y	Type	E	D (m)	WS	SWL	Q(l/s)	s	S.C (l/s/m)	T (m^2/d)	Source
GW27	Shaga/guaye mender/AmlakTadese well	352450	1323310	dug well	1789								This study
GW28	Rike well	349070	1326168	dug well	1787								This study
GW29	Woreta town supply/Jicaa borehole	359326	1319721	borehole	1800	76							This study
GW30	Infranz town	350405	1355601	dug well	1927								This study
GW31	Alem Ber/Gala terara	382592	1317900	dug well cold	2092								This study
GW32	Serba Maryiam/Amora gedel tsebel	382171	1317731	spring	2066								This study
GW33	Maksegne village supply	369675	1319117	borehole	1907	63							This study
GW34	Shinasim/Rib	359629	1326220	borehole	1808								This study
GW35	Ager Kirigna Maryam	349582	1339614	dug well	1789								This study
GW36	Ambo Meda/Gaja bahir	378623	1339111	borehole	2014								This study
GW37	Addis Zemen town supply/Alabo No.1	367852	1341230	borehole	1934	137?							This study
GW38	Sene hiwot Gebrel tsebel/Licha town	378630	1288023	dug well	2326								This study
GW39	Gebtsawit/Burat/Jorit	344604	1301015	dug well	1983								This study
GW40	Hamusit town supply	342182	1301222	borehole cold	1958								This study
GW41	Huzet/Gerarge	407710	1301117	spring	3016				0.5				This study
GW42	Guramba Kidanemheret hot spring	367474	1296586	hot spring	1933								This study
GW43	Zege town supply	315618	1292050	borehole	1799	124							This study
GW44	Ygodit-Tentela/Robit supply	305914	1289672	borehole	1833	68							This study
GW45	Chimba town/Kedam Gebeya	299930	1294970	dug well cold	1814								This study
GW46	Andesa Giorgis spring	334463	1275160	spring cold	1714								This study
GW47	Tikurit	332023	1273035	spring cold	1721								This study
GW48	Lomi	312011	1282351	spring	1831								This study
GW49	Yebab Chincha	313802	1278243	borehole	1862	30?							This study
GW50	Entedit	315512	1276884	borehole cold	1884	90-150?							This study
GW51	Dengel Ber town	282623	1322572	spring	1803								This study
GW52	Norway (kinder Garden, delgi)	287461	1348655	dug well	1822								This study

ID	Site	X	Y	Type	E	D (m)	WS	SWL	Q(l/s)	s	S.C (l/s/m)	T (m^2/d)	Source
GW53	Chewa Diba/upstream	290594	1363251	dug well	1894	6							This study
GW54	Chan Diba primary school	286468	1371255	dug well	2045	6.5							This study
GW55	Zenzelma	336244	1287877	borehole	2021								This study
GW56	Dima/Rim	304851	1251073	borehole	2061								This study
GW57	Gordena village	323949	1278668	borehole	1781								This study
GW58	Sebat Amit primary schoole supply	326865	1275920	borehole cold	1780	60							This study
GW59	Merawi	294931	1262786	spring	1994								This study
GW60	Durebete town supply	279925	1256936	borehole cold	1925								This study
GW61	Adis Kidan/Bilt Sar	267819	1227044	spring	2416								This study
GW62	Garagi Mender2	262933	1249103	dug well cold	2103								This study
GW63	Gish Abay tsebel	303191	1213249	spring	2730								This study
GW64	Gish Abay town supply	303983	1215080	borehole cold	2690								This study
GW65	Zerehe spring	270524	1218850	spring	2567				25				This study
GW66	Lalibela town supply	275792	1273946	borehole cold	1940								This study
GW67	Yesemala town supply	270701	1282194	spring	2063								This study
GW68	Meshenti town supply	314710	1270547	borehole	1921	78							This study
GW70	Workaye/salini camp borehole	278365	1312813	borehole									This study
GW71	Fageta	286172	1224672	borehole cold									This study
GW72	Areke	312689	1281731	spring									This study
GW73	Awramba	366915	1319849	borehole cold		126		9					This study
GW74	Awrajit/Tis Abay	347880	1269740	spring									This study
GW75		322745	1361257	dug well									This study
GW76		337388	1300444	borehole									Sogreah (2012)

ID	Site	X	Y	Type	E	D (m)	WS	SWL	Q(l/s)	s	S.C (l/s/m)	T (m^2/d)	Source
													Sogreah (2012)
GW77		350673	1289346	dug well									
GW78		355301	1303244	dug well									Sogreah (2012)
GW79		351627	1312039	dug well									Sogreah (2012)
GW80		350855	1312346	dug well									Sogreah (2012)
GW81		352169	1305490	dug well									Sogreah (2012)
GW82		275719	1293422	borehole									Sogreah (2012)
GW83		348926	1314362	dug well									Sogreah (2012)
GW84		265321	1246161	borehole									Sogreah (2012)
GW85		321386	1377648	dug well									Sogreah (2012)
GW86		350949	1309679	borehole									Sogreah (2012)
GW87		354299	1304392	cold spring									Zelalem (2009)
GW88		349036	1310444	dug well									Zelalem (2009)
GW89		397071	1309085	dug well									Zelalem (2009)
GW90		373206	1286508	borehole									Zelalem (2009)
GW91		372073	1288388	borehole									Zelalem (2009)

ID	Site	X	Y	Type	E	D (m)	WS		SWL	Q(l/s)	s	S.C (l/s/m)	T (m^2/d)	Source
GW92		332828	1396792	borehole	2170	108			10.78	2.65	17.22	0.15	15.8	Bayisa (2003)
GW93		335237	1396189	borehole	2150	65			6.05	6.28	46.95	0.13	13.7	Bayisa (2003)
GW94		335329	1395787	borehole	2170	174			0.8	2	148.2	0.01	1.1	Bayisa (2003)
GW95		335027	1396846	borehole	2160	72			18.6	6.56	4.4	1.49	157.1	Bayisa (2003)
GW96		335253	1398706	borehole	2210	56			13.56	2.7	17.35	0.16	16.9	Bayisa (2003)
GW97		334766	1393328	borehole	2160	120			Artesian	17				Bayisa (2003)
GW98		331708	1391268	borehole	2150	92			4.6	2.45	15.7	0.16	16.9	Bayisa (2003)
GW99		333197	1390747	borehole	2023	250.6			37	2.5				Bayisa (2003)
GW100		317470	1373657	borehole	1851	44	10,20		5.34	6.5	12.2	0.53	55.87	Bayisa (2003)
GW101		319453	1371157	borehole	1802	286			13	37.5	42.3	0.83	71.5	This study
GW102		319274	1375676	borehole	1841	116.5			3.6	4			11.8	This study
GW103	Gonder zuria/Mikael Debre	328667	1383951	borehole	1989	107			24	10				ADSWE, 2009
GW104	Gonder zuria/Mikael Debre	329509	1383528	borehole	1947	150			12.5	10				ADSWE, 2009
GW105	Gonder zuria/Mikael Debre	328345	1383860	borehole	1990	150			37.1	4	42.9	0.09		ADSWE, 2009
GW106	Gonder zuria/Mikael Debre	328636	1383450	borehole	1970	144			46	12	15.49	0.47		ADSWE, 2009
GW107	Gonder zuria/Mikael Debre	328372	1383264	borehole	1965	188			31.8	6	45.57	0.13		ADSWE, 2009
GW108	Gonder zuria/Mikael Debre	328492	1383100	borehole	1955	210			26.5	2	153.1	0.01		ADSWE, 2009
GW109	Gonder zuria/Mikael Debre	328346	1383257	borehole	1965	175			8.8	12.5	101.13	0.12		ADSWE, 2009
GW110	Gonder zuria/Mikael Debre	327947	1382786	borehole	1973	180			13.61	1.5	136.73	0.01		ADSWE, 2009
GW111	Dembia/Azezo/azezo meat factory	329615	1388410	borehole	2051	116								Sogreah, 2012
GW112	Dembia/Chewahit kebele/Chewahit	301700	1368928	borehole	1851	136.7			0.6	3.58	35.63	0.1	6.04	Sogreah, 2012
GW113	Dembia/Gondar medical science collage	332727	1394474	borehole	2130	120				2				Sogreah, 2012
GW114	Dembia/Gorgorabh2	311477	1355834	borehole	1827	92.5			0.75	3	46.05	0.0651466		Bayisa (2003)
GW115	Dembia/Teda well	333959	1379880	borehole	1930	84				1				Sogreah, 2012
GW116	Dembia/Tedabh5	333959	1379880	borehole	1930	40				2.5				Sogreah, 2012
GW117	Dembia/Chwahit no3	310283	1361874	borehole	1837	54		13	Artesian	3.58				Sogreah, 2012
GW118	Kola Diba area	318949	1371348	borehole	1804	120/96			Artesian					Sogreah, 2012
GW119	Kola Diba area	327124	1373044	borehole	1829	320								Sogreah, 2012
GW120	Gonder malt factory/Chilomaryam/dembia	319367	1375883	borehole	1837	116.5			12.3	4	19.92	0.2008032	11.8	This study
GW121	Gonder zuria/angerb	333290	1390954	borehole	2010	250.6			37	2.5				This study
GW122	Kola Diba test well(Tew8)	319035	1370799	borehole	1803	301			9	15				This study
GW123		315823	1386169	dug well	2052									sogreah, 2012

ID	Site	X	Y	Type	E	D (m)	WS	SWL	Q(l/s)	s	S.C (l/s/m)	T (m^2/d)	Source
GW124		321293	1377441	dug well	1933								Getachew, 2008
GW125		315015	1371379	dug well	1808								Getachew, 2008
GW126		308527	1366191	dug well	1896								Getachew, 208
GW127		331196	1380074	borehole	1884								Getachew, 2008
GW128		330033	1384286	borehole	1958								Getachew, 2008
GW129		328517	1384497	borehole	2020								Girum,2010
GW130		300350	1367758	dug well	1855								Girum,2010
GW131		319520	1367241	dug well	1798								Girum,2010
GW132		320946	1360264	dug well	1791								Getachew, 2008
GW133		312777	1368477	borehole	1834								Baysa, 2003
GW134		332393	1394346	borehole	2111	65.9		6.32	2.1				ADSWE, 2009
GW135		332555	1394838	borehole	2122	120			1.14				ADSWE, 2009
GW136		332690	1394965	borehole	2134	91.7		3.24	4.64				ADSWE, 2009
GW137		330372	1391367	borehole	2106	140		6.67	7				ADSWE, 2009
GW138		330073	1391898	borehole	2130	80.9		3	3				ADSWE, 2009
GW139		329717	1382309	borehole	1920	150		3.24	2.38				ADSWE, 2009
GW140		329717	1381878	borehole	1910	150		34.5	3.15				ADSWE, 2009
GW141		330951	1383121	borehole	1918	98		12.2	2				ADSWE, 2009
GW142		330383	1381691	borehole	1899	182			dry				ADSWE, 2009
GW143		330326	1390335	borehole	2073	54		3.9	4.5				ADSWE, 2009
GW144		329721	1386603	borehole	2005	84		5	2				ADSWE, 2009
GW145		330205	1390482	borehole	2079	156			1				ADSWE, 2009
GW146		330205	1390482	borehole	2079	156		18	<1				ADSWE, 2009
GW147		320526	1384051	borehole	2024	53			3				ADSWE, 2009
GW148		331649	1381201	borehole	1865	85			1				ADSWE, 20093
GW149		330526	1384051	borehole	1933				1				ADSWE, 2009

ID	Site	X	Y	Type	E	D (m)	WS		SWL	Q(l/s)	s	S.C (l/s/m)	T (m^2/d)	Source
GW150		333712	1381032	borehole	1948	90				dry				ADSWE, 2009
GW151		326643	1384178	borehole	2022	150				dry				ADSWE, 2009
GW152		318528	1374810	borehole	1829	44			4.5	6 to 8				ADSWE, 2009
GW153		314867	1385700	borehole	2004									This study
GW154	Tach Teda	332718	1378687	dug well	1886	60								This study
GW155	within the campus	330171	1391540	borehole	2107	150				2				This study
GW156		340290	1390112	borehole	1970	45			5.75	2				Bayisa (2003)
GW157	Durdurit gote	304881	1365942	dug well	1827	8								This study
GW158		285440	1347883	borehole	1811	59		18	4	1.01	33.14	0.03	3.16	Bayisa (2003)
GW159		367337	13413121	borehole	1980	137			8	4.6	21	0.22	23.2	Bayisa (2003)
GW160		390085	1312467	borehole	2640	72			2	1.5	56	0.03	3.16	Bayisa (2003)
GW161		396613	1310232	borehole	2640	122			7.31	4	47.32	0.08	8.4	Bayisa (2003)
GW162		393349	1311349	borehole	2690	110			8.03	1.5	24.35	0.04	4.2	Bayisa (2003)
GW163		395345	1257158	borehole	2570	72			3.5	6	20	0.3	31.6	Bayisa (2003)
GW164		361200	1336289	borehole	1867	43			3	2				Bayisa (2003)
GW165		285346	1347691	borehole	1802	129			0.71	4			22.6	This study
GW166		277462	1256650	borehole	2000	30			12	4	5	0.8	84.3	Bayisa (2003)
GW167		277462	1256650	borehole	2000	30			13	4	4.5	0.89	93.8	Bayisa (2003)
GW168		265371	1245683	borehole	2150	104			26.8	2	19.2	0.1	10.5	Bayisa (2003)
GW169		265156	1246127	borehole	2150	57.9			30.76	2	19.78	0.1	10.5	Bayisa (2003)
GW170		265156	1246127	borehole	2150	122			22.02	3	38.05	0.08	8.4	Bayisa (2003)
GW171		265254	1244577	borehole	2160	124								Bayisa (2003)
GW172		297449	1262070	borehole	2004	107.7			47.7	6.54			97.7	This study
GW173		284709	1184202	borehole	2021	120			5.04	40			0	This study
GW174		351040	1346920	borehole	1910	100			16	2.2	16.4	0.13	13.7	Bayisa (2003)
GW175		353227	1349121	borehole	1910	54				3				Bayisa (2003)
GW176		387927	1318004	borehole	1810	60			20	6				Bayisa (2003)
GW177		354142	1313724	borehole	1870	55				3				Bayisa (2003)
GW178		363887	1300408	borehole	2000	118		12,103	5.2	2.1	103.6	0.02	2.1	Bayisa (2003)
GW179		353656	1326083	borehole	1798	60			4					Bayisa (2003)
GW180	Rim/Aba golo	304291	1251423	cold spring	2019					4.0				Sogreah (2012)

ID	Site	X	Y	Type	E	D (m)	WS	SWL	Q(l/s)	s	S.C (l/s/m)	T (m^2/d)	Source
GW181	Chemba village	303719	1250906	borehole	2055	45		34.5					Sogreah (2012)
GW182	Durbete town	277716	1256074	borehole	1973	34		27	2.5				Sogreah (2012)
GW183		258584	1319500	borehole	1793	88		1	40	7.41	5.4	569	Sogreah (2012)
GW184		357037	1296661	cold spring	2111								Molla (2004)
GW185		369975	1286019	cold spring	2426								Molla (2004)
GW186		348963	1301585	cold spring	1871								Molla (2004)
GW187		371566	1289547	cold spring	2248								Molla (2004)
GW188		384974	1292336	cold spring	2212								Molla (2004)
GW189		384856	1286072	cold spring	2404								Molla (2004)
GW190		387477	1287409	cold spring	2480								Molla (2004)
GW191		379775	1291860	cold spring	2230								Molla (2004)
GW192		380043	1289223	cold spring	2302								Molla (2004)
GW193		380856	1286769	cold spring	2370								Molla (2004)
GW194		383385	1288933	cold spring	2344								Molla (2004)
GW195		400153	1292426	cold spring	2784								Molla (2004)

ID	Site	X	Y	Type	E	D (m)	WS	SWL	Q(l/s)	s	S.C (l/s/m)	T (m^2/d)	Source
GW196		400965	1294412	cold spring	2742								Molla (2004)
GW197		400150	1292421	cold spring	2776								Molla (2004)
GW198		405200	1297185	cold spring	2967								Molla (2004)
GW199		405108	1298402	cold spring	3021								Molla (2004)
GW200		388524	1310709	cold spring	2658								Molla (2004)
GW201		387645	1303757	cold spring	2278								Molla (2004)
GW202		388444	1301792	cold spring	2057								Molla (2004)
GW203		386106	1302910	cold spring	2186								Molla (2004)
GW204		385457	1302255	cold spring	2072								Molla (2004)
GW205		403734	1300666	cold spring	2910								Molla (2004)
GW206		403821	1300869	cold spring	2896								Molla (2004)
GW207		403688	1301788	cold spring	2904								Molla (2004)
GW208		391104	1307711	cold spring	2532								Molla (2004)
GW209		397542	1308887	cold spring	2625								Molla (2004)
GW210		388549	1308304	cold spring	2357								Molla (2004)

ID	Site	X	Y	Type	E	D (m)	WS	SWL	Q(l/s)	s	S.C (l/s/m)	T (m^2/d)	Source
GW211		389048	1310283	cold spring	2440								Molla (2004)
GW212		385789	1308196	cold spring	2335								Molla (2004)
GW213		385288	1313484	cold spring	2551								Molla (2004)
GW214		384847	1311360	cold spring	2450								Molla (2004)
GW215	Beles out flow area	218472	1227178	cold spring									This study
GW216	Beles out flow area	213512	1245227	borehole									This study
GW217	Beles out flow area	235559	1258458	cold spring									This study
GW218	Beles out flow area	201829	1246070	cold spring									This study
GW219	Beles out flow area	222087	1246820	borehole									This study
GW220	Beles out flow area	236405	1264429	dug well									This study
GW221	Beles out flow area	242553	1256973	borehole									This study
GW223	Beles out flow area	226137	1280453	cold spring									This study
GW224	Beles out flow area	271840	1308196	cold spring									This study
GW225	Beles out flow area	278458	1313020	borehole		110?							This study
GW226	Bahir Dar test well	316070	1282376	test well		500		36.3	53	43.6		108	This study

D: borehole depth, WS: depth to groundwater level strike, SWL: depth to static groundwater level, S.C: specific capacity, T: transsmissivity

Appendix 2a. Field and laboratory measured hydrochemical parameters for groundwater.

ID	Type	X	Y	Depth (m)	Field EC (µS/cm)	Field pH	Field Temp (ºC)	Sampling date	Lab. pH	Lab.EC (µS/cm)
GW1	borehole	343291	1370434		703	6.89	26.4	16/3/2012	7.4	697
GW2	borehole	312606	1355049	121	453	7.14	28.2	13/3/2012	8	462
GW3	borehole	328564	1383745	301	302	9.37	29.7	12/3/2012	9.62	294
GW4	dug well	324513	1359981						7.49	7900
GW5	dug well	334446	1380606		539	7.07	23	16/3/2012	7.26	521
GW6	borehole	363781	1285984	95.6	344	7.426	18.7	29/3/2012	7.08	283
GW7	borehole	386114	1282962	90	289	7.822	24.4	29/3/2012	7.88	284
GW8	borehole	284766	1313751	70	285	6.93	26.3	1/5/2012	6.85	357
GW9	borehole	396407	1313342	109	2100	6.521	21.6	2/4/2012	6.47	2390
GW10	borehole	407117	1304322	42	256	7.257	14.9	2/4/2012	7.45	249
GW11	borehole	350291	1292521	62.8	253	8.074	24.4	30/3/2012	8.96	249
GW12	borehole	285626	1258237	38/65?	628	6.831	24.1	27/4/2012	6.93	623
GW13	borehole	323134	1280503	82	369	8.369	25.7	2/5/2012	8.52	369
GW14	borehole	319628	1280330	80	379	7.654	25.6	19/4/2012	7.67	382
GW15	borehole	359714	1334645	60	519	8.745	28	28/3/2012	8.19	512
GW16	hot spring	355780	1303277		199	10.134	39.3	8/3/2012	9.58	198
GW17	dug well	342822	1316411	12	647	7.08	21.6	"	7.37	613

ID	Type	X	Y	Depth (m)	Field EC (µS/cm)	Field pH	Field Temp (ºC)	Sampling date	Lab. pH	Lab.EC (µS/cm)
GW18	dug well cold	354487	1312034		136.9	6.559	25	9/3/2012	6.86	164
GW19	spring	355164	1309272		179	6.71	23	"	7.45	144
GW20	dug well	347199	1306740	12	302	6.74	30	"	7.08	306
GW21	borehole	334578	1392871	173?	620	7.759	24.4	12/3/2012	7.86	590
GW22	borehole	319108	1371888	286/72-75?	851	7.316	29.3	12/3/2012	7.57	841
GW23	dug well	324386	1362994	10	1699	7.37	22.3	13/3/2012	7.43	1657
GW24	dug well cold	324540	1362647	10	4500	7.389	21.3	13/3/2012	7.39	4730
GW25	spring	300883	1368388		100	7.603	24.8	13/3/2012	7.70	459
GW26	dug well	307771	1364312	4	640	7.328	29	13/3/2012	7.47	600
GW27	dug well	352450	1323310		3700	7.218	21.6	15/3/2012	7.55	3980
GW28	dug well	349070	1326168		619	7.301	23.5	15/3/2012	7.28	607
GW29	borehole	359326	1319721	76	547	7.108	25.7	15/3/2012	7.46	541
GW30	dug well	350405	1355601		468	6.486	24	16/3/2012	6.8	462
GW31	dug well cold	382592	1317900		387	7.368	22.8	27/3/2012	7.11	388
GW32	spring	382171	1317731		13,800	7.091	20.5	27/3/2012	7.5	14030

ID	Type	X	Y	Depth (m)	Field EC (µS/cm)	Field pH	Field Temp (ºC)	Sampling date	Lab. pH	Lab.EC (µS/cm)
GW33	borehole	369675	1319117	63	569	7.967	23	27/3/2012	7.69	575
GW34	borehole	359629	1326220		833	7.555	25.6	27/3/2012	7.26	819
GW35	dug well	349582	1339614		1014	7.909	24.2	28/3/2012	7.13	994
GW36	borehole	378623	1339111		627	7.512	25.2	28/3/2012	6.78	614
GW37	borehole	367852	1341230	137?	511	7.47	26.8	28/3/2012	7.30	475
GW38	dug well	378630	1288023		101.8	6.362	21.5	29/3/2012	6.61	111
GW39	dug well	344604	1301015		243	6.455	25	30/3/2012	6.55	244
GW40	borehole cold	342182	1301222		130.2	6.738	26.5	30/3/2012	6.96	143
GW41	spring hot	407710	1301117		91.1	7.3	16	4/4/2012	7.01	99
GW42	spring	367474	1296586		203	9.451	40	5/4/2012	9.48	192
GW43	borehole	315618	1292050	124	627	8.438	21.1	6/4/2012	8.55	609
GW44	borehole	305914	1289672	68	161	6.811	22.2	6/4/2012	6.54	158
GW45	dug well cold	299930	1294970		256	6.565	26.4	6/4/2012	6.48	252
GW46	spring cold	334463	1275160		5150	6.977	23.4	18/4/2012	7.19	4410
GW47	spring	332023	1273035		320	6.936	26.1	18/4/2012	7.13	327

ID	Type	X	Y	Depth (m)	Field EC (µS/cm)	Field pH	Field Temp (ºC)	Sampling date	Lab. pH	Lab.EC (µS/cm)
GW48	cold spring	312011	1282351		192	6.479	23.1	19/4/2012	6.53	192
GW49	borehole	313802	1278243	30?	377	7.195	25.2	19/4/2012	7.44	381
GW50	borehole	315512	1276884	90-150?	374	7.134	23.2	19/4/2012	7.16	375
GW51	cold spring	282623	1322572		301	7.64	27.2	23/4/2012	7.53	299
GW52	dug well	287461	1348655		661	7.634	27.2	23/4/2012	7.33	652
GW53	dug well	290594	1363251	6	397	7.069	21.6	24/4/2012	6.8	395
GW54	dug well	286468	1371255	6.5	574	7.256	21.8	24/4/2012	7.25	568
GW55	borehole	336244	1287877			7.14	nd	23/4/2012	7.07	229
GW56	borehole	304851	1251073		168	6.81	23.2	25/4/2012	6.64	269
GW57	borehole	323949	1278668		357	8.776	25.6	26/4/2012	8.69	350
GW58	borehole	326865	1275920	60	430	7.681	24.6	26/4/2012	7.88	431
GW59	cold spring	294931	1262786		238	6.961	22.5	27/4/2012	6.59	220
GW60	borehole	279925	1256936	30	341	8.24	23.8	27/4/2012	8.05	344
GW61	cold spring	267819	1227044		151	7.883	20	27/4/2012	7.25	149
GW62	dug well	262933	1249103		170	6.584	23.5	27/4/2012	6.49	176

ID	Type	X	Y	Depth (m)	Field EC (µS/cm)	Field pH	Field Temp (ºC)	Sampling date	Lab. pH	Lab.EC (µS/cm)
GW63	cold spring	303191	1213249		86	7.533	16.6	30/4/2012	6.65	83
GW64	borehole	303983	1215080		215	7.936	21.2	30/4/2012	7.77	211
GW65	cold spring	270524	1218850		153	7.4	17.4	30/4/2012	6.83	157
GW66	borehole	275792	1273946		138	6.97	26.1	1/5/2012	6.72	217
GW67	cold spring	270701	1282194		10	7.22	20.8	1/5/2012	6.98	112
GW68	borehole	314710	1270547	78	421	7.759	26	2/5/2012	7.56	417
GW69	dug well	321622	1284199		459	7.901	21.2	4/5/2012	7.41	449
GW71	borehole	286172	1224672		162.7	7.29	25	28/2/12	7.53	158
GW72	cold spring	312689	1281731		188	6.58	23.3	26/3/2012	6.8	187
GW73	borehole	366915	1319849	126	522	6.4	26.3	6/4/2012	7.85	502
GW74	cold spring	347880	1269740		510	7.13	23	4/4/2012	7.6	507
GW75	dug well	322745	1361257						7.37	7200
GW76	borehole	337388	1300444						6.6	198
GW77	dug well	350673	1289346						6.8	164

ID	Type	X	Y	Depth (m)	Field EC (µS/cm)	Field pH	Field Temp (ºC)	Sampling date	Lab. pH	Lab.EC (µS/cm)
GW78	dug well	355301	1303244						7.1	147
GW79	dug well	351627	1312039						7.5	700
GW80	dug well	350855	1312346						7	330
GW81	dug well	352169	1305490						7.1	363
GW82	borehole	275719	1293422						7.3	293
GW83	dug well	348926	1314362						8.4	442
GW84	borehole	265321	1246161						9.1	332
GW85	dug well	321386	1377648						7.1	414
GW86	borehole	350949	1309679						7.5	511
	cold									
GW87	spring	354299	1304392						6.67	249
GW88	dug well	349036	1310444						7.16	803
GW89	dug well	397071	1309085						7.86	216
GW90	borehole	373206	1286508						7.62	270
GW91	borehole	372073	1288388						7.63	276
	cold									
GW215	spring	218472	1227178		402	6.977	23.9	8/4/2012	7.4	398
GW216	borehole	213512	1245227		863	7.048	29.3	8/4/2012	7.27	826

ID	Type	X	Y	Depth (m)	Field EC (µS/cm)	Field pH	Field Temp (ºC)	Sampling date	Lab. pH	Lab.EC (µS/cm)
GW217	cold spring	235559	1258458		235	6.652	25.6	8/4/2012	6.87	202
GW218	cold spring	201829	1246070		359	7.38	31.6	9/4/2012	7.5	383
GW219	borehole	222087	1246820		337	7.02	25.1	9/4/2012	6.93	401
GW220	dug well	236405	1264429		383	6.8	28.4	6/4/2012	6.97	424
GW221	borehole	242553	1256973		376	7.9	29.1	6/4/2012	8.03	418
GW222	borehole	228858	1279859		77.6	6.12	28.4	6/4/2012	6.45	144
GW223	cold spring	226137	1280453		131	6.83	27.4	6/4/2012	7.27	210
GW224	cold spring	271840	1308196		271	6.457	24.9	1/5/2012	6.65	272
GW225	borehole	278458	1313020	110?	578	7.483	25.6	1/5/2012	7.24	567
GW226	test well			500					7.08	1247

Appendix 2b. Laboratory measured hydrochemical data for groundwater.

ID	Type	X	Y	Depth (m)	Na	K	Ca	Mg	HCO3	CO3	Cl	F	SO4	NO3	SiO2	Br
GW1	borehole	343291	1370434		25	0.8	71.0	35	438	0	8	0.38	10	9	59	0.2
GW2	borehole	312606	1355049	121	120	4.0	0.30	3	304	0	7	1.20	19	0.4	45	0.28
GW3	borehole	328564	1383745	301	64	0.3	0.1	8.0	161	32	9	0.60	11	0.4	32	0.44
GW4	dug well	324513	1359981		680	2	680	400	800	0	1489	0.06	2297	6.2	10	18.4
GW5	dug well	334446	1380606		20	0.5	48.0	19	267	0	16	0.32	13	5	61	0.26
GW6	borehole	363781	1285984	95.6	7	1.9	35.2	10	183	0	1.0	0.53	3	0.44	24	0.08
GW7	borehole	386114	1282962	90	9	5.1	35.9	7	178	0	1	0.31	3	3.50	28	0.11
GW8	borehole	284766	1313751	70	12	2.0	35	16	222	0	3	0.38	2.4	7.1	58	0.59
GW9	borehole	396407	1313342	109	504	14.9	61.0	34	1684	0	8	2.8	8	0.00	24	0.23
GW10	borehole	407117	1304322	42	19	8.3	19.0	5	137	0	7	0.2	5	3.50	32	0.19
GW11	borehole	350291	1292521	62.8	46	0.7	7.5	2	156	11	2	0.25	1	0.40	21	0.11
GW12	borehole	285626	1258237	38/65?	53	3.0	19	30	344	0	2	0.20	3.5	6.2	66	0.54
GW13	borehole	323134	1280503	82	72	3.9	8	5	220	0	4	0.51	4.1	0.4	20	0.6
GW14	borehole	319628	1280330	80	40	3.3	18	14	243	0	1	0.35	3.3	7.5	46	0.61
GW15	borehole	359714	1334645	60	107	0.6	13.4	3	329	0	11	0.11	9	2.20	26	0.19

ID	Type	X	Y	Depth (m)	Na	K	Ca	Mg	HCO3	CO3	Cl	F	SO4	NO3	SiO2	Br
GW16	hot spring	355780	1303277		38	0.2	0.1	10.2	56	34	2	0.90	1	0.4	62	nd*
GW17	dug well	342822	1316411	12	49	1.4	55.8	6.4	300	0	15	0.70	3	4	42	nd
GW18	dug well	354487	1312034		5	1.6	20.0	3.5	65	0	6	0.40	17	9	48	0.5
GW19	cold spring	355164	1309272		5	0.3	11.0	10.0	88	0	1	0.30	6	8	44	0.38
GW20	dug well	347199	1306740	12	5.3	0.8	39.0	13.0	168	0	6	0.30	4	3	54	0.42
GW21	borehole	334578	1392871	173?	90	1.5	25.0	0.1	293	0	18	0.30	12	9	52	0.76
GW22	borehole	319108	1371888	286/72-75?	46	0.4	30.0	57.0	490	0	21	0.50	10	22	58	0.51
GW23	dug well	324386	1362994	10	178	0.6	123.0	58.0	914	0	38	0.50	78	16	39	0.82
GW24	dug well	324540	1362647	10	370	1.3	297.0	255.0	667	0	876	0.50	1011	32	42	9.9
GW25	cold spring	300883	1368388		23	2.5	46.0	19.3	294	0	3	0.70	11	0.4	81	0.16
GW26	dug well	307771	1364312	4	13	0.4	73.0	26.0	403	0	3	0.60	10	7	50	0.22
GW27	dug well	352450	1323310		625	1.0	0.1	100	780	0	580	1.10	7	7	23	9.2
GW28	dug well	349070	1326168		65	1.0	32.0	17	320	0	28	0.28	17	5	39	0.61
GW29	borehole	359326	1319721	76	4	10.0	69.0	24	317	0	14	0.51	15	1	90	0.26
GW30	dug well	350405	1355601		20	2.0	44.0	12	198	0	22	0.31	9	10	68	0.28

ID	Type	X	Y	Depth (m)	Na	K	Ca	Mg	HCO3	CO3	Cl	F	SO4	NO3	SiO2	Br
GW31	dug well cold	382592	1317900		40	0.6	36.0	9	234	0	3	1.50	12	1	40	0.12
GW32	spring	382171	1317731		3700	88.0	0.0	25	7893	0	1071	5.5	10	1	47	0.1
GW33	borehole	369675	1319117	63	110	2.0	28.0	8	354	0	10	0.54	14	9	35	0.22
GW34	borehole	359629	1326220		40	1.0	78.0	31	430	0	13	0.35	15	0.4	40	0.73
GW35	dug well	349582	1339614		30	8.1	103.0	37	400	0	106	0.32	6	1.30	50	1.1
GW36	borehole	378623	1339111		25	1.2	68.9	17	290	0	26	0.26	9	57.50	63	0.39
GW37	borehole	367852	1341230	137?	90	0.6	23.0	9	305	0	3	0.38	9	4.00	49	0.11
GW38	dug well	378630	1288023		3	0.8	12.2	3	49	0	3	0.34	14	9.30	13	0.15
GW39	dug well	344604	1301015		2	0.5	25.2	9	127	0	5	0.16	2	18.60	25	0.16
GW40	borehole cold	342182	1301222		7	0.4	13.1	5	80	0	1	0.14	1	7.10	17	0.09
GW41	spring hot	407710	1301117		4	2.8	10.8	2	49	0	3	0.21	3	4.00	24	0.14
GW42	spring	367474	1296586		40	1	1	0.1	27	36	5	0.41	6	0.4	37	0.18
GW43	borehole	315618	1292050	124	133	4	11	5	360	9	15	0.98	4	0.9	17	0.41
GW44	borehole	305914	1289672	68	4	1	14	9	69	0	3	0.17	2	28.8	18	0.12
GW45	dug well	299930	1294970		7	1	20	14	65	0	14	0.13	27	22.0	17	0.33

ID	Type	X	Y	Depth (m)	Na	K	Ca	Mg	HCO3	CO3	Cl	F	SO4	NO3	SiO2	Br
GW46	cold spring	334463	1275160		543	10.7	56	364	3550	0	30	0.25	36.2	0.4	107	2
GW47	cold spring	332023	1273035		12	2.2	23	18	185	0	4	0.16	5.0	14.6	54	0.57
GW48	cold spring	312011	1282351		8	1.2	14	9	99	0	1	0.12	3.2	14.4	48	0.84
GW49	borehole	313802	1278243	30?	17	5.8	47	13	238	0	2	0.44	2.6	0.4	66	0.78
GW50	borehole	315512	1276884	90-150?	26	4.0	27	15	235	0	4	0.34	5.6	4.9	56	0.98
GW51	cold spring	282623	1322572		13	2.0	31	8	156	0	5	0.33	4.4	2.7	44	0.89
GW52	dug well	287461	1348655		22	0.7	65	25	397	0	3	0.31	5.7	15.5	54	1.5
GW53	dug well	290594	1363251	6	20	0.4	39	9	178	0	2	0.47	7.7	22.2	58	1.9
GW54	dug well	286468	1371255	6.5	13	1.5	59	18	189	0	3	0.20	5.6	73.0	48	2.7
GW55	borehole	336244	1287877		6	1.3	25	8	124	0	1	0.24	1	15.9	68	0.59
GW56	borehole	304851	1251073		7	1.0	29	9	163	0	2	0.29	1.0	4.9	68	2.7
GW57	borehole	323949	1278668		72	2.4	6	4	222	0	9	0.50	3.1	0.4	22	1.7
GW58	borehole	326865	1275920	60	83	3.4	16	8	262	0	14	0.64	3.0	1.8	24	1.5
GW59	cold spring	294931	1262786		5	1.6	17	12	128	0	1	0.16	1.0	6.2	42	0.92

ID	Type	X	Y	Depth (m)	Na	K	Ca	Mg	HCO3	CO3	Cl	F	SO4	NO3	SiO2	Br
GW60	borehole cold	279925	1256936	30	35	1.5	29	13	234	0	1	0.21	3.5	0.4	38	0.37
GW61	spring	267819	1227044		6	1.7	10	7	76	0	2	0.14	2.2	11.1	34	0.54
GW62	dug well cold	262933	1249103		3	1.4	17	7	88	0	2	0.37	5.0	9.3	38	0.61
GW63	spring	303191	1213249		2	1.5	8	4	39	0	1	0.29	1.5	9.7	22	0.44
GW64	borehole cold	303983	1215080		8	1.7	23	8	130	0	1	0.23	2.0	7.1	32	0.56
GW65	spring	270524	1218850		11	5.6	9	5	85	0	1	0.28	4.5	10.2	34	0.55
GW66	borehole cold	275792	1273946		17	5.9	17	4	124	0	1	0.39	4.3	2.7	76	0.54
GW67	spring	270701	1282194		3	0.9	12	4	52	0	1	0.41	4.0	9.3	30	0.33
GW68	borehole	314710	1270547	78	38	1.8	28	16	281	0	2	0.42	3.6	0.9	38	0.55
GW69	dug well	321622	1284199		12	1.8	43	25	293	0	2	0.28	1.3	1.8	46	0.44
GW71	borehole cold	286172	1224672		6	1.1	16	2	86	0	1	0.12	1.1	2.7	28	nd
GW72	spring	312689	1281731		8	1.0	17	9	105	0	1	0.1	4.0	12	47	nd
GW73	borehole	366915	1319849	126	76	3.0	22	10	332	0	5.7	0.35	19.1	0	23.5	nd

ID	Type	X	Y	Depth (m)	Na	K	Ca	Mg	HCO3	CO3	Cl	F	SO4	NO3	SiO2	Br
GW74	cold spring	347880	1269740		26	1.1	39	25	307	0	7.8	0.17	17.8	4.4	49.6	nd
GW75	dug well	322745	1361257		870	0.4	230	320	767	0	1872	0.3	779	0.58	24	13.64
GW76	borehole	337388	1300444		5	1.0	20	9	94.8	0	2.7	0.50	0.2	0	nd	nd
GW77	dug well	350673	1289346		3	2.6	27	5	94.8	0	5.5	0.50	0.2	0	nd	nd
GW78	dug well	355301	1303244		7	0.5	16	6	81.1	0	7.6	0.50	0.2	0	nd	nd
GW79	dug well	351627	1312039		40	0.6	62	25	431	0	7.6	0.50	11.5	0	nd	nd
GW80	dug well	350855	1312346		5	0.4	30	19	149	0	6.6	0.50	48	0	nd	nd
GW81	dug well	352169	1305490		13	0.6	48	13	200	0	15.1	0.50	1.8	0	nd	nd
GW82	borehole	275719	1293422		18	1.1	31	12	201	0	2.9	0.50	0.4	0	nd	nd
GW83	dug well	348926	1314362		43	0.6	30	25	195	24	10.6	0.50	29.9	0	nd	nd
GW84	borehole	265321	1246161		80	0.8	4	2	110	48	4.8	0.60	0.2	0	nd	nd
GW85	dug well	321386	1377648		20	0.6	50	15	268	0	7.7	0.50	0.8	0	nd	nd
GW86	borehole	350949	1309679		22	1.0	56	15	300	0	9.1	0.60	5.5	0	nd	nd
GW87	cold spring	354299	1304392		6.5	0.7	33	11	139	0	2.8	0.48	3.3	12	nd	nd
GW88	dug well	349036	1310444		92	1.3	76	22	525	0	3.8	0.32	29.7	4.3	nd	nd
GW89	dug well	397071	1309085		8.01	1.3	38	2.7	128	0	2.7	0.15	2.53	9	nd	nd
GW90	borehole	373206	1286508		6.02	1.8	33	14	166	0	3.2	0.08	0.14	15	nd	nd

ID	Type	X	Y	Depth (m)	Na	K	Ca	Mg	HCO3	CO3	Cl	F	SO4	NO3	SiO2	Br
GW91	borehole cold	372073	1288388		6.32	1.5	29	13	174	0	2.3	0.15	0.25	11	nd	
GW215	spring	218472	1227178		7	1.0	59	11	254	0	2	0.3	5.0	22.2	25	0.29
GW216	borehole cold	213512	1245227		27	1.9	119	19	354	0	35	0.3	27.4	90.8	23	1.1
GW217	spring cold	235559	1258458		7	0.6	18	11	122	0	0	0.2	2.1	5.8	31	0.2
GW218	spring	201829	1246070		11	0.7	41	16	217	0	0	0.3	1.4	25.7	83	0.42
GW219	borehole	222087	1246820		9	0.5	39	18	214	0	6	0.2	0.9	44.3	72	0.44
GW220	dug well	236405	1264429		10	0.3	41	23	279	0	4	0.2	2.5	6.7	68	0.37
GW221	borehole	242553	1256973		87	1.5	10	4	262	0	6	0.5	3.4	<0.4	63	nd
GW222	borehole cold	228858	1279859		8	1.1	20	6	93	0	2	0.2	1.4	<0.4	56	0.03
GW223	spring cold	226137	1280453		9	1.6	22	9	143	0	1	0.2	2.4	2.7	72	0.22
GW224	spring	271840	1308196		17	2.7	25	8	126	0	6	0.38	5.6	24.8	62	0.64
GW225	borehole	278458	1313020	110?	54	9.6	58	19	371	0	4	0.45	5.1	0.4	90	0.53
GW226	test well	315977	1282169	500	189.5	14.66	41	47	830	0	13.04	0.41	0.41	1.77	88.17	nd

*nd: not determined

Appendix 2c. Field and laboratory measured hydrochemical parameters for rainfall and surface waters.

ID	Site	Type	X	Y	Field EC (µS/cm)	Field pH	Field Temp. (ºC)	Sampling date	Lab. pH	Lab. EC (µS/cm)
Rain1	Gilgel Beles	Rain	209521	1235107				July	6.66	33.00
Rain2	Bahir Dar	Rain	321196	1282803				August	6.60	25.00
								Mean		
Rain3	Gonder	Rain	332613	1395124				July&Aug.	7.00	44.00
Rain4	Gasay	Rain	406941	1304349				August	7.03	31.00
								mean		
Rain5	Sekela	Rain	304802	1215226				July&Aug.	6.63	30.50
SW4	Megech river at the bridge	River	331417	1381243	417	8.21	21.2	16/3/2012	7.92	421
SW6	Gelda river at the bridege	River	337015	1296526	186	7.76	19.4	5/4/2012	7.55	183
SW7	Emba Wenze/Chan stream	River	359131	1300704	168	8.67	26.1	5/4/2012	9.58	152
SW9	Gilgel Abay at Chimba	River	300407	1295158	182	7.68	24.1	6/4/2012	7.63	178
SW10	Abay at Tis Abay	River	345129	1270503	187	8.51	24.1	18/4/2012	7.67	194
SW12	Abay R. at the bridge	River	326649	1283913	162	7.89	23.7	23/4/2012	7.52	163
SW14	Gilgel Abay at the bridge	River	285785	1257172	87.1	8.60	23.7	25/4/2012	7.39	190
SW20	Abat Beles river at the bridge	River	207965	1239179	157	8.21	24.9	8/4/2012	7.25	160
SW21	Gumara river at the bridge	River	351381	1309268	272	8.39	24	8/3/2012	7.73	273
SW23	Gumara river upstream	River	401474	1296161	100.2	6.10	24	6/4/2012	7.99	144
SW24	Dirma	River	320033	1385779					8	286
		Tana								
SW1	Achera-Ashewa bahir	Lake	320908	1357598	164	7.79	22.6	13/3/2012	7.27	163
		Tana								
SW3	Gorgora port hotel	Lake	315386	1353588	154	8.57	24.4	13/3/2012	7.23	156

ID	Site	Type	X	Y	Field EC (µS/cm)	Field pH	Field Temp. (ºC)	Sampling date	Lab. pH	Lab. EC (µS/cm)
SW5	Ager Kirigna Maryam	Tana Lake	349526	1339504	134	10.30	23.5	28/3/2012	7.35	152
SW8	Zege	Tana Lake	316535	1293039	162	8.03	21.2	6/4/2012	7.86	157
SW11	Delgi	Tana Lake	287811	1347944	175	8.46	25.2	23/4/2012	7.83	159
SW13	Korata	Tana Lake	331321	1300702		8.40	nd	23/4/2012	8.32	158
SW15	Kunzila	Tana Lake	285791	1314323	157	8.74	26.9	1/5/2012	7.14	163
SW16	Tana Lake at the center	Tana Lake	324699	1284793	170	8.44	23.3	3/5/2012	7.92	163
SW17	Tana Lake at the center	Tana Lake	320124	1308650	156	8.36	23.3	3/5/2012	7.68	167
SW18	Tana Lake at the center	Tana Lake	318801	1318504	156	8.26	22.8	3/5/2012	7.71	156
SW19	Tana Lake	Tana Lake	314898	1328628	154	8.31	23	3/5/2012	6.45	144
SW2	Achera-Ashewa bahir	Wet land	320555	1357949	246	6.72	18.3	13/3/2012	6.60	232
SW22	Wagtera	Wet land	342175	1317257	249	9.32	27	8/3/2012	7.03	274

Appendix 2d. Laboratory measured hydrochemical data for rainfall and surface waters.

ID	Site	Type	X	Y	Na	K	Ca	Mg	HCO_3	CO_3	Cl	F	SO_4	NO_3	SiO_2	Br
Rain1	Gilgel Beles	Rain	209521	1235107	0.70	0.18	4.25	0.72	14.00	0	0.50	0.14	2.22	2.66	1.00	0.26
Rain2	Bahir Dar	Rain	321196	1282803	0.42	0.10	3.04	0.14	8.00	0	1.13	0.10	0.10	2.66	0.40	0.22
Rain3	Gonder	Rain	332613	1395124	0.75	0.25	6.90	0.25	16.78	0.00	1.18	0.10	2.11	2.44	0.30	0.26
Rain4	Gasay	Rain	406941	1304349	0.50	0.14	3.70	0.20	12.00	0	1.28	0.10	0.10	1.77	0.20	0.21
Rain5	Sekela	Rain	304802	1215226	0.78	1.27	3.02	0.69	7.50	0.00	1.20	0.10	3.13	6.43	0.10	0.25
SW4	Megech river at the bridge	River	331417	1381243	20	2.0	27.0	22	216	0	9	0.29	20	0.4	35	0.2
SW6	Gelda river at the bridege	River	337015	1296526	7	2.4	17.8	6	110	0	3	0.18	4	0.44	10	0.2
SW7	Emba Wenze/Chan stream	River	359131	1300704	5	2	15	5	54	13	2	0.2	3	0.4	12	0.13
SW9	Gilgel Abay at Chimba	River	300407	1295158	6	2	18	9	92	0	0.1	0.24	3	22.2	12	0.16
SW10	Abay at Tis Abay	River	345129	1270503	7	2.4	18	8	101	0	3	0.29	6.3	1.3	10	0.58
SW12	Abay R. at the bridge	River	326649	1283913	6	2.9	15	6	89	0	1	0.36	7.6	0.9	10	0.73
SW14	Gilgel Abay at the bridge	River	285785	1257172	5	2.3	17	8	112	0	1	0.24	4.4	1.8	18	2
SW20	Abat Beles river at the bridge	River	207965	1239179	6	2.1	17	6	89	0	3	0.3	12.2	<0.4	4.9	0.44
SW21	Gumara river at the bridge	River	351381	1309268	11.7	2.7	21	12.6	171	0	3.5	0.13	3	0.4	33	0.4
SW23	Gumara river upstream	River	401474	1296161	10.1	3.8	13.4	2	61	0	3.5	0.26	23.7	0.9	21.4	nd*
SW24	Dirma	River	320033	1385779	13	2.4	26	15	159	0	9.1	0.40	1.2	0	nd	nd
SW1	Achera-Ashewa bahir	Tana Lake	320908	1357598	10	1.5	17.0	5.3	82	0	3	0.70	24	0.4	7	0.17
SW3	Gorgora port hotel	Tana Lake	315386	1353588	21	1.0	10.0	4	89	0	3	0.34	7	0.4	7	0.19

ID	Site	Type	X	Y	Na	K	Ca	Mg	HCO_3	CO_3	Cl	F	SO_4	NO_3	SiO_2	Br
SW5	Ager Kirigna Maryam	Tana Lake	349526	1339504	9	2.1	16.0	5	72	0	3	0.31	30	0.4	12	0.21
SW8	Zege	Tana Lake	316535	1293039	6	2	17	6	93	0	3	0.41	4	0.4	4	0.18
SW11	Delgi	Tana Lake	287811	1347944	5	2.3	14	6	78	0	5	0.33	5.3	0.4	10	0.92
SW13	Korata	Tana Lake	331321	1300702	6	2.2	15	6	74	0	2	0.53	10.5	0.4	10	8.2
SW15	Kunzila	Tana Lake	285791	1314323	6	2.3	26	6	107	0	4	0.45	8.3	0.4	8	0.48
SW16	Tana Lake at the center	Tana Lake	324699	1284793	6	2.4	15	6	85	0	2	0.63	9.3	0.4	8	0.71
SW17	Tana Lake at the center	Tana Lake	320124	1308650	6	2.2	15	5	88	0	3	0.49	5.9	0.4	8	0.57
SW18	Tana Lake at the center	Tana Lake	318801	1318504	6	2.4	15	5	89	0	2	0.41	6.4	0.4	8	0.56
SW19	Tana Lake at the center	Tana Lake	314898	1328628	8	1.1	20	6	93	0	1.8	0.16	1.43	0.4	4	0.54
SW2	Achera-Ashewa bahir	Wet land	320555	1357949	7	0.5	33.0	9.3	157	0	1	0.70	11	0.4	7	0.08
SW22	Wet land	Wet land	342175	1317257	23	2.9	20.0	3.3	118	0	18	0.90	1.0	3	6	nd

*nd: not determined

Appendix 3a. Isotopic data of groundwater samples.

ID	Site	Type	X	Y	Well depth	$\delta^{18}O$ (‰)	$\delta^{2}H$ (‰)	^{3}H (TU)
GW1	Maksegniet town supply	borehole	343291	1370434		0.4	4.79	1.16
GW2	Gorgora town supply/Kes Mender	borehole	312606	1355049	121	-2.52	-7.92	0.5
GW3	Dashen brewery borehole 1B/Lashka	borehole	328564	1383745	301	-3.9	-18.52	0.52
GW5	Tseda town	dug well	334446	1380606		0.01	11.86	
GW6	Arb gebeya town supply	borehole	363781	1285984	95.6	-5.96	-10.81	1.65
GW7	Jib Asra town supply	borehole	386114	1282962	90	-5.96	-15.74	
GW8	Kunzila town supply	borehole	284766	1313751	70	-2.15	-7.11	1.6
GW9	Debretabore town supply/Gafat No.10	borehole	396407	1313342	109	-5.3	-26.95	0.51
GW10	Gasay town supply	borehole	407117	1304322	42	-5.3	-24.21	0.37
GW11	Anbesame town supply	borehole	350291	1292521	62.8	-5.96	-11.63	3.14
GW12	Wetete Abay town supply	borehole	285626	1258237	38/65?	-1.87	0.62	2.39
GW13	AWWCE borehole	borehole	323134	1280503	82	-1.81	-3.42	2.06
GW14	Dudu/Amhara PVC factory	borehole	319628	1280330	80	-2.41	-2.48	6.18
GW15	Yifag town supply	borehole	359714	1334645	60	-5.83	-17.33	
GW16	Wonzaye	hot spring	355780	1303277		-5.01	-16.83	0.82
GW17	Wagtera school	dug well	342822	1316411	12	0.04	12.66	2.71
GW18	Mesno cllinic	dug well	354487	1312034		-1.22	4.87	

ID	Site	Type	X	Y	Well depth	$\delta^{18}O$ (‰)	$\delta^{2}H$ (‰)	^{3}H (TU)
GW19	Tanku Gebriel/Medehaniealem tsebel	cold spring	355164	1309272		-2.02	0.59	6.28
GW20	Zarak/Showble school	dug well	347199	1306740	12	-1.31	4.18	
GW21	Angereb 6/NW5	borehole	334578	1392871	173?	-0.62	4.98	2.74
GW22	Kola diba town borehole/Wonfela	borehole	319108	1371888	286/64-75?	-0.46	6.45	1.13
GW23	Robit village supply	dug well	324386	1362994	10	-1.12	-0.82	
GW24	Robit Medihanealem tsebel	dug well	324540	1362647	10	-1.99	-3.78	0.92
GW25	Gurehae/Beles	cold spring	300883	1368388		-3.06	-11.29	1.48
GW26	Cewayit supply	dug well	307771	1364312	4	0.27	10.3	
GW27	Shaga/Gguaye mender/Amlak tadese well	dug well	352450	1323310		-1.37	5.31	3.34
GW28	Rike well	dug well	349070	1326168		-1.84	3.28	6.08
GW29	Woreta town supply/Jicaa borehole	borehole	359326	1319721	76	-5.83	-31.21	0.63
GW30	Infranz town	dug well	350405	1355601		-1.53	3.7	
GW31	Alem Ber/Gala terara	dug well	382592	1317900		-1.24	4.95	
GW32	Serba Maryiam/Amora gedel tsebel	cold spring	382171	1317731		-7.9	-35.27	0.43

ID	Site	Type	X	Y	Well depth	$\delta^{18}O$ (‰)	$\delta^{2}H$ (‰)	^{3}H (TU)
GW33	Maksegne village supply	borehole	369675	1319117	63	-1.3	2.7	
GW34	Shinasim/Rib	borehole	359629	1326220		-1.42	2.35	
GW35	Ager Kirigna Maryam	dug well	349582	1339614		-1.99	-5.32	6.06
GW36	Ambo Meda/Gaja bahir	borehole	378623	1339111		-1.99	-2.12	
GW37	Addis Zemen town supply/Alabo No.1	borehole	367852	1341230	137?	-1.99	2.68	3.43
GW40	Hamusit town supply	borehole	342182	1301222		-5.3	-0.52	5.11
GW41	Huzet/Gerarge	cold spring	407710	1301117		-2.07	-3.26	
GW42	Guramba Kidanemheret hot spring	hot spring	367474	1296586		-5.19	-25.4	0.67
GW43	Zege town supply	borehole	315618	1292050	124	-1.93	-4.84	1.29
GW44	Ygodit-Tentela/Robit supply	borehole	305914	1289672	68	-5.88	-6.54	5.09
GW45	Chiba town/Kedam Gebeya	dug well	299930	1294970		-0.92	1.82	6.41
GW46	Andesa Giorgis spring	cold spring	334463	1275160		-4.95	-16.13	3
GW47	Tikurit	cold spring	332023	1273035		-1.06	3.54	5.71
GW48	Lomi	spring	312011	1282351		-1.75	1.05	5.71

ID	Site	Type	X	Y	Well depth	$\delta^{18}O$ (‰)	$\delta^{2}H$ (‰)	^{3}H (TU)
GW49	Yebab Chincha	borehole	313802	1278243	30?	-2.67	-7.75	
GW50	Entedit	borehole cold	315512	1276884	90-150?	-3.71	-14.55	1.94
GW51	Dengel Ber town	spring	282623	1322572		-0.32	9.18	
GW52	Norway (kinder Garden, delgi)	dug well	287461	1348655		0.04	9.04	1.95
GW53	Chewa Diba/upstream	dug well	290594	1363251	6	-0.46	12.61	5.79
GW54	Chan Diba primary school	dug well	286468	1371255	6.5	-0.16	11.34	
GW55	Zenzelma	borehole	336244	1287877		-1.55	1.88	4.58
GW56	Dima/Rim	borehole	304851	1251073		-1.71	1.24	3.21
GW57	Gordena village	borehole	323949	1278668		-1.98	-5.41	
GW58	Sebat Amit primary schoole supply	borehole cold	326865	1275920	60	-1.94	-4.12	
GW59	Merawi	spring	294931	1262786		-1.66	2.52	6.03
GW60	Durebete town supply	borehole cold	279925	1256936	30	-1.85	-0.96	
GW61	Adis Kidan/Bilt Sar	spring	267819	1227044		-1.94	0.16	
GW62	Garagi Mender2	dug well cold	262933	1249103		-1.4	-3.68	4.73
GW63	Gish Abay tsebel	spring	303191	1213249		-1.56	-0.64	

ID	Site	Type	X	Y	Well depth	$\delta^{18}O$ (‰)	$\delta^{2}H$ (‰)	^{3}H (TU)
GW64	Gish Abay town supply	borehole cold	303983	1215080		-3.41	-8.53	4.66
GW65	Zerehe spring	spring	270524	1218850		-1.2	-0.61	5.54
GW66	Lalibela town supply	borehole cold	275792	1273946		-2.74	-8.96	1.48
GW67	Yesemala town supply	spring	270701	1282194		-1.28	-3.55	
GW68	Meshenti town supply	borehole	314710	1270547	78	-3.23	-10.56	
GW69	Baeta tsebel	dug well cold	321622	1284199		-1.82	2.87	
GW74	Awrajit/Tis Abay	spring cold	347880	1269740		-1.38	-0.87	
GW215	Abatachen spring	spring	218472	1227178		-0.92	11.03	5.47
GW216	Mender 4/Felege Selam	borehole cold	213512	1245227		1.79	9.91	5.13
GW217	Ali spring	spring cold	235559	1258458		1.79	8.98	1.23
GW218	Mender46 spring	spring	201829	1246070		-1.17	7.97	
GW219	Mender28 supply	borehole	222087	1246820		-1.44	9.35	
GW220	Emba Ser village supply	dug well	236405	1264429		-0.09	10.88	

ID	Site	Type	X	Y	Well depth	$\delta^{18}O$ (‰)	$\delta^{2}H$ (‰)	^{3}H (TU)
GW221	Work Meda village supply/Kaba	borehole cold	242553	1256973		-2.83	-11.8	
GW223	Addis Woyne/Jawe town	spring cold	226137	1280453		-0.43	5.94	
GW224	Dusman/Charman spring	spring	271840	1308196		-1.13	3.7	5.58
GW225	Workaye/salini camp borehole	borehole	278458	1313020	110?	-4.15	-22.27	1.46
GW226	Bahir Dar test well	test well	316070	1282376	500	-3	-15.45	2.25

Appendix 3b. Isotopic data of surface waters.

ID	Site	Type	X	Y	$\delta^{18}O$ (‰)	$\delta^{2}H$ (‰)
SW4	Megech river at the bridge	River	331417	1381243	1.67	17
SW6	Gelda river at the bridege	River	337015	1296526	1.34	16.54
SW7	Emba Wenze/Chan stream	River	359131	1300704	-0.84	-3.2
SW9	Gilgel Abay at Chimba	River	300407	1295158	-0.92	9.35
SW10	Abay at Tis Abay	River	345129	1270503	3.84	28.2
SW12	Abay R. at the bridge	River	326649	1283913	5.79	43.57
SW14	Gilgel Abay at the bridge	River	285785	1257172	3.18	24.13
SW20	Abat Beles river at the bridge	River	207965	1239179	4.05	32.78
SW21	Gumara river at the bridge	River	351381	1309268	2.2	22.68
SW23	Gumara river upstream	River	401474	1296161	1.31	13.02
SW1	Achera-Ashewa bahir	Tana Lake	320908	1357598	4.67	38.11
SW3	Gorgora port hotel	Tana Lake	315386	1353588	4.22	39.47
SW5	Ager Kirigna Maryam	Tana Lake	349526	1339504	1.85	32.3
SW8	Zege	Tana Lake	316535	1293039	5.69	44.5
SW11	Delgi	Tana Lake	287811	1347944	5.49	42.86
SW13	Korata	Tana Lake	331321	1300702	5.99	46.03
SW15	Kunzila	Tana Lake	285791	1314323	5.42	38.36
SW16	Tana Lake center	Tana Lake	324699	1284793	4.93	38.12
SW17	Tana Lake center	Tana Lake	320124	1308650	4.8	39.78
SW18	Tana Lake center	Tana Lake	318801	1318504	3.66	37.53
SW19	Tana Lake center	Tana Lake	314898	1328628	4.4	40
SW25	Koga reservoir	Reservoir	297278	1254865	4.46	29.89
SW26	Angereb reservoir	Reservoir	335378	1394862	1.96	18.77
SW2	Achera-Ashewa bahir	Wet land	320555	1357949	6.63	52.41
SW22	Wagtera marsh	Wet land	342175	1317257	16.55	108.93

Appendix 3c. Isotopic data of rainfall.

ID	Month	Station	Altitude (m)	$\delta^{18}O$ (‰)	$\delta^{2}H$ (‰)
BD5	May	Bahir Dar	1808	-0.47	12.19
BD6	June	Bahir Dar	1808	-0.64	17.74
BD7	July	Bahir Dar	1808	-5.3	-17.81
BD8	August	Bahir Dar	1808	-4.05	-8.16
BD9	September	Bahir Dar	1808	-1.92	10.75
GAS6	June	Gassay	2789	-0.08	26.43
GAS7	July	Gassay	2789	-4.51	-9.53
GAS8	August	Gassay	2789	-5.11	-17.1
GAS9	September	Gassay	2789	-2.15	5.35
GAS10	October	Gassay	2789	-6.21	-30.81
GO4	April	Gonder	2125	-0.79	13.42
GO5	May	Gonder	2125	-2.32	3.12
GO6	June	Gonder	2125	-0.55	15.88
GO7	July	Gonder	2125	-3.82	-12.33
GO8	August	Gonder	2125	-4.06	-11.86
GO9	September	Gonder	2125	-2.23	4.26
GO10	October	Gonder	2125	-0.37	11.59
S5	May	Sekela	2710	-0.39	16.2
S6	June	Sekela	2710	-0.87	16.24
S7	July	Sekela	2710	-4.91	-19.79
S8	August	Sekela	2710	-6.49	-33.77
S9	September	Sekela	2710	-1.32	14.07
S10	October	Sekela	2710	-1.87	9.14
GB5	May	Gilgel Beles	1040	0.47	17.35
GB6	June	Gilgel Beles	1040	-0.33	18.33

ID	Month	Station	Altitude (m)	$\delta^{18}O$ (‰)	$\delta^{2}H$ (‰)
GB7	July	Gilgel Beles	1040	-4.25	-13.95
GB8	August	Gilgel Beles	1040	-3.97	-9.86
GB9	September	Gilgel Beles	1040	-0.99	16.3
GB10	October	Gilgel Beles	1040	3.32	50.89

Appendix 4. Groundwater subgroups.

ID	Site	Type	X	Y	Well depth (m)	Subgroup	Group
GW19	Tanku Gebriel/Medehaniealem tsebel	cold spring	355164	1309272		3	2
GW40	Hamusit town supply	borehole	342182	1301222		3	2
GW41	Huzet/Gerarge	cold spring	407710	1301117		3	2
GW44	Ygodit-Tentela/Robit supply	borehole	305914	1289672	68	3	2
GW45	Chiba town/Kedam Gebeya	dug well	299930	1294970		3	2
GW48	Lomi	cold spring	312011	1282351		3	2
GW55	Zenzelma	borehole	336244	1287877		3	2
GW56	Dima/Rim	borehole	304851	1251073		3	2
GW59	Merawi	cold spring	294931	1262786		3	2
GW61	Adis Kidan/Bilt Sar	cold spring	267819	1227044		3	2
GW63	Gish Abay tsebel	cold spring	303191	1213249		3	2
GW67	Yesemala town supply	cold spring	270701	1282194		3	2
GW72	Areke	cold spring	312689	1281731		3	2
GW217	Ali spring	cold spring	235559	1258458		3	2
GW218	Mender46 spring	cold spring	201829	1246070		3	2
GW219	Mender28 supply	borehole	222087	1246820		3	2
GW220	Emba Ser village supply	dug well	236405	1264429		3	2
GW223	Addis Woyne/Jawe town	cold spring	226137	1280453		3	2
GW6	Arb gebeya town supply	borehole	363781	1285984	95.6	3	2
GW7	Jib Asra town supply	borehole	386114	1282962	90	3	2
GW8	Kunzila town supply	borehole	284766	1313751	70	3	2
GW10	Gasay town supply	borehole	407117	1304322	42	3	2
GW12	Wetete Abay town supply	borehole	285626	1258237	38/65?	3	2

ID	Site	Type	X	Y	Well depth (m)	Subgroup	Group
GW14	Dudu/Amhara PVC factory	borehole	319628	1280330	80	3	2
GW18	Mesno cllinic	dug well	354487	1312034		3	2
GW20	Zarak/Showble school	dug well	347199	1306740	12	3	2
GW25	Gurehae/Beles	cold spring	300883	1368388		3	2
GW29	Woreta town supply/Jicaa borehole	borehole	359326	1319721	76	3	2
GW35	Ager Kirigna Maryam	dug well	349582	1339614		3	2
GW47	Tikurit	cold spring	332023	1273035		3	2
GW49	Yebab Chincha	borehole	313802	1278243	30?	3	2
GW50	Entedit	borehole	315512	1276884	90-150?	3	2
GW51	Dengel Ber town	cold spring	282623	1322572		3	2
GW60	Durebete town supply	borehole	279925	1256936	30	3	2
GW62	Garagi Mender2	dug well	262933	1249103		3	2
GW64	Gish Abay town supply	borehole	303983	1215080		3	2
GW65	Zerehe spring	cold spring	270524	1218850		3	2
GW66	Lalibela town supply	borehole	275792	1273946		3	2
GW68	Meshenti town supply	borehole	314710	1270547	78	3	2
GW69	Baeta tsebel	dug well	321622	1284199		3	2
GW215	Abatachen spring	cold spring	218472	1227178		3	2
GW224	Dusman/Charman spring	cold spring	271840	1308196		3	2
GW225	Workaye/salini camp borehole	borehole	278458	1313020	110?	3	2
GW54	Chan Diba primary school	dug well	286468	1371255	6.5	3	2
GW1	Maksegniet town supply	borehole	343291	1370434		3	2
GW5	Tseda town	dug well	334446	1380606		3	2
GW22	Kola diba town borehole/Wonfela	borehole	319108	1371888	286/64-75?	3	2
GW23	Robit village supply	dug well	324386	1362994	10	3	2
GW26	Cewayit supply	dug well	307771	1364312	4	3	2
GW28	Rike well	dug well	349070	1326168		3	2

ID	Site	Type	X	Y	Well depth (m)	Subgroup	Group
GW30	Infranz town	dug well	350405	1355601		3	2
GW31	Alem Ber/Gala terara	dug well	382592	1317900		3	2
GW34	Shinasim/Rib	borehole	359629	1326220		3	2
GW36	Ambo Meda/Gaja bahir	borehole	378623	1339111		3	2
GW37	Addis Zemen town supply/Alabo No.1	borehole	367852	1341230	137?	3	2
GW52	Norway (kinder Garden, delgi)	dug well	287461	1348655		3	2
GW53	Chewa Diba/upstream	dug well	290594	1363251	6	3	2
GW74	Awrajit/Tis Abay	cold spring	347880	1269740		3	2
GW216	Mender 4/Felege Selam	borehole	213512	1245227		3	2
GW32	Serba Maryiam/Amora gedel tsebel	cold spring	382171	1317731		1a	1
GW27	Shaga/guaye mender/Amlak tadese well	dug well	352450	1323310		1b	1
GW9	Debretabore town supply/Gafat No.10	borehole	396407	1313342	109	1c	1
GW4		dug well	324513	1359981		1d	1
GW24	Robit Medihanealem tsebel	dug well	324540	1362647	10	1d	1
GW46	Andesa Giorgis spring	cold spring	334463	1275160		1d	1
GW75		dug well	322745	1361257		1d	1
GW16	Wonzaye	hot spring	355780	1303277		2a	2
GW42	Guramba Kidanemheret hot spring	hot spring	367474	1296586		2a	2
GW2	Gorgora town supply/Kes Mender	borehole	312606	1355049	121	2	2
GW3	Dashen brewery borehole 1B/Lashka	borehole	328564	1383745	301	2	2
GW11	Anbesame town supply	borehole	350291	1292521	62.8	2	2
GW13	AWWCE borehole	borehole	323134	1280503	82	2	2
GW15	Yifag town supply	borehole	359714	1334645	60	2	2
GW17	Wagtera school	dug well	342822	1316411	12	2	2
GW21	Angereb 6/NW5	borehole	334578	1392871	173?	2	2
GW33	Maksegne village supply	borehole	369675	1319117	63	2	2

ID	Site	Type	X	Y	Well depth (m)	Subgroup	Group
GW43	Zege town supply	borehole	315618	1292050	124	2	2
GW57	Gordena village	borehole	323949	1278668		2	2
GW58	Sebat Amit primary schoole supply	borehole	326865	1275920	60	2	3
GW73	Awramba	borehole	366915	1319849	126	2	2
GW221	Work Meda village supply/Kaba	borehole	242553	1256973		2	2